AN EVALUATION OF A NOVEL METHOD FOR THE INHIBITION OF SULPHIDE STRESS CORROSION CRACKING IN STEEL.

A Thesis Submitted for the Degree of

Doctor of Philosophy

to

Council for National Academic Awards

by

Thurairajah Sriskandarajah

This Work was Carried out at Middlesex Polytechnic
in Collaboration with The City University and
Supported by the Department of Energy, Great Britain.

To My Wife Sakthy and Children .....

ACKNOWLEDGEMENTS

I am indebted to my supervisors, Dr. H.C. Chan of the School of Civil Engineering, Middlesex Polytechnic, and Professor A.C.C. Tseung of the Department of Chemistry, The City University, for their guidance and encouragement throughout this work. I would like to extend my gratitude to my advisory supervisor, Dr. J. Golden, of Middlesex Polytechnic, for his assistance and encouragement during this study.

My sincere and grateful thanks are due to my colleagues, particularly Messers. R.A. Smith and F. Jones of the School of Civil Engineering, Middlesex Polytechnic and Mr. P. Rasiyah of the Department of Chemistry, The City University, for many valuable discussions. Sincere and grateful thanks are also due to the technical and library staff of the Middlesex Polytechnic, especially Messers. F. Hyde, M. Bodger, T. Rube, G. Aide, L. Lambley and I. Oliver for helping on numerous aspects of the work and Mrs. K. Scales for persisting with a difficult manuscript.

I would also like to acknowledge the general assistance given by the Middlesex Polytechnic and the financial support received from the Department of Energy, Great Britain. The Financial support by the NRDC for patenting this work is also acknowledged.

Finally I would like to extend my deepest gratitude to my parents for their encouragement and financial support throughout my studies.

ABSTRACT

Sulphide stress corrosion cracking, (SSCC) is one of the major problems encountered by the petroleum industry throughout the world. The problem is likely to increase in severity for the North Sea oil and gas industries as the fields get older and platforms are moved to deeper waters. This is because the hydrogen sulphide concentration increases as the fields get older and deeper water explorations require higher strength steels. The protective measures taken at present to combat SSCC are not adequate. Therefore a novel method was developed to inhibit SSCC in steel. This method is based on using an active hydrogen evolution sulphide electro-catalyst, more active than steel, as a coat on the surface of the steel, such that the hydrogen evolution will take place on the catalyst surface, instead of on the corroding steel surface. Therefore, the amount of hydrogen diffusing through the steel is greatly reduced. Hence, SSCC in the steel is effectively inhibited. Electrochemical and mechanical experimental studies were carried out to confirm the validity of this method.

A computer-aided literature survey on SSCC and its prevention in oil- and gas-well equipment is presented.

The viability of three sulphide electro-catalysts, $NiCo_2S_4$, MoS_2 and WS_2 for this method were studied in various experiments, namely, electrochemical polarization, hydrogen diffusion studies and corrosion weight loss measurements. The experimental studies carried out in NACE solution, consisting of a 5 percent (mass/volume) NaCl and 0.5 percent (volume/volume) acetic acid, with a continuous flow of H_2S at 1 atmospheric pressure, indicated that hydrogen evolution performances were in the following order:

in the absence of H_2S, $NiCo_2S_4 > WS_2 > MoS_2 \gg$ EN 42 steel

in the presence of H_2S, $MoS_2 > WS_2 > NiCo_2S_4 \gg$ EN 42 steel.

MoS_2 was found to be the most stable catalyst in the sour corrosive environment. Evans diagrams, constructed to predict corrosion rates, indicate that the corrosion current ratio of the MoS_2 - EN 42 steel couple and EN 42 steel did not change significantly when the catalyst loading was reduced. The

hydrogen diffusion studies confirmed that an MoS_2/FEP (fluoro ethylene polymer) adherent coat with higher catalyst to FEP ratio was the most effective of three adherent coats. The corrosion weight loss measurements showed that the corrosion rates of steel coupons partially coated with MoS_2/FEP coat were higher than those of uncoated coupons for up to 50 hours but thereafter they reduced significantly below those of uncoated coupons.

Mechanical studies carried out to evaluate the effectiveness of this method were helped by a literature survey on stress corrosion test methods and interpretation of results. Slower straining/loading rate tests and sustained load tests were selected to study the changes in various mechanical parameters on different types of specimens when protected with MoS_2/FEP coat. In addition to these tests, Charpy impact tests were also carried out. The mechanical parameters measured on the specimens are:

a) for compact tension specimens
   - stress intensity factor at failure
   - total energy required for fracturing the specimen
   - average energy consumed for unit length of crack extension
   - crack opening displacement
   - crack growth rate
   - time to failure

b) for three-point bend specimens
   - crack opening displacement

c) for Charpy V-notch impact test specimens
   - fracture energy.

All these mechanical parameters confirm the effectiveness of the MoS_2/FEP coat to inhibit SSCC in steel. Scanning electron microscopic examinations of the specimens also confirmed the viability of the novel protective method. The sour-corrosion fatigue tests showed that the MoS_2/FEP coat could be used effectively in environments where a cyclic loading pattern is inevitable.

These studies confirm that the proposed protective technique could be used effectively in the oil and gas industries to inhibit SSCC.

CONTENTS

Page.

LIST OF FIGURES

LIST OF TABLES

Page.

LIST OF PLATES

CHAPTER ONE

INTRODUCTION

CHAPTER 1.

INTRODUCTION.

The internal sour corrosion of hot risers carrying crude oil and gas mixtures from geological strata to production platforms and the pipelines carrying these products to refineries is one of the major problems faced by the petroleum industry throughout the world. This sour corrosion in steel can be represented by the anodic reaction:

$$Fe_{(substrate)} - 2e^- \rightarrow Fe^{a+}_{(aqueous)}$$

The conjugate cathodic reaction is either or both, of the following reactions:

$$2H_3O^+ + 2e^- \rightarrow 2H_2O + H_2$$

$$H_2S + 2e^- \rightarrow S^{a-} + H_2$$

These cathodic hydrogen evolution reactions proceed via the formation of H atoms, adsorbed on the steel surface, followed by desorption to form H_2 gas. In the presence of hydrogen sulphide much of the adsorbed atomic hydrogen enters the steel rather than bubbling off at the surface as molecular hydrogen. This atomic hydrogen in the steel has a serious deleterious effect on the physical properties of the steel. Hence, the steel can fail at stresses well below the yield stress and this phenomenon is designated as sulphide stress corrosion cracking, (SSCC).

At present, inhibitors and protective metallic or non-metallic coatings are used as protective measures to minimise the general corrosion, and hence reduce the SSCC, in industry. The addition of inhibitors is currently the most favoured method. However, inhibitors have to be added either continously or at specific time intervals and it is not certain whether they would be very effective in sour pipes since the inhibitors cannot completely stop the reaction between H_2S and

steel. Pores and cracks may develop in coatings over a period of time and severe localised attacks can result. Moreover, it is not possible to detect or repair immediately any defect of existing protective coatings. Hence, it is clear that the methods employed at present are not adequate for the prevention of SSCC. Therefore,extensive research has carried out in this field to find suitable methods to prevent SSCC in steels which are used in the petroleum industry. Through this research a novel method has been found.

The novel method is based on using an active hydrogen evolution sulphide electro-catalyst, more active than steel, as a coat on the steel surface, such that hydrogen evolution will take place on the catalyst surface, instead of on the corroding steel surface. Therefore the amount of atomic hydrogen diffusing through the steel is greatly reduced. Hence, SSCC in the steel is effectively inhibited. Although the proposed method appears to be straight forward there are a number of problems and doubts that need to be resolved. Hence, an extensive study was carried out from the electrochemical and mechanical points of view and this work is reported in detail in parts 1 and 2 of this thesis respectively.

A computer-aided literature survey on sulphide stress corrosion cracking and its prevention in oil- and gas- well equipment was carried out and is reported in Chapter 2. This literature survey greatly helps us understand the factors that control SSCC in steel and the prevention measures taken in the industry to combat it. Chapter 3 introduces the novel method and early work carried out on it. It also gives the problems and doubts that are to be resolved and the work to be carried out to evaluate the method. Chapter 4 describes hydrogen evolution studies carried out on three sulphide electro-catalysts $NiCo_2S_4$, MoS_2 and WS_2 and on EN 42 steel. Although the studies reported in Chapter 4 do not yield the selection of a sulphide catalyst for further studies it certainly provides an understanding of the fundamental characteristics of the hydrogen evolution reaction on the three sulphides and EN 42 steel. Chapter 5 serves as a key for the selection of a sulphide electro-catalyst to inhibit SSCC in steel. In this Chapter the corrosion rates of the steel and

sulphide-steel couples are evaluated by constructing Evans diagrams and hydrogen diffusion experiments, carried out to assess the effectiveness of the three sulphides are reported. Chapter 6 describes corrosion weight loss measurements carried out to gain information on the corrosion rate, nature of corrosion products, and the effect of the corrosion products on corrosion rate of the steel.

A literature survey on stress corrosion test methods and interpretation of test results is given in Chapter 8. This literature survey shows the advantages and disadvantages of the various stress corrosion test methods available at present; it also helps to select test methods and specimen types used throughout the mechanical studies reported in Part 2 of this thesis. Chapter 9 describes continuous slower straining/loading rate tests carried out on compact tension specimens. Also, it gives in detail all the preliminary studies carried out to select a suitable loading rate and the studies carried out on how and where to apply the protective coat on the compact tension specimens. The information on the kinetic parameters of SSCC, crack-growth-rate and time-to-failure, obtained from sustained load tests using compact tension specimens are given in Chapter 10. Chapter 11 describes tests carried out to evaluate the long-term sour corrosion effects on mechanical properties of steels protected with the MoS_2/FEP (fluoro-ethylene-polymer) coat. It gives the information on the changes of mechanical parameters such as stress intensity factor at failure, total fracture energy required for fracturing the specimen, average energy consumed for unit length of crack extension, crack opening displacement and impact fracture energy. Chapter 12 provides the information on the tests carried out to study the viability of the MoS_2/FEP coat to inhibit SSCC in actual environmental conditions where a cyclic loading pattern is inevitable.

Although the experimental studies presented in this thesis were carried out with a view of evaluating the proposed technique to inhibit SSCC in steel, they also provide a wider knowledge of the experimental techniques that could be used to study stress corrosion cracking in general. The mechanical tests developed, such as the slower straining/loading rate tests on pre-cracked compact tension specimens and the techniques employed in the sustained load tests and corrosion fatigue tests to measure growing crack length without interrupting the tests were fruitful outcomes of this study.

PART ONE

THE ELECTROCHEMICAL ASPECTS

CHAPTER TWO

LITERATURE SURVEY ON SULPHIDE STRESS CORROSION CRACKING AND ITS PREVENTION IN OIL- AND GAS-WELL EQUIPMENT

CHAPTER 2.

LITERATURE SURVEY ON SULPHIDE STRESS CORROSION CRACKING AND ITS PREVENTION IN OIL- AND GAS- WELL EQUIPMENT.

2.1 Search and Methodology

A computer literature search, using the facilities and expertise of the Information Science Section of The Middlesex Polytechnic Library was carried out. The following data bases were used; Compendex, Chemical Abstracts, U.S. Government Report, Metals and Technology Index. This search mainly covered a period of 15 years (1966-1981) and was complemented by additional manual search yielding over 400 references.

Most of the papers, especially those relating to actual experience in the field, are authored by scientists and engineers working in the U.S.A. This is due to the greater amount of experience accumulated by the Americans in the oil and gas industries over the last 50 years. This accumulated experience and experimental results may not be directly or entirely applicable to the North Sea oil and gas industries since composition of downwell fluids and gas respectively may be different.

2.2 Types of Corrosion of Oil- and Gas-Well Equipment.

For practical considerations, corrosion in oil- and gas-well production can be classified into three main types.

1. Sweet corrosion occurs as a result of the presence of carbon dioxide and fatty acids in the absence of oxygen and hydrogen sulphide. Carbon dioxide is noncorrosive in the absence of moisture, but when moisture is present, carbondioxide dissolves and forms carbonic acid. This carbonic acid causes a reduction in pH of the water which makes it

quite corrosive to steel. This sweet corrosion can occur in either oil or gas wells.

2. Sour corrosion is designated as corrosion in oil and gas wells producing even trace quantities of hydrogen sulphide. Although hydrogen sulphide is noncorrosive in the absence of moisture, if moisture is present the gas becomes corrosive. It becomes very severely corrosive where carbondioxide or oxygen are also present.

3. Oxygen corrosion occurs wherever equipment is exposed to atmospheric oxygen. It occurs most frequently in off shore installations, brine-handling and injection systems, and shallow producing wells where air is allowed to enter the annular space.

Sour corrosion is the only one dealt with further in this literature survey, since this research programme is confined to inhibition of sulphide stress corrosion cracking. Also it is beyond the scope of this thesis to cover in detail all the types of corrosion encountered in oil and gas-well equipment.

2.3 Sour Corrosion and its Effects

Sour corrosion is exhibited in a variety of corrosion forms, namely, general corrosion, pitting corrosion and corrosion-erosion. General corrosion resulting from chemical attack usually occurs on that part of pipe well which is alternatively wet and dry when ratio of water to oil in the flowlines is considerably higher. Pitting corrosion results from a chemical attack at low points where fluids settle and accumulate in the piping systems. Corrosion-erosion results from impingement of fluids and corrosion substance on the pipe surface at high flow velocity.

The general mechanism of sour corrosion can be simply, though not completely stated[1] chemically as follows:

H_2S	+	Fe	+	H_2O	→	FeS_x	+	2H
Hydrogen Sulphide		Iron		Water		Iron Sulphide		Hydrogen

Another reaction which occurs with hydrogen sulphide corrosion is that the hydrogen released in the foregoing reaction enters into the steel where it can alloy with the steel to embrittle it, or form molecular hydrogen which leads to the formation of blisters and cracks well below the working stresses. This phenomenon is termed as sulphide stress corrosion cracking (SSCC).

The degree of SSCC attack varies since the mechanism of the sour corrosion is dependent on a number of parameters, such as pH, the concentration of chloride ion, oxygen, carbon dioxide and hydrogen sulphide in the solution, the ratio of water to hydrocarbon content, composition of the steel, microstructure, cold work, temperature, pressure and the flow of solution, etc.[1-7] Figure 2.1[8] shows the various factors affecting the sulphide stress corrosion cracking. These factors are critically reviewed in the following sections.

2.4 Electrochemical Variables.

2.4.1. Hydrogen Evolution on Steel Surface and Diffusion of Atomic Hydrogen.

The corrosion of steel[9] can be simply represented by the anodic reaction;

$$Fe_{(sub)} - 2e^- \rightarrow Fe^{2+}(aq) \quad \ldots\ldots\ldots\ldots\ldots (A)$$

The conjugate cathodic reaction can be;

$$2H_3O^+ + 2e^- \rightarrow 2H_2O + H_2 \quad \ldots\ldots\ldots\ldots\ldots (B)$$

$$O_2 + 2H_2O + 4e^- \rightarrow 4OH^- \quad \ldots\ldots\ldots\ldots\ldots (C)$$

$$H_2S + 2e^- \rightarrow S^{2-} + H_2 \quad \ldots\ldots\ldots\ldots\ldots (D)$$

The nature of the cathodic reactions depends on the corrosion medium, pH of the solution and the local conditions of the environment. In the case of oil and gas pipe lines, the cathodic reaction process is likely to be (B) and (D).

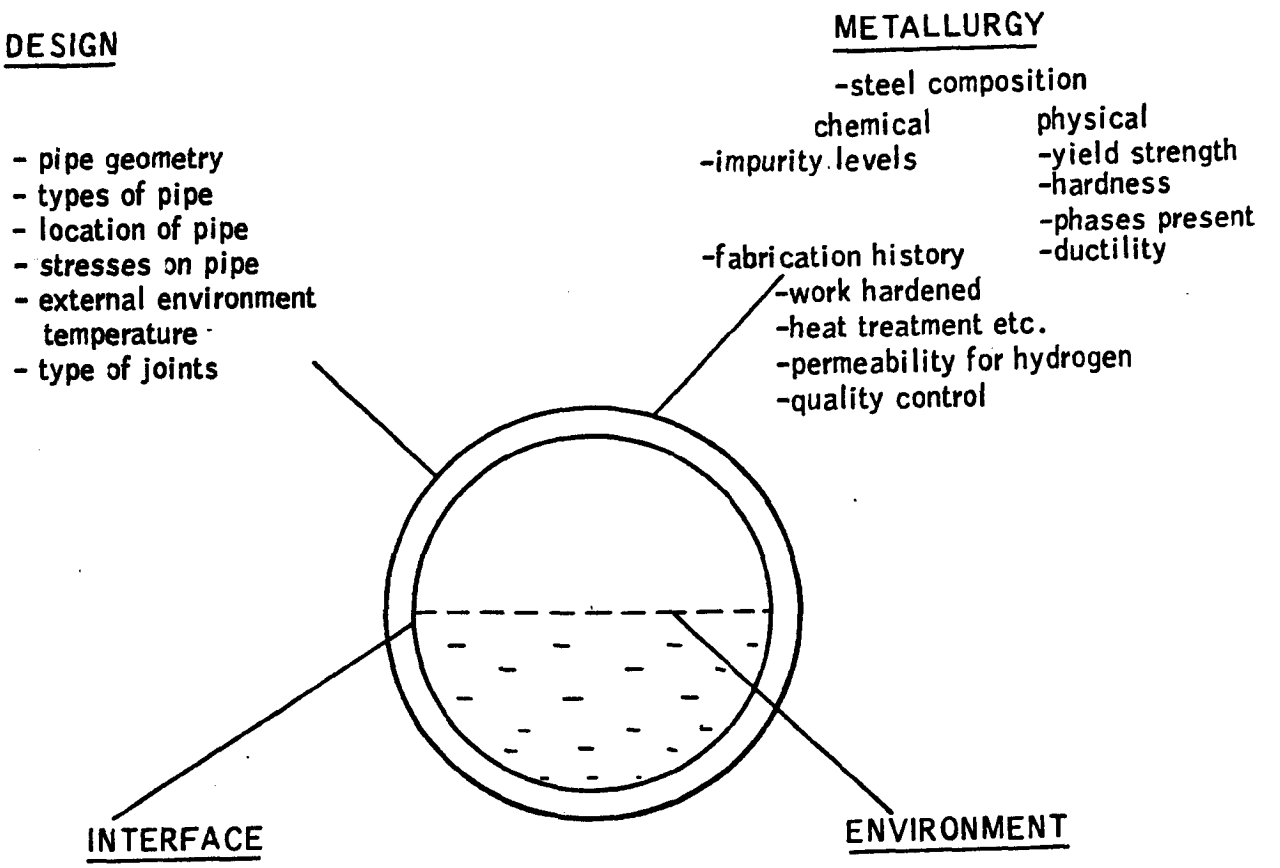

Figure 2.1. Factors which affect the sulphide stress corrosion cracking of steels,[8].

In practice, the cathodic hydrogen evolution reaction proceeds via the formation of H atoms, adsorbed on the steel surface, followed by desorption to form H_2 gas[10,11]. Some of the adsorbed H atoms diffuse into the bulk of the steel:

$$Fe - H_{ads} \underset{K_{b \to s}}{\overset{K_{s \to b}}{\rightleftharpoons}} Fe - H_{abs} \quad \ldots\ldots\ldots\ldots\ldots\ldots (E)$$

Where $K_{s \to b}$ is the rate constant for surface to bulk reaction and $K_{b \to s}$ is the rate constant for bulk to surface reaction.

If void sites are present in the metal, e.g. in iron, other equilibrium reactions to be considered are;

$$Fe - H_{ads.ext.} \rightleftharpoons Fe - H_{interstitial} \rightleftharpoons Fe - H_{void\ surface} = \tfrac{1}{2}H_{2\,in\ void.}$$

The formation of hydrogen gas inside the voids in steel would set up high internal pressures, leading to blisters and weakening of the metallic structure. The rate of hydrogen dissolution in steel is known to be influenced by the composition, structural defects such as interstitial sites, grain boundaries, and dislocations, which provide hydrogen diffusion paths in steel[12]. These structural defects are enlarged in size or number by the presence of residual or applied tensile stress. These lead to enhanced hydrogen diffusion into steel, resulting in hydrogen embrittlement and sulphide stress corrosion cracking[13].

Research studies have shown that the rate at which steels absorb hydrogen from the environment has an important effect on their sensitivity to Hydrogen Stress Cracking in the environment. As the severity of the hydrogen charging conditions decreased, the time for failure increased at a given applied stress.

Beck et al[14] investigated the effect of H_2S, CN^-, NO_2^- and OH^- on the hydrogen permeation rate in steel. They showed that hydrogen dissolution and subsequent diffusion increased in the order of $OH^- < NO_2^- < CN^- < H_2S$ in steel. On the basis of these results, Kabozer and

Montblannova[15] suggested that H_{ads} recombination reaction is the rate determination step. They suggested that the adsorbtion of anions leads to the lowering of M-H_{ads} bond. However, since there is no significant change in activation energy for M-H_{ads} in these environments, Bockris et.al[10] and Glass et.al[14] hold the view that the chemisorbed anion on the iron surface decreases the recombination rate of hydrogen atoms. This would then lead to a higher concentration of H_{ads} and hence higher hydrogen permeation rate.

2.4.2. Thermodynamics of Sour Corrosion System.

Pourbaix and his co-workers[16,17] have calculated the phases at equilibrium for M/H_2O systems at 25° C from the chemical potentials of the species involved in the equilibria, and have expressed the data in the form of equilibrium diagrams having pH Vs E, the equilibrium potential (Vs S.H.E.) as ordinates. These diagrams provide a thermodynamic basis for the study of corrosion reactions, although, as emphasised by Pourbaix, their limitations in relation to the practical problems must be appreciated.

Figure 2.2 gives a potential/pH equilibrium diagram construced for the ternary system Fe-S-H_2O by Horvath et.al[77]. The diagram is based on the general formulae developed by Pourbaix and his collaborators. When this system was compared to the Fe-H_2O system they noted that the stability zones of FeS and FeS_2 correspond with the incomplete passivation of iron. It is also noted that although FeS and FeS_2 have stable domains (at certain potential and pH values) according to the E-pH diagrams, but this does not necessarily mean that films are continuous and protective. Horvath concluded that in acidic and neutral pH ranges the sulphide ions are effective anodic simulators for iron and steel. They suggested that iron can be protected in an H_2S aqueous environment by raising the iron potential into the passive region where the sulfide ions are unstable. This could be achieved either by applying an external electro motive force (E.M.F.) or by the addition of an oxidising agent capable of raising the iron potential above the sulphide-oxide transormation level, e.g. by Chromates.

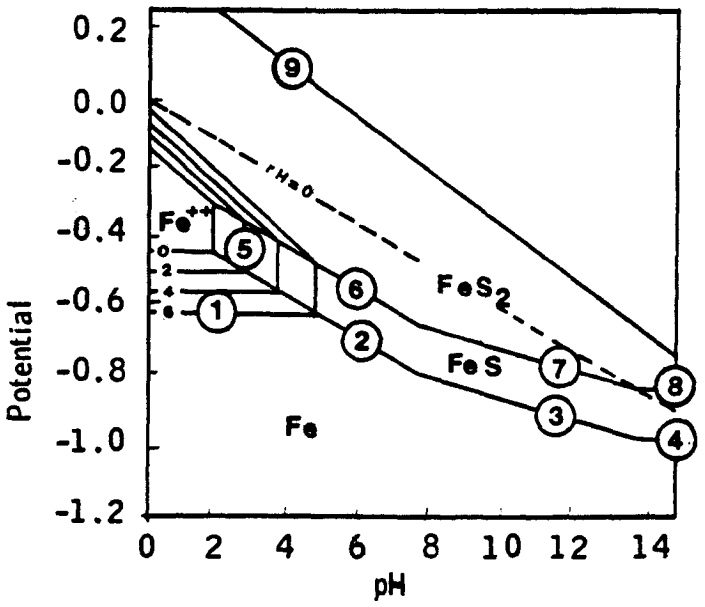

Fig.2.2. Potential - pH equilibrium diagram of the ternary system Fe-S-H_2O,(77).

French[18] has summarised the stability domains for various sulphide species (HS^-, H_2S and S^{2-}) at different pH values. The bisulphide ion (HS^-) is not present in appreciable concentrations until pH = 5. The H_2S and HS^- concentrations are approximately equal at pH = 6.8. The H_2S concentration is nil above pH = 8 and the sulphide ion (S^{2-}) is not present until pH = 13. French concludes that H^+ ions are the cathodic depolarisers at pH < 5 whilst between pH8 and 13, the HS^- is the cathodic depolarizer.

2.4.3. Effect of Applied Potential.

The work done by McIntyre on precracked specimens[19] shows (Fig.2.3) that the rate of stress corrosion crack growth in sodium chloride solution is significantly influenced by applied polarization, being greatest with cathodic polarization and least with anodic polarization. This observation supports the early work done by Brown[20] on pre-cracked specimens. Also it is consistent with a stress corrosion mechanism which is principally associated with the uptake of hydrogen by the test piece since cathodic polarization favours the evolution of hydrogen at the steel

surface. Conversely, anodic polarization would suppress the availability of hydrogen at the crack tip, thus promoting an overall reduction in crack growth rate.

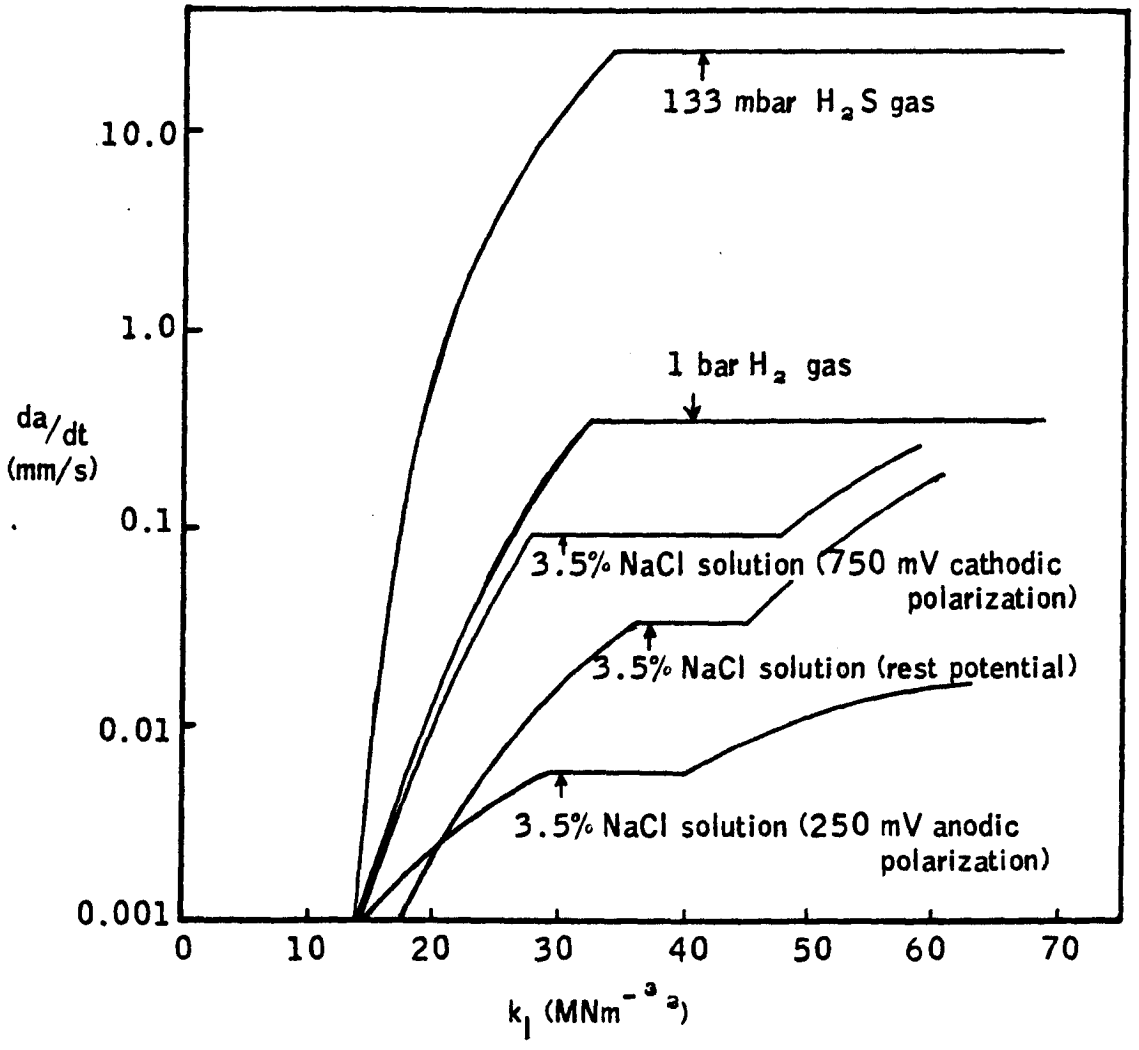

Fig.2.3 The influence of applied polarization on crack growth rate as a function of stress intensity,[19]

The dependence of crack growth rate on polarization is not, however, consistent with the dependence of time to failure on polarization, as shown in Figure 2.4[19].. This indicates a reduction in time to failure on anodic as well as on cathodic polarization of the test piece for tests conducted at stress intensity levels just above the threshold value. The implication of this behaviour is that at such stress intensity levels a considerable proportion of the overall time to failure is associated with

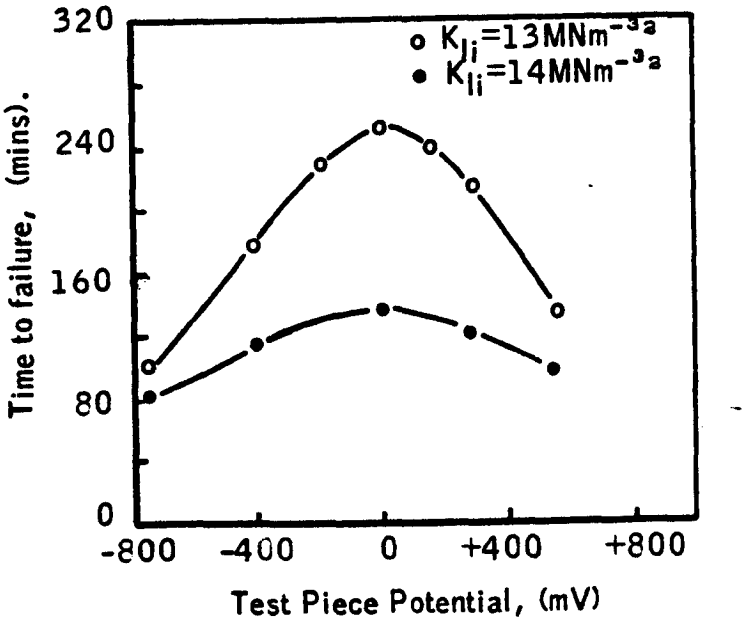

Fig.2.4 Influence of applied polariation on time to failure,[19].

crack initiation rather than with crack propagation and that the application of anodic polarization facilitates crack initiation although it retards propagation. The overall effect is thus a reduction in the total time to failure. Townsend[21] reported that on bent smooth wire specimens the time to failure was increased greatly by anodic polarization, while cathodic polarization was reduced, in 3.0% sodium chloride and 0.5% acetic acid aquous solution saturated with H_2S at room temperature (figure 2.5).

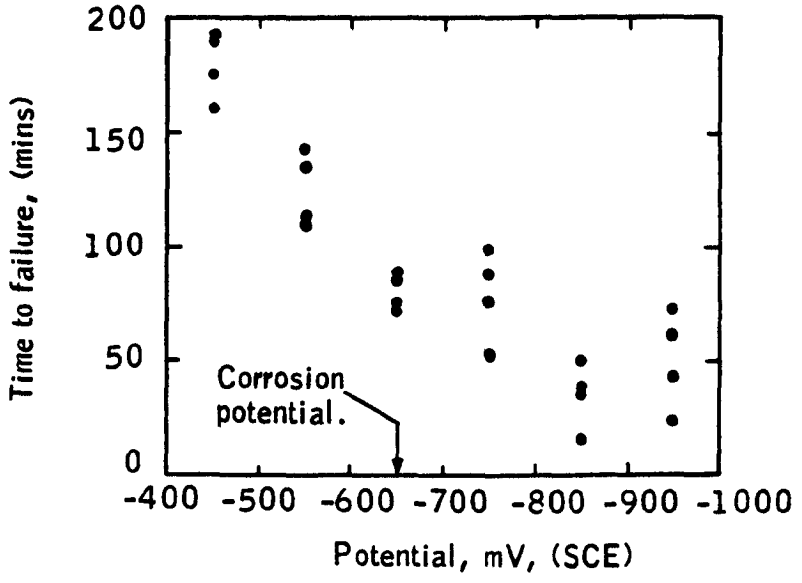

Fig.2.5. Time to failure of bent wire specimens as a function of applied potential at room temperature in H_2S solutions,[21].

The effect of electrochemical potential on delayed failure and hydrogen permeation for AISI 4340 and HP 9-4-45 Steels was studied by Barth, et al[22]. Failure times for both steels were decreased by cathodic polarization. The steels had an approximate tensile stress of 1680 N/mm². The steels were tested as 0.762 mm foils, stressed to 345 N/mm². Figure 2.6 shows the effects of applied potential on hydrogen permeation and delayed failure times. For the case of HP 9-4-45 steel the decrease in failure time by anodic polarization was accompanied by pitting corrosion. The occurrence of pitting is expected[23] to produce similar electrochemical conditions, at the base of the pit, as those found at stress corrosion crack tips[24].

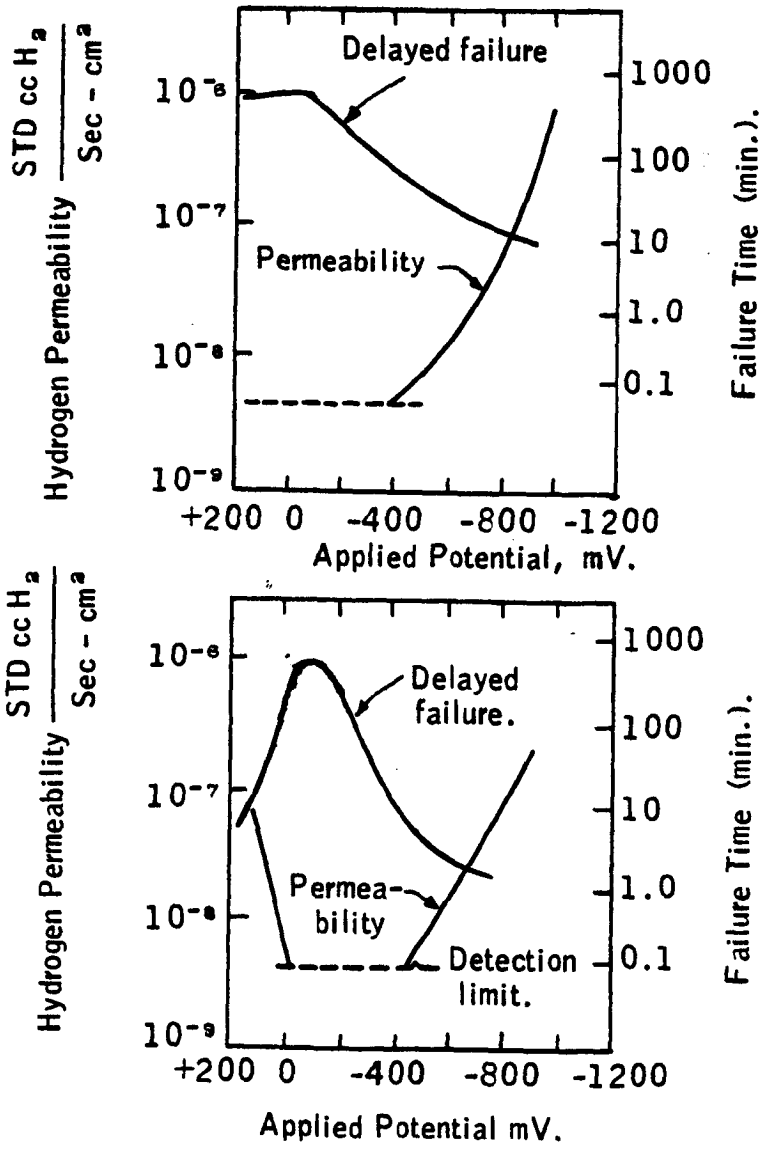

Fig.2.6. Effect of applied potential on delayed failure and hydrogen permeation rate for stressed foils (50 kpsi) of AISI 4340 and HP 9-4-45 steels in 3.0 N NaCl solution,[22].

2.5 Environmental Variables.

2.5.1. Hydrogen Sulphide Concentration.

As might be expected, work done by several investigators [2,25-27] shows that the tendency to sulphide stress corrosion cracking increases with increasing concentration of H_2S. Field experience has shown definite embrittlement problems with conventional oil field tubular steels of 550 N/mm² and higher yield stresses when exposed to natural gas containing 0.01 atm (34 ppm) partial pressure hydrogen sulphide[25]. Also failure have been reported for 9% chromium steel tubing, with a yield stress of approximately 894 N/mm², in wells where the partial pressure of hydrogen sulphide was not known exactly, but was considered to be significantly below 0.01 atm (34 ppm)[26]. Hudgins et al[26] also studied the effect of hydrogen sulphide concentration on SSCC, employing a steel which had a hardness value of HRC 21. Their experimental results show (figure 2.7) that only a 1 ppm H_2S concentration in 5% NaCl solution is effective enough to produce a SSCC failure in the steel. In support of this, Hudson, et al[27] found that hydrogen absorption was

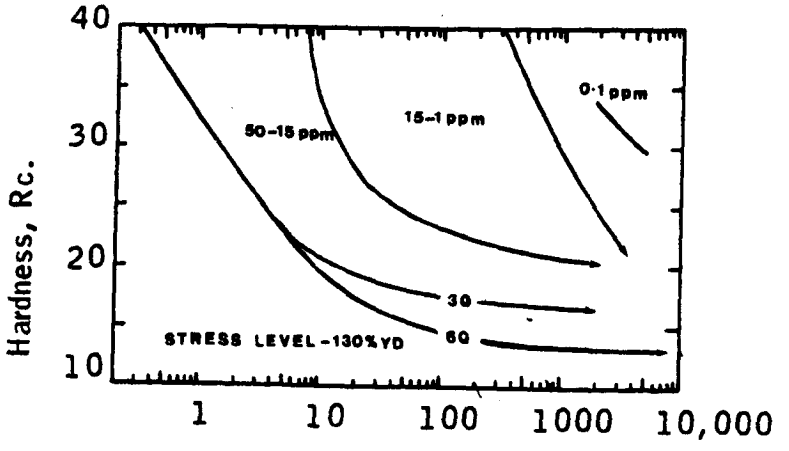

Fig.2.7. Approximate correlation of failure time to hardness in 5% NaCl containing various concentrations of H_2S,[26].

increased significantly by as little as 0.01 ppm. sulphide presence (as Na_2S) and considerably by only 0.36 ppm. sulphide in tests where the absorption of hydrogen by steel studied under cathodic protection. Treseder and Swanson[2] found cracking of API P-110 and 9 Ni steels in a 0.001 atms. hydrogen sulphide partial pressure (3 ppm), 0.5% acetic acid solution and stated that this partial pressure was their criterion for defining a sour environment. Greco and Brickell[28] studied hydrogen permeation rates in AISI 1020 steel as a function of H_2S concentration and found that 0.5 percent partial pressure of hydrogen sulphide produced significant amount of hydrogen permeation in the steel. Also they found that higher concentrations produced more hydrogen permeation. In another study Greco, et al[29] concluded that the lowest level of hydrogen sulphide concentrations that produced embrittlement was a partial pressure of 0.02 atm (68 ppm) as evidenced by blister formation in the steel.

The conclusion from the above is that for high strength steels of major interest to the oil industry (i.e. steels with yield stresses of 80,000 - 130,000 psi (550 - 895 N/mm^2)) the embrittlement problem exists until the hydrogen sulphide concentration falls below some value in the range of 0.0001 - 0.001 atm. partial pressure (0.34 - 3.4 ppm).

2.5.2. Variation in pH.

Many investigators[2,30,31] have studied the effect of pH on cracking of steels and found a correlation between decreased pH (increased acidity) and increased tendency to sulphide stress corrosion cracking. For example, according to Treseder and Swanson[2], remarkable increases in cracking suceptibility are obtained by decreasing pH from 5 to 3 (Fig. 2.8). The same trend is reported (Fig.2.9) i.e., susceptibility to SSCC increased when pH decreased from 8 to 3, by Dvoracek[30].

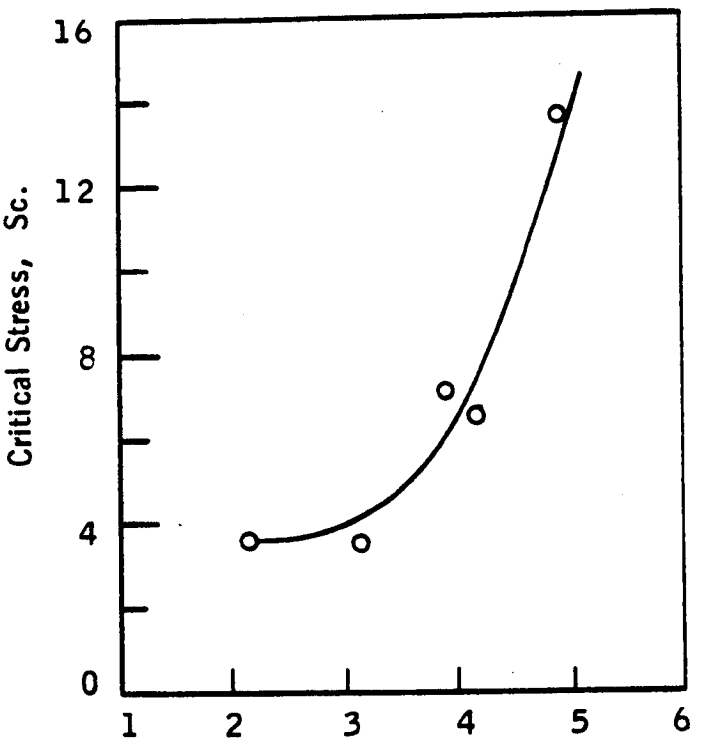

Fig.2.8. Effect of pH on sulphide stress cracking for p-110 casing samples. Acetic acid-sodium acetate buffer used to obtain indicated pH in saturated H_2S solution,[2].

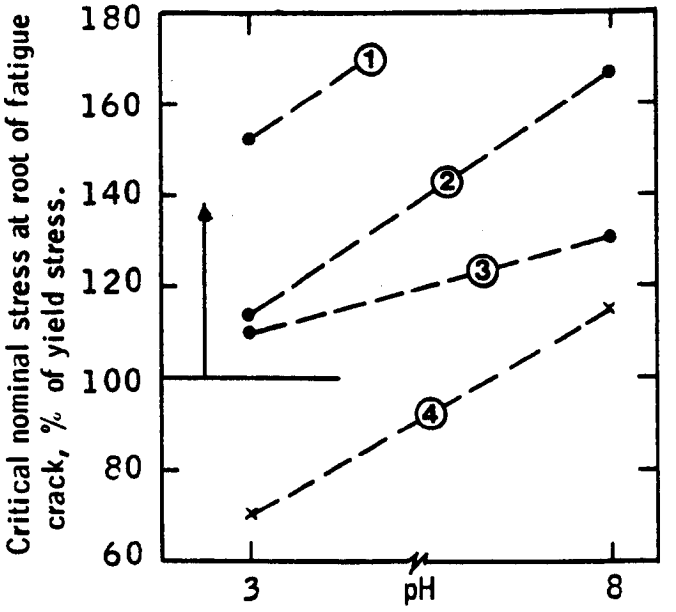

Fig.2.9. Effect of H_2S and pH on sulphide stress cracking of casing. (1) 25 ppm, (2) 150 ppm, (3) 300ppm, (4) 2800 ppm H_2S,[30].

Hudgins[31] has reported on the effect of pH over the range 1 to 10 and finds a similar general trend to that reported above, with the exception that he found the cracking tendency to be independent of pH in the range 2 to 5 (Fig. 2.10). Dvoracek concluded that embrittlement would not be a

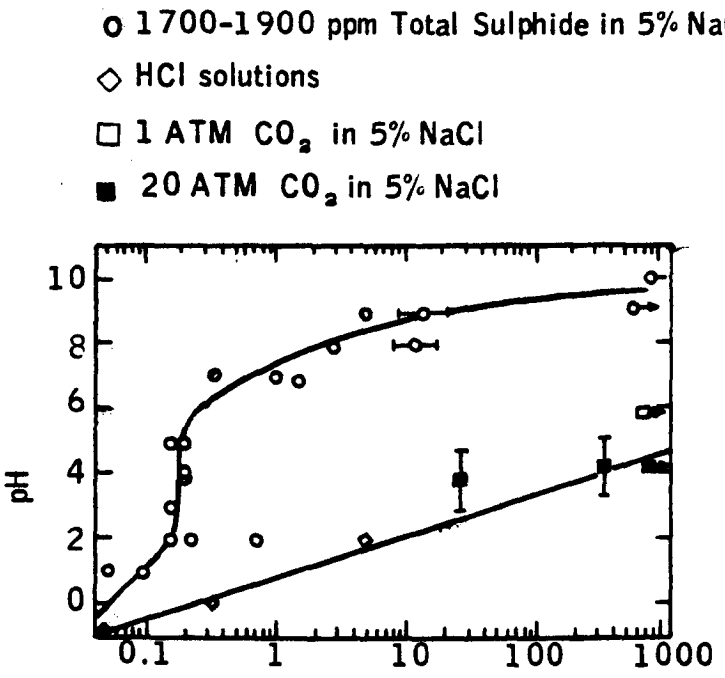

Fig.2.10. Effects of solution pH and H_2S additions on failure of unnotched high strength steel specimens in 5% NaCl solution. All the notched-ring specimens RC 33±1 and stressed to 115% YD.[31].

problem with a 132,000 psi (910 N/mm²) yield stress steel at pH 8. This marked effect of increasing pH on reducing embrittlement effects is in agreement with service experience[4]. Presumably the effect results from the reduction of corrosion with increasing pH and the corresponding reduction of hydrogen entry into the steel.

This does not imply that there is no embrittlement problem in alkaline sulphide systems. Work done by Skei, et al[32] on the hydrogen blistering problem showed that hydrogen entry into steels could occur in certain alkaline sulphide solutions, but that it was reduced markedly by the presence of oxidizing agents such as air. Many laboratory embrittlement tests are subject to sufficient air contamination to have a possible

inhibiting effect on the corrosion reactions leading to hydrogen entry into the steel. This could lead to an erroneous conclusion in tests designed to simulate a field condition where oxygen contamination is not possible.

2.5.3. Chloride Concentration.

Treseder, et al[2] and Dvoracek[30] have studied the effect of chloride ion concentration on sulphide stress corrosion cracking and hydrogen embrittlement. They have concluded that the presence of several percent sodium chloride in hydrogen sulphide solution has no significant effect on embrittlement of low alloy steels, but may increase the severity of the environment for those alloys for which chloride ion has a strong adverse effect on passivity e.g. 12% Chromium Steels.

2.5.4. Micro-Organisms

It has been shown by various investigators[33-35] that micro-organisms can greatly affect corrosion rates. In order for micro-organisms to accelerate corrosion, the environment must be suitable for their growth and multiplication. Moisture, essential minerals, organic matter, an energy source, and a suitable pH must be provided. In many cases, when steel structures are in contact with the earth or water, all the necessary requirements are met.

Micro-organisms such as the Desulfocibrio (sulphate reducing bacteria) can cause sulphide corrosion, hence, sulphide stress corrosion cracking, in the absence of atmospheric oxygen (anaerobic conditions)[25]. These organisms utilize hydrogen formed by electrochemical corrosion during their growth and reduce sulphate (SO_4) to sulphide (H_2S). Both hydrogen utilization and H_2S formation cause increased sour corrosion rates and are therefore of great concern.

2.5.5. Temperature Variation.

Possible beneficial effects of elevated temperature in reducing SSCC and hydrogen embrittlement have recently received attention[36]. It is generally agreed that SSCC and HE effects in steels will be most severe at room temperature, and less severe at higher and lower temperatures. Townsend[37] studied the temperature effect with high strength carbon steel wire (yield stress, 212,000 psi (1470 N/mm^2)) and found a maximum susceptibility to cracking at 77^0 F (25^0 C)(Fig.2.11). The

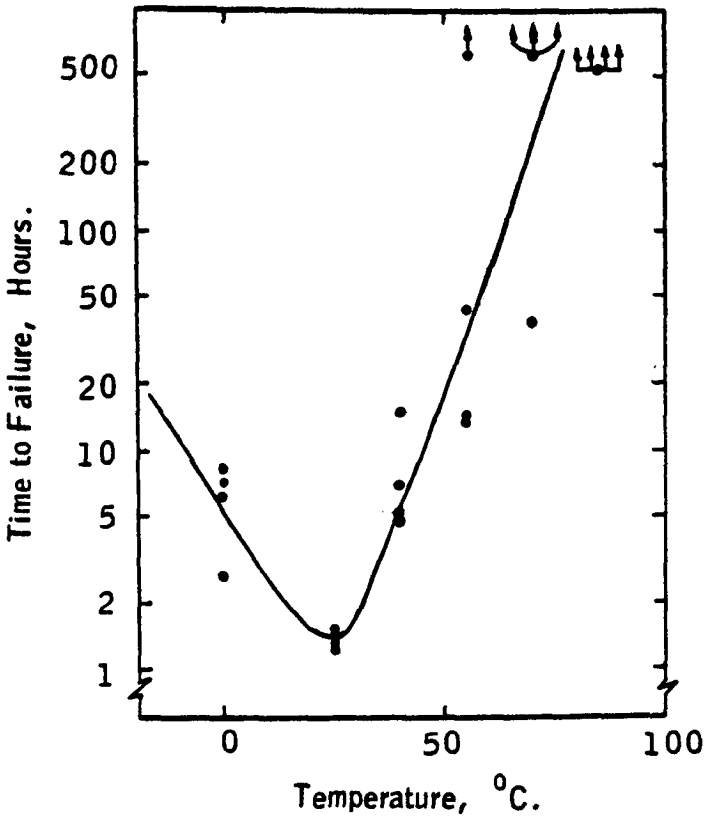

Fig.2.11. Effect of temperature on sulphide stress cracking of 212 kpsi yield strength wire line steel. Three percent NaCl, 0.5% acetic acid, H_2S saturated solution,[37].

cracking tendency was slightly reduced at temperatures near the freezing point but considerably reduced at temperatures in the vicinity of 175^0 F (80^0 C); many of the specimens were not cracked at the expiration of the test period. Greer[38] used notched C-ring specimens in a NACE solution (5% sodium chloride + 0.5% acetic acid solution saturated with hydrogen sulphide) and concluded that above 150^0 F (65^0 C) API Grade

P-110 steel could be considered equivalent to lower strength steels, which are considered satisfactory for sour gas service at 75° F (24° C). Similar results have been obtained when Dvoracek[30] performed a few comparative sulphide stress corrosion cracking test at room temperature and at 300° F (149° C).

Comparable data also have been reported for other embirttling systems. Greer, et al[39] observed that tendency for cracking of high strength steels in 15% hydrochloric acid decreased with increasing temperature; failure of a 165,000 psi (1138 N/mm²) yield stress steel was not observed above 150° F (65° C) and a 190,000 psi (1310 N/mm²) yield stress level above 300° F (149° C).

As discussed above the beneficial effect of increased temperature is of considerable engineering importance. That the effect is observed in systems where the hydrogen is introduced by any of the three common methods, corrosion, cathodic charging, and exposure to hydrogen gas, indicates that the temperature effect is related to effects within the steel rather than to a surface corrosion reaction effect. Any mechanism proposed for sulphide stress corrosion cracking must also provide an explanation for this pronounced temperature effect.

2.5.6. Sulphide Film:

In practice it has been found that the iron sulphide film formed, due to the reaction of H_2S with steel in aqueous media, tends to cause localized attack since the film is more cathodic to the steel, i.e., pitting corrosion results[8]. Ideally, however if the iron sulphide film is continuous and adherent, the corrosion rate would be reduced, but in practice the film will be affected by other parameters namely sulphide concentration, pH, CO_2, oxygen etc.

Shannon and Boggs[40] observed the formation of protective, hard and adherent FeS scale at sulphide concentrations above 515 ppm in an oil-

brine-H_2S system, whilst at a lower concentration the FeS film was non-protective, gelatinous and non-adherent. Ewing[41] and Sardisco, et al[42] have reported that the composition and protectiveness of the iron sulphide scale was affected by the initial pH of the systems: the least protective, predominantly mackinawite scale was formed preferentially when the initial pH was between 6.5 and 8.8, a more protective pyrrhotite-pyrite scale forming outside this pH range[42].

The presence of CO_2 and H_2O in the system tends to make the environment very corrosive. The CO_2 dissolves in water to form carbonic acid and thus causing a reduction in pH.

$$CO_2 + H_2O \rightarrow H_2CO_3$$

$$Fe + H_2CO_3 \rightarrow FeCO_3 + H_2$$

The carbonic acid also makes the FeS film on the surface very unstable[43].

The iron sulphide film is formed when iron corrodes in the presence of H_2S and therefore the corrosion rate is determined by either the exchange rates at the Metal/film or film/solution interface or by transfer rates in the film. However,it has been found[52] that sulphide corrosion is extremely sensitive to the presence of minute quantities of oxygen. The corrosion rate in the presence of H_2S at pH 4.2 with the exclusion of oxygen shows a parabolic decrease in corrosion rate as the film thickness increases.

2.6 Mechanical and Metallurgical Variables.

2.6.1. Microstructure and Heat-Treatment.

It has been reported by many investigators that the microstructure has a considerable effect on sulphide stress corrosion cracking and hydrogen embrittlement. There is general agreement that untempered martensite

promotes sulphide stress corrosion cracking and environmental embrittlement[44-46]. This appears to be in large part due to the brittle nature of the martensite plates[44]. Specifically, it has been suggested that the high elastic stresses associated with plate formation are the major factor in embrittlement, since it was found that high residual stresses promote hydrogen-induced cracking even in the absence of martensite[26]. Such a conclusion would be in agreement with results on Trip steels in hydrogen[47,48]. Diffusion does not seem important since hydrogen diffuses more slowly in untempered than in tempered martensite[38].

At high strength levels, it appears that the best environmental resistance, for hydrogen blistering or cracking, occurs in well-tempered martensite or bainite microstructures[49]. Snape[44] has claimed that a double temper technique designed to transform any retained austenite to martensite can produce exceptional resistance to sulphide stress corrosion cracking. Medium and low strength levels are somewhat more difficult to assess, but such assessment is important because of the widespread use of steels in this range. A specific difficulty is that grain size and composition effects can modify the ranking of microstructures[50]. With these constraints in mind, however, it may be possible to list the microstructures from best to poorest environmental performance. The order would be as follows[51]; quenched and tempered bainite or martensite is best, followed by a spheroidized structure of uniformly dispersed carbides, with fine carbides being prefered to coarse ones, a normalized structure is poorest, although exceptions can be found, particularly for spheroidal and pearlitic structures.

2.6.2. Chemical Composition of Steels.

Composition and residuals of a steel normally dominate its mechanical properties. The mechanical properties are improved or changed as required by control or elimination of certain elements. This tends to be the case for hydrogen embrittlement and sulphide stress corrosion cracking as well. Normally the elements in an alloy steel classified into two categories, interstitial elements and substitutional elements. It may be

easier to look separately at its effects on SSCC.

2.6.2.1. Interstitial Elements:

The important interstitial elements in steel are carbon and nitrogen, and their behaviour seems generally predictable. An increase of the carbon concentration in structural steel leads to larger internal stresses during quenching due to the formation of martensite[7]. Snape[44], and Masamiti, et al[54] have shown that with increasing carbon concentrations in the steel the susceptibility to hydrogen embrittlement increase in media containing hydrogen sulphide. However, according to Masamiti, et al[54] an increase of the carbon concentrations from 0.15% to 0.30% in quenched and tempered steels alloyed with 1% Mn has no effect on susceptibility to SSCC. Snape has studied the effect of carbon on susceptibility to SSCC in structural steel alloyed with 2.0% Cr, 0.3% Al, and 0.2 Mo at two different concentration levels (0.04 and 0.13% C). The steel with 0.04% C was tested after quenching and tempering, and the steel with 0.13% C after normalization and tempering to equal strength (UTS 795 N/mm^2). The results show that raising the carbon concentration lowers resistance to SSCC. In similar steels heat treated to equal strength the failure stress decreases from 590 to 345 N/mm^2 under the same experimental conditions when the carbon concentration is raised from 0.04 to 0.45%. It should be noted, however, that the effect of carbon on the susceptibility of steels to SSCC may be affected greatly by differences in microstructure. Obviously, the effect of carbon on SSCC is best determined with steels having an identical structure. Apparently the negative effect of carbon on the resistance of steel to SSCC is due to the formation of carbide phase, whose boundary with the matrix may serve as a collector for hydrogen and thus for nucleation of cracks.

2.6.2.2. Substitutional Elements.

The common substitutional additions to steels are chromium, manganese, silicon, nickel and molybdenum. Elements of lesser importance are vanadium aluminium, titanium and cobalt.

Raising the concentration of chromium from 1% to 3.85% in structural steels has been shown to decrease the diffusivity of hydrogen and to increase the SSCC resistance of the steel[7]. These effects of chromium are due to the fact that chromium is a carbide former and imparts high strength levels while increasing the tempering temperature.

Since manganese is a strong anstenite former, it is normally expected that manganese will show a negative resistance to sulphide stress corrosion cracking and hydrogen embrittlement[53]. Vereshchagin, et al[55] study on quenched and tempered steels of 16 GS and 10G2S types shows that the resistance to SSCC and HE decreases when manganese concentration is raised from 0.8% to 1.6%. The detrimental effects of increasing manganese concentration on SSCC were studied by Ward, et al[53] who reported that when manganese concentration increased from 0.5 to 2.0 percent level the sulphide stress corrosion cracking resistance decreased by 40 percent. Manganese levels below 0.40% are not practical as manganese is required to tie up sulfur in order to prevent hot shortness during blooming and rolling.

There have been few studies of the effect of nickel on hydrogen embrittlement and sulphide stress corrosion cracking and there is no agreement concerning its effect in steel intended for operation in hydrogen-containing media[7]. Snape[44] reported that raising the nickel concentration to 2.92% in steels within the range of 824 to 1510 N/mm^2 ultimate tensile stress has almost no effect on resistance to SSCC. However, with increasing strength the resistance to SSCC decreases. Waid, et al[53] have studied the effect of nickel on AISI 4340 type steels to SSCC resistance. Their results show that nickel contents up to about 1.0 percent have no effect on SSCC resistance. Also they have shown that

above 1.0 percent nickel content could cause a detrimental effect on resistance to sulphide stress corrosion cracking.

Grobner, et al[56] found in a study of the effect of Molybdenum on the properties of quenched and tempered steel (yield stress 824 N/mm²) that raising the molybdenum concentration from 0.25 to 1.0 percent has a favourable effect on resistance to SSCC. Waid, et al[53] also reported that molybdenum improves SSCC resistance for medium carbon alloy steels (0.30% C, 2.00% Cr, 0.20% V) heat treated to a yield stress of 827 N/mm². In a particular experimental condition, failure stress increases about 20 percent with an increase in molybdenum content from 0.25% to 0.62%. A further increase in molybdenum content to 0.87% produced a decrease in SSCC resistance of the steel, indicating the optimum level to be in the range of 0.60 to 0.70 percent.

Waid, et al[53] published results, in a study of the effect of vanadium on medium carbon alloy steels (0.20% C, 2.00% Cr, 0.80% Mo) at a yield stress level of 760 N/mm², showing that increasing vanadium concentration from 0 to 0.2 percent increased the sulphide stress corrosion cracking resistance of the steels. At higher vanadium levels, i.e. above 0.2 percent, no additional improvement in SSCC was observed. The beneficial effect of vanadium is thought to result from its role as a carbide former which, therefore, allows the use of higher tempering temperatures to reach a given strength level.

2.6.3. Cold Work (Plastic Deformation)

It is generally agreed that cold working (plastic deformation) has an adverse effect on resistance to hydrogen embrittlement and sulphide stress corrosion cracking. When steel is bent or straightened cold (below about 1000° F; 538° C), hardness can increase and residual stresses up to the yield stress of the metal may be present. It is very difficult to predict the magnitude and direction of these residual stresses which may be additive to service or applied stresses[36]. The NACE publication on Sulphide Cracking Resistance Materials[57] recommends that,

subsequent to any cold deformation, the part should be heat-treated at 1150° F (621° C) minimum to a hardness of HRC 22 maximum. Baldy[58] demonstrated that an N80 steel subjected to a 1% cold work (about the same as in cold straightening a tube) lowered its sulphide environment load carrying capacity from 483 - 517 N/mm² to 310 - 345 N/mm². An 1150° F (621° C) temper subsequent to cold working, is recommended by NACE publication[57], increased its capacity to the 448 - 552 N/mm² range.

Treseder and Swanson[2] studied the effects of cold work up to 30% reduction in area and found a marked reduction in critical stress values at 10% reduction. API grades J-55 and X-52 also poor SSCC performance after cold work even though hardness was below HRC 22.

2.6.4. Hardness (Strength Level):

In the early days of the sulphide stress corrosion cracking problem when it became apparent that the susceptibility to cracking increased with increasing strength of the steel. Steels were categorised as being resistant to cracking in sulphide systems if their hardness were below HRC 20 and with experience this was soon raised to HRC 22 (approximate tensile stress of 775 N/mm² or less)[57]. Hardness was selected because it was a convenient and nondestructive way of measuring strength. However, it became apparent that such a simplified approach was inadequate to meet the engineering demands for materials that were in the strength range approaching or exceeding this critical hardness value.

Tresder and Swanson[2], found that three classes of steel did not qualify as resistant to sulphide stress corrosion cracking in their laboratory tests even though their hardness was comparatively low. Bates[59] also reported a sulphide stress corrosion cracking failure of steel with a yield

stress of only 365 N/mm². Hill, et al[60] found that hardness was not consistently related to resistance to sulphide stress corrosion cracking and in fact demonstrated susceptibility to cracking in a steel with a hardness of only HRC 15. They concluded that specification of a hardness or strength level will not necessarily assure good resistance to attack by aqueous hydrogen sulphide. It was also shown that all the factors that dictate the metallurgical properties of a steel could have an influence on its resistance. Therefore it became necessary to define such steels in terms of composition, heat treatment, and mechanical working.

Current practice within the energy industry is to accept steels as being resistant to cracking in sulphide service if they meet the requirements set forth in NACE Publication IF166[57]. In this standard acceptable steels are defined in terms of their API, ASTM, or AISI specifications with an over-riding requirement of a maximum hardness of Rockwell C22. There is some interest in modifying this approach so that steels would be qualified on the basis of a performance test. Progress in this direction awaits adoption of the standardised laboratory acceptance test mentioned above. In the meantime individual laboratory acceptance tests are used to evaluate new materials.

2.7 Sour Corrosion Control.

2.7.1. Design and Operating Techniques.

Design and operating techniques can be used to restrict sour corrosion in two ways. The original design can be chosen: 1, to reduce the severity of corrosion; and 2, to allow mitigation procedures to be easily applied if corrosion appears in a well. Selection of tubing to reduce corrosion caused by high flow rates, designing the christmas tree and surface flow lines to reduce turbulence, and designing rod strings are all applications of this principle. Also it should be emphasised that in flow lines, the velocities

should be kept high enough to prevent buildup of scale. All blind ends or obstructions which could serve as traps for scale should be eliminated. In gas lines, all low spots should be equipped with adequate means for removing any water which might collect. In oil wells sometimes the water-oil ratio can be reduced by squeezing off water bearing formations. Poor or questionable operating techniques can be the difference between success or failure of a mitigation program.

An important consideration in the selection of the piping configuration is the required operating flexibility of the gathering system. The operating pressure for the gathering system should be selected on the basis of projected production and pressure decline data and delivery pressure to the field treating plant. Also this type of information would help to design or install required equipment, which could operate well within its physical limits, and generally increase its life many-fold.

There are a number of standards developed over the years to help engineers in designing offshore pipelines and installations in view of reducing adverse effect of corrosion. Particularly the National Association of Corrosion Engineers Standard RP-06-75[61] gives guide-lines to accommodate following installations to facilitate pipeline internal corrosion control programs.

1. Access and related fittings adaptable to use of internal monitoring equipment.
2. The installation of identifiable markers to serve as location check points during internal monitoring evaluation.
3. Access fittings for the insertion of corrosion coupons.
4. Fittings to permit injection of chemical inhibitors.
5. Storage space for inhibitor containers.
6. Dehydration facilities.
7. Pigging facilities. etc.

2.7.2. Inhibition.

2.7.2.1. Inhibitors.

Probably the most widely used method of controlling sulphide corrosion in oil and gas production equipment is by chemical inhibition. Since corrosion is a surface reaction, any modification of the steel-environment interface will affect the rate of corrosion. Certain chemicals which, when added to a corrosive system, modify this interface to reduce the corrosion rate, are called inhibitors.

Corrosion inhibitors are usually selected on the basis of solubility or dispersibility in the fluids which are to be inhibited. Selection of a corrosion inhibitor for use in a pipeline carrying crude oil and water is very important. The corrosion inhibitor selected can be either oil soluble, oil soluble-water dispersible, or water soluble.

Selection of an oil soluble corrosion inhibitor for use in pipelines designed to transport crude oil is, frequently, made simply because crude oil is in the pipeline[62]. While this is a logical premise, it may prove to be a costly procedure at some later date. For instance, most pipelines and flowlines carrying small volumes of water and large quantities of oil fail from corrosion on the bottom portion of the pipe rather than top. Usually, the upper portion of the pipe is found to be well protected against corrosion. There is evidence that the oil soluble inhibitor is protecting the portion of the pipe occupied by the crude oil emulsion.

Use of an oil soluble-water dispersible corrosion inhibitor is widespread in systems handling both oil and water. This type of inhibitor may do a good job protecting oil wells, gas wells, or small diameter flowlines due to high velocity and/or turbulent flow that promotes mixing of the inhibitor and produced fluids. However, it may not provide the desired protection in larger flowlines or pipelines carrying these same fluids due to reduction in velocity and/or turbulence. Hence, the fluids must have an optimum velocity for the inhibitor to be effective.

Water soluble corrosion inhibitors are also widely used in the oil field, especially in waterfloods and salt water disposal systems. Due to the relative short film life of water soluble corrosion inhibitors, they are continuously injected as opposed to the batch treatment method. One might assume a water soluble inhibitor is the answer to treating a pipeline carrying crude oil and water, because water on the bottom of the pipe is the primary source of the corrosion problem. However, another problem must be considered. The portion of pipe occupied by the oil and water emulsion is also a corrosive environment. Under such a condition, a water soluble inhibitor would probably not provide adequate protection. However, there is laboratory evidence that a portion of some water soluble inhibitors is absorbed into the oil, which could provide some protection in the oil phase.

2.7.2.2. Requirements for Inhibitors:

Gatlin[63] summarised the characteristics of inhibitors that are required for wet, sour gas transmission systems, particularly for the Hudson's Bay Oil and Gas Kaybob system in Alberta, Canada, (17.5% H_2S and 3.5% CO_2), to be;

1. Soluble and dispersible in both brine and fresh waters.
2. Negligible partioning into a condensate phase.
3. Non-emulsifying in either condensate or waters.
4. Effective in removing and preventing iron sulphide deposition.
5. At least 90% effective in inhibiting uniform corrosion.
6. Effective in preventing pitting and blistering.
7. Effective at an economical injection rate.

Dijk and Capelle[64] state that the secondary requirements which have to be fulfilled by corrosion inhibitors are;

1. No foaming.

2. Separation of inhibitors must be easy.

3. No damage to the environment.

4. Compatibility with the system.

5. Stability over a wide temperature range.

Gatlin states that the pipe walls are continuously water wet at a high gas velocities (7.6 m/s; 25 ft/s and up) and at liquid-to-gas ratios of 34 ± 28 L/km^3 (6 ± 5 btls/MMSCF). At high liquid-to-gas ratios the spray flow consists of an annular ring of liquid with a core of gas. At even higher liquid-to-gas ratios, the water present having a lower velocity, the flow becomes stratified with the accumulation of water in low spots.

For inhibitors to be effective, they must reach the corrosive areas and because the presence of water plays an essential role during corrosion it is for this reason that water dispersible and water soluble inhibitors have shown improved inhibitions[18]. However, it has been found by Hausler, et al[78], that iron sulphide is hydrocarbon wettable and provided the hydrocarbon contains some water to solvate the exchanged ion, the organic water-insoluble inhibitor can easily be adsorbed on the sulphide scale.

2.7.2.3. Inhibitors in Practice.

The first specific sulphide oil-field inhibitor was formaldehyde and was introduced in 1944[1]. This compound formed a sulphide-iron-formaldehyde film on the surface of the metal which was effective in reducing the corrosion rate. In the Groningen gas field[65] an oil soluble/water dispersible inhibitor was mixed with condensate and added to the production stream. This inhibitor has been found to be successful from the corrosion control point of view. It was added in batches every fortnight for well-bore tubing and continuously for the flow lines and surface equipment. An increase in production and hence

an increase in gas velocities over 11-13 m/s had been found to be deleterious for the inhibitor film formed on the tubes. This was overcome by incorporating a continuous feed of the inhibitor through the injection hole so that any removal of inhibitor from the surface would be immediately replaced by a fresh supply of inhibitor. This system ensures that the corrosion is controlled and allows a maximum flow rate of 15-17 m/s.

Lyle, et al[66], found that an addition of ethylamine plus amine phosphate (USA manufacturer) in environments of low and high sulphur gave a low corrosion rate. Oxygen present in the solution was found to increase the amount of inhibitor required to achieve the low corrosion rate.

Bregman[67] summarised the inhibitors used in the petrolium industry. For pipeline applications, Bregman divided the inhibitors in use to water-soluble and oil-soluble inhibitors. Water soluble inhibitors are mainly inorganic, e.g., sodium nitrite and sodium chromate and function by maintaining a protective film. Where water is a minor phase, it is necessary to inject sufficient inhibitor to give a 2 percent concentration in water samples withdrawn from downstream water dropouts.

2.7.2.4. Mechanism of Sour Corrosion Inhibition.

Hausler et al[52] have studied the mechanism of hydrogen sulphide corrosion inhibition and reported that organic water-insoluble inhibitors are more effective than water-soluble ones. This is because the iron sulphide is hydrocarbon wettable. Provided the hydrocarbon contains some water to solvate the exchanged ion, the inhibitor can easily be adsorbed on the sulphide scale. The organic nature of the inhibitor helps to exclude water from the scale surface and thus reduces the rate of the interfacial exchange even more. The reduction in corrosion reaction is dependent upon the concentration of the inhibitor.

The protective iron sulphide film being very thin and of constant thickness, little corrosion is needed to push inhibitor, once adsorbed, into a nonprotective scale layer. The adsorption being rapid but quite irreversible, the inhibitor then becomes inactive. This means that inhibitor transport to the corroding surface has to be at least as fast as its consumption at the surface. This transport rate may not be a problem in systems where the hydrocarbon-to-water ratio is much larger than one, but in systems where there is much more water than hydrocarbon, abnormally high inhibitor concentrations may become necessary in order to keep the inhibitor transfer rates sufficiently rapid.

Hackl et al[68] studied the mechanism of the action of amine-type inhibitors in the presence of hydrogen sulphide. The efficiency of inhibitors was determined by cathodic and anodic galvanostatic polarization in a deaerated 3 percent Na_2SO_4 solution at pH = 1. They concluded that the "active" hydrogen associated with the N atom of the inhibitors has no decisive role in the presence of hydrogen sulphide and that the inhibiting effect of sulphur-containing organic compounds is associated with the pre-adsorption of the HS^- ions which are formed during the reduction of these compounds.

2.7.3. Protection with Coatings.

Internal coating of pipelines provides a physical barrier between the steel and the corrosive substances being transported and is being considered as an internal corrosion measure. It also ensures[69] the characteristics such as, product purity, prevents contamination from corrosive products, reduces maintenance and labour costs, provides protection of the pipe interior against the accumulation of deposits, and improves the flow rate due to the reduction of friction.

The NACE standard RP-06-75[61], the recommended practice of control of corrosion on offshore steel pipelines, states the main requirements of coatings to be;

1. Ease of application.

2. Ease of repair.

3. Good adhesion to pipe surface.

4. Ability to resist environments to which the coating will be exposed.

5. Ability to resist damage due to handling, storage, and installation.

6. Ability to resist cracking.

7. Resistance to disbondment.

The NACE standard also gives numerous references to specific coating standards.

An approach which is gaining acceptance in the oil and gas industry is the use of epoxy coatings[71]. The first epoxy internal coating of a natural gas line was applied in March, 1953[69]. A thin film of 1.5-3 mils (37-75 microns) was made by spraying on the cleaned surface of a 20 inch diameter pipeline. Periodic checks were subsequently made on this line for five years, but these were discontinued as no performance failure was observed. Practical tests and experience have shown that application of such a film results in the following savings for gas line service[69];

1. Increase in throughput of 5-8%: the increase will be maintained for many years. However, there is a substantial margin, since it is generally considered that even a 1% improvement in throughput justifies internal coating.

2. Pipe length protected prior to laying : there is no corrosion which would impair the smoothness, and create product contamination.

3. Easier and faster cleaning of the transmission line after laying, and more rapid drying after hydrostatic testing.

4. Reduction in paraffin and other deposition which lower gas flow.

5. Reduced pumping costs, which are maintained in service.

6. Reduced maintenance because frequency of cleaning is substantially reduced.

7. Product purity; there is no contamination from corrosion product which might block, or damage appliances.

8. Aids pipe inspection because the light-reflecting internal coating shows up lamination and other pipe defects.

Apart from the liquid spraying method using solvents, dry powdered thermosetting epoxy coatings, cured in situ (200 - 250 microns thick) have been developed since the early sixties[70]. The advantages of the powder coating may be briefly summarised as follows;

1. No solvent - (a) no solvent carrier wastage, (b) no solvent fire hazards, thus reduced precautions; (c) no atmospheric pollution, (d) health hazards reduced, (e) no possibility of retained solvent impairing film properties (coatings have lower porosity), (f) less air changes required in work area.

2. One coat; high build, uniform application, particularly by electrostatic spraying.

3. Approaching 100% effective use of the powder coating can be attained. It is essential to use a powder recovery unit (re-using overspray powder): 98% - 99% effective powder utilisation is possible.

4. Sagging, bridging, poor coverage at edges and other surface defects liable to occur with solvent-bearing paints do not arise.

5. Economic advantages such as savings in finishing operations and one-coat operation.

6. None, or minimal, damage of epoxy powder coated articles during subsequent rough handling or transport.

Signal Oil, and Gas Co.[72], reported the successful in-situ coating and operation of a 24 mile long, 12 inch diameter, offshore gathering pipeline for sour crude oil. This coating was selected for other applications, e.g. SLAM operation, on the basis of a proven background and successful record.

A more recent development is the use of glass flake reinforced plastics[73]. The plastic is a combination of C-glass particles, three to four microns thick. The selected plastic coating meet the anti-corrosion and mechanical requirements of the petroleum industry. This system has improved the abrasion and erosion resistance of the coating and also reduced the permeability of the coating since a lining may have as many as 300 overlapping flakes in a 2 mm thick lining, thus making it difficult for vapour or liquid to penetrate. An additional feature of this type of coating is its ability to closely match the coefficient of expansion of steel and this avoids thermal stresses and ensures good adhesion to the steel surface (up to 170° C).

2.7.4. Development of New Materials.

From experience it became apparent that the most effective method for control of SSCC and hydrogen embrittlement would be development of more hydrogen sulphide resistant materials[74]. The first development of an H_2S - resistant steel resulted in the recommendation of a maximum hardness of 22 HRC and 775 N/mm² maximum yield stress material. In 1963, NACE published "Tentative NACE Specification 60, Tubular Goods", and API published "Tentative API Specification 5AC Casing and Tubing". These specifications required a restricted yield stress of 517 to 620 N/mm²; a 655 N/mm² minimum ultimate tensile stress, restricted chemical composition; a specific heat treatment of normalize and temper with minimum time and temperature, no cold working other than normal straightening and no cold die stamping.

Also, in the early 1960's a quenching and tempering heat treatment of seamless pipe was used to achieve high physical properties. At the time the NACE and API specifications were written it was general practice to

use pipes at the 550 N/mm² yield strength by the normalizing heat treatment, which these specifications required. When quenching and tempering became widely accepted, the API included it as an acceptable heat treatment for grade C-75 in 1965.

Domestically produced quenched and tempered grade modified N-80 appeared on the market in 1971 and met all requirements of API standard -5AC. This grade N-80, a carbon-manganese fully killed steel, used to ensure sufficient hardenability to obtain a fully martensitic structure and uniformity of properties. Due to large tonnages of this grade being used, modified N-80 was revised and incorporated into API standard -5AC in April 1975 as grade L-80[74].

With grade L-80 in general use, the next immediate goal of this industry was for a yet higher strength material that offered at least the same SSCC resistance. Trials involving the use of boron-treated 4130, vanadium-treated 4130, and regular 4130 grade steels using only an external quench system were conducted, but the desired properties were never attained. Numerous other elements and combinations were tried but finally it was realized that to produce the heavy walls needed for a 90,000 psi (620 N/mm²) minimum yield stress casing (C-90) and to meet the demanding physical requirements, an internal-external quench system was necessary. The internal-external quench system has proven highly successful on casing and coupling stock with wall thickness up to 1.5 inch. A modified AISI 4130 steel is now used for this grade which is marketed by Republic Steel Corp., Ohio, as RS-90 and first introduced in 1976. The grade has a yield stress of 90,000 to 105,000 psi (620 to 725 N/mm²) and minimum ultimate tensile stress of 105,000 psi (725 N/mm²).

Geological formations now being explored require drilling depths below 20,000 ft with bottom hole pressures and temperatures greater than 24,000 psi (165 N/mm²) and 500° F[79] respectively. Material requirements for these deeper, sour wells challenged the capabilities of materials being used[79]. To develop a casing steel for this need,

various alloying elements were systematically investigated over a seven-year period to determine their influence on sulphide stress corrosion cracking resistance[74]. Most of the alloys studied in this investigation were of the medium carbon Cr-Mo type, and in most cases these alloys were quenched and tempered to yield strengths in the range of 110,000 to 120,000 psi (760 to 830 N/mm^2).

As a result of these evaluations, the experimental alloy steel RS-115 (now being patented by Republic Steel Corp.) developed. It exhibits excellent sulphide stress cracking resistance at yield strength levels in the range of 110,000 to 130,000 psi (760 to 900 N/mm^2). The newly developed RS-115 has much greater temper resistance compared to API L-80 and C-90 casing steels. When RS-115 is heat-treated to the same yield stress levels of L-80 and C-90, it has SSCC resistance 50% greater than API L-80 and 25% greater than C-90. With SSCC resistance equivalent to either of the two grades, the new steel had yield strength 25% to 35% higher.

The new steel is not expected to replace grades L-80 and C-90 for applications where these grades are use-and cost-effective. Enlargement of the "family" of SSCC-resistant steels is expected to give oil and gas producers a broader choice of materials, especially for drilling and completing at depths below 20,000 ft, (6,100 m).

2.8 Corrosion Monitoring.

Corrosion monitoring has received great emphasis in the petroleum industry. The main aims of corrosion monitoring may be classified as follows;

1. to determine whether corrosive conditions exist in the system,
2. to determine and predict corrosion rates,
3. to evaluate the effectiveness of various corrosion control procedures,
4. to optimize corrosion control procedures,
5. to monitor the continuity of effective corrosion control.

A number of tests have been devised to measure and assess the amount of corrosion that has occurred in a particular system. The tests can be classified under three headings;

(a) inspection of structures,
(b) intermittent testings,
(c) cumulative testings.

Inspection of structures includes, visual inspection, equipment failure-records, nondestructive testing, internal caliper survey, ultrasonic testing, internal wall thickness logs etc. The best method to determine the extent and severity of corrosion is use of equipment-failure records. These records are very helpful in determining not only the amount but the cost of corrosion, both before and after treatment. Typical nondestructive testing can include X-ray studies of failed equipment. This is very valuable for critical, high pressure service equipment such as christmas trees and valves[75]. However, it is not likely that X-rays of each piece of equipment can be obtained and certainly, the full length of a high pressure flow line is not likely to be X-rayed. Ultrasonic testing with various instruments is limited largely to surface facilities and it is necessary to make many readings because the searching probe can "see" so little of the surface area involved. Ultrasonic studies and surveys are of value when many spot tests are made frequently.

Internal caliper survey is widely used in the petrolium industry and is a direct measurement of the damage that has caused in the pipelines and casings by corrosion. The tool consists of a number of peripheral feelers which bear against the inner surface of the pipe. The feelers actuate a stylus that records the greatest pit depth at the location of the feelers. The possibility of the feelers missing some pits or only partly entering other pits must be considered. The use of caliper surveys in coated tubing is considered as a poor practice. The feelers are hard metal and bear against the pipe with considerable force. Damage to the coating usually occurs at the end of the joint as the feelers spring out into the collar.

Intermittent testing includes testing of corrosivity of the environment by sampling and analysis of stream, iron content analysis, residual inhibitor analysis, electrical resistance probes, and polarization resistance probes. There are a number of factors that should be considered when using iron content and stream sample analysis to predict corrosion rate. The iron content of water from a gas-condensate well has more significance than the iron content of water from an oil well. Though the iron content of gas-condensate waters varies widely, as a survey gave an average of 310 ppm (parts per million) for corrosive wells and 125 ppm for noncorrosive wells[1], in practice, many corrosive wells have as little as 100 ppm iron. It has been possible to reduce the iron content of corrosive wells to as low as 10 to 25 ppm by effective inhibition. The iron content of corrosive wells may range from 5 ppm up to several hundred parts per million where large concentrations of iron are present in formation water.

Electrical resistance probes provide the added benefit of permitting the monitoring of the progress of corrosion on a day to day basis[75]. Such probes are usually installed in a system for several months and may be more representative of what is occurring in the system than most corroding specimens, frequently replaced on a regularly scheduled basis, perhaps once a month. The electrical resistance probes are subject to damage from flowing conditions, i.e., high velocity or abrasion.

Polarization resistance probes measurements are quite satisfactory as long as there is complete coverage of the electrodes in an aqueous or conductive environment. In this type of probe measurement the error can be quite pronounced, if the surface area of metal that is used to correlate corrosion rates, is exposed partially to hydrocarbon or other nonconductive media.

Cumulative testing includes testing of the corrosivity of the environment by using corrosion coupons, hydrogen probes and removable test pools. The corrosion test coupon is a tool used to evaluate the corrosion rate. The coupon is a small specimen, usually low-carbon steel, which is exposed to the well fluids for 2- to 4-week periods. The loss in weight is used as a measure of corrosion and is reported as "mils per year" (mpy) penetration.

This method of evaluation assumes that the corrosion is uniform which may not be true because the loss in weight may be caused by pitting. One obvious limitation of coupons is that they indicate the corrosion only at the point of exposure. Scale and paraffin depositions on the coupon can produce erroneous indications. These factors should be considered when evaluating a coupon survey.

Hydrogen probes are useful, especially in high pressure gas condensate wells where gas, condensate and water are present at high velocities and under high pressure. The probe has got an advantage that it can give a day-to-day reading to indicate the fluctuation in corrosion. The measurement of hydrogen diffused in steel is important for sour corrosion system since dissolved hydrogen is the major cause for sulphide stress corrosion cracking and hydrogen embrittlement. The methods employed in the measurement of absorbed hydrogen[76] are usually based on vacuum ion gauges and on electrochemical cells. The electrochemical cell is based on the Devanathan and Stachurski[11] technique on measuring absorbed hydrogen.

CHAPTER THREE

A NOVEL METHOD FOR INHIBITION OF SULPHIDE STRESS CORROSION CRACKING IN STEEL

CHAPTER 3.

A NOVEL METHOD FOR INHIBITION OF SULPHIDE STRESS CORROSION CRACKING IN STEEL.

3.1 Introduction

Sour corrosion and consequently, sulphide stress corrosion cracking, is one of the major concerns of the petroleum industry. There are three conditions that must be satisfied in order for sulphide stress corrosion cracking (SSCC) to occur. These conditions, which are interdependent, are[6],

(a) The steel must be above a particular strength level where it is susceptible to sulphide stress corrosion cracking.

(b) The steel has to be subjected to a sustained tensile stress above some value that is dependent upon the strength level and the hydrogen content.

(c) The steel must contain atomic hydrogen that is free to diffuse either along a concentration or stress gradient. (The hydrogen content required to initiate cracks generally appears to be inversely related to the strength level and the applied stress).

Elimination or reduction of one of the three conditions could provide a path for prevention of sulphide stress corrosion cracking. In practice the energy industry cannot tolerate any reduction in ultimate tensile stress of the steel, (condition a), or the applied stress, (condition b), as the trend for deeper and higher pressure wells continues. Hence, control of the amount of atomic hydrogen formed and absorbed on the steel surface that diffuses through (condition c), is the only possible way left to reduce or prevent the SSCC. This way of approach is already being employed in the form of coating steel pipelines with various types of material and by addition of inhibitors into pipelines, where normal corrosion of substrate steel, is reduced; hence a reduction in the amount of atomic hydrogen formed is achieved. Also a number of new alloys and various heat treatment conditions have been developed to combat sulphide stress corrosion cracking. With changing chemical composition of the alloys the same principle, i.e., reduction in atomic hydrogen formed and diffused through is achieved by producing more corrosion

resistance alloys and by the resistriction of the hydrogen diffusion path with suitable metallurgical structure.

Metallic or non-metallic coatings have the disadvantage that over a period of time, because pores and cracks develop and severe localized attacks result. Development of new alloys and various metallurgical treatments encounter a difficult task in that the possible combinations of chemical elements and heat-treatments are running-out. Also the development of new alloys could not be phased in with the increasing demands. At present, the most favoured protection method is the addition of inhibitors.. Inhibitors have to be added either continuously or at specific time intervals and it is not certain whether they would be very effective in sour pipes, since the inhibitors cannot completely stop the reaction between hydrogen sulphide and steel[8]. Therefore, there is a need to devise a more efficient and reliable method for preventing sulphide stress corrosion cracking.

3.2 A Novel Method.

It has been discussed in detail in the literature survey, that when steel is corroded in the absence of oxygen, the conjugate cathodic reaction would be hydrogen evolution and could be written as:

$$H_3O^+ (aq.) + e^- \rightarrow H_2O (aq.) + H_{(ads)} \quad \ldots\ldots\ldots (2.1)$$

$$H_{(ads)} + H_{(ads)} \rightarrow H_2 (gas) \quad \ldots\ldots\ldots (2.2)$$

When H_2S is present in the environment (sour environment), it will react with steel to form iron sulphides. On such surfaces in the sour environment, reaction (2.2) is the rate determining step[14] and this in turn leads to the diffusion of hydrogen atoms into the steel, leading to hydrogen embrittlement and sulphide stress corrosion cracking.

One novel approach to the problem is to coat the steel surface with an active hydrogen evolution electro-catalyst, such that the hydrogen evoluation will take place on the active catalyst surface, instead of on the corroding steel surface. This ensures that the concentration of H atoms on the steel surface is reduced to a minimum, thus, the amount of atomic hydrogen absorbed on the steel surface

for diffusion is greatly reduced. The significance of the use of more active hydrogen evolution sulphide-electro-catalysts, ($NiCo_2S_4$, FeS) is that these catalysts have lower hydrogen evolution overpotential [8,80] and can operate in both sour (corrosion due to the presence of H_2S) and sweet (corrosion due to the presence of CO_2 and H_2O) corrosion environments without being poisoned, since these catalyst preparations involve a reaction between base metals and hydrogen sulphide.

3.3 Previous Work on the Method.

The effectiveness of a sulphide electro-catalyst, $NiCo_2S_4$, for hydrogen evolution has been studied at The City University, London [81,82]. This catalyst gave a performance of 1.0 A/cm² current density in 5N KOH, 70° C at a potential -150 mV vs RHE (reversible hydrogen electrode) stable for over 3000 hours comparable to the performance of platinum black [83]. Furthermore this catalyst gave a hydrogen evolution performance of 250 mA/cm² at -50 mV vs RHE under chlor-alkali conditions, i.e., 17 percent NaCl solution at 75° C. However, the performance of steel cathodes under similar condition is lower, 250 mA/cm² at -300 mV vs RHE [84]. Onuchukwa [80] used $NiCo_2S_4$ catalyst to carry out the initial work on the proposed method. The $NiCo_2S_4$ catalyst was prepared by reacting freeze - dried $NiCo_2O_4$ with H_2S at 300° C for 8 hours. The sulphide-catalyst was then mixed with ICI GP1 Teflon dispersion in the ratio of 10:3. The mixture was painted onto 100 mesh nickel screen, followed by curing at 300° C for 1 hour to form a Teflon-bonded electrode. Hydrogen evolution studies were carried out on the $NiCo_2S_4$ electrode and on EN 42 steel in 3.5 percent NaCl solution, both in the absence and presence of H_2S. The results showed (Figure 3.1) that in both cases, $NiCo_2S_4$ was more active than EN 42 steel for the hydrogen evolution reaction. Therefore it has been concluded that if a $NiCo_2S_4$ electrode is electrically connected to an EN 42 steel electrode, it would act as the hydrogen evolution cathode and protect the steel against any hydrogen attack. This was confirmed by hydrogen diffusion measurements through EN 42 steel foil, using the bielectrode membrane technique, originally devised by Devanathan and Starchuski [11]. Figure 3.2 shows the effect of connecting the Teflon-bonded $NiCo_2S_4$ electrode to the steel

Figure 3.1. Hydrogen evolution current-potential curves on $NiCo_2S_4$ and EN 42 steel in the presence and absence of H_2S in 3.5% sodium chloride solution at 25° C.

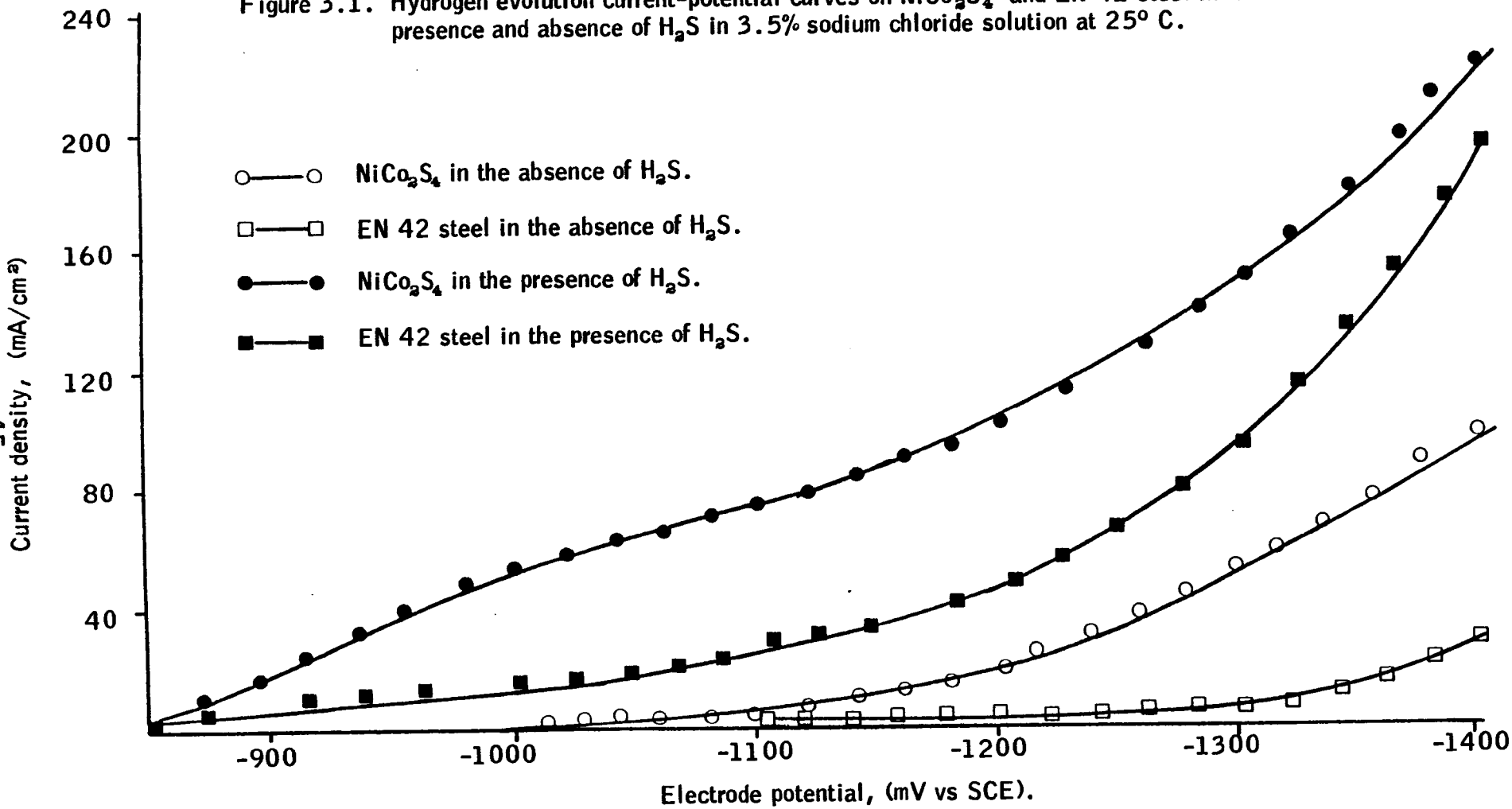

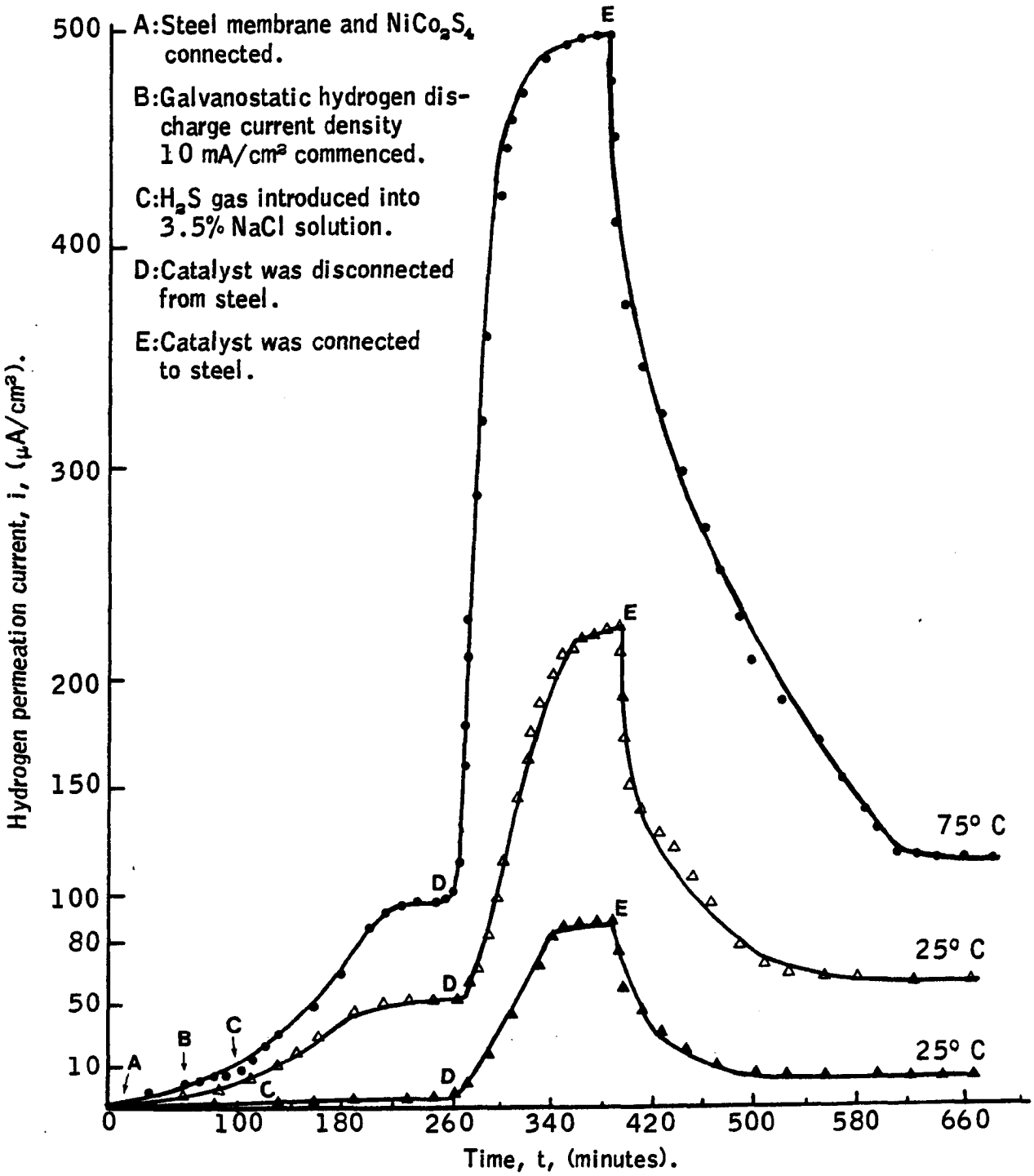

Figure 3.2. Effect of connecting a Teflon bonded $NiCo_2S_4$ electrode on the hydrogen permeation current through a EN 42 steel membrane in 3.5% NaCl solution.

membrane on the hydrogen permeation current in the presence and absence of H_2S. This shows that there was very little hydrogen diffusion current monitered while the $NiCo_2S_4$ electrode remains connected to the steel membrane, particularly at 25° C. On disconnecting the electrode from the steel membrane, the hydrogen permeation current increases significantly. There after, on re-connection, the hydrogen permeation current decreases back to the original level.

Russ[8] carried out further studies on the proposed novel method and employed a technique similar to that of Onuchukwa. He also reported the same trend of results, i.e., when a $NiCo_2S_4$ electrode was connected to a steel membrane, the hydrogen diffusion current was reduced, although the experimental conditions differed from those of Onuchukwa.

While carrying out hydrogen diffusion experiments, Russ[8] noticed that the $NiCo_2S_4$ electrode disintegrated with time. In addition, the solution around the vicinity of the electrode was found to become olive green in colour, and dark coloured particles were visible in the solution. Such phenomena have not been observed in electrodes coated on 100 mesh nickel screens. There are two possible explanations;

(a) In the case where 100 mesh nickel screen was used, the GP 1 - catalyst coating can wrap around each individual wire, thus imparting a greater adhesion.

(b) Another possibility is the corrosion of $NiCo_2S_4$ under those experimental conditions.

The corrosion of $NiCo_2S_4$ under these experimental conditions was investigated by the author[85]. In his experimental set up, Russ had the $NiCo_2S_4$ electrode very close to the platinum anode, (1-2 cm separation). Therefore it is possible for the chlorine evolved at the platinum anode to dissolve in the electrolyte to form hypochlorous acid and to attack the $NiCo_2S_4$ chemically. To investigate the hypothesis two experiments were carried out.

(a) When a $NiCo_2S_4$ electrode was placed in a 1N NaCl solution and Cl_2 gas was bubbled, there were signs of physical disintegration and dissolution.

(b) When a $NiCo_2S_4$ (cathode) and platinum electrode (anode) were polarized at a current density of 10 mA/cm^2 in a U tube at an electrode separation of approximately 12 cm there was no sign of its physical deterioration and dissolution of the $NiCo_2S_4$ electrode for the first hour. Thereafter, there was some sign of physical deterioration and dissolution.

These results confirmed that the corrosion of $NiCo_2S_4$ was due to the attack of hypochlorite or hypochlorous acid. In a natural corrosion situation, no hypochlorite will be produced since the corrosion potential is far below the decomposition potential of brine.

3.4 Proposal for Further Evaluation of the Proposed Method.

Although the previous experimental studies on the proposed novel method are encouraging, it is clearly understood that the work done is only at its initial stages. There are a number of problems and doubts to be resolved in the process of evaluation of the proposed novel method and these may be listed as follows;

(a) Previous work done by Onuchukwa and Russ indicated that the various catalysts, such as $NiCo_2S_4$, FeS and FeSx have different degrees of effectiveness in different media for preventing the amount of hydrogen diffused through a steel membrane. Hence it would be necessary to look for more suitable catalysts for sour environments.

(b) While the active electro-catalyst reduces the formation of atomic hydrogen on a corroding steel surface, it would enhance normal corrosion. This is a problem of the utmost importance in the evaluation of the proposed method.

(c) When a steel -pipe is coated with an active catalyst, the ratio of the cathodic to anodic area would be increased by many folds if the catalyst coat is damaged and thus exposing the pipe-steel. Then the pipe might fail due to anodic dissolution rather than due to hydrogen embrittlement or sulphide stress corrosion cracking.

(d) The experimental technique employed in the previous studies only shows that the hydrogen diffusing through a steel membrane is reduced under the protection. This hydrogen diffusion studies could not give any indication of reduction in sulphide stress corrosion cracking failure in terms of mechanical properties concerned.

(e) The proposed technique should effectively inhibit SSCC in actual environmental conditions, where a cyclic loading pattern and hence a corrosion fatigue condition, is inevitable.

In view of the problem (a), it is necessary to study other sulphide electrocatalysts, which may be more active and stable than $NiCo_2S_4$. Considering the stability of the catalysts, tungsten sulphide, WS_2 and molybndenum sulphide, MoS_2 are selected together with $NiCo_2S_4$ for further evaluation since Mo and W are more acid resistant than Ni or Co.

It is normally accepted that when an active cathode is electrically connected to a corroding metal piece, it would increase normal corrosion as clarified in the problem (b). In this proposed novel technique, connecting an active cathodic electrode to a corroding steel is the basic concept for the protection, hence enhanced normal corrosion is inevitable. A comprehensive program is included, in view of this problem, in future evaluation, to predict enhancement of the corrosion rate by employing an Evans diagram and also a series of experiments, to monitor actual corrosion weight loss and to study the effect of corrosion product formed on corroding steel surfaces.

To overcome the problem, discussed in (c), it is proposed to use another non-conducting layer on top of the catalyst coating, hence, if any part of the coating is damaged, the area ratios will be kept within the acceptable limit. Also the

activity of $NiCo_2S_4$ and its analogues relative to steel may be controlled by reducing the catalysts-loading, because it has been shown that activity of hydrogen evolution catalyst is dependent on the catalyst-loading[83,87].

Previous experimental studies on the proposed novel method only concentrated on the use of a separate Teflon-bonded $NiCo_2S_4$ electrode, electrically connected to the steel membrane in the hydrogen diffusion tests. Though this is convenient for laboratory experimental studies, it cannot give any indication or assessment in terms of improvement of mechanical properties due to the application of the novel method. Hence to find an answer for the problem 'd' a series of mechanical tests with the aid of fracture mechanic concepts, is included in this research program. Also, another set of tests is included to evaluate the changes in mechanical properties of specimens coated with the proposed electro-catalyst coating and being subjected to sour corrosive environment as a function of time.

To find an answer for the problem (e), that is, the applied electrocatalyst coating should be effective in actual environmental conditions where a cyclic loading pattern is inevitable, it was decided to carry out a preliminary study on corrosion fatigue problem.

CHAPTER FOUR

HYDROGEN EVOLUTION PERFORMANCE STUDIES ON SULPHIDE ELECTRO-CATALYSTS AND STEEL

CHAPTER 4.

HYDROGEN EVOLUTION PERFORMANCE STUDIES ON SULPHIDE ELECTRO-CATALYSTS AND STEEL.

4.1 Introduction.

As a first step for further evaluation of the proposed novel method for inhibition of sulphide stress cracking in steel, this study aims at comparing the hydrogen evolution performance of three sulphide catalysts, $NiCo_2S_4$, MoS_2 and WS_2 and EN 42 steel. To achieve this comparative study, this investigation proposes to determine:

(a) the hydrogen evolution current density - electrode potential relationship for the three sulphides and EN 42 steel, at different temperatures both in the presence and absence of H_2S in the NACE solution.

(b) the basic electro-kinetic parameters, such as, Tafel parameters, pseudo-exchange current density and Arrhenius activation energy for the sulphides and EN 42 steel in the different media.

A porous electrode system is selected for the hydrogen evolution studies of the sulphide catalyst. The porous electrode consists of an electrocatalyst, distributed uniformly in the form of small particles, in a porous and conducting substrate. A study[83] on a porous electrode as a function of sulphide catalyst loading shows that the hydrogen evolution activity on the porous electrode increases with increased catalyst loading until a catalyst loading of approximately 15 mg/cm^2 is reached. Then the activity is maintained at the same level until the catalyst loading reaches approximately 30 mg/cm^2. Hence for this comparative hydrogen evolution study on the sulphides, the catalyst loading is kept between 17 and 22 mg/cm^2.

To aid the experimental studies a short review on hydrogen evolution reaction and electrocatalysts was carried out.

4.2 A Short Review on the Hydrogen Evolution Reaction and on Electrocatalysts.

4.2.1. Introduction.

The reaction in which hydrogen is evolved from aqueous solution is a very important one in the history of electrochemistry[88]. The considerable importance of this reaction lies in its technological importance and its application to industrial purposes. The fact, that the hydrogen gas evolves on a great number of metals, permits the rate of hydrogen evolution reaction to be studied upon a much larger number of electrocatalysts than any other reaction. Furthermore, the hydrogen evolution reaction plays a dominant role in the theory of the corrosion of metals.

Pure hydrogen is mainly obtained by electrolysis of water in electrolysers containing a large number of unit cells[89]. One main contribution to the price of the hydrogen produced by electrolysis is the cost of the electrical energy. Obviously the electrical energy consumed in electrolysers is dominated by the overpotential developed at cathode and anode electrodes. The overpotential can be related to the cell potential E, by

$$E = E_{rev} + \eta_a + \eta_c + \eta_{iR}$$

where, E_{rev} is the reversible potential for water electrolysis

η_a is the activation polarization at the electrodes

η_c is the concentration polarization in the electrolyte

η_{iR} is the ohmic losses in the electrolyte and across the membrane.

Activation polarization at the electrodes results from charge transfer inhibition at the electrodes and is determined by the catalytic activity of the electrodes and surface roughness. Concentration polarization results from concentration gradients which exist in the neighbourhood of the electrodes. Ohmic losses in the electrolysis cell is the sum of the η_{iR} terms due to electrolyte, membrane, and electrode resistances Gas bubbles also contribute to the ohmic losses.

4.2.2. Electrocatalysts

Extensive studies are being carried out in search of an electrocatalyst having low overpotential for hydrogen evolution reaction[83,87,91-94]. The hydrogen evolution overpotential on metals has been shown to vary periodically with atomic number of the metals[90]. Figure 4.1 illustrates the hydrogen evolution reaction on two groups of metals in terms of exchange current density and hydrogen adsorption energy[89]. The first group,

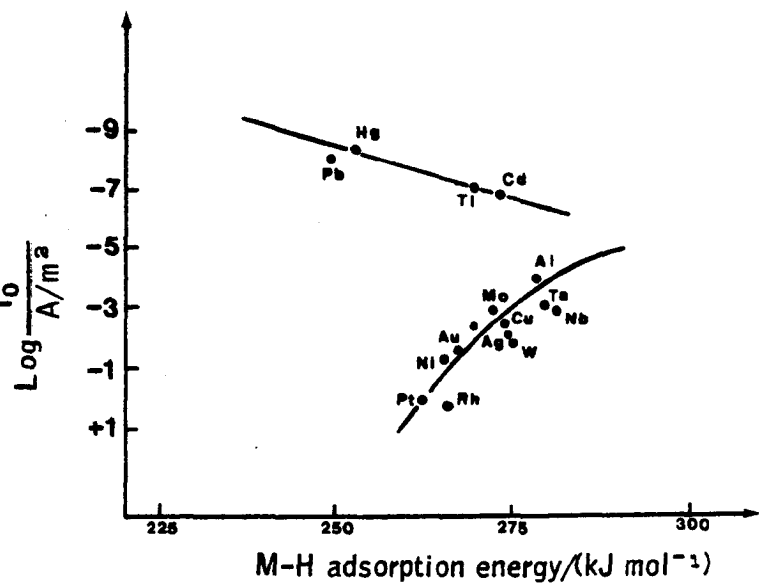

Fig.4.1. Rate of hydrogen evolution reation (log i_0) at different metals versus M-H energy.

mercury, cadmium, lead and thallium, shows that with small values of hydrogen-adsorbtion energy the rate of the hydrogen evolution reaction at the equilibrium potential is also relatively small. As the strength of the bond of hydrogen to the metal increases, the current density, i_0, at the equilibrium potential increases. For the second group of metals, nickel, platinum, tungsten, etc., at higher values of the hydrogen-metal bond, the direction of the log i_0 - MH bond strength relation changes. In this group as the energy of adsorption increases, the hydrogen evolution relation rates decreases. However, one cannot interpret these facts very conclusively without more information,such as hydrogen evolution mechanism,

rate determining steps, electronic configurations of the elements, etc.

Many workers have combined elements by doping to achieve compounds with suitable electronic properties that will give high hydrogen evolution performance[91-93]. Tungsten oxide doped with platinum, and sodium tungsten bronze are two such compounds which have shown enhanced hydrogen evolution performance[93]. The performance of the newly developed electrocatalysts has discouraged the common use of steel for hydrogen evaluation. Platinum is often an alternative choice to steel, but this element is not only expensive but often very susceptible to poisoning by trace impurities from the cell component and electrolyte.

Tseung and Man[81] developed a novel catalyst, nickel-cobalt-sulphide ($NiCo_2S_4$) for hydrogen evolution purposes in alkaline media. The Teflon-bonded electrodes of the sulphide catalyst gave a hydrogen evolution performance of $1 A/cm^2$ at -150 mV vs RHE (reversible hydrogen electrode) in 5N KOH at 70^0 C. The life tests in the same media have confirmed that Teflon bonded $NiCo_2S_4$ cathode catalyst can operate at 70^0 C, with the performance of $1 A/cm^2$ at -150 mV vs RHE, for over 3000 hours without any deterioration. Recently British Petroleum Research Centre[94] has developed a proprietary electrocatalyst for hydrogen evolving cathodes in alkaline media. The electrodes exhibit a low overvoltage of 70 to 90 mV vs RHE at 70^0 C for $1 A/cm^2$ hydrogen evolution current density in 5N KOH.

4.2.3. Mechanism of Hydrogen Evolution.

The discharge of hydrogen ions from an acid solution may occur through a series of stages and could be summarized as follows[95];

(1) $(H_3O^+)_B \xrightarrow[\text{Diffusion}]{\text{Migration}} (H_3O^+)_E$

$(H_3O^+)_B$: Hydrated ion in bulk of solution.

$(H_3O^+)_E$: Hydrated ion near electrode.

(2) (H_3O^+) + e^- $\xrightarrow[\text{Dehydration}]{\text{Discharge}}$ M-H + H_2O

ion — electron from metal M — H atom adsorbed on M.

(3a) M-H + M-H $\xrightarrow{\text{Combination}}$ H_2

(3b) $(H_3O^+)_E$ + M-H + e^- $\xrightarrow[\text{discharge}]{\text{Secondary}}$ H_2

If one of these steps is much slower than any of the others, it will determine the rate of the process, the reactants and products of the other steps maintaining equilibrium with one another in the steady conditions imposed by the slow step. Much theoretical and practical effort has been directed towards discovering the mechanism of the hydrogen evolution reaction, and it is now possible to measure certain parameters, the values of which are diagnostic of various reaction mechanisms. For example a value of 0.03 for the slope b of the Tafel line ($\eta = a + b \log i$) at ordinary temperatures is characteristic of a rate-determining combination step 3a. Similarly a slope of 0.12 is characteristic of a rate-determining discharge step 2 or secondary discharge step 3b[95]. However it has been pointed out that in some cases different rate-determining steps can give the same slope[89]. Hence it is necessary to carry out transient studies which give information on surface conditions, which directly helps to confirm the mechanism.

4.3 Experimental Procedures.

4.3.1. Materials and Methods.

4.3.1.1. Sulphide - Electro - Catalysts.

The $NiCo_2S_4$ for this work was prepared by employing a co-precipitation technique[96]. Initially 50 g of potassium polysulphide, was dissolved in 150 ml distilled water and filtered. Then 15 g of $Ni(NO_3)_2 \cdot 6H_2O$ and 30 g of $Co(NO_3)_2 \cdot 6H_2O$ were dissolved in 50 ml of

distilled water. The polysulphide solution was then added to the mixed nitrate solution with continuous stirring. This preparation produced about 15 g of $NiCo_2S_4$, which was filtered off and dried under N_2 at 125^0 C overnight.

The MoS_2 and WS_2 were supplied by Alpha Chemicals. These two sulphides were subjected to vacuum grinding in a vibratory ball-mill to increase their surface area.

4.3.1.2. Electrolyte

The electrolyte solution recommended by the NACE (National Association of Corrosion Engineers) for sour environmental studies was used for this study. The NACE solution consists of a 5 percent (mass/volume) sodium chloride and 0.5 percent (volume/volume) acetic acid with a continuous flow of H_2S at 1 atmospheric pressure. The sodium chloride and acetic acid used were of Analar grade and were supplied by BDH Chemicals. Distilled and deionized water was used to prepare the solution.

4.3.1.3. Electrode Preparation

The sulphide electrocatalysts prepared were of polycrystalline powder form. To fabricate electrodes, the hydrophobic particulate polymer, Fluoro-ethylene-polymer (FEP, obtained from ICI Plastics) was used to bind the electrocatalyst to the nickel-mesh current collector. The FEP bonded electrodes were prepared as follows;

A weighed amount of the sulphide electrocatalysts (200 mg) was mixed with the appropriate quantity of FEP dispersion of 55% concentration by weight and 3 ml of methanol. The catalyst/FEP ratio was optimized initially and was found to be 1:1 for $NiCo_2S_4$ and 1:0.85 for MoS_2 and WS_2. The mixture was throughly dispersed by means of a magnetic stirrer and painted onto 1 cm^2 100 mesh nickel-screens (ultrasonically degreased in

acetone and weighed) and dried with a hair-drier. This process was repeated until the nickel screen is completely covered with the catalyst. The electrodes were then pressed at a pressure of 0.8 kN/cm^2 for 3 minutes, followed by curing at 300^0 C for 1 hour in a stream of nitrogen, N_2.

EN 42 steel foil of 0.15 mm thickness was used in this study. A 1 cm^2 steel piece was spot welded to a 1.5 mm x 0.15 mm x 15 cm piece of EN 42 steel for current collection. This electrode was cleaned ultrasonically in acetone for a minimum of 30 minutes before polarization studies were carried out.

4.3.1.4. Test Cell.

A 3-compartment glass test cell (Figure 4.2) was used for this study. A 3 cm x 2 cm platinum mesh was used as the counter electrode. A saturated calomel electrode (SCE) was used as the reference electrode. The working electrode compartment and the secondary electrode compartment were separated by means of a Nafion membrane (E.I. Du Pont De Nemours and Company, U.S.A.). The use of a Nafion membrane effectively prevents the diffusion of hypochlorous acid, formed at the anode compartment due to the evolution of Cl_2 at the counter electrode, from reaching the cathode compartment. To facilitate passage of hydrogen sulphide, H_2S, in the working electrode compartment, it was necessary to use an Agar salt bridge in the reference electrode compartment. The out-going H_2S gas was removed as a lead sulphide precipitate by bubbling through lead acetate solution.

4.3.1.5. Electrochemical Test Procedure.

Initial experiments indicated that reproducible results could only be obtained on pre-cathodised electrodes. For example a freshly-prepared, FEP-bonded $NiCo_2S_4$ electrode performance was 64 mA/cm^2 at -800 mv (Vs SCE) in NACE solution at 20^0 C without H_2S, whereas the

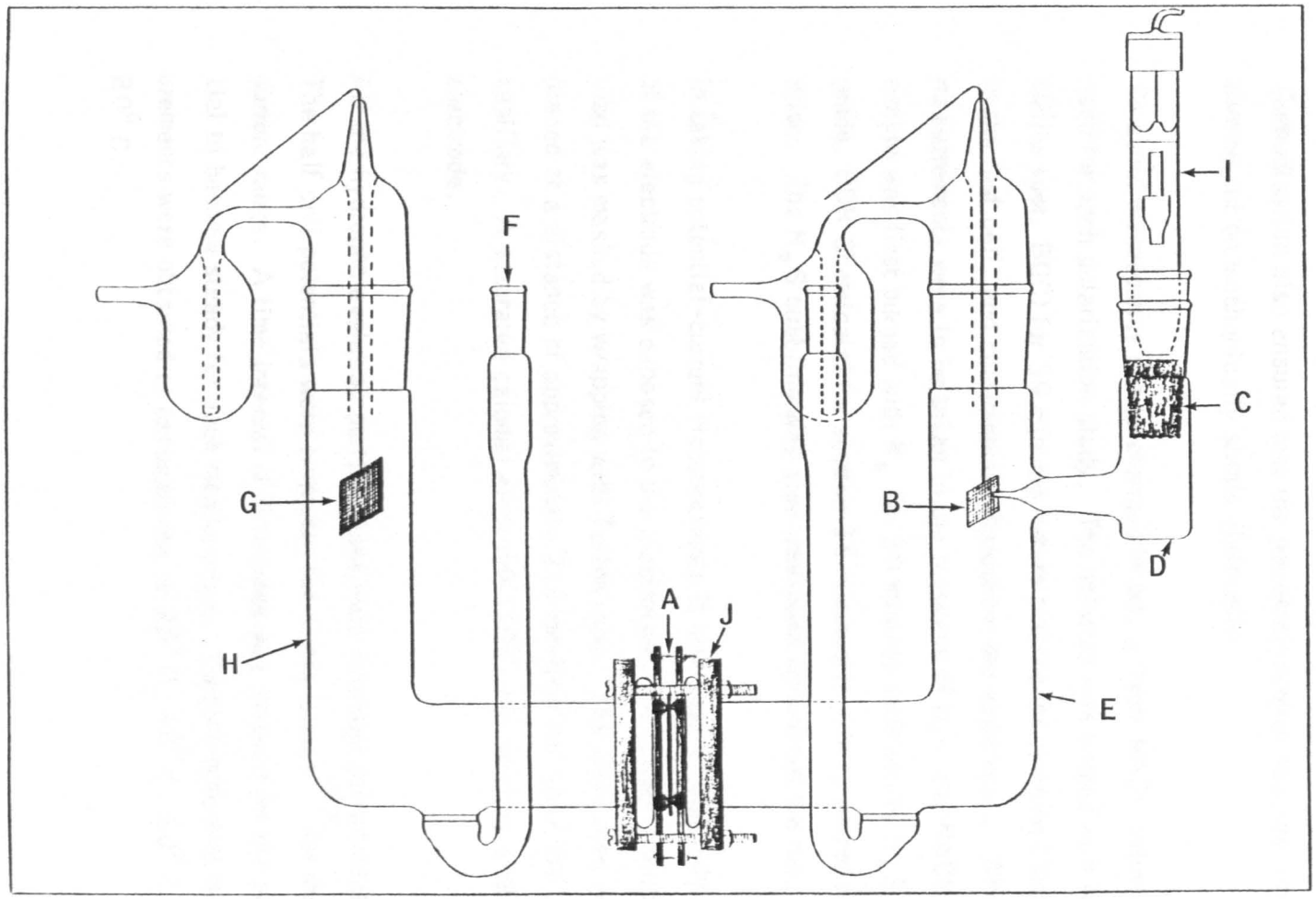

Fig.4.2. Three-compartment cell assembly for current-potential measurement.
A: Nafion membrane. B: Working electrode. C: Agar bridge. D: Reference compartment.
E: Working compartment. F: Gas inlet, G: Counter electrode. H: Counter compartment.
I: Saturated calomel electrode. J: Aluminium bracket.

performance, after cathodisation for 3 hours at 500 mA/cm^2 was 105 mA/cm^2 under the same conditions. Therefore in the determination of the hydrogen evolution activity of the sulphides, electrodes were cathodised for approximately 12 hours at 500 mA/cm^2 at 60^0 C. Cathodisation also ensured that the potential-current measurements were carried out on mechanically stable electrodes.

To avoid discrepancy due to changes in pH, a fresh NACE solution was used for each polarization study. The solution was purged with N_2 (white spot, BOC) for 30 minutes before placing the working electrode in the test cell, and continuously throughout the experiment. When V-i measurements were to be taken in the presence of H_2S, the NACE electrolyte was first purged with N_2 for 30 minutes followed by H_2S (analar grade, BDH Chemicals) for another 30 minutes to ensure proper saturation. The H_2S bubbling was also continued throughout the run.

In taking potential-current measurements it was ensured that only 1 cm^2 of the electrode was exposed to the electrolyte, the current collector lead was masked by wrapping with Teflon tape. The electrodes were placed at a distance of approximately 2.5 mm from the tip of the Luggin capillary. A saturated calomel electrode (SCE) was used as a reference electrode.

All the hydrogen evolution performances were obtained galvanostatically. The half cell potentials were corrected for ohmic losses[97] for the complete current range. A time interval of 5 minutes was allowed for the potential to become steady for each measurement. Current-potential measurements were obtained at temperatures of 25^0 C, 40^0 C, 60^0 C and 80^0 C.

4.3.2. Electrocatalysts Characterization.

The sulphur content of the $NiCo_2S_4$, prepared by the co-precipitation technique and the ball-milled MoS_2 and WS_2, were determined by a Schoniger combustion unit. This analytical technique is basically the

combustion of a weighed quantity of sulphide in a stream of oxygen. The effluent gases are dissolved in a solution of hydrogen peroxide of known concentration to form sulphate ions. This solution is titrated against barium chloride solution using thorin solution as indicator.

The surface area measurements of the sulphide catalysts, before and after the ball-milling in the case of MoS_2 and WS_2, were carried out on a Micrometric Surface Area Analyzer. This instrument facilitates the measurement of the surface area by determining the quantity of the inert gas, N_2, necessary to form a monolayer on the sulphide representative sample. The sulphide samples were kept at an elevated temperature of 200° C for 4 hours under a stream of pure nitrogen to ensure freedom from vapours. Then 1 gram of sulphide sample was taken for the analysis. The actual numerical value of the surface area measurement is calculated from the BET equation.

Since there is a tendency for sulphides to be electrochemically reduced at cathodic polarization and sulphur to be leached away, it was found necessary to determine the quantity of sulphur in the sulphides after enhanced polarization. Therefore the sulphide electrodes, made as detailed in 4.3.1.3., were subjected to a cathodic current density of 500 mA/cm^2 at 60° C in the NACE solution for 12 hours both in the presence and absence of H_2S. After this pre-cathodization, the catalysts coatings were removed from the electrodes and the quantity of sulphur analysed in the Schoniger combustion unit.

4.4 Results.

Figures 4.3 to 4.6 give the current potential curves for hydrogen evolution at the current density range of 0.5 to 15 mA/cm^2 on $NiCo_2S_4$, MoS_2, WS_2 and EN 42 steel electrodes respectively in NACE solution both in the presence and absence of H_2S, at 25° C, 40° C, 60° C and 80° C. The catalyst loading of the $NiCo_2S_4$, MoS_2 and WS_2 electrodes was 17 mg/cm^2, 19 mg/cm^2 and 22 mg/cm^2 respectively.

Figure 4.3. Hydrogen evolution current-potential characteristics on FEP bonded $NiCo_2S_4$ (17 mg/cm²), MoS_2 (19 mg/cm²), and WS_2 (22 mg/cm²) electrodes and on EN 42 steel, in NACE solution, in the presence and absence of H_2S at 25° C.

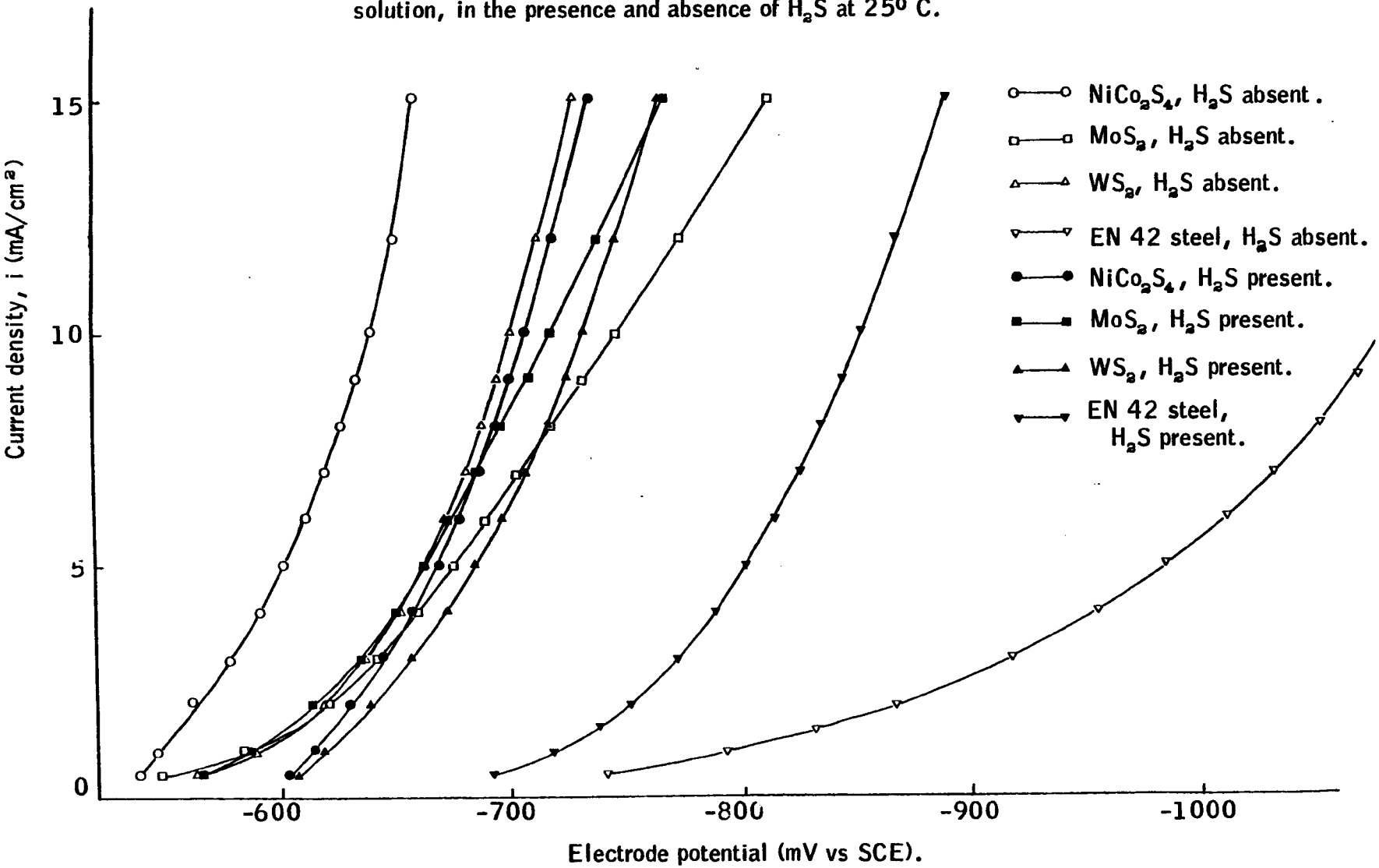

Figure 4.4. Hydrogen evolution current-potential characteristics on FEP bonded $NiCo_2S_4$ (17 mg/cm²), MoS_2 (19 mg/cm²), and WS_2 (22 mg/cm²) electrodes and on EN 42 steel, in NACE solution, in the presence and absence of H_2S at 40° C.

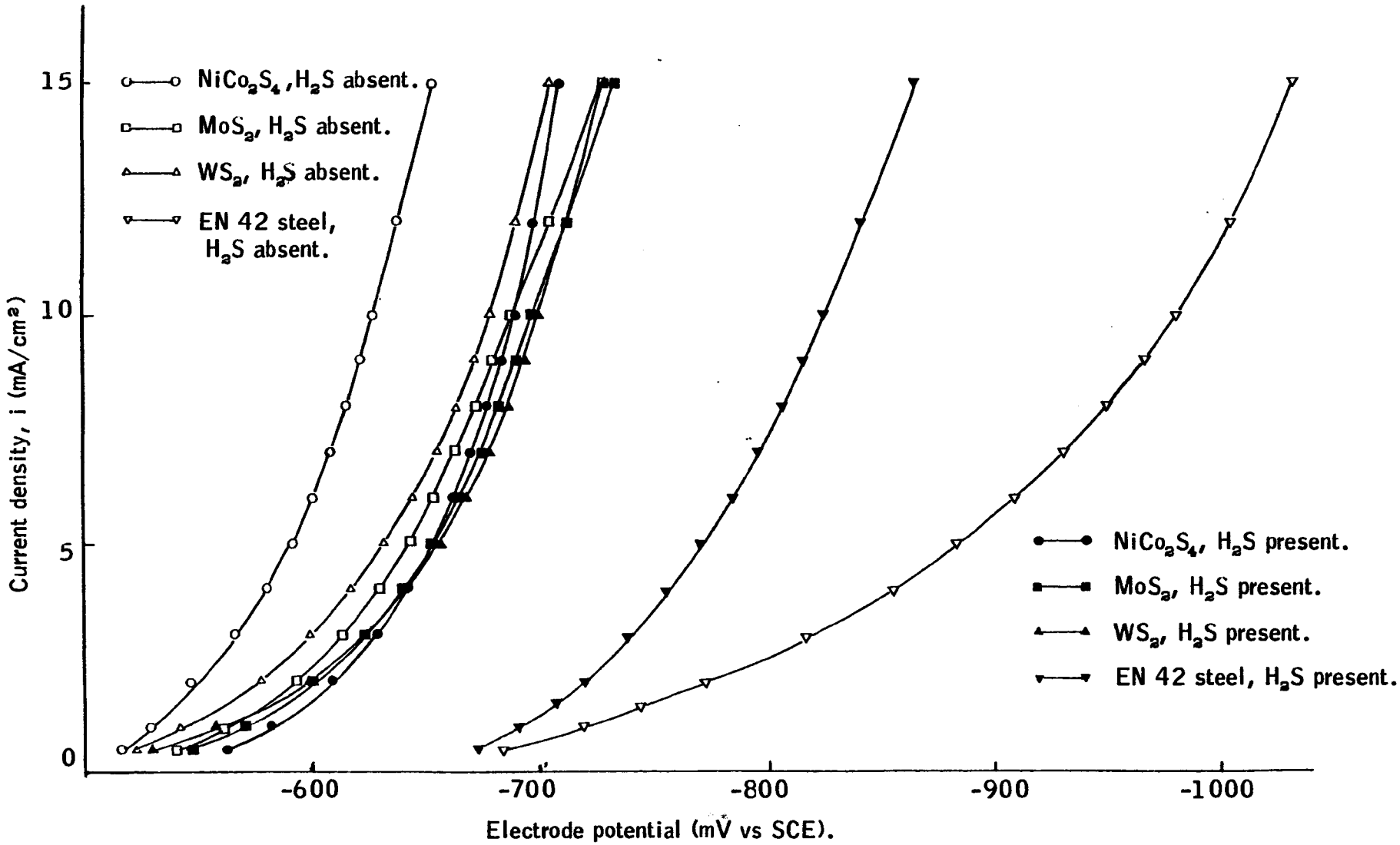

Figure 4.5. Hydrogen evolution current-potential characteristics on FEP bonded $NiCo_2S_4$ (17 mg/cm²), MoS_2 (19 mg/cm²), and WS_2 (22 mg/cm²) electrodes and on EN 42 steel, in NACE solution, in the presence and absence of H_2S at 60° C.

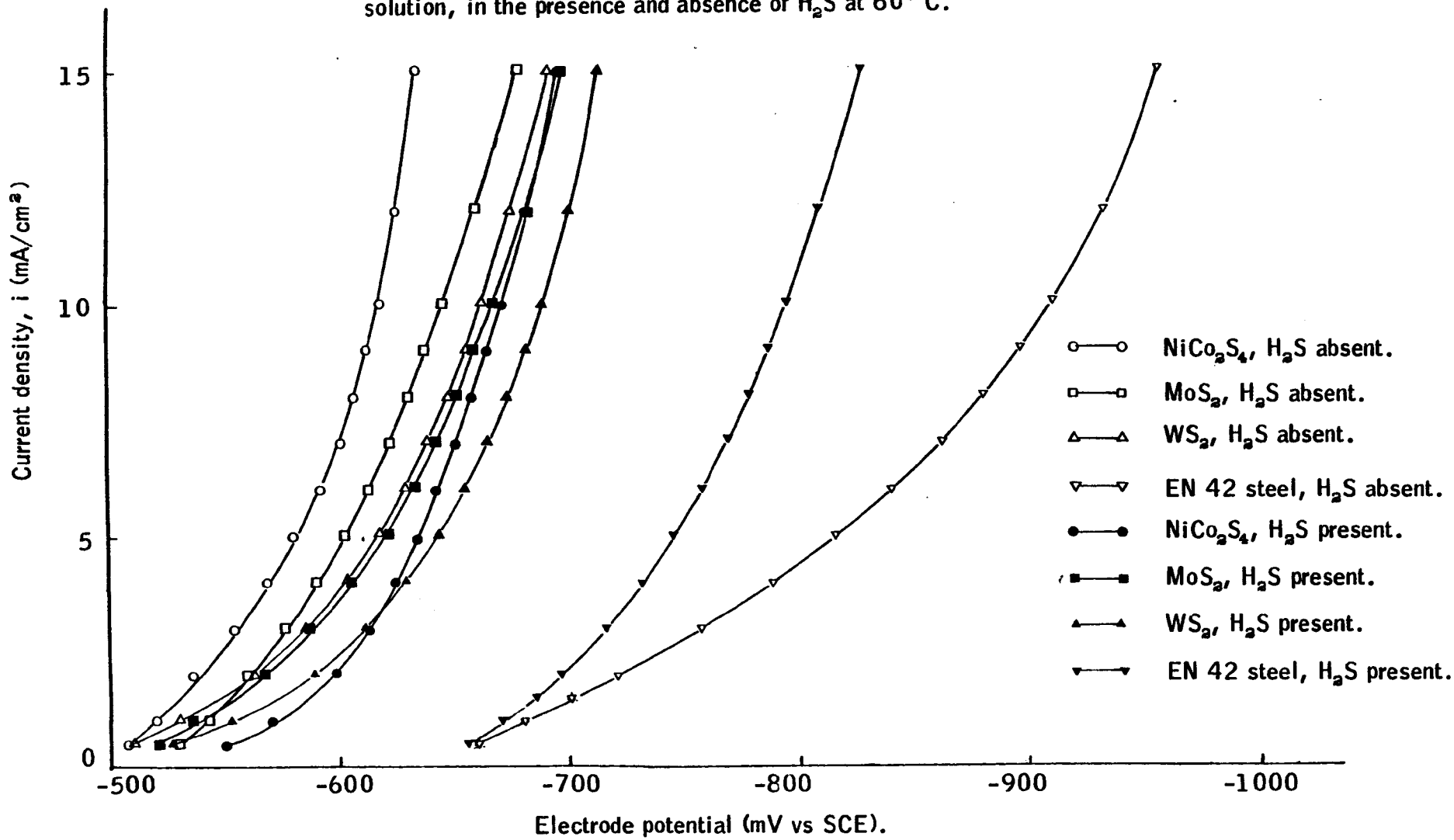

Figure 4.6. Hydrogen evolution current-potential characteristics on FEP bonded $NiCo_2S_4$ (17 mg/cm²), MoS_2 (19 mg/cm²), and WS_2 (22 mg/cm²) electrodes and on EN 42 steel, in NACE solution, in the presence and absence of H_2S at 80° C.

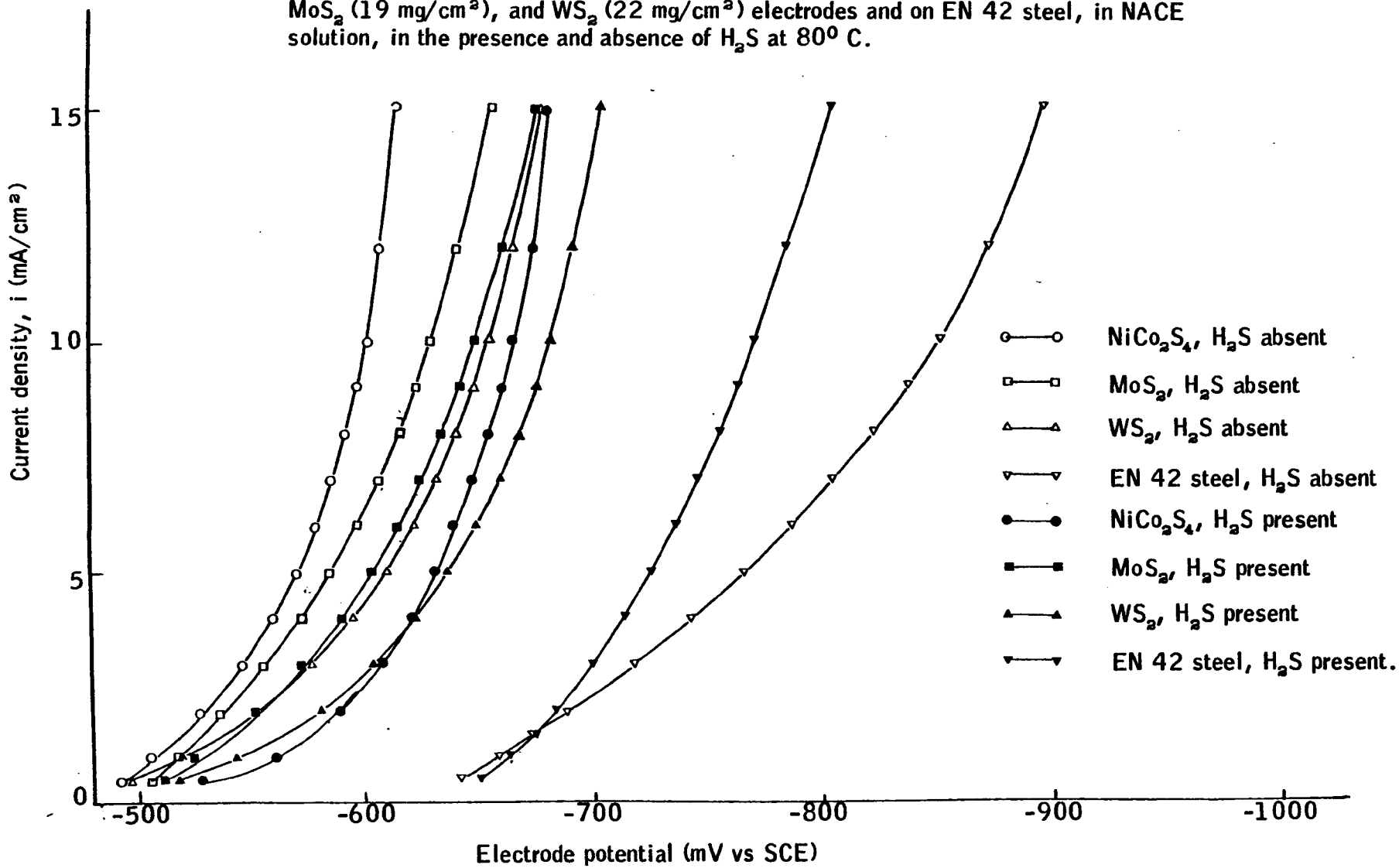

Figures 4.7 to 4.10 show the Tafel plots for hydrogen evolution reaction on $NiCo_2S_4$, MoS_2 and WS_2 electrodes at 25° C, 40° C, 60° C and 80° C in NACE solution, both in the presence and absence of H_2S. Figure 4.11 gives the Tafel plot for EN 42 steel at 25° C in NACE solution, both in the presence and absence of H_2S. The pseudo-exchange current densities (per geometric area of the electrode) obtained from the Tafel plots are given in Table 4.1.

Figure 4.12 gives the log i (at constant potential) versus $\frac{1}{T}$ plots for the sulphides and EN 42 steel electrodes, in NACE solution, in the absence of hydrogen sulphide. Figure 4.13 gives the corresponding log i versus $\frac{1}{T}$ plots in the presence of hydrogen sulphide for the four electrodes. The apparent activation energies for hydrogen evolution reaction on the three sulphides and EN 42 steel were estimated from the slope of the log i versus $\frac{1}{T}$ curve in each case and are given in Table 4.2. Every effort was made to take the measurements in the low over-voltage region in order to avoid or minimise contributions due to ohmic and concentration overpotentials. Hence current density values at potentials of -620 mV and -740 mV (Vs SCE) were taken for the sulphides and steel electrodes respectively.

Table 4.3 gives the sulphur content and the BET surface area analysis of the three sulphide catalysts. Table 4.4 gives the changes in the sulphur content of $NiCo_2S_4$, MoS_2 and WS_2 electrodes after cathodization (500 mA/cm² at 60° C for 12 hours) in NACE solution, in both the presence and absence of H_2S.

4.5 Discussion.

From Figures 4.3 to 4.6, it can be seen that the $NiCo_2S_4$ is more active for the hydrogen evolution reaction than the other sulphides in NACE solution, in the absence of H_2S. However MoS_2 appears to be most effective catalyst around a practical potential of -600 mV (Vs SCE) at all temperatures except 40° C, in NACE solution, in the presence of H_2S. Furthermore the three sulphides seems to be far more active for the hydrogen evolution reaction than the EN 42 steel in the two media that were studied. The hydrogen evolution performance of the sulphides are in the following descending order, particularly at low current densities.

Figure 4.7. Tafel plots for the hydrogen evolution reaction on $NiCo_2S_4$ (17 mg/cm²), MoS_2 (19 mg/cm²), and WS_2 (22 mg/cm²) electrodes in NACE solution, in the presence and absence of H_2S at 25° C.

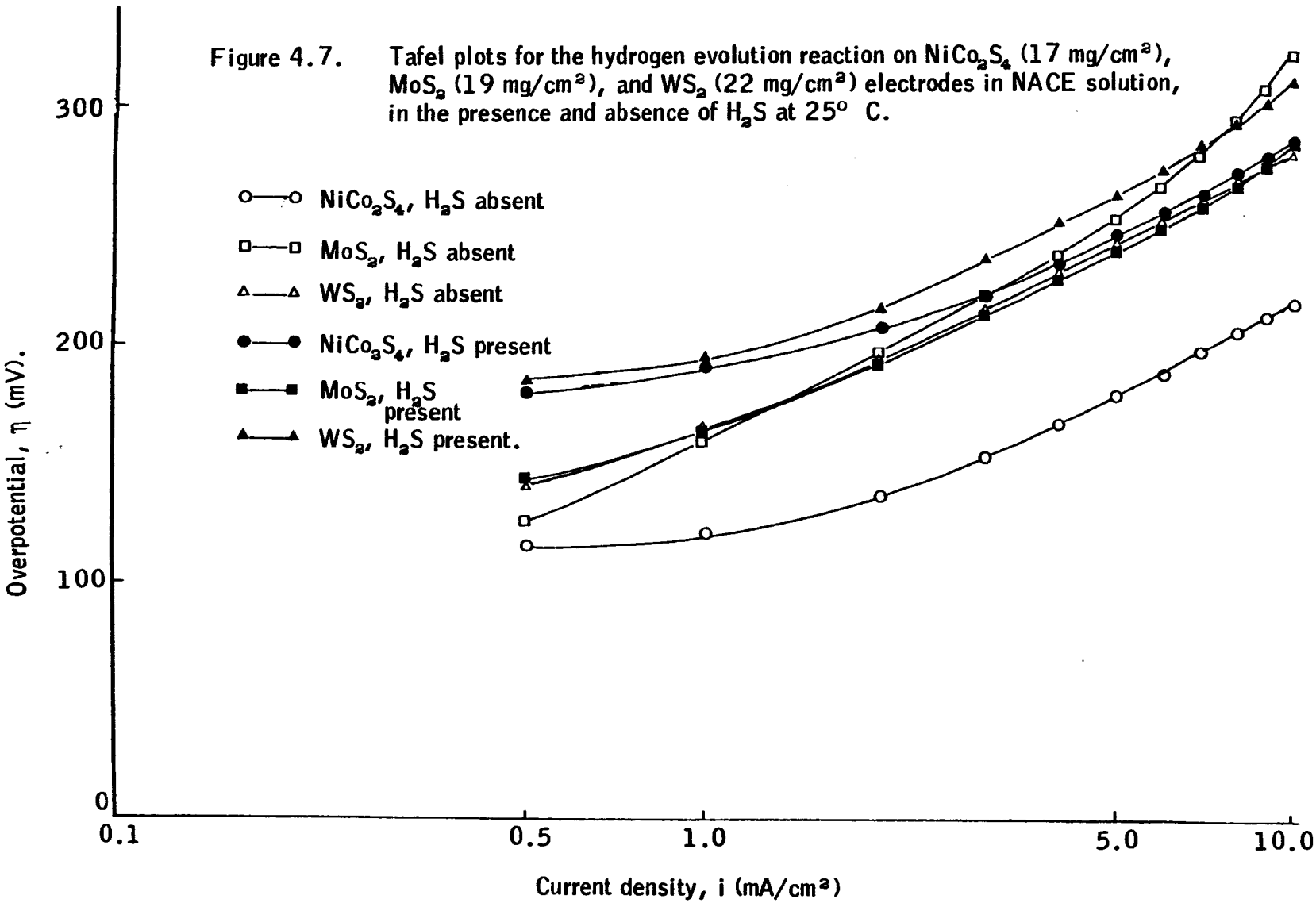

Figure 4.8. Tafel plots for the hydrogen evolution reaction on $NiCo_2S_4$ (17 mg/cm²), MoS_2 (19 mg/cm²), and WS_2 (22 mg/cm²) electrodes in NACE solution, in the presence and absence of H_2S at 40° C.

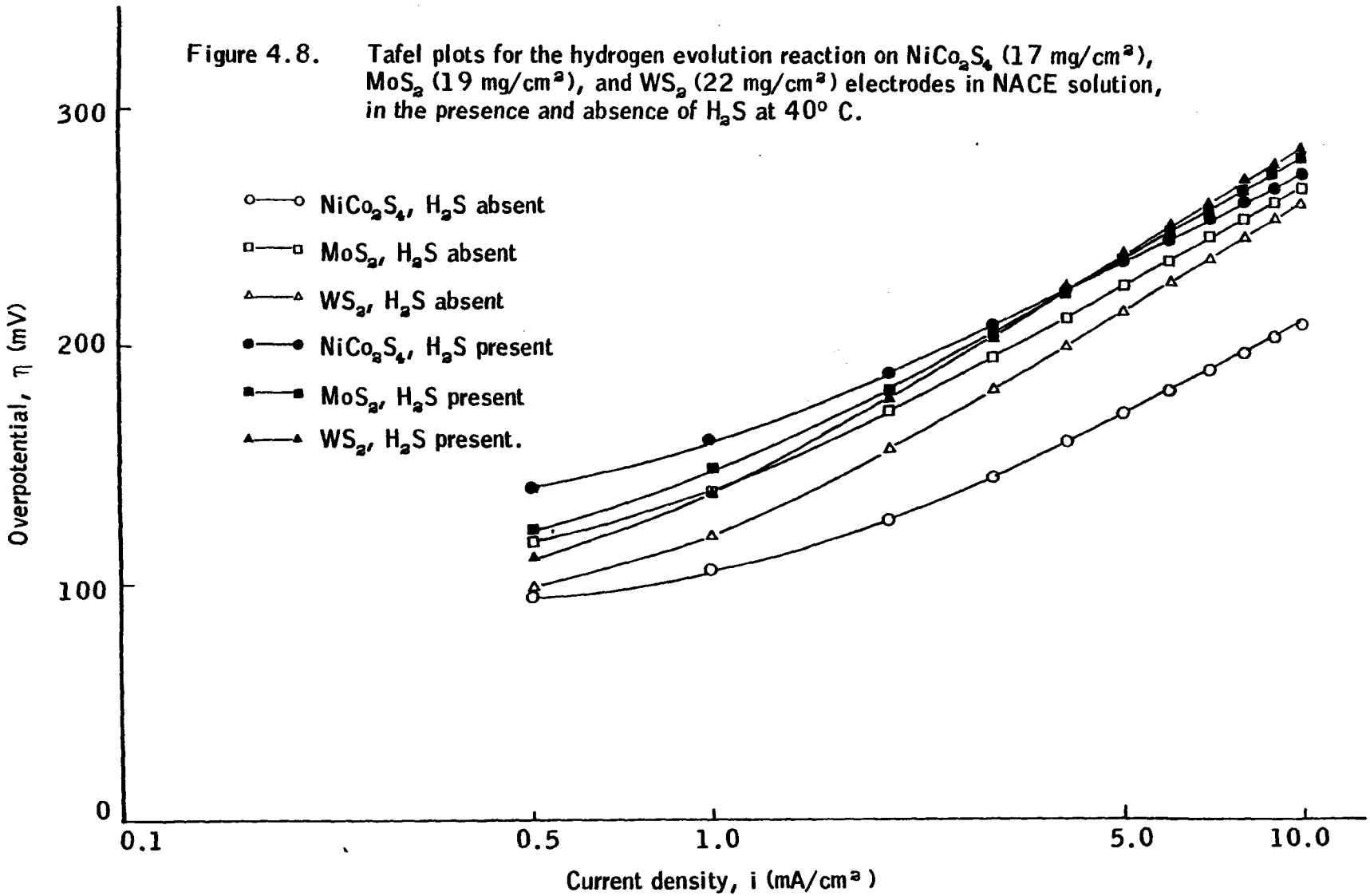

Figure 4.9. Tafel plots for the hydrogen evolution on $NiCo_2S_4$ (17 mg/cm²), MoS_2 (19 mg/cm²) and WS_2 (22 mg/cm²) electrodes in NACE solution, in the presence and absence of H_2S at 60° C.

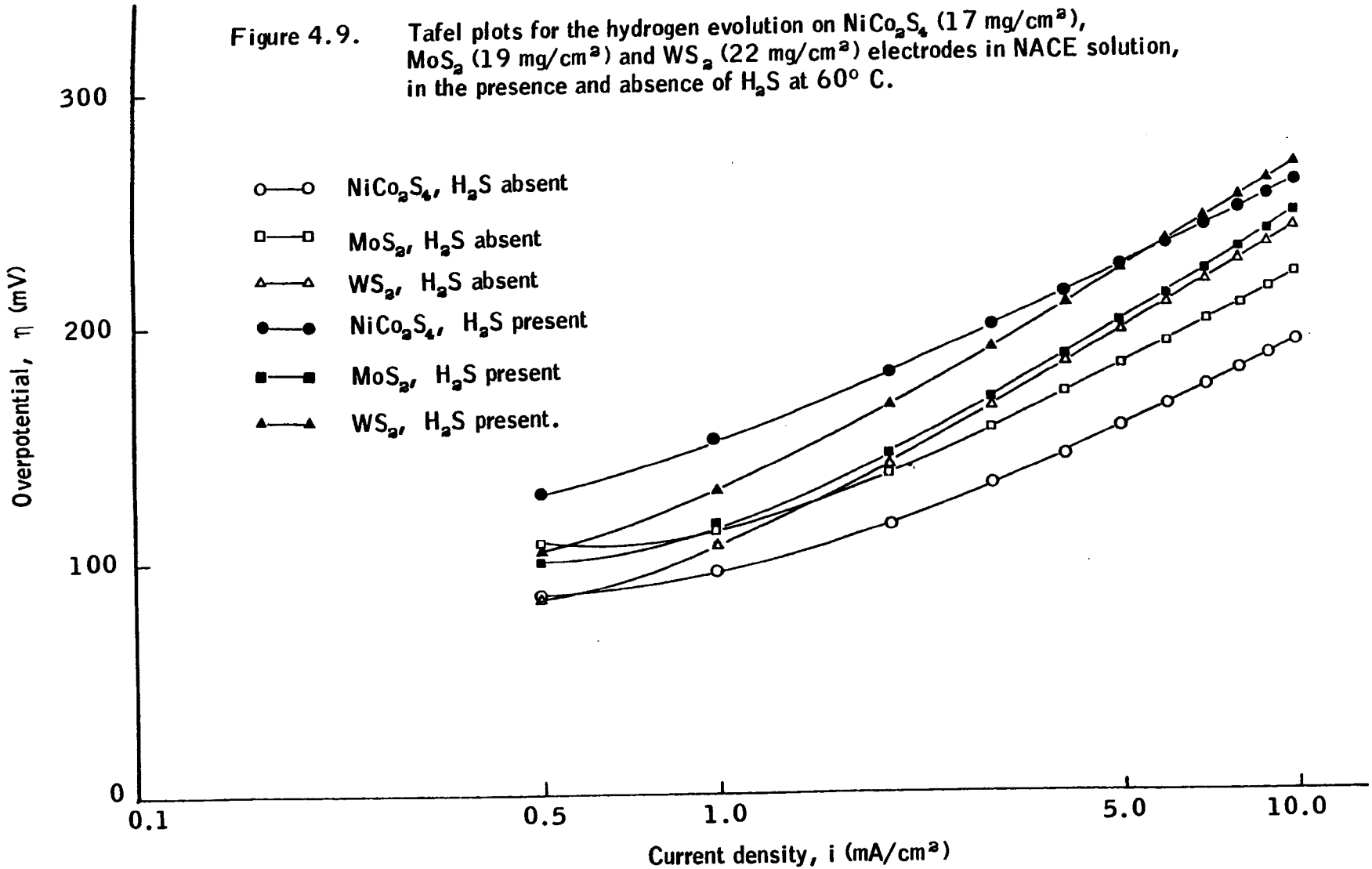

Figure 4.10. Tafel plots for the hydrogen evolution on $NiCo_2S_4$ (17 mg/cm²), MoS_2 (19 mg/cm²) and WS_2 (22 mg/cm²) electrodes in NACE solution, in the presence and absence of H_2S at 80° C.

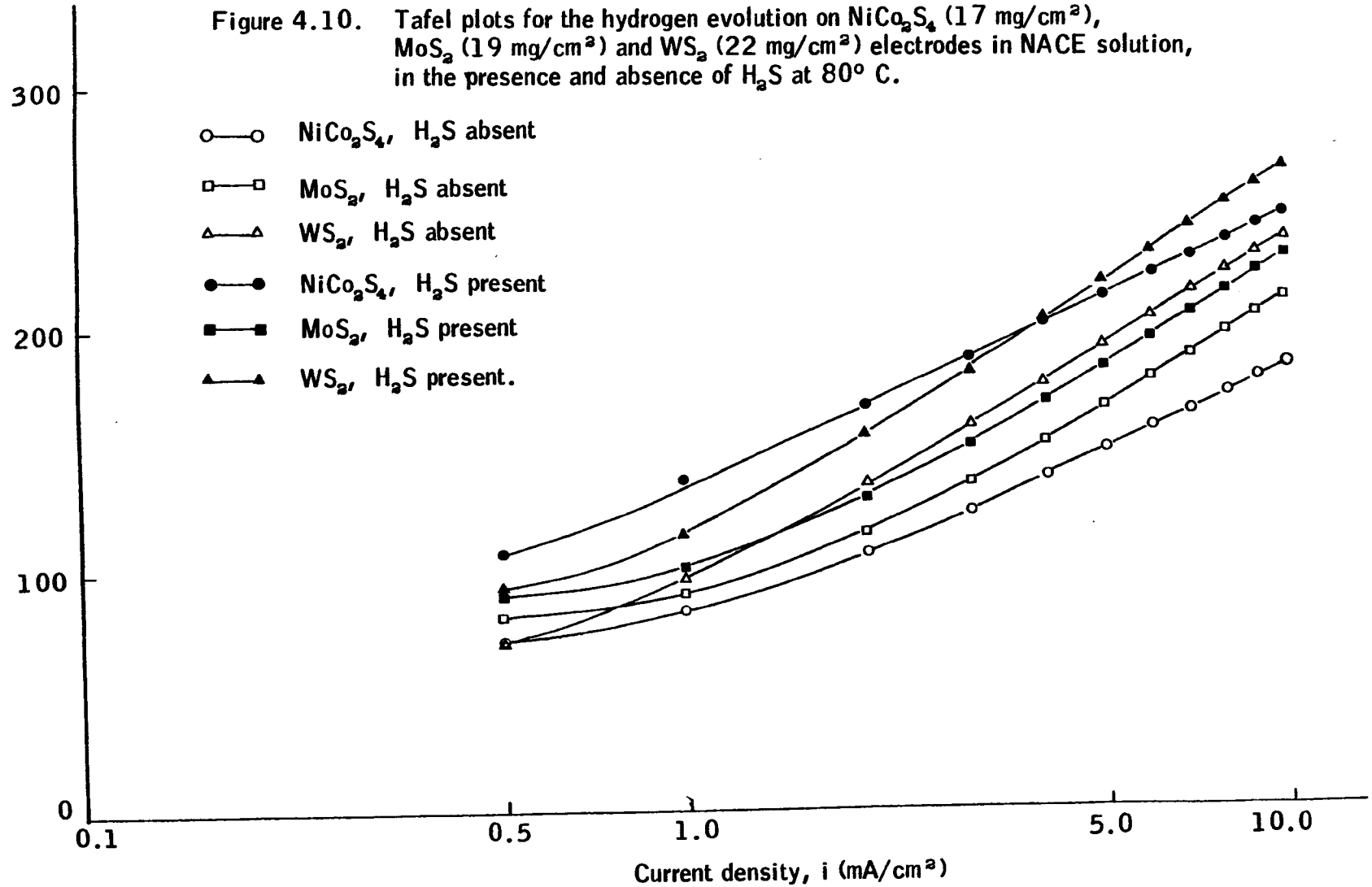

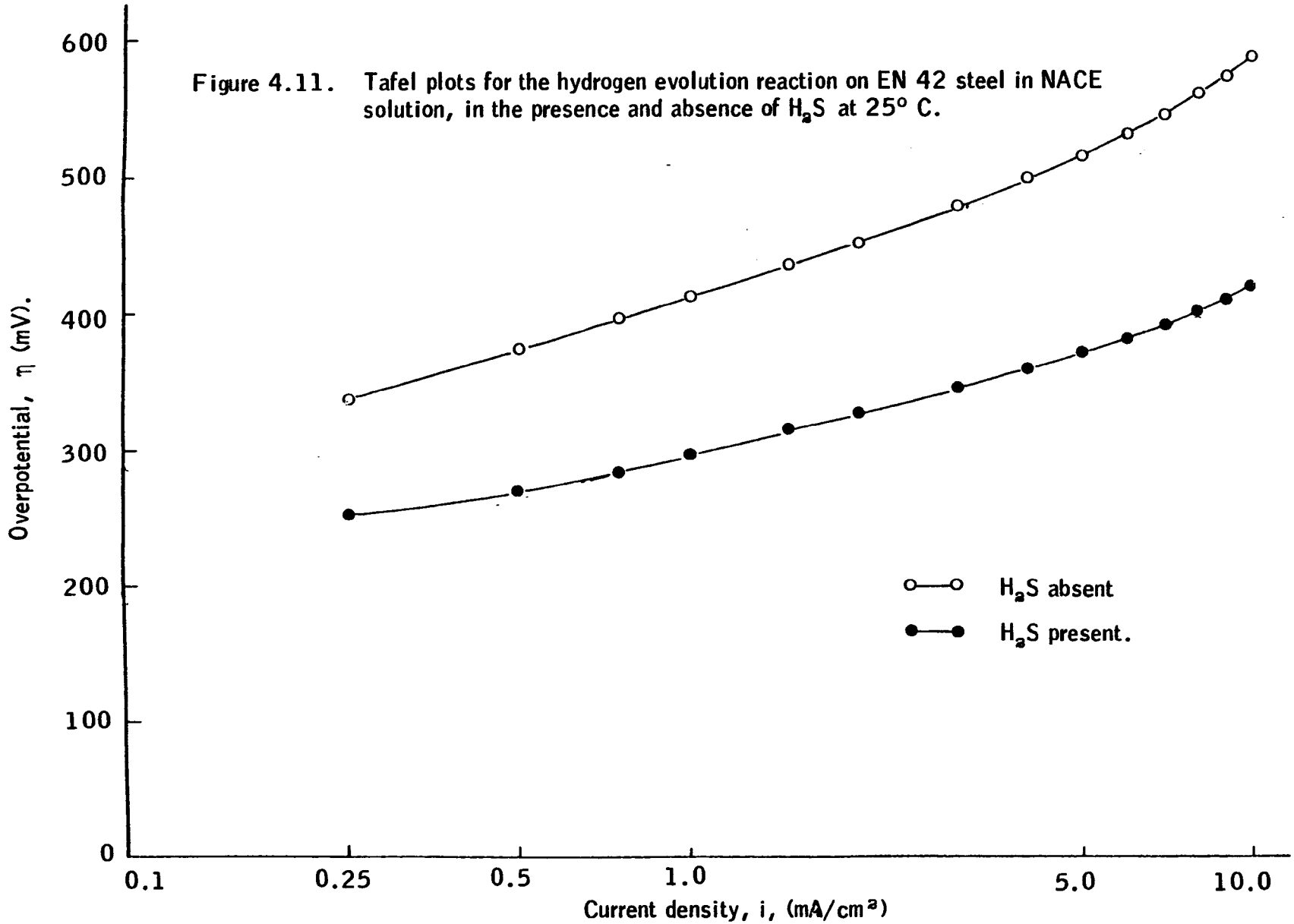

Figure 4.11. Tafel plots for the hydrogen evolution reaction on EN 42 steel in NACE solution, in the presence and absence of H_2S at 25° C.

TABLE 4.1. Pseudo-exchange current densities of $NiCo_2S_4$, MoS_2, WS_2 and EN 42 steel in the presence and absence of H_2S at 25° C, 40° C, 60° C and 80° C in NACE solution.

Temperature	$NiCo_2S_4$		MoS_2		WS_2		EN42 steel	
	Presence of H_2S (mA/cm^2)	Absence of H_2S (mA/cm^2)	Presence of H_2S (mA/cm^2)	Absence of H_2S (mA/cm^2)	Presence of H_2S (mA/cm^2)	Absence of H_2S (mA/cm^2)	Presence of H_2S (mA/cm^2)	Absence of H_2S (mA/cm^2)
25° C	0.050	0.191	0.060	0.050	0.032	0.047	0.0021	0.00054
40° C	0.056	0.200	0.095	0.118	0.133	0.170	-	-
60° C	0.060	0.220	0.208	0.160	0.153	0.210	-	-
80° C	0.069	0.248	0.270	0.331	0.198	0.250	-	-

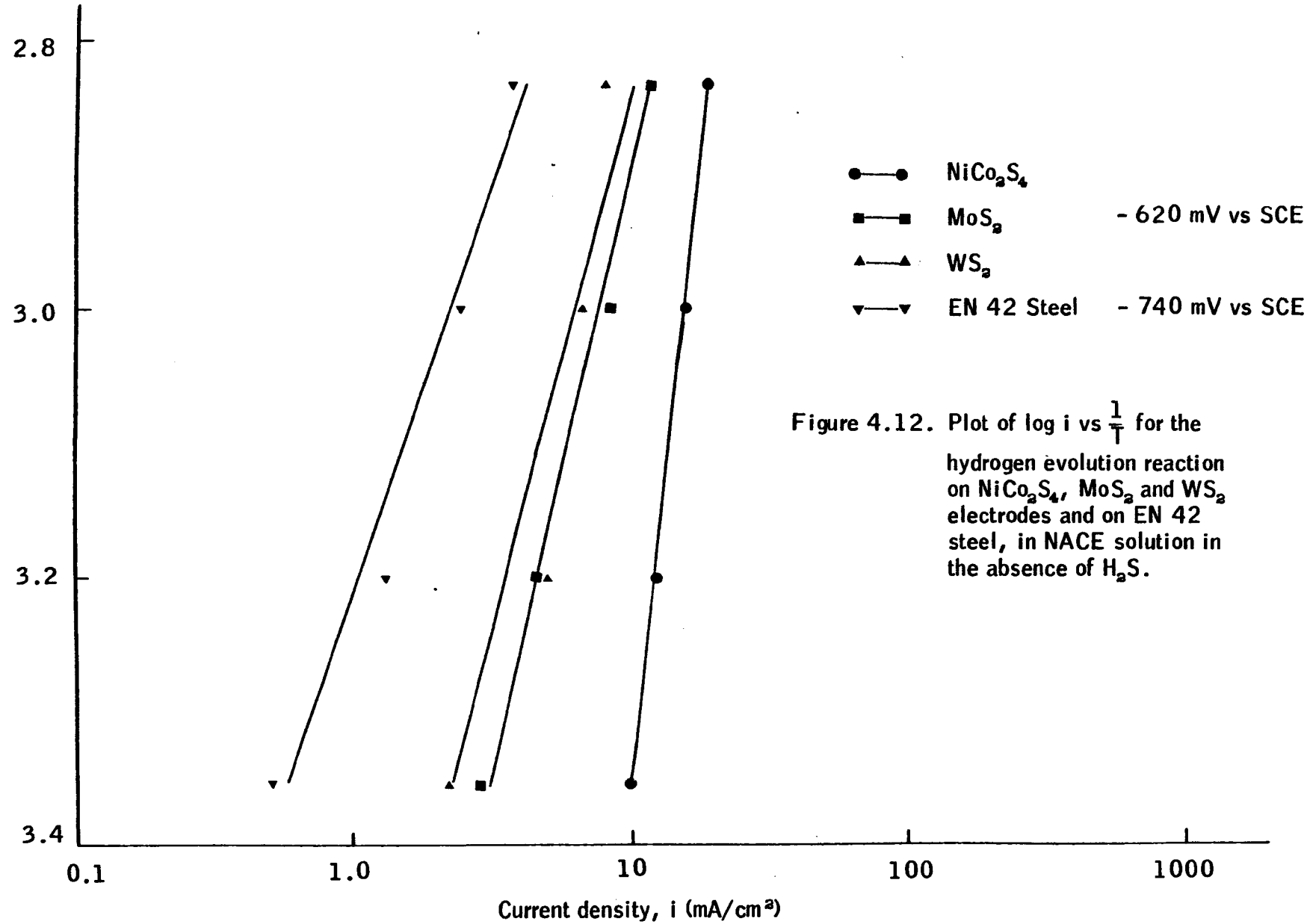

Figure 4.12. Plot of log i vs $\frac{1}{T}$ for the hydrogen evolution reaction on $NiCo_2S_4$, MoS_2 and WS_2 electrodes and on EN 42 steel, in NACE solution in the absence of H_2S.

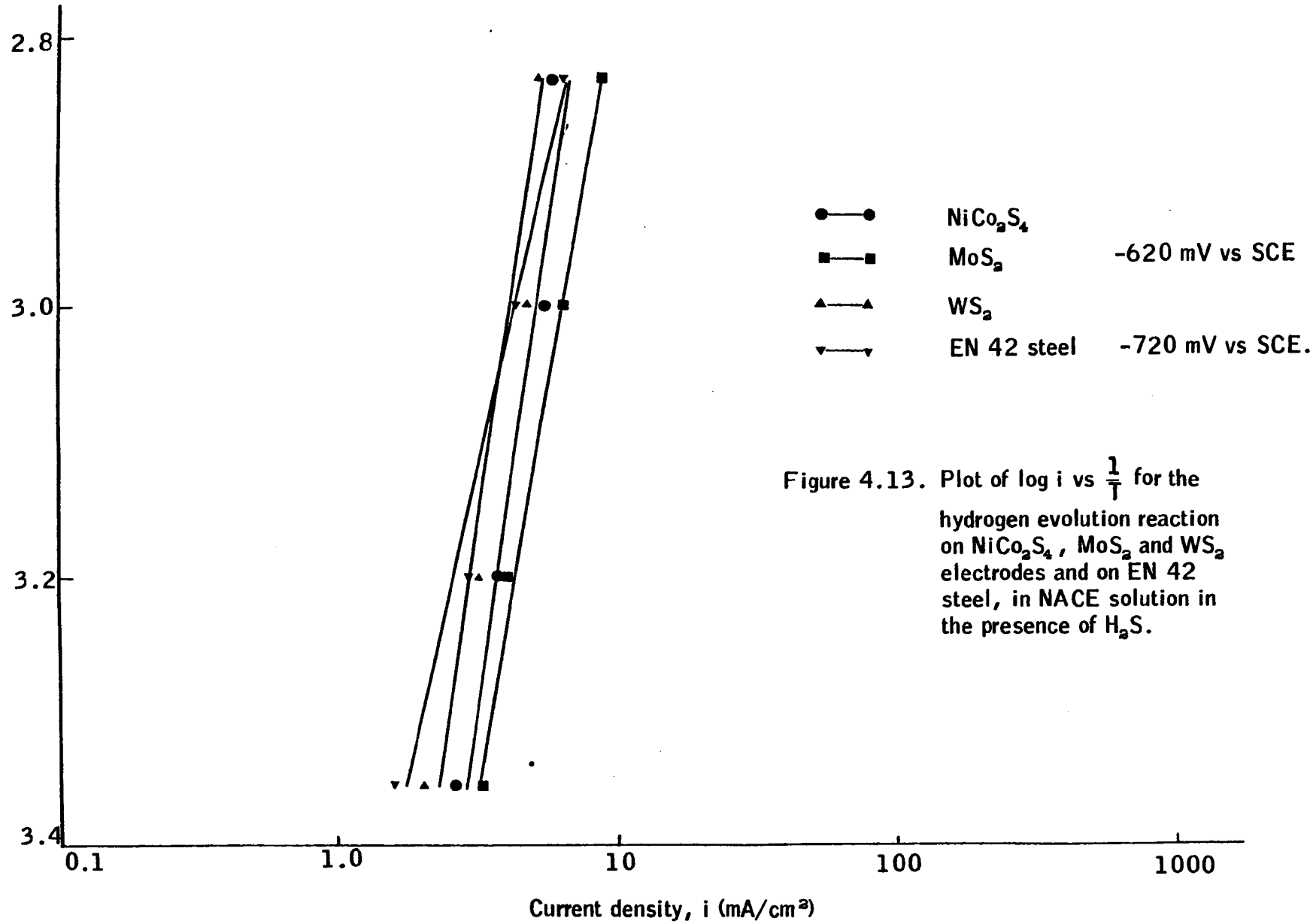

Figure 4.13. Plot of log i vs $\frac{1}{T}$ for the hydrogen evolution reaction on $NiCo_2S_4$, MoS_2 and WS_2 electrodes and on EN 42 steel, in NACE solution in the presence of H_2S.

TABLE 4.2 The apparent activation energies for hydrogen evolution on $NiCo_2S_4$, MoS_2, WS_2 and EN 42 steel in NACE solution in the presence and absence of H_2S.

Electrode	Catalyst loading (mg/cm^2)	Absence of H_2S (joules/mole)	Presence of H_2S (joules/mole)
$NiCo_2S_4$	17	4389	5898
MoS_2	19	9363	7194
WS_2	22	10626	6082
EN 42 steel	-	13961	9238

TABLE 4.3. Sulphur content and surface areas of $NiCo_2S_4$, MoS_2 and WS_2.

Sample	Theoretical sulphur content (percent)	Actual sulphur content (percent)	Surface area (m^2/g)	
			before ball milling	after ball milling
$NiCo_2S_4$	42.07	40.77	8.22	-
MoS_2	40.44	34.60	5.01	8.6
WS_2	25.80	20.52	6.07	11.05

TABLE 4.4.

Changes in the sulphur content of $NiCo_2S_4$, MoS_2 and WS_2 electrodes after being cathodized at 500 mA/cm² current density for 12 hours in NACE solution, in the presence and absence of H_2S at 60° C.

Electrode	Catalyst:FEP (ratio)	Before Test (percent)	After Test	
			with H_2S (percent)	without H_2S (percent)
$NiCo_2S_4$	1 : 1	26.30	10.84	4.68
MoS_2	1 : 0.85	23.58	24.88	23.14
WS_2	1 : 0.85	13.98	16.00	13.60

in the absence of H_2S, $NiCo_2S_4 > WS_2 > MoS_2$

in the presence of H_2S, $MoS_2 > WS_2 > NiCo_2S_4$

The pseudo-exchange current densities calculated for the sulphide catalysts in the same media, given in the Table 4.1, also supports the order outlined above for the hydrogen evolution performance. The pseudo-exchange current for the sulphide catalysts is 15 to 28 times higher than that of EN 42 steel at 25^0 C when tested in the presence of H_2S and 87 to 354 times higher when tested in the absence of H_2S at 25^0 C. It was not possible to estimate the actual exchange current density using an electrochemically active area, because it is difficult, in the absence of transient measurements to ascertain the available surface area used during the hydrogen evolution reaction. Moreover, the surface roughness of the steel has not been measured in this experiment. Though the pseudo-exchange current of EN 42 steel has not been measured at higher temperatures, it is expected that the above relationship will still be valid since the activation energy for the hydrogen evolution reaction on the sulphide catalysts is significantly less than that on the EN 42 steel.

The apparent activation energies given in Table 4.2, for hydrogen evolution reaction on the three sulphides and EN 42 steel electrodes show the following trend,

$$\text{Steel} >> MoS_2 \approx WS_2 > NiCo_2S_4 .$$

The apparent activation energy on the $NiCo_2S_4$ electrode was found to increase, whereas that on the other electrodes decreased in the presence of H_2S.

Sulphur analysis (Table 4.4) on the pre-cathodized $NiCo_2S_4$ electrodes indicated a considerable loss of sulphur. The sulphur content of the MoS_2 and WS_2 electrodes indicated a very little loss after pre-cathodization, either in the presence or absence of H_2S. In terms of stability, the three sulphides may be arranged as follows;

$$MoS_2 \approx WS_2 > NiCo_2S_4$$

The above discussions indicate that MoS_2 electrocatalyst is the most effective for hydrogen evolution reaction, in terms of performance and stability in the presence of hydrogen sulphide. However at this stage it is very difficult to select one catalyst for further studies on the novel method since it is not known to what extent hydrogen permeation will be reduced by this catalyst and by how much general corrosion enhancement will take place. Hence it was decided to study the three sulphide catalysts further.

CHAPTER FIVE

SELECTION OF A SULPHIDE-ELECTRO-CATALYST FOR INHIBITION OF SULPHIDE STRESS CORROSION CRACKING

CHAPTER 5.

SELECTION OF A SULPHIDE-ELECTRO-CATALYST FOR INHIBITION OF SULPHIDE STRESS CORROSION CRACKING.

5.1 Introduction.

The hydrogen evolution performance of the sulphide electro-catalysts, $NiCo_2S_4$, MoS_2 and WS_2 was reported in the previous chapter in terms of current-potential measurements and kinetic parameters. It was concluded that it is necessary to study the characteristic of the sulphide catalysts further, before selecting a catalyst for the inhibition of sulphide stress corrosion cracking. The selection of a catalyst for the proposed method is mainly dependent on two parameters;

(1) The degree of effectiveness of the catalyst to reduce the diffusion of hydrogen, which is formed on the steel surface due to sour corrosion.

(2) The extent to which the catalyst would enhance normal corrosion of the steel, in the event of any damage to the non-conducting, protective top-layer.

Therefore the sulphide-catalyst to be selected should have more activity to reduce the diffusion of the atomic hydrogen effectively, while providing as little as possible enhancement of normal corrosion. Hence the electrocatalyst should have a balance between the two extreme conditions, to be good enough to satisfy the basic requirements of the proposed method.

To evaluate the effectiveness of the three sulphides, $NiCo_2S_4$, MoS_2 and WS_2, in view of the conditions discussed, electrochemical studies were conducted in the following two directions.

(I) Evans diagrams - to predict the corrosion rate of freely corroding steel and a steel partially coated with an active catalyst.

(2) Electrochemical hydrogen diffusion studies (developed by Devanathan and Stachurski[11]) - to assess the reduction in the amount of atomic hydrogen diffusing through a steel membrane, which could give a qualitative assessment of various boundary conditions.

In both experiments a different range of electro-catalysts loadings was used either in the form of electrodes or adherent coating, because it has been shown that when the sulphide catalyst was used as an electrode, the activity for hydrogen evolution depends on catalyst loading[83].

5.2 Evans Diagram - A Graphical Method of Expressing Corrosion Rates.

Evans has developed[98] a graphical method which shows how the corrosion rate, $I_{corr.}$ is dependent on the extent of the polarization of the anodic and cathodic reactions constituting the corrosion reaction. He used the co-ordinates E and I to illustrate how the electrochemical mechanism of corrosion could be applied to a variety of corroding systems. The cathodic and anodic partial reactions constituting the overall corrosion reaction are presented in the 'Evans' diagrams as linear E-I curves that converge and intersect at a point, which defines the corrosion potential $E_{corr.}$ and corrosion current $I_{corr.}$ (Figure 5.1)

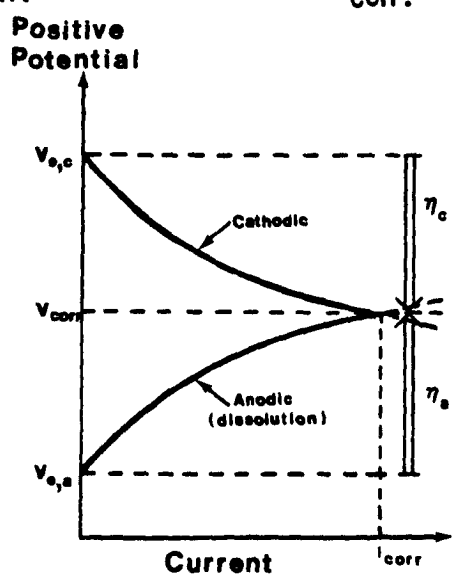

Figure 5.1. Typical Evans diagram employs linear current-potential coordinates. The rates of anodic and cathodic reactions are equal on the corroding metal,[98].

However, it is convenient to use the logarithmic scale for current, in Evans diagrams, i.e. semi-logarithmic curve. Plotting currents in a logarithmic form will enable the identification of electron transfer process and mass transfer process of the anodic and cathodic process. Figure 5.2 gives the semi-logarithmic curve, which shows the roles of exchange current densities, i_0, and gradients ($RT/\alpha F$), for both processes in determining the corrosion rate (the intersection point).

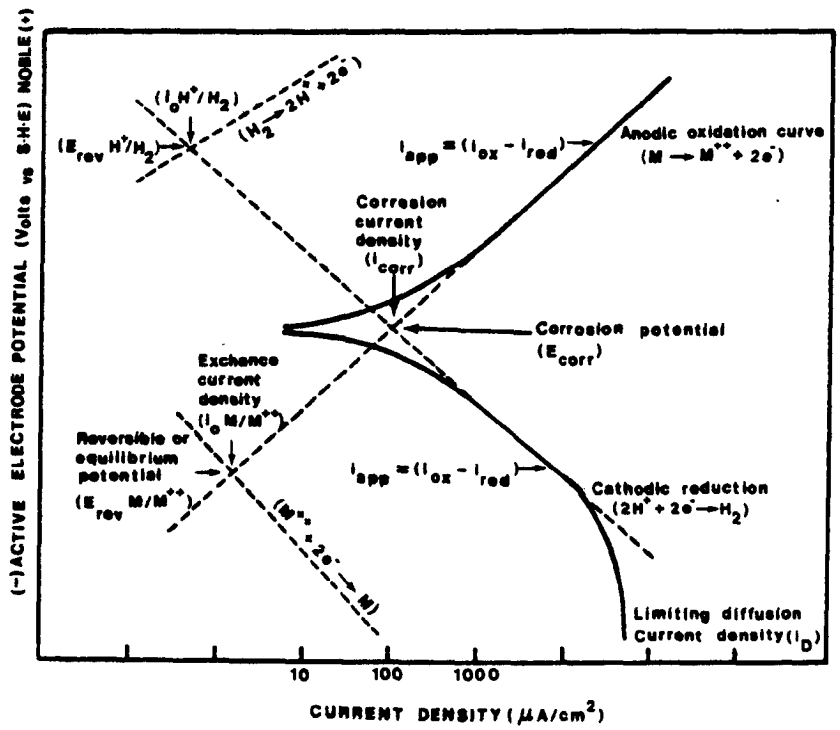

Figure 5.2. Semi-logarithmic curves for the corrosion of a metal in acidic media in which there are two exchange processes involving oxidation of metal and reduction of hydrogen ion. (78)

Figure 5.3 shows, a typical semi-logarithmic Evans diagram for a steel freely corroding and a steel-sulphide couple in acidic medium. It may be noticed that the corrosion current is enhanced when the activity of the cathodic reaction is increased due to connection of a sulphide electrode. Also it should be noted that the corrosion potential of the steel-sulphide couple increased towards the anodic direction. This is due to the high exchange current density and the relatively low overpotential for hydrogen evolution reaction of the sulphide electrode.

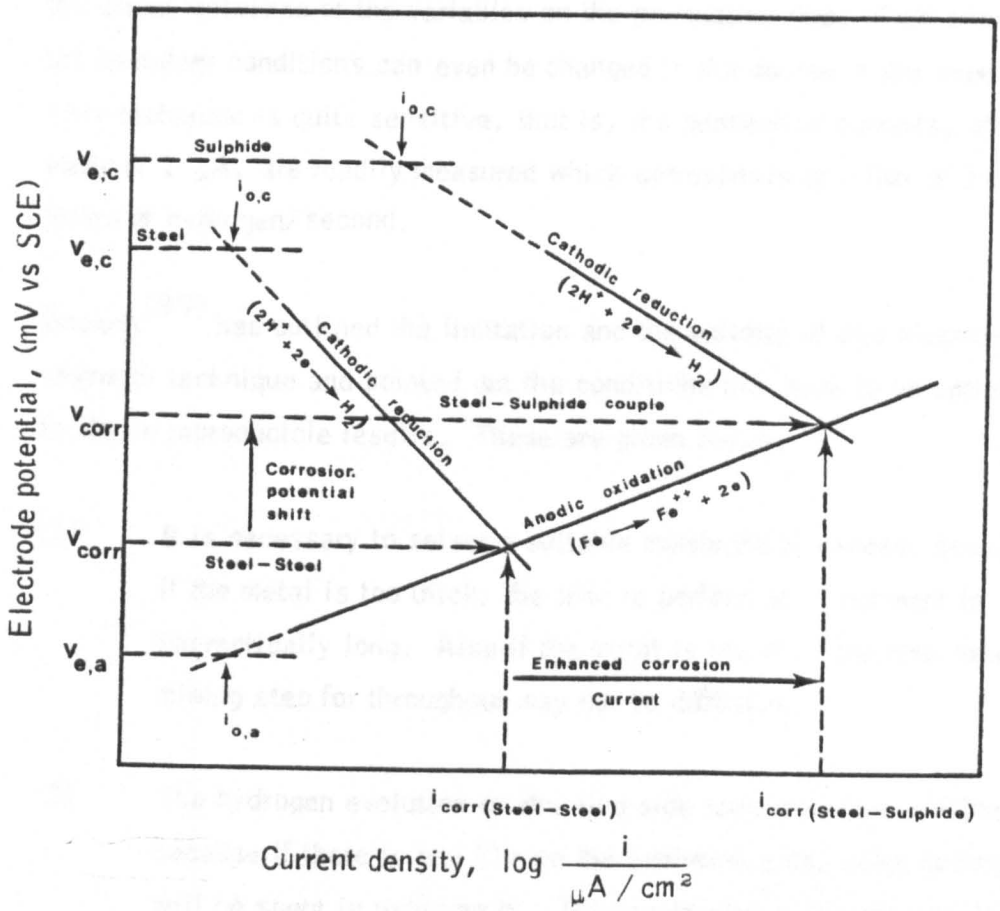

Figure 5.3. Typical semi-logarithmic Evans diagram for freely corroding steel and a steel-sulphide couple in acidic media, (e.g. NACE solution pH = 3).

5.3 An Electrochemical Technique for the Study of Hydrogen Permeation in Iron-Base Alloys.

5.3.1. Advantages and Limitations of the Electrochemical Technique.

An electrochemical technique to study the diffusion of atomic hydrogen through a steel membrane, was developed by Devanathan and Stachurski[11]. In this method, a thin steel membrane is cathodically charged to form hydrogen or subjected to normal corrosion on one side, while the other side is maintained at a constant potential sufficiently anodic to oxidize all of the hydrogen diffusing through. This bi-electrode membrane technique is much more convenient than the conventional gas phase studies for hydrogen permeation studies. The experimental boundary conditions such as solution composition, applied potential, pH, temperature, gas phase composition, etc, can be easily changed. Hence it would be possible to measure

the direct influence of the variables on the permeation rate. Furthermore, the boundary conditions can even be changed in the course of the experiment. This technique is quite sensitive, that is, the permeation currents, of the order of 1 μA, are readily measured which corresponds to a flux of 10^{-11} moles of hydrogen/second.

Bockris[99] has outlined the limitation and the validity of this electrochemical technique and pointed out the conditions that have to be satisfied to obtain reproducible results. These are given below.

(1) It is necessary to select a suitable membrane thickness, because if the metal is too thick, the time to perform an experiment is impractically long. Also if the metal is too thin, the rate-determining step for throughput may not be diffusion.

(2) The hydrogen evolution or charging side should be free of films, because if there is any film on the evolution side, some hydrogen will be spent in reducing it. This could give a descrepancy in calculating diffusion parameters.

(3) Anodic dissolution of the iron on the throughput side could contribute to the hydrogen oxidation current. One solution is to plate a thin layer of adhering palladium onto the anodic side. The palladium film thickness should be appropriate to offer no resistance against the throughput of hydrogen, while protecting the iron from dissolution.

(4) Impurities in the anode compartment electrolyte could interfere or contribute to the hydrogen oxidation current if one tries to measure a diffusion current in the region of 0.1 to 1 $\mu A/cm^2$. Pre-electrolytic purification could be effective in such experiments.

5.3.2. Previous Work on the Technique Using Solution Containing "Cathodic Poisoners".

It has been recognized that a number of chemical species have the effect of increasing the speed of the hydrogen entry into iron, steel and ferritic alloys. The generic terms "Cathodic poison and cathodic promoter are applied to these species because they are said to poison the recombination reaction and therefore promote hydrogen absorption. The cathodic promoters are mainly, phosphorus, arsenic, antimony and bismuth from Group V-A of the periodic table and sulphur, selenium and tellurium from Group VI-A of the periodic table. Other species which increase hydrogen permeation are the halide ions, particularly iodine in acid solution, and cyanide ions in alkaline solution. Radhakirishnan and Shreir[100] investigated the specific effects of Group V and VI element additions to electrolytic hydrogen charging, utilizing the electrochemical technique. The solution in the hydrogen charging compartment was 0.1 N H_2SO_4 and the solution at the anodic side was 0.1 N NaOH. The variation in the steady state permeation current as a function of the charging current density for the various promoters is given in Figure 5.4. Arsenic is the most effective of the poisoners studied.

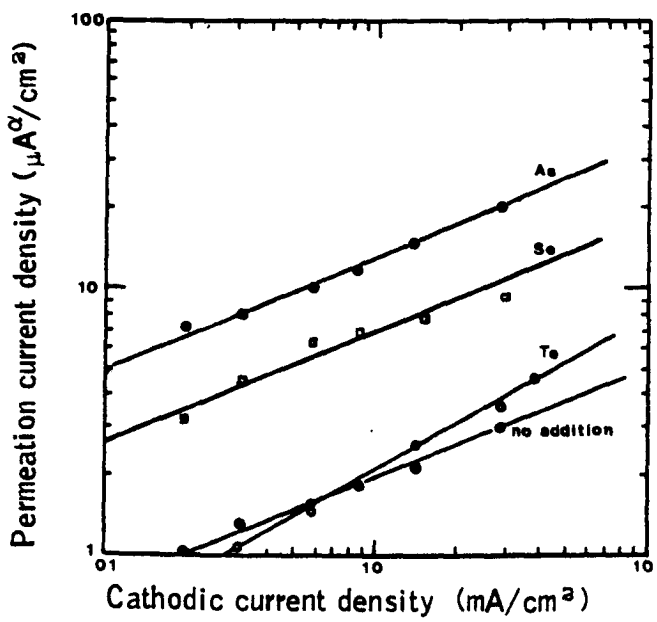

Figure 5.4. Relationship between the applied cathodic charging current density and the steady state permeation current. Shim steel in 0.1 N H_2SO_4 with various additon,[100].

Zakroczniski, et.al[101], studied the effect of the elements phosphorus, arsenic, antimony, sulphur, selenium and tellurium on the permeation of hydrogen through steel in a medium of pH range 1 to 14 as a function of element concentration. They observed that the enhancement of the hydrogen permeation current occurred only under conditions when the hydride of the elements were formed at the cathodic side of the membrane. Furthermore the elements or the anions did not enhance the hydrogen permeation. They concluded that the element hydrides do not modify the hydrogen permeation process, but affect only the velocity, by enhancing the transmission of hydrogen atoms across the electrolyte/metal interface. Furthermore the rate of hydrogen permeation in steel is known to be influenced by composition, and structural defects such as interstitial sites, grain boundaries dislocation etc., which provide hydrogen diffusion paths in the steel. These structural defect paths for hydrogen permeation are enlarged in size or number by the presence of residual or applied tensile stress as a function of temperature.

5.4 Experimental Procedures.

5.4.1. Materials and Method to Construct Evans Diagrams.

5.4.1.1. Materials Preparation.

The co-precipitated $NiCo_2S_4$ and ball-milled MoS_2 and WS_2 were prepared as outlined in section 4.3.1.1. Sulphide electrodes of loading ranging from 17 to 22 mg/cm^2 and 5 to 8 mg/cm^2 were fabricated as described in section 4.3.1.3. The NACE solution,both in the presence and absence of H_2S, recommended for sour environmental studies was used as electrolyte in this study. The three-compartment cell as shown in figure 4.2 was used with the Nafion membrane separating the anodic and cathodic compartments. The use of the Nafion membrane effectively prevents the diffusion of the hypochlorous acid from the anodic to cathodic compartment.

5.4.1.2. The Test Procedure.

The sulphide electrodes were pre-cathodized at a current density of 500 mA/cm^2 for approximately 12 hours at 60^0 C to obtain reproducible results. To avoid a discrepancy due to changes in pH, a fresh NACE solution was used for each polarization study. The electrolyte was purged with nitrogen for 30 minutes before placing the working electrode in the test cell and continuously throughout the experiment. When the current-potential measurements were to be taken in the presence of H_2S, the NACE electrolyte was first purged with N_2 for 30 minutes followed by H_2S for another 30 minutes to ensure proper saturation. The H_2S bubbling was also continued throughout the run.

In taking current-potential measurements it was ensured that only 1 cm^2 of the electrode was exposed to the electrolyte, the current collector lead was masked by wrapping with Teflon tape. A saturated calomel electrode (SCE) was used as a reference electrode. The half cell potentials were corrected for ohmic losses for the complete current range.

Cathodic current-potential measurements were taken for the three sulphides, with two different ranges of catalysts loading, at different temperatures. For EN 42 steel electrodes cathodic and anodic polarization measurements were taken under the same conditions.

5.4.2. Materials and Methods for the Hydrogen Permeation Study.

5.4.2.1. Materials Preparation.

EN 42 steel foil was used as diffusion membrane for this study. The steel was supplied in the form of a foil of thickness 0.15 mm and 50 mm width. Table 5.1 gives the chemical composition of the EN 42 steel. The steel foil was cut into a 40 mm x 40 mm piece and was polished with 600 grade silicon carbide paper until a smooth surface was obtained. The polished membrane was degreased and cleaned ultrasonically in acetone for 30 minutes.

Three different groups of steel membranes were prepared for the hydrogen diffusion studies. The first group of membranes was used as prepared with the sulphide electrodes electrically connected from the beginning of the tests. The second and third groups of membranes were used as sulphide coats applied on the cathodic side of the membranes. The composition of the two sulphide coats are given in Table 5.2. The sulphide coatings were prepared as follows. A weighed amount of sulphide (200 mg) was mixed with the appropriate quantity of FEP dispersion and 3 ml of methanol. The mixture was thoroughly dispersed by means of a magnetic stirrer and painted on to the cleaned steel membrane for the required area and dried with a hair-drier. The prepared membrane was cured at 300^{0} C for 1 hour in a stream of argon. In the case where the sulphide/FEP ratio was high,methanol was not added to the mix during preparation of the coat. The membranes were cured at 300^{0} C for 10 minutes in a stream of argon.

5.4.2.2. Test Cell.

The diagramatic representation of the diffusion test cell used in this study is given in Figure 5.5. Basically this test cell consists of a steel membrane placed between two carefully ground glass flanges, which are bolted together with the aid of aluminium brackets and a water tight seal produced by using O-ring washers. The steel membrane separates the test cell into two similar compartments which are the cathodic and anodic compartments. In the cathodic compartment, hydrogen would be produced either by cathodic charging or natural corrosion reaction, which would diffuse through the steel membrane. The potential on the anodic side of the steel membrane is controlled by a potentiostat at an anodic potential sufficient to oxidize the hydrogen. Hence any hydrogen diffusing through the steel membrane would be oxidized. The anode compartment has a provision to accommodate a saturated calomel electrode, (SCE) as a reference electrode. The reference compartment is drawn into a luggin capillary pointing close to the anodic side of the membrane. A piece of platinum foil is used as a counter electrode to complete the potentiostatic circuit.

TABLE 5.1. Percentage chemical composition of EN 42 Steel.

Carbon	0.75	Silicon	0.30
Manganese	0.65	Sulphur	0.05
Phosphorus	0.05	Nickel	-
Chromium	-	Molybdenum	-
Vanadium	-		

TABLE 5.2. Composition of sulphide coats applied on the cathodic side of the steel membranes used for hydrogen diffusion studies.

Group	Sulphide	Status	Catalyst/FEP
2	$NiCo_2S_4$	as prepared	1 : 1
2	MoS_2	ball-milled	1 : 0.85
2	WS_2	ball-milled	1 : 0.85
3	$NiCo_2S_4$	as prepared	1 : 1.12
3	MoS_2	un-ballmilled	1 : 1.12
3	WS_2	un-ballmilled	1 : 1.12

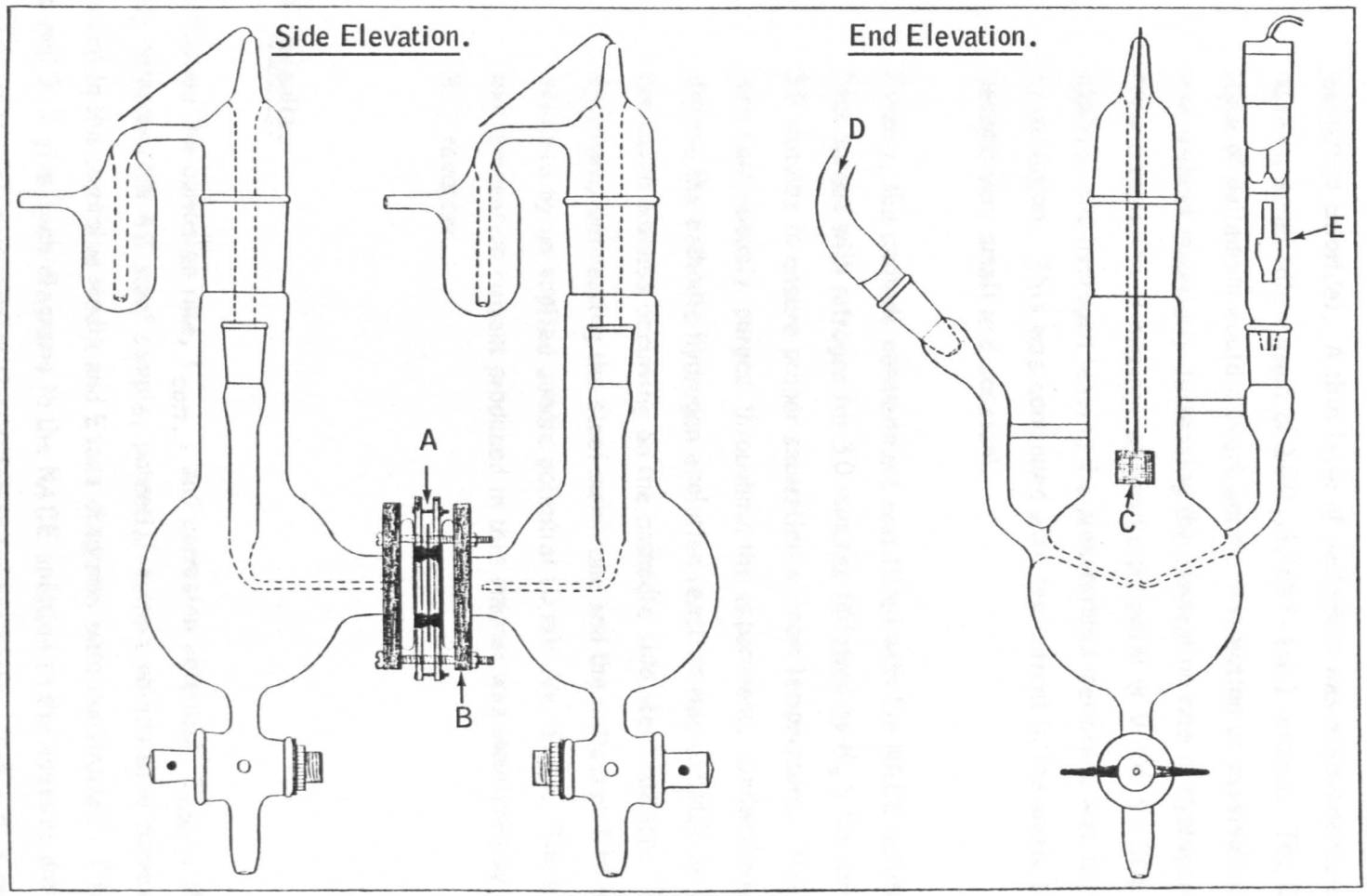

Figure 5.5. Two-compartment hydrogen diffusion cell assembly used in this study. A: Steel membrane placed between O-rings. B: Aluminium bracket. C: Counter Pt electrode. D: Gas inlet. E: Saturated calomel electrode.

5.4.2.3. Test Procedures.

The anode compartment was filled with the pre-electrolyzed 0.1 N NaOH solution containing 2 drops of palladium plating solution (0.1 N palladium chloride). A thin layer of palladium was electrodeposited by passing a cathodic current of 100 $\mu A/cm^2$ for 1 minute. The thin layer of palladium would prevent anodic dissolution or passivation of iron without materially decreasing the permeation rate of hydrogen atoms. After completion of plating, an anodic potential of 0 mV Vs SCE was applied, and hydrogen leaving the presaturated membrane was removed by oxidation. This was continued until the current in the anode circuit became very small and constant.

Finally, the cathode compartment was filled with the NACE solution first purged with nitrogen for 30 minutes followed by H_2S for another 30 minutes to ensure proper saturation at room temperature. The H_2S was continuously purged throughout the experiment. Under these conditions the cathodic hydrogen evolution reaction was dictated by the corrosion process occurring on the cathodic side steel surface. The hydrogen, permeating the steel membrane and the palladium film was oxidized by an applied anodic potential (0 mV Vs SCE). The hydrogen permeation current produced in this manner was monitored by the X-Y recorder.

5.5 Results.

To estimate the corrosion rate, $I_{corr.}$, and corrosion potential, $E_{corr.}$, of the freely corroding EN 42 steel sample, potential-current polarization curves were obtained in the corrosive media and Evans diagrams were constructed. Figures 5.6 and 5.7 give such diagrams in the NACE solution in the absence and presence of H_2S respectively at four different temperatures. Table 5.3 gives the corrosion current and corresponding corrosion potential of the EN 42 steel observed from the points of interception of the anodic and cathodic semi logarithmic polarization curves.

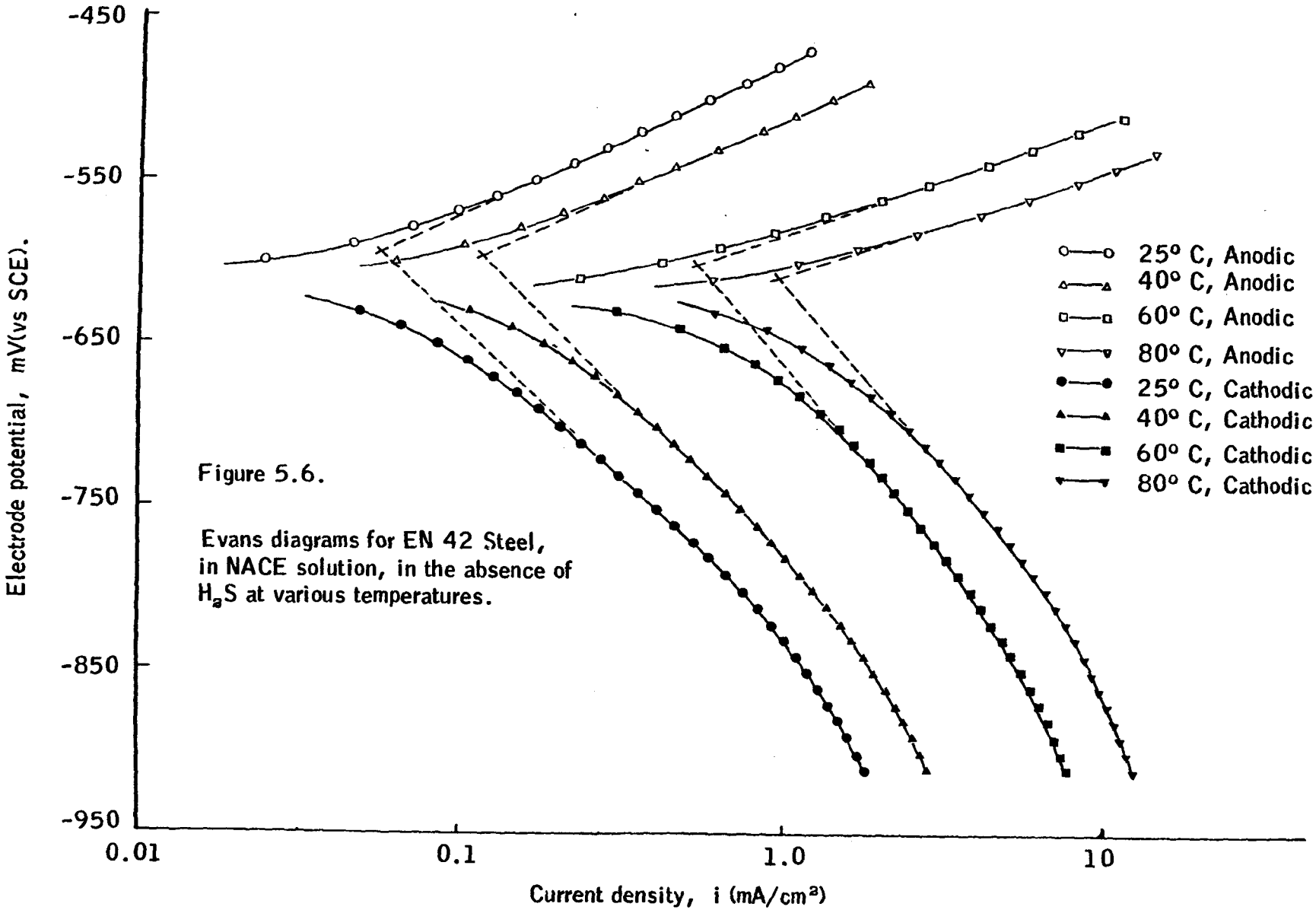

Figure 5.6.

Evans diagrams for EN 42 Steel, in NACE solution, in the absence of H_2S at various temperatures.

Figure 5.7. Evans diagrams for EN 42 steel in NACE solution, in the presence of H_2S, at various temperatures.

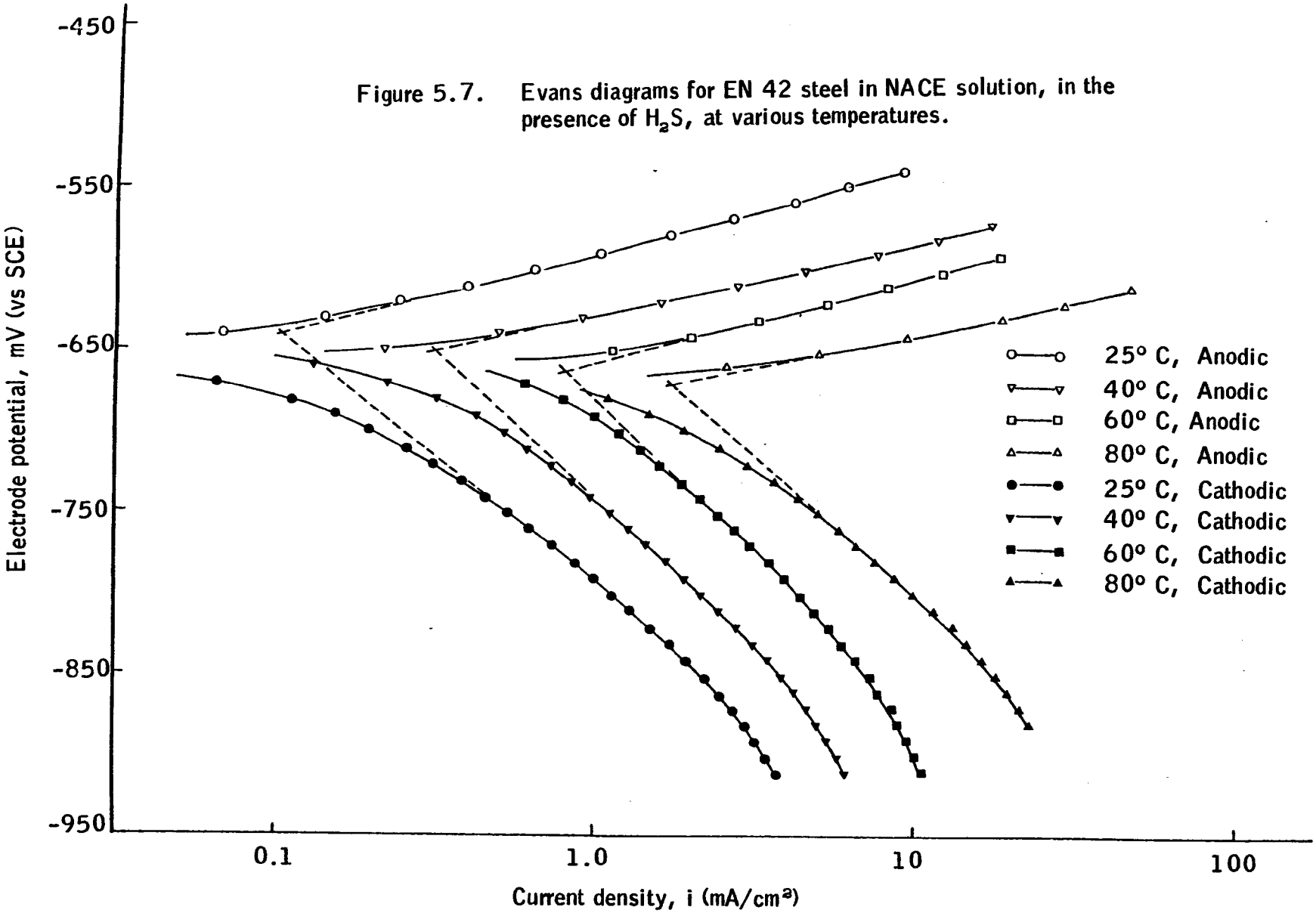

TABLE 5.3.

Corrosion potentials and corresponding currents of freely corroding EN 42 steel in NACE solution, both in the presence and absence of H_2S at various temperature.

Temperature	In the presence of H_2S		In the absence of H_2S	
	Potential (mV vs SCE)	Current (μA)	Potential (mV vs SCE)	Current (μ A)
25° C	-641	105	-594	57
40° C	-651	324	-596	115
60° C	-662	813	-601	535
80° C	-670	1778	-608	951

Evans diagrams, incorporating the anodic polarization curves for EN 42 steel and cathodic polarization cures for the sulphides, ($NiCo_2S_4$ - 17 mg/cm^2 , MoS_2 - 19 mg/cm^2 , WS_2 - 22 mg/cm^2) at different temperatures and in both the presence and absence of H_2S are plotted in Figures 5.8 to 5.15. The corresponding curves for the low loading sulphide electrodes ($NiCo_2S_4$ - 6 mg/cm^2 , MoS_2 - 5 mg/cm^2 , WS_2 - 6 mg/cm^2) and the EN 42 steel are given in Figures 5.16 to 5.19. Table 5.4 summarises the corrosion currents and corresponding potential when the sulphide electrodes are connected to a steel electrode at 25^0 C, 40^0 C, 60^0 C and 80^0 C in the media studied. Table 5.5 gives the ratio of predicted corrosion current between EN 42 steel - sulphide couples and EN 42 steel - EN 42 steel couple at 25^{0}C and 60^0 C in the presence and absence of H_2S.

Figure 5.20 gives the hydrogen diffusion current (oxidation current) through the EN 42 steel membrane protected with the three sulphides, $NiCo_2S_4$, MoS_2 and WS_2, in NACE solution in the presence of H_2S at room temperature. The protection was applied in the form of separate electrodes (catalyst loading, $NiCo_2S_4$ - 18 mg/cm^2 , MoS_2 - 17 mg/cm^2 , WS_2 - 20 mg/cm^2), which were electrically connected to the steel membrane. Also the diffusion current through a similar membrane without any protection in the same media is presented in the Figure 5.20. Figure 5.21 gives the corresponding hydrogen diffusion current when the steel membrane was protected with low loading sulphide electrodes, (catalyst loading, $NiCo_2S_4$ - 6 mg/cm^2 , MoS_2 - 5 mg/cm^2 , WS_2 - 8 mg/cm^2) in the same media.

Figure 5.22 gives the hydrogen permeation current through the EN 42 steel membrane protected with an adherent sulphide coating in NACE solution, in the presence of H_2S at room temperature. The adherent protective coatings were made with the catalyst to FEP ratio of 1 : 0.85 for MoS_2 and WS_2 and 1:1 for $NiCo_2S_4$, as used for the electrodes. The coating was applied in the middle of the steel membrane and the area of the sulphide coat to the exposed steel was kept approximately 1:2. The corresponding diffusion current of the EN 42 steel membrane protected with higher FEP content sulphide coat in the same media is given in Figure 5.23. The denser coating was prepared with the catalyst to FEP ratio of 1:1.12 and cured for 10 minutes at 300^0 C in an argon environment.

Figure 5.8. Evans diagram of anodic polarization of EN 42 steel and cathodic polarization of $NiCo_2S_4$ (17mg/cm²), MoS_2 (19 mg/cm²) and WS_2 (22 mg/cm²) in NACE solution, in the absence of H_2S at 25° C.

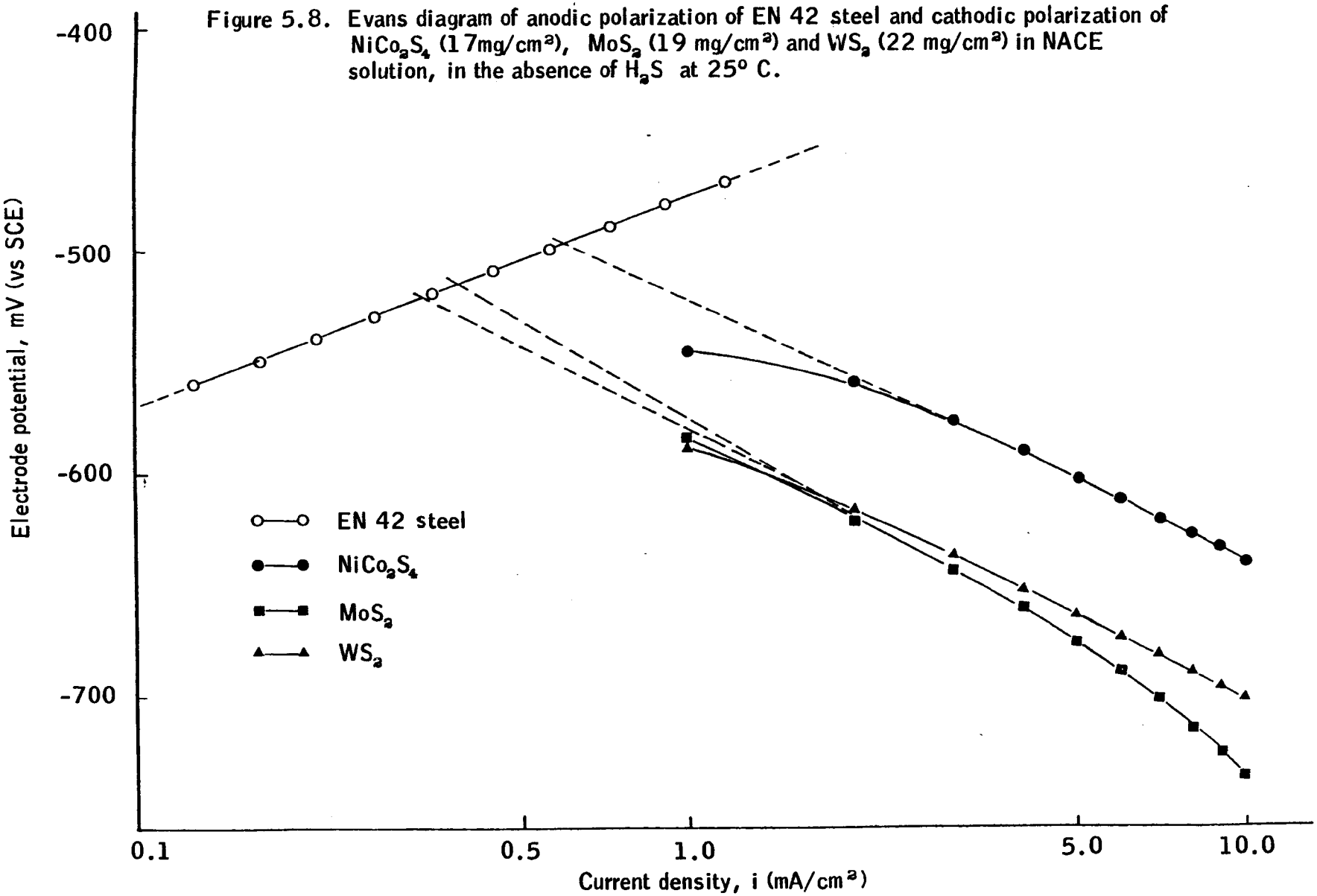

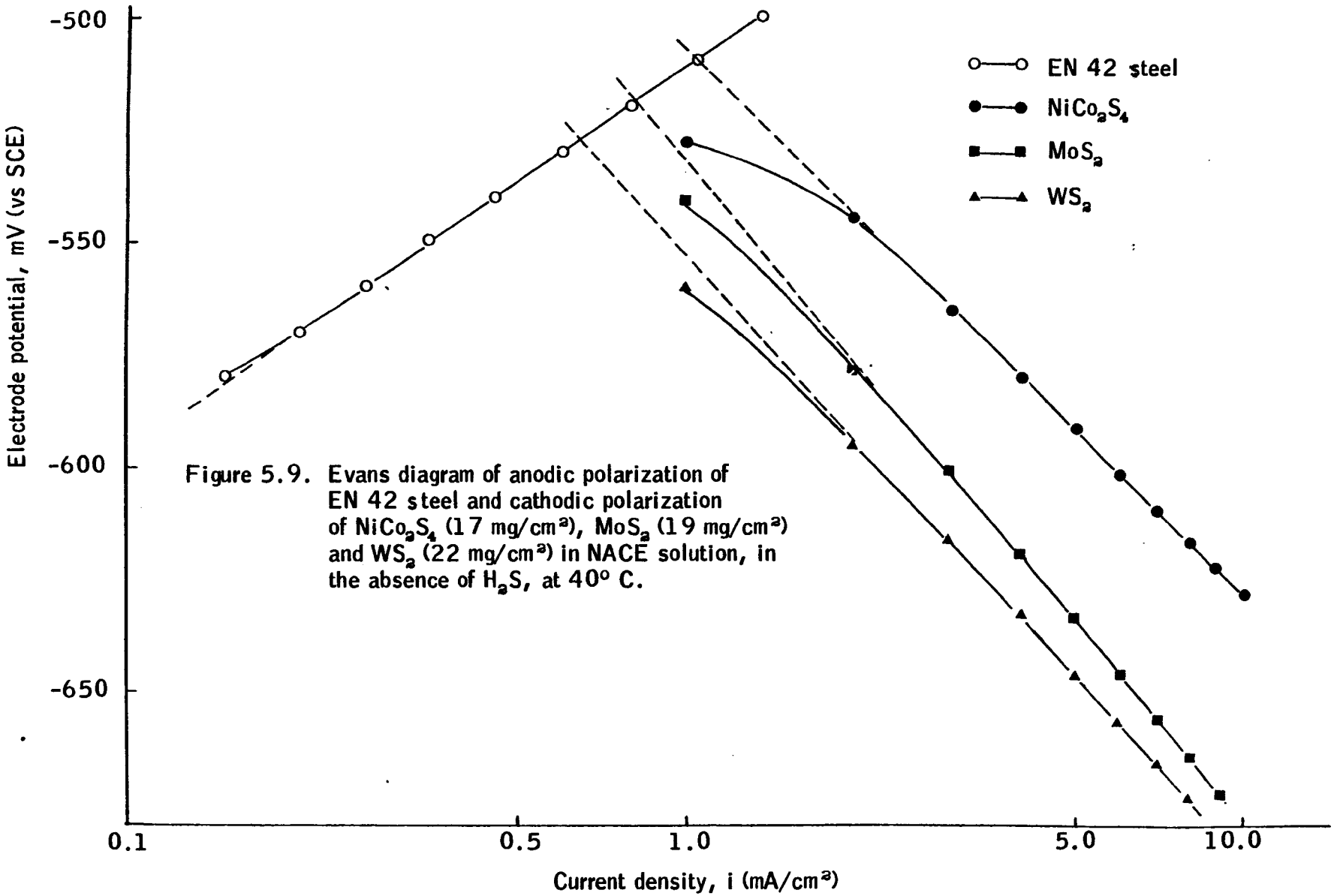

Figure 5.9. Evans diagram of anodic polarization of EN 42 steel and cathodic polarization of $NiCo_2S_4$ (17 mg/cm²), MoS_2 (19 mg/cm²) and WS_2 (22 mg/cm²) in NACE solution, in the absence of H_2S, at 40° C.

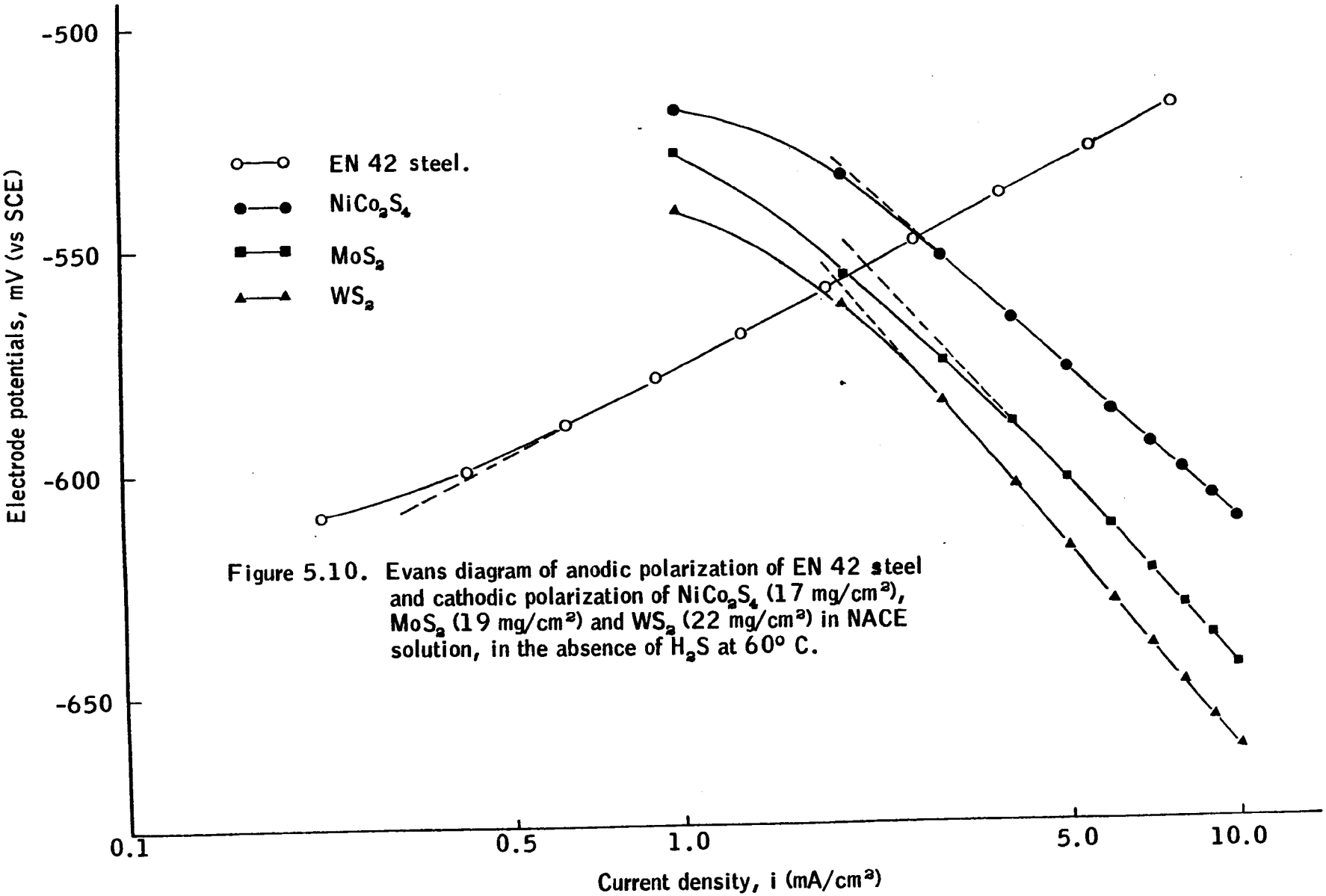

Figure 5.10. Evans diagram of anodic polarization of EN 42 steel and cathodic polarization of $NiCo_2S_4$ (17 mg/cm²), MoS_2 (19 mg/cm²) and WS_2 (22 mg/cm²) in NACE solution, in the absence of H_2S at 60° C.

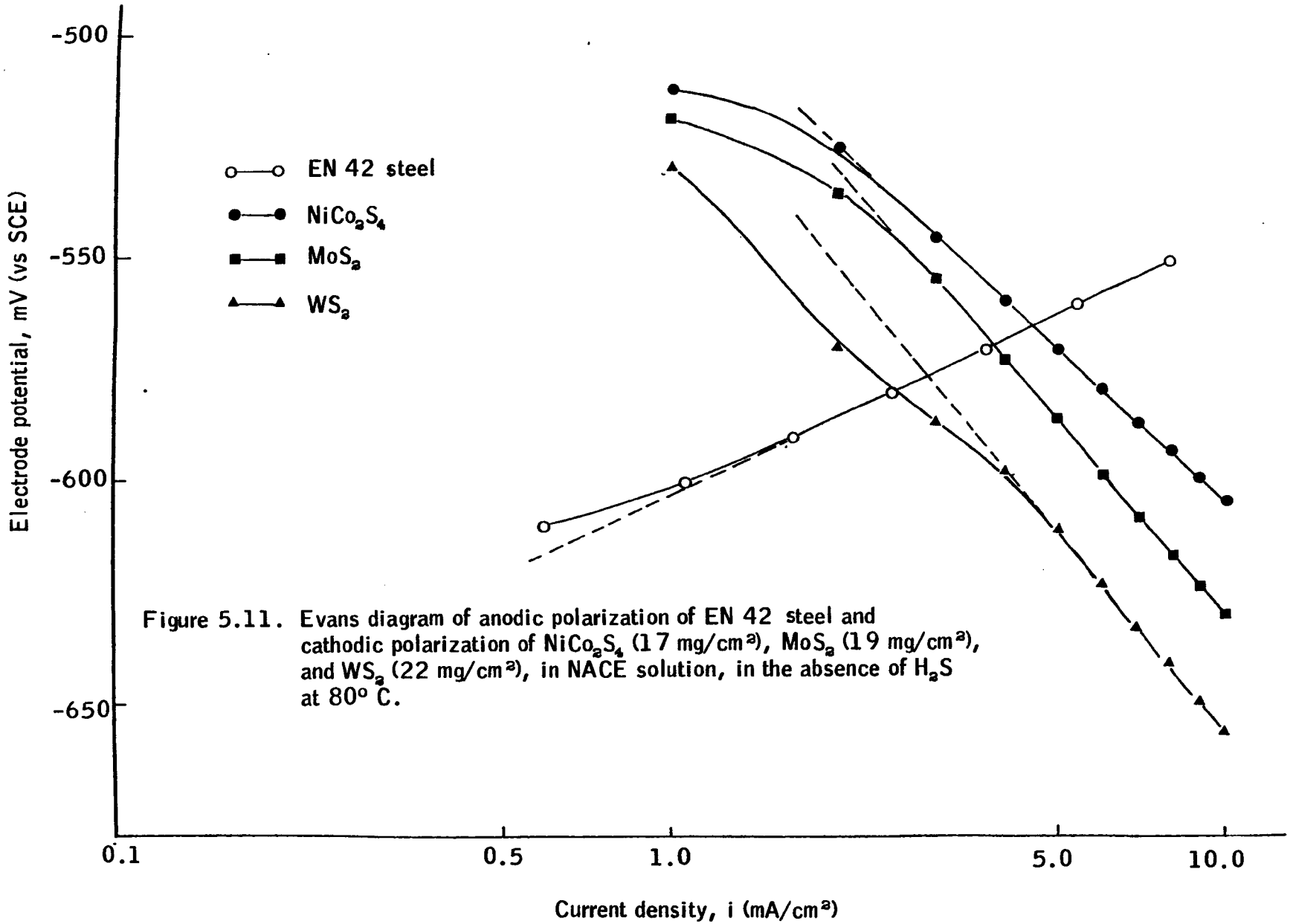

Figure 5.11. Evans diagram of anodic polarization of EN 42 steel and cathodic polarization of $NiCo_2S_4$ (17 mg/cm²), MoS_2 (19 mg/cm²), and WS_2 (22 mg/cm²), in NACE solution, in the absence of H_2S at 80° C.

Figure 5.12. Evans diagram of anodic polarization of EN 42 steel and cathodic polarization of $NiCo_2S_4$ (17 mg/cm²), MoS_2 (19 mg/cm²) and WS_2 (22 mg/cm²) in NACE solution, in the presence of H_2S at 25° C.

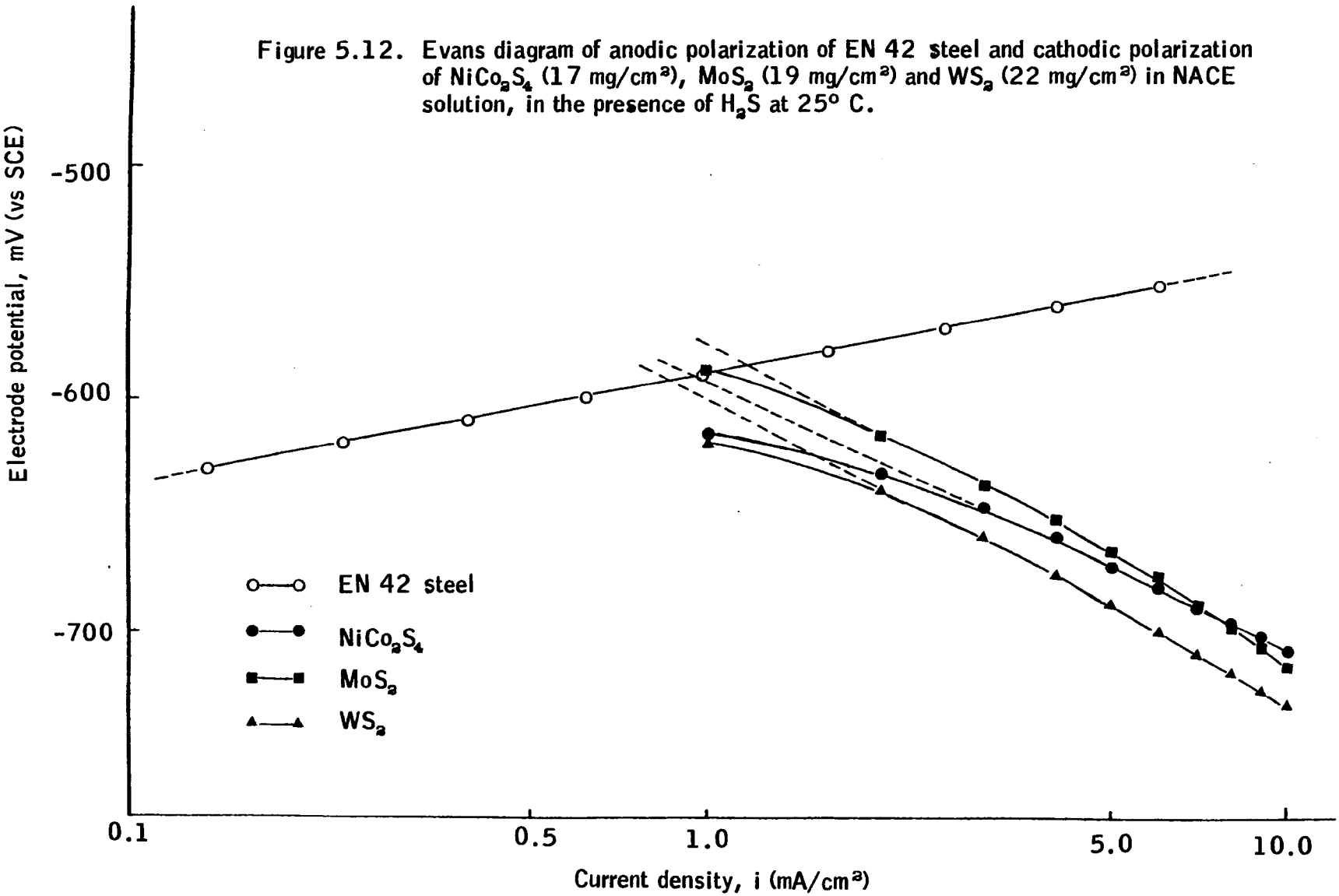

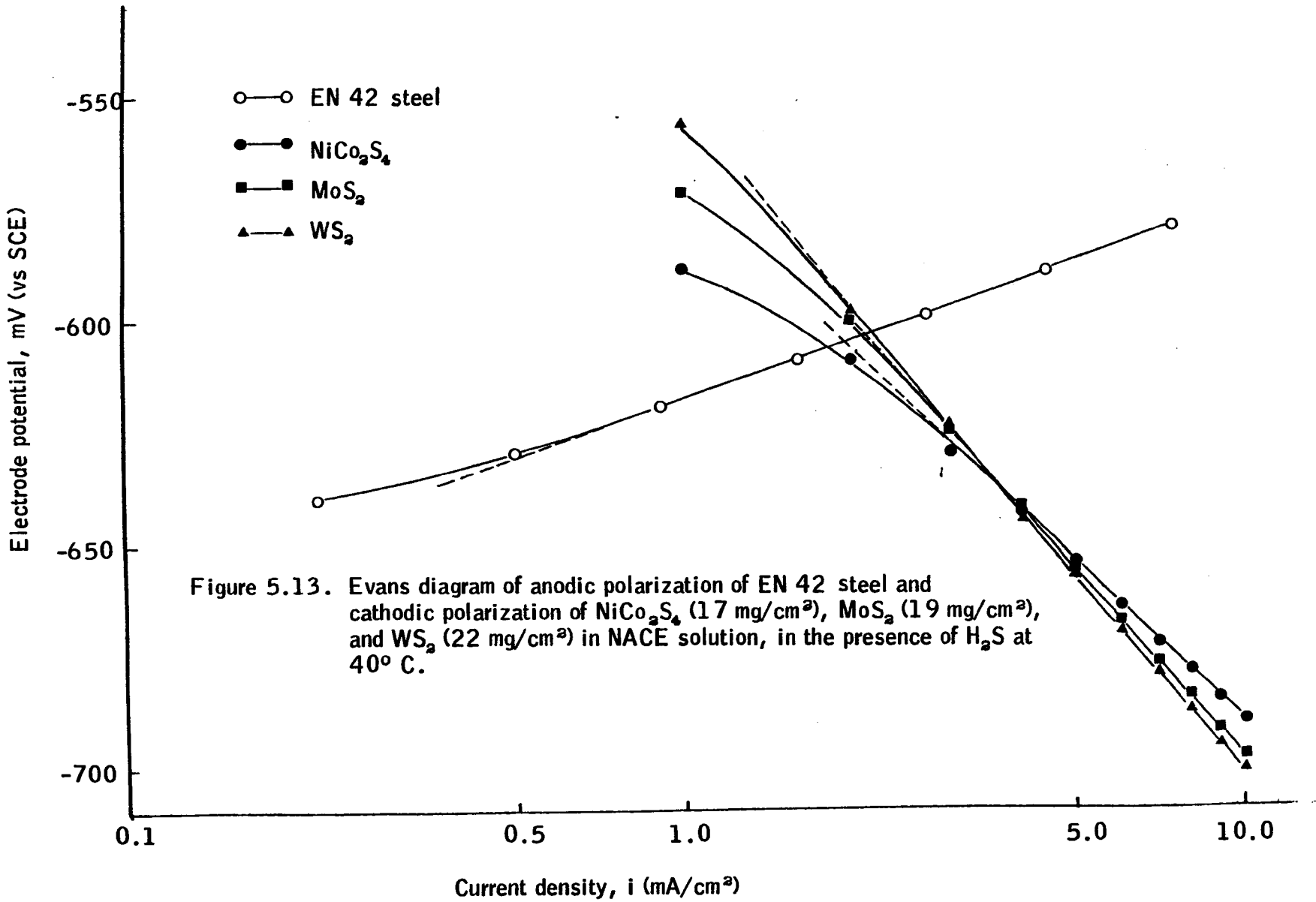

Figure 5.13. Evans diagram of anodic polarization of EN 42 steel and cathodic polarization of $NiCo_2S_4$ (17 mg/cm²), MoS_2 (19 mg/cm²), and WS_2 (22 mg/cm²) in NACE solution, in the presence of H_2S at 40° C.

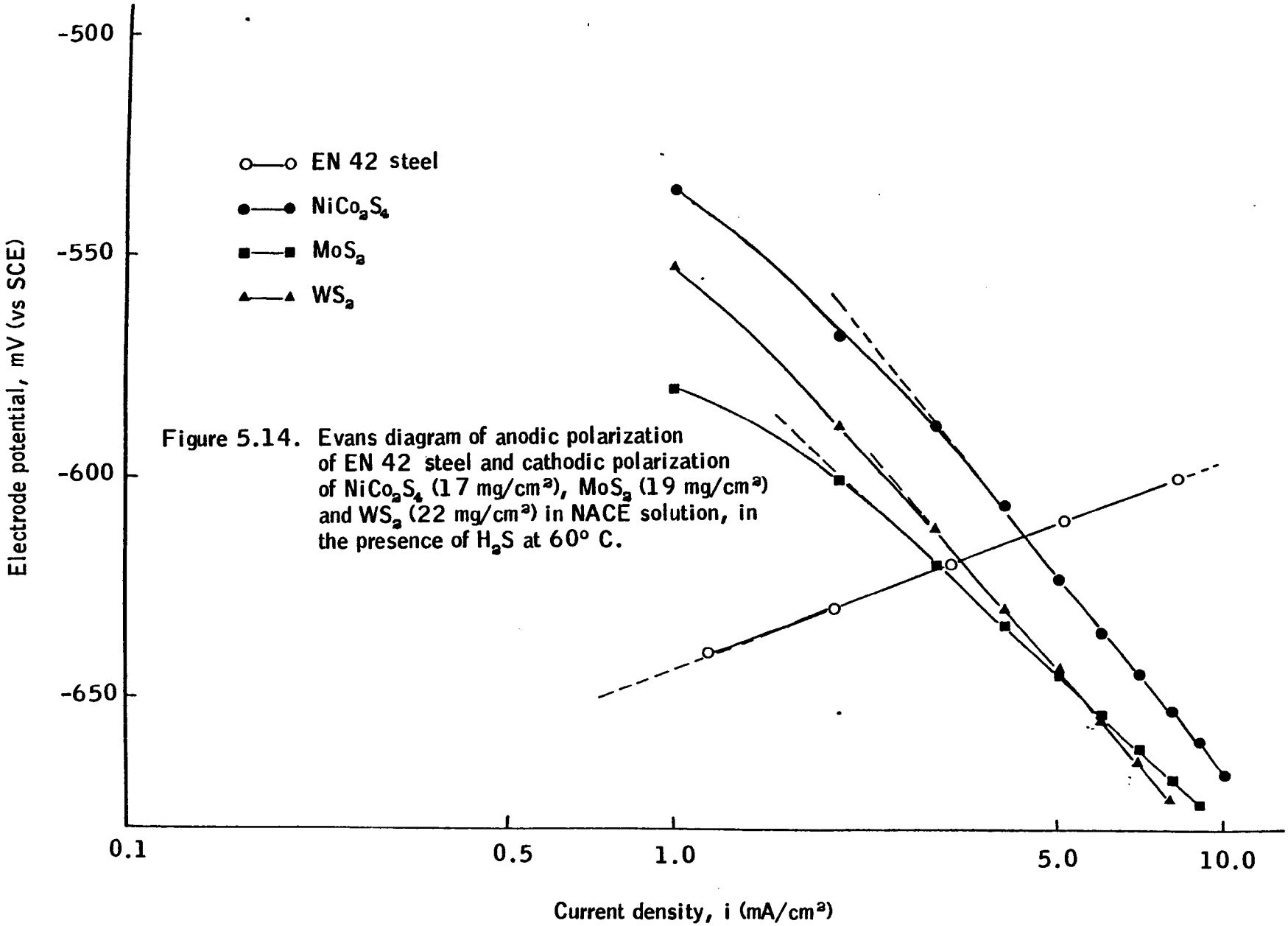

Figure 5.14. Evans diagram of anodic polarization of EN 42 steel and cathodic polarization of $NiCo_2S_4$ (17 mg/cm²), MoS_2 (19 mg/cm²) and WS_2 (22 mg/cm²) in NACE solution, in the presence of H_2S at 60° C.

Figure 5.15. Evans diagram of anodic polarization of EN 42 steel and cathodic polarization of $NiCo_2S_4$ (17 mg/cm²), MoS_2 (19mg/cm²), and WS_2 (22 mg/cm²) in NACE solution in the presence of H_2S at 80° C.

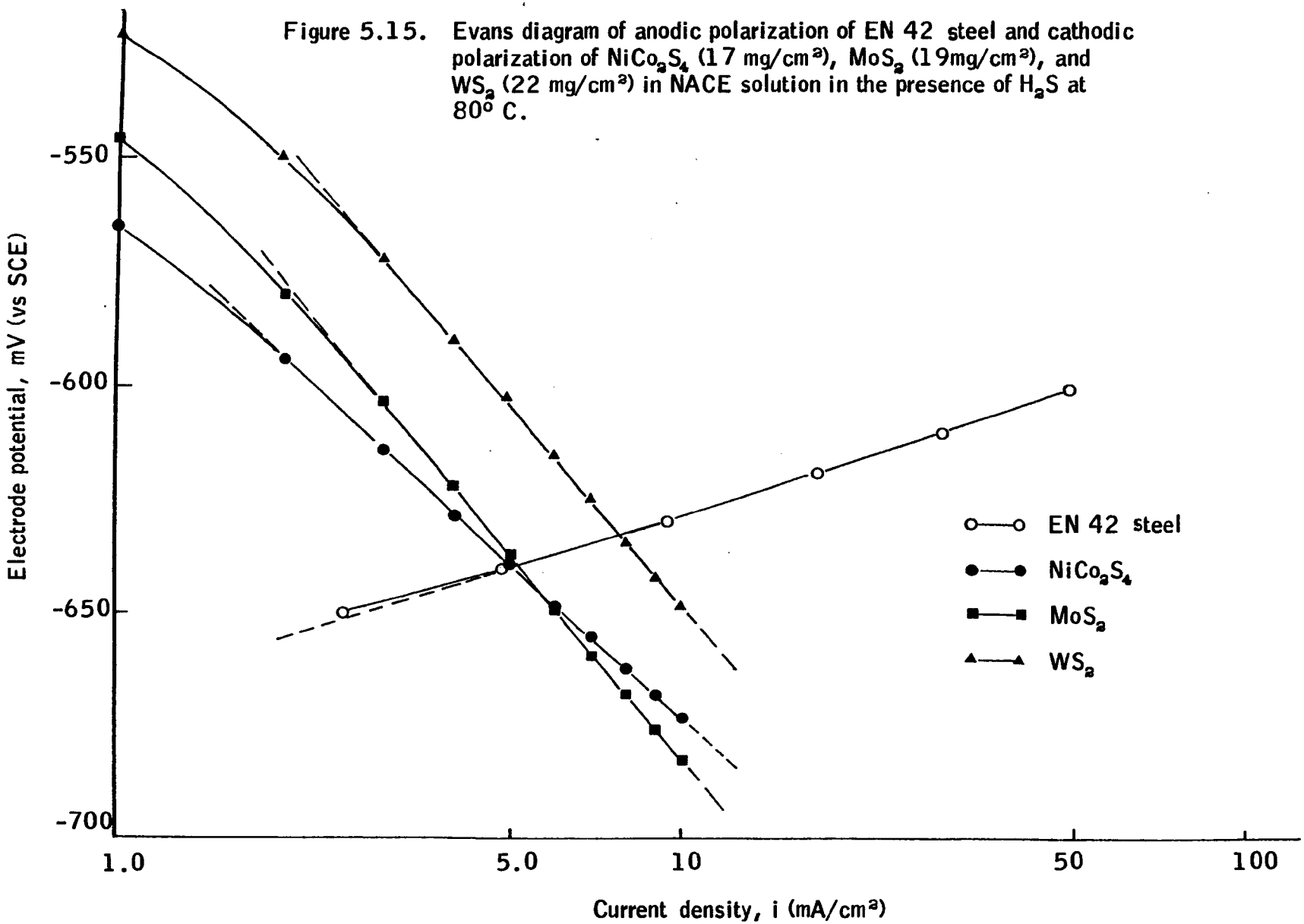

Figure 5.16. Evans diagram of anodic polarization of EN 42 steel and cathodic polarization of $NiCo_2S_4$ (6 mg/cm²), MoS_2 (5 mg/cm²) and WS_2 (6 mg/cm²) in NACE solution, in the absence of H_2S at 25° C.

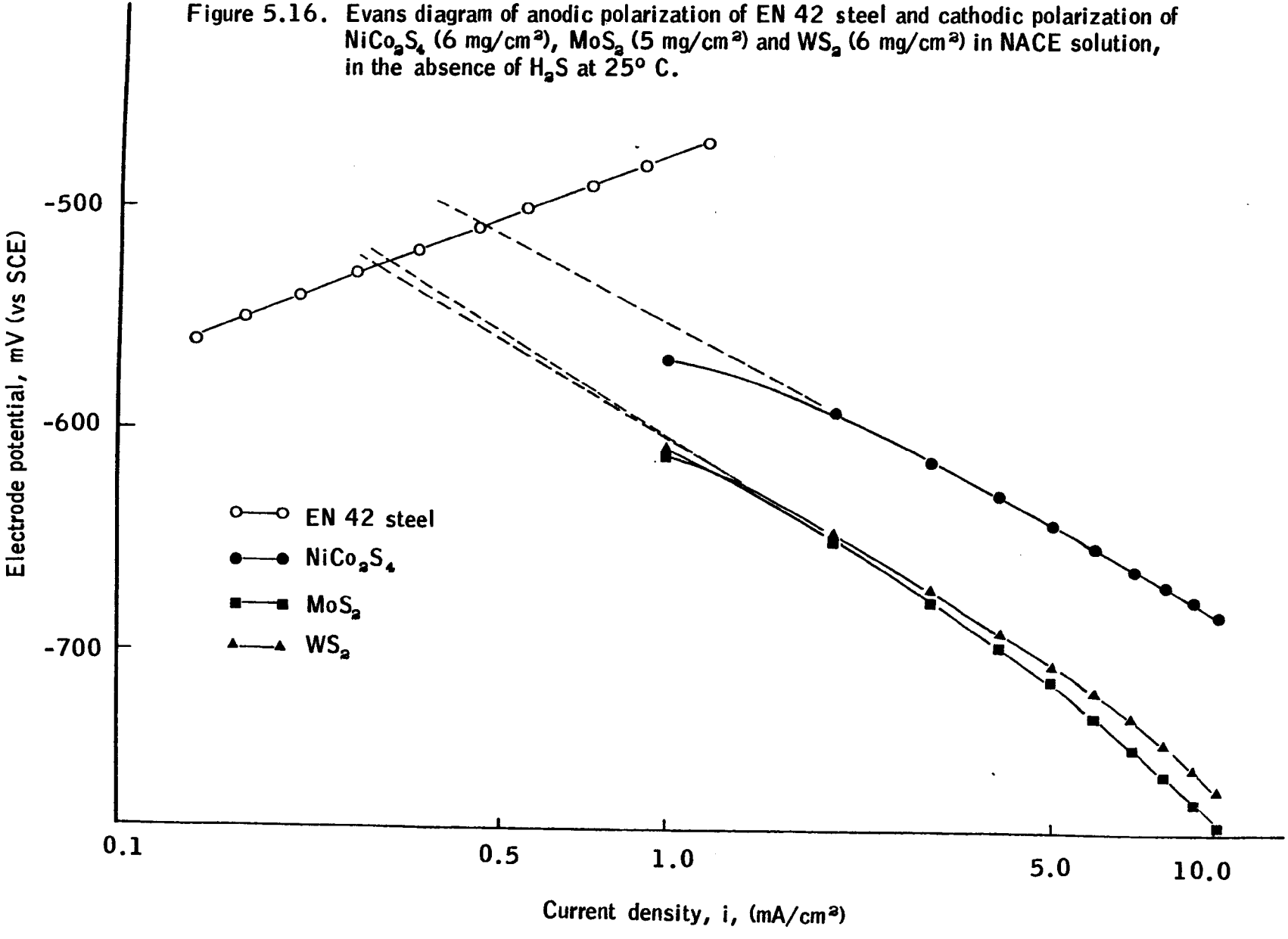

Figure 5.17. Evans diagram of anodic polarization of EN 42 steel and cathodic polarization of $NiCo_2S_4$ (6 mg/cm²), MoS_2 (5 mg/cm²), and WS_2 (6 mg/cm²) in NACE solution, in the absence of H_2S at 60° C.

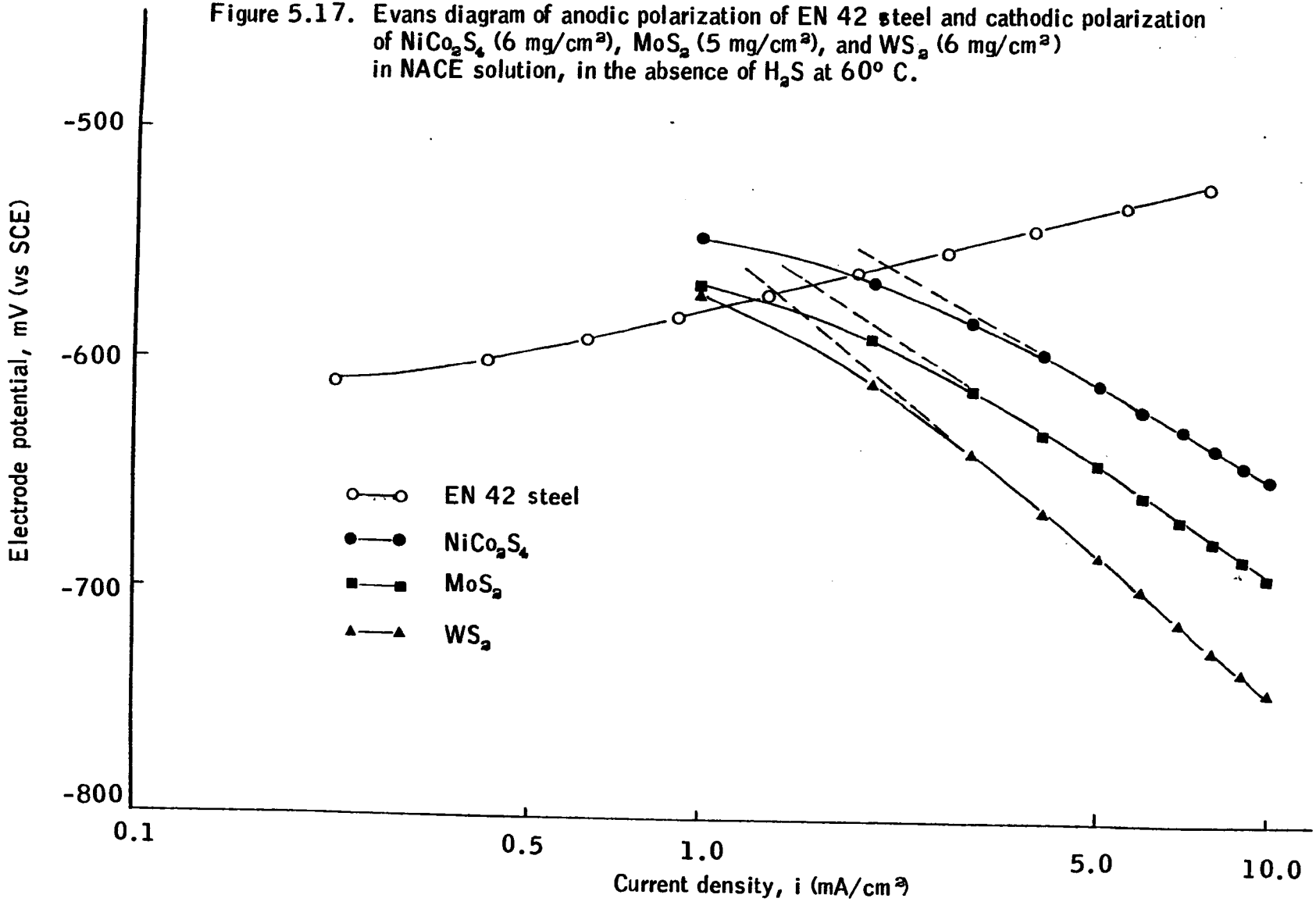

Figure 5.18. Evans diagram of anodic polarization of EN 42 steel and cathodic polarization of $NiCo_2S_4$ (6 mg/cm²), MoS_2 (5 mg/cm²) and WS_2 (6 mg/cm²) in NACE solution, in the presence of H_2S at 25° C.

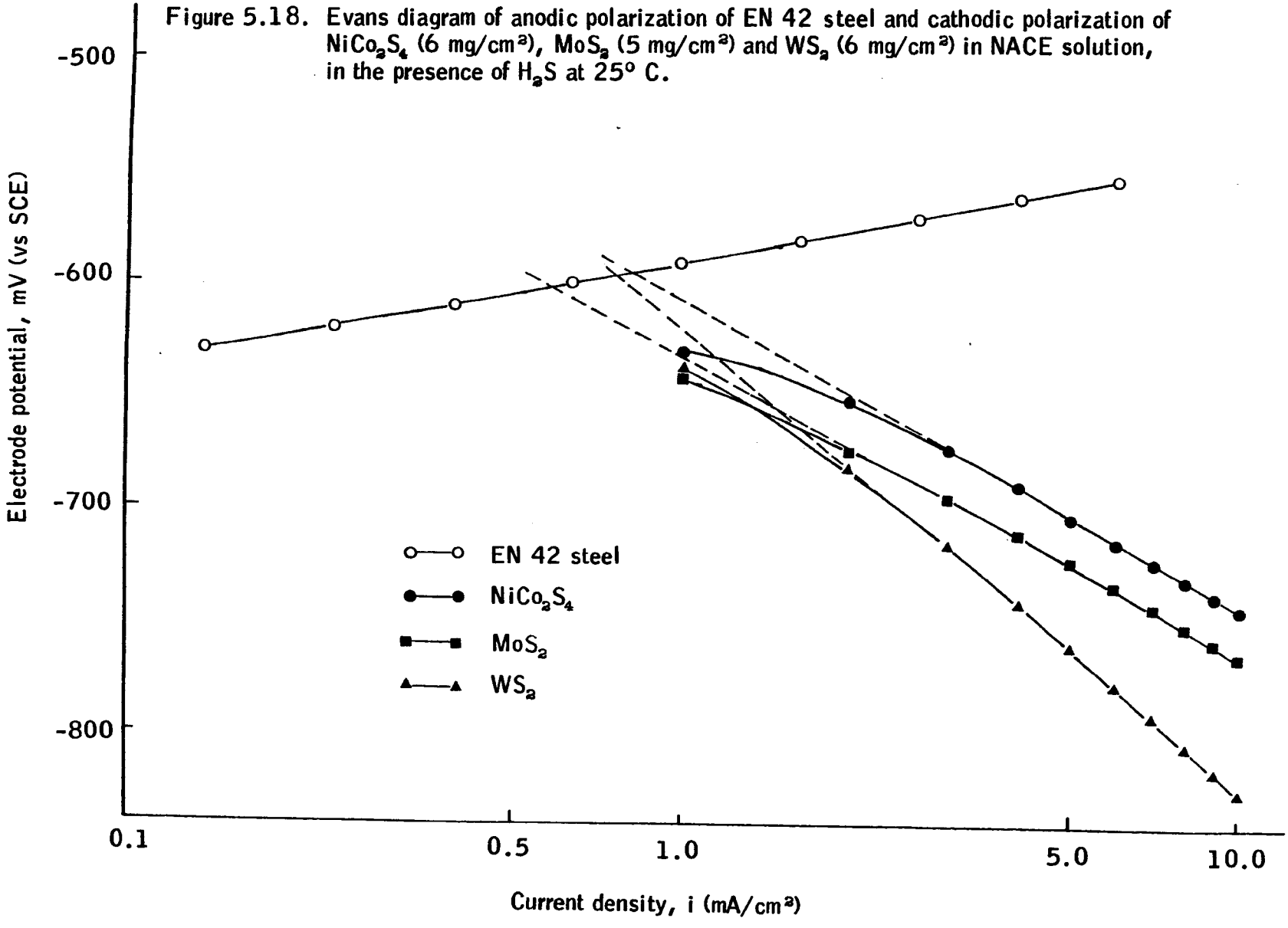

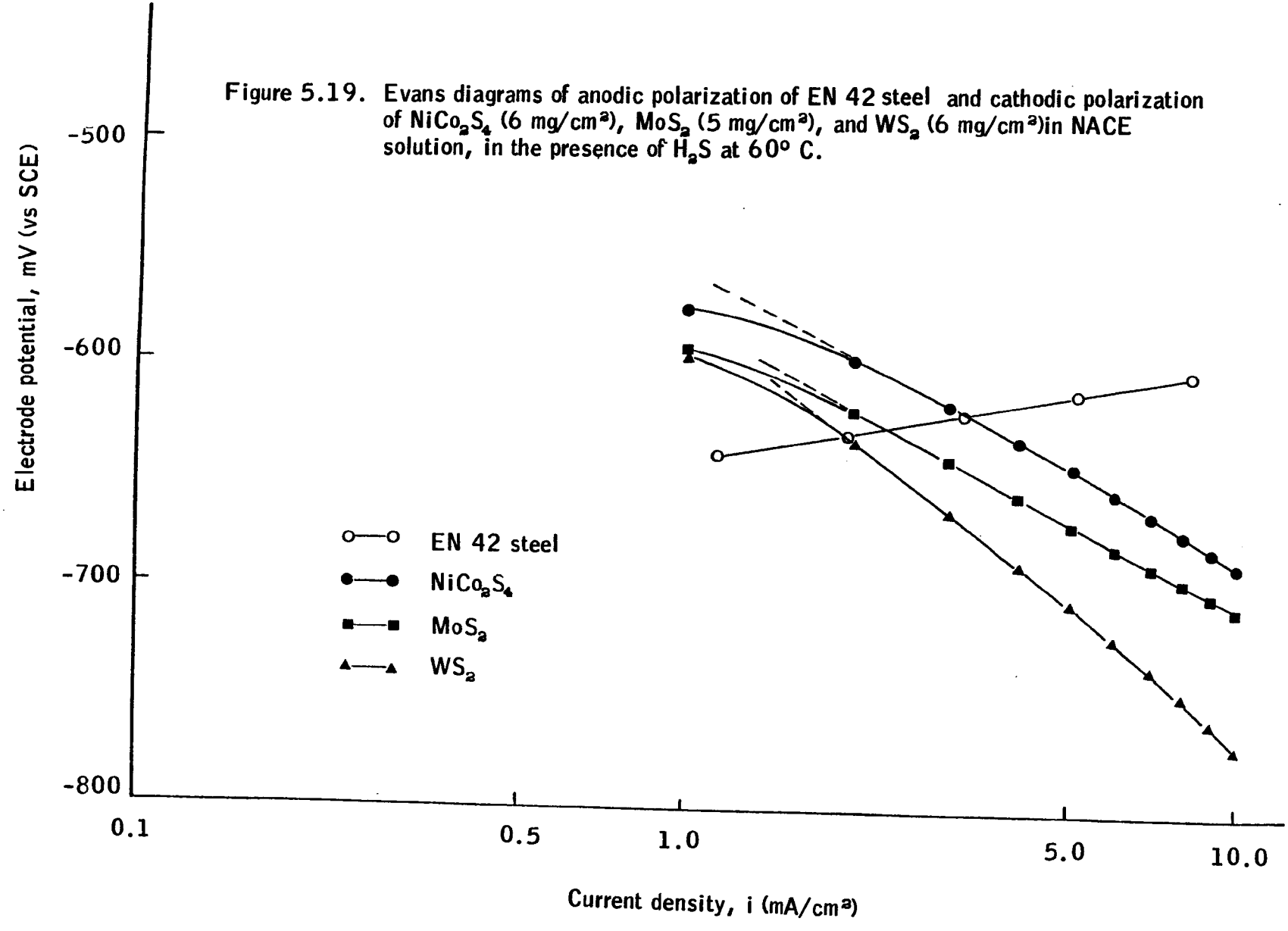

Figure 5.19. Evans diagrams of anodic polarization of EN 42 steel and cathodic polarization of $NiCo_2S_4$ (6 mg/cm²), MoS_2 (5 mg/cm²), and WS_2 (6 mg/cm²)in NACE solution, in the presence of H_2S at 60° C.

TABLE 5.4. The predicted corrosion protentials and corresponding currents when the $NiCo_2S_4$, MoS_2 and WS_2 electrodes are connected to the EN 42 steel at various temperatures in NACE solution, in the presence and absence of H_2S.

Temp.	Steel + $NiCo_2S_4$ (17 mg/cm²)				Steel + MoS_2 (19 mg/cm²)				Steel + WS_2 (22 mg/cm²)			
	Absence of H_2S		Presence of H_2S		Absence of H_2S		Presence of H_2S		Absence of H_2S		Presence of H_2S	
	(mV)	(μA)	(mV)	(μA)	(mV)	(μA)	(mV)	(μA)	(mV)	(μA)	(mV)	(μA)
25° C	-494	600	-588	950	-514	395	-584	1180	-520	320	-593	850
	-508	460	-594	815	-526	298	-602	585	-524	315	-598	765
40° C	-509	1060	-606	1950	-517	850	-604	2095	-527	627	-604	2160
60° C	-548	2780	-612	4400	-554	2220	-621	3100	-559	1930	-619	3350
	-556	2110	-620	3250	-504	1550	-626	2300	-568	1350	-630	1910
80° C	-564	4525	-639	5000	-569	3780	-632	5200	-575	2910	-639	7800

Note: (1) Second figures for 25° C and 60° C are for catalyst loading of $NiCo_2S_4$, 6 mg/cm²; MoS_2, 5 mg/cm²; and WS_2, 8 mg/cm².

(2) Potentials, mV are values measured with reference to saturated electrode, (SCE).

TABLE 5.5.

Ratio of predicted corrosion current between EN 42 steel-sulphide couple/freely corroding EN 42 steel in NACE solution, in the presence and absence of H_2S.

Corrosion couple	Temperature 25° C		Temperature 60° C	
	Absence of H_2S	Presence of H_2S	Absence of H_2S	Presence of H_2S
EN 42 - $NiCo_2S_4$ (17 mg/cm²)	10.5	9.04	5.2	5.4
EN 42 - $NiCo_2S_4$ (6 mg/cm²)	8.07	7.10	3.94	3.99
EN 42 - MoS_2 (19 mg/cm²)	6.92	11.2	4.14	2.89
EN 42 - MoS_2 (5 mg/cm²)	5.22	5.57	3.81	2.82
EN 42 - WS_2 (22 mg/cm²)	5.61	8.09	3.60	4.12
EN 42 - WS_2 (8 mg/cm²)	5.52	7.28	2.52	2.37

Figure 5.20. Effect of connecting Teflon bonded sulphide electrodes on the hydrogen permeation current through EN 42 steel membrane in NACE solution, in the presence of H_2S at room temperature.

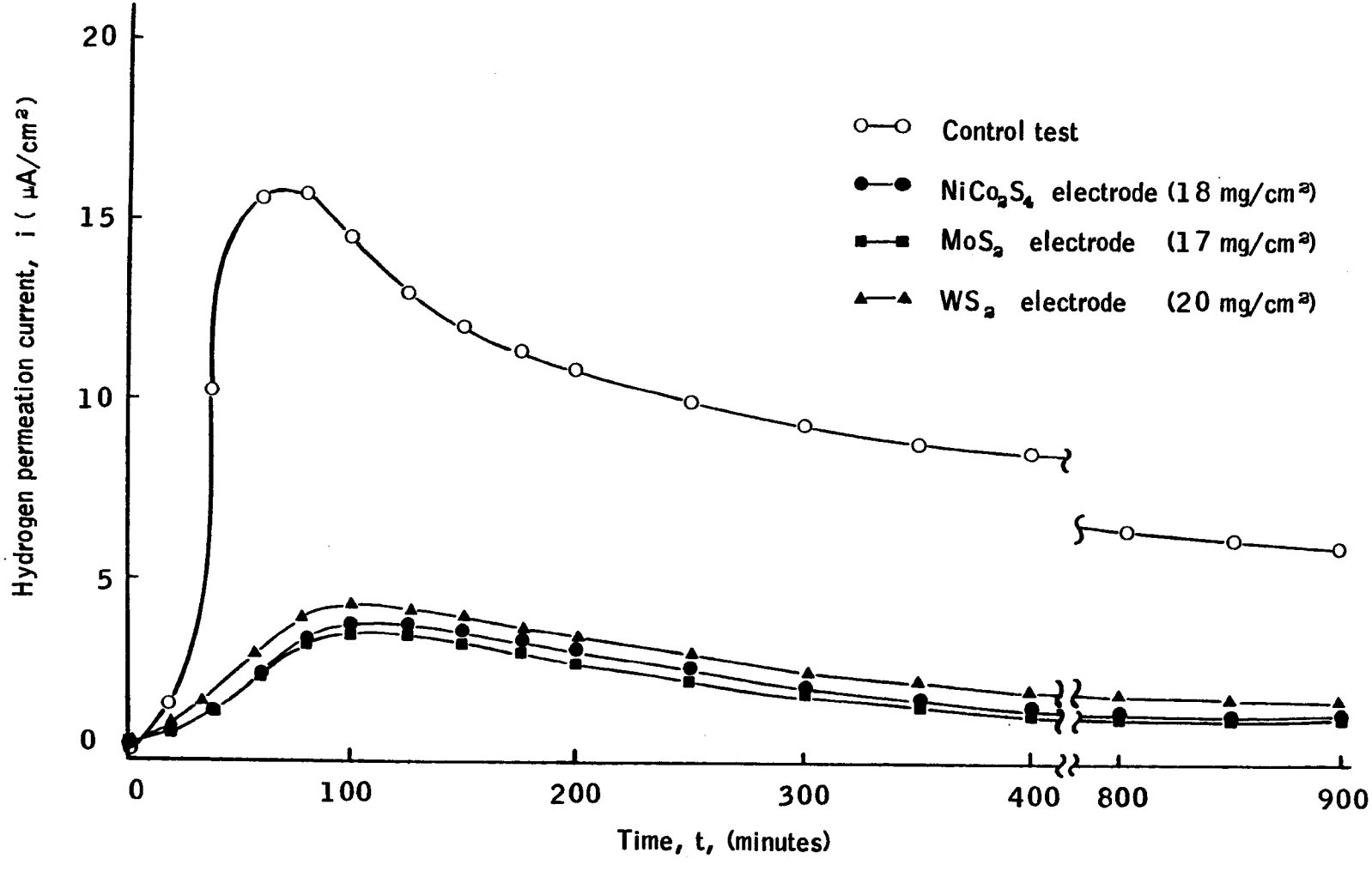

Figure 5.21. Effect of connecting Teflon bonded sulphide electrodes on the hydrogen permeation current through EN 42 steel membrane in NACE solution, in the presence of H_2S at room temperature.

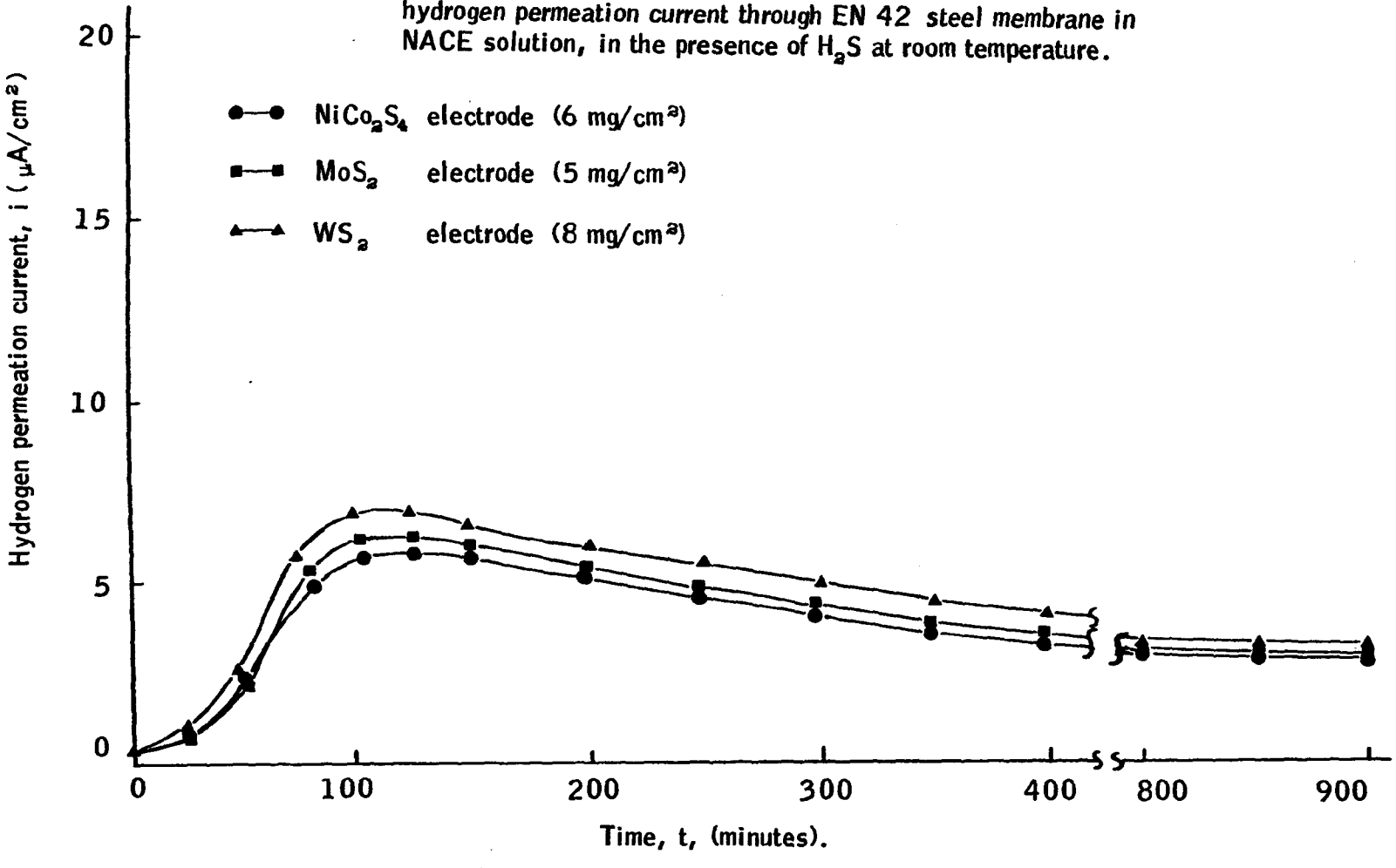

Figure 5.22. Effect of adherent sulphides coating (MoS_2 and WS_2 are ball-milled) on the hydrogen permeation current through EN 42 steel membrane in NACE solution, in the presence of H_2S at room temperature.

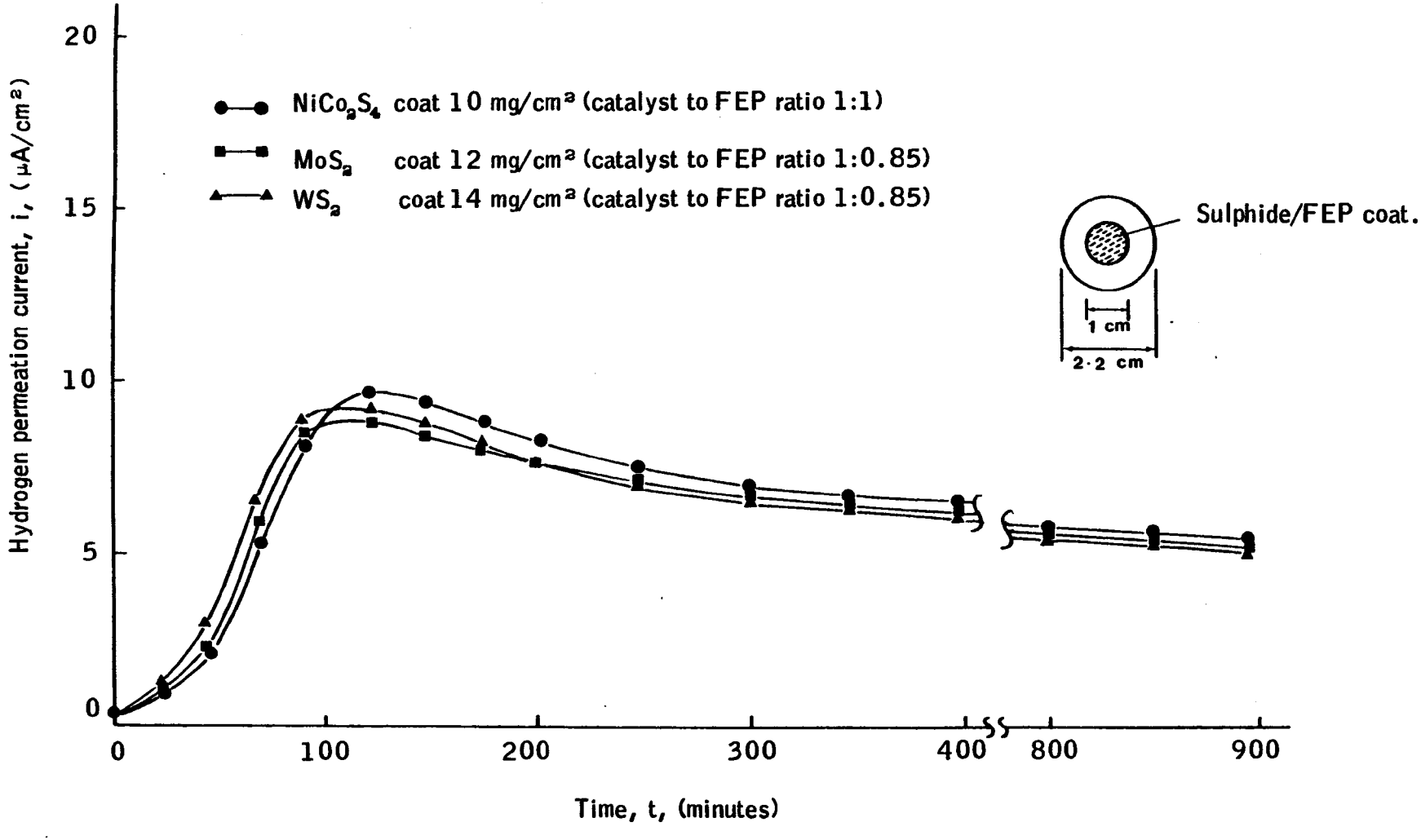

Figure 5.23. Effect of adherent sulphide coating (MoS_2 and WS_2 are unball-milled) on the hydrogen permeation current through EN 42 steel membrane in NACE solution, in the presence of H_2S at room temperature.

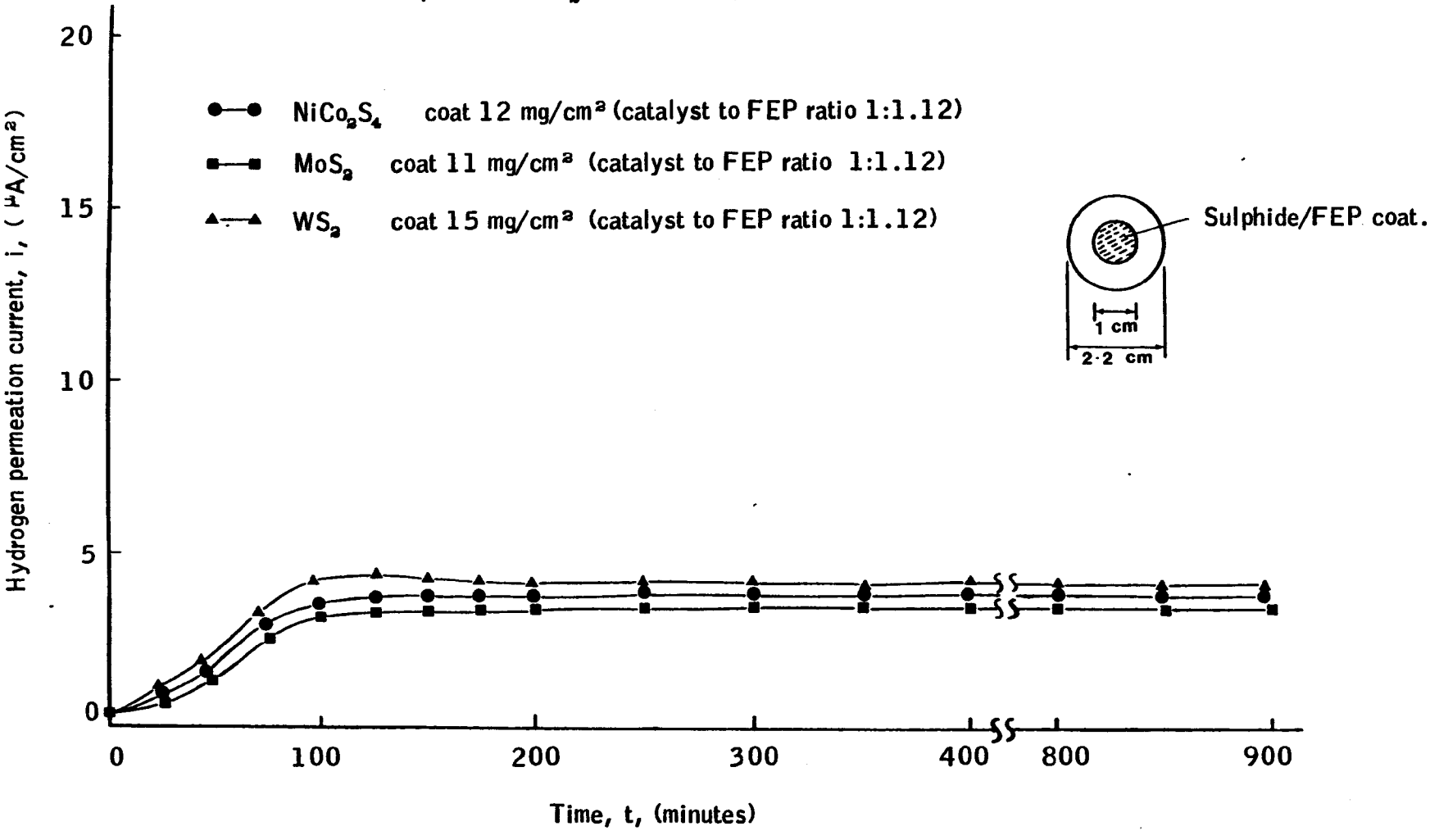

5.6 Discussion.

The Evans diagrams have been constructed to predict, the corrosion current, $I_{corr.}$ and corresponding corrosion potential, $E_{corr.}$, for freely corroding steel and steel coupled with sulphide electrodes. The corrosion current, calculated from the Figures 5.6 and 5.7 shows (Table 5.3) that the current increases considerably with increasing temperature. Particularly when the temperature increases from 25° C to 80° C the corrosion current increases about 18 times regardless of whether H_2S was present or not. Also the corrosion potentials became more cathodic with increasing temperature both in the presence and absence of H_2S. Furthermore the corrosion potentials were more cathodic in the presence of H_2S compared to those obtained without H_2S in NACE solution, possibly, due to the shift in the reversible potential of the steel.

Table 5.4 summarises the corrosion current and corresponding potential predicted from the Evans diagrams (Figures 5.8 to 5.19) when the sulphide electrodes were connected to the EN 42 steel in NACE solution, in the presence of H_2S at different temperatures. It shows a considerable increase in corrosion current and corrosion potential, towards anodic direction than when the steel corroding freely. This increase is apparently due to the very high exchange current density and low over-potentials of the sulphide electrodes for the hydrogen evolution reaction. Also this corrosion potential increase towards the anodic direction confirms that the steel electrode was protected against hydrogen attack by the sulphide electrodes in the media studied. Furthermore, it may be seen in the Table 5.3 and 5.4 that as the temperature was increased, the corrosion rate increases in both cases, but at a faster rate in the case of freely corroding steel.

The results in Table 5.4 indicate that there was a significant decrease in corrosion current when the catalyst loading was reduced from 17-22 mg/cm^2 to 5-8 mg/cm^2, although the decrease in the predicted corrosion current was not directly proportional to the decrease in catalyst loading.

The ratios of predicted corrosion currents of various EN 42 steel - sulphide couples with freely corroding steel show (Table 5.5) that the best steel-sulphide couple was EN 42 steel-low loading WS_2 couple. It shows that the predicted corrosion rate was only increased 2.37 times more than the steel corroding freely in NACE solution at 60° C with continuous H_2S bubbling. The EN 42 steel - WS_2 (low loading) couple was significantly better than the EN 42 steel - $NiCo_2S_4$ couple, but was similar to that of the EN 42 steel - MoS_2 couple.

The hydrogen diffusion study on EN 42 steel membrane protected with a sulphide electrode connected electrically, in the presence of H_2S showed (Figure 5.20) that the diffusion current was reduced considerably when the steel membrane was protected. The three sulphide electrodes (catalyst loading, $NiCo_2S_4$ - 18 mg/cm^2 , MoS_2 - 17 mg/cm^2 , WS_2 - 20 mg/cm^2] gave almost the same amount of protection, that is, the maximum diffusion current of 16 μ A/cm^2 in the case of unprotected steel membrane has been reduced by 12 μA/cm^2 to 4 μA/cm^2 when protected. Figure 5.21 shows the corresponding hydrogen diffusion current when the steel membrane is electrically connected with low loading ($NiCo_2S_4$ - 6 mg/cm^2 , MoS_2 - 5 mg/cm^2 , WS_2 - 8 mg/cm^2) sulphide electrodes. It shows that the maximum diffusion currents of the protected steel membranes varied between 5.5 and 7 μA/cm^2 , despite the fact the catalyst loadings were reduced at least by a factor of two. These results indicate that the protection given by the sulphide electrodes were not proportional to the catalyst loading. Probably an effectiveness factor plays a major role in the activity of the Teflon bonded porous electrodes. It may be seen from the results that the three sulphides could be arranged in terms of performance to reduce the hydrogen permeation as follows;

$$NiCo_2S_4 \approx MoS_2 > WS_2$$

Although the hydrogen diffusion studies discussed above show the effectiveness of the proposed method to inhibit the sulphide stress corrosion cracking, the technique used, i.e. connecting a sulphide electrode electrically to the steel membrane, was in contrast to the industrial situation. Hence the sulphide coatings were applied to the steel membranes to simulate the actual situation and the same diffusion studies were carried out. Figure 5.22 shows that when the sulphide coatings were applied partially to the steel membrane, the maximum

diffusion current was not reduced considerably. The protected membranes gave a maximum hydrogen diffusion current of 8 to 9.5 $\mu A/cm^2$, whereas an unprotected membrane gave only 16 $\mu A/cm^2$. It has been found that the sulphide/FEP coatings (catalyst to FEP ratio, 1: 0.85 for MoS_2 and WS_2 and 1:1 for $NiCo_2S_4$) were porous and not properly bonded with the substrate. When the steel membrane coatings were removed and examined under a microscope, corrosion was found under the sulphide/FEP coatings. To overcome this problem a new coating was developed with a higher FEP content and unball-milled sulphides. These coatings were used in the similar hydrogen diffusion experiment to evaluate their effectiveness. The results (Figure 5.23) show that the coats having higher FEP content gave better protection against hydrogen permeation as the sulphide electrode was electrically connected to the corroding steel membrane. Also the coats were dense and better protected the substrate against corrosion. The sulphides coat ability to reduce the hydrogen permeation through the steel membrane could be arranged as follows;

$$MoS_2 \quad > \quad NiCo_2S_4 \quad > \quad WS_2$$

The above discussions and the work discussed in the previous chapter indicate that MoS_2 is the most effective hydrogen evolution electrocatalyst to be selected for further studies to evaluate the effectiveness of the proposed method. Also it is encouraged by the fact that MoS_2 is already available in commercial quantities because of its use as a solid lubricant. Hence it was chosen for further studies without any reservation.

CHAPTER SIX

EVALUATION OF THE PROPOSED PROTECTIVE COAT (MoS_2/FEP) FOR INHIBITION OF SSCC IN STEEL BY CORROSION WEIGHT LOSS TESTS

CHAPTER 6.

EVALUATION OF THE PROPOSED PROTECTIVE COAT (MoS_2/FEP) FOR INHIBITION OF SSCC IN STEEL BY CORROSION WEIGHT LOSS TESTS.

6.1 Introduction.

The corrosion rate of freely corroding EN 42 Steel and EN 42 Steel - sulphides electrode couples were predicted and assessed theoretically by construction of Evans diagrams in the previous chapter. Although this assessment gave valuable information which led to the selection of one sulphide-catalyst, MoS_2 from three, for further studies, it could not reveal information on actual corrosion rate, nature of corrosion products and the effect of the corrosion products on corrosion rate of the steel. Hence it was decided to carry out a series of corrosion weight loss tests to determine the extent of these factors.

There are numerous corrosion standards[102], developed over the years to conduct various types of corrosion experiments relating to different types of corrosion, under laboratory conditions. Laboratory corrosion weight loss tests are mainly classified into four groups;

1) Total immersion test - In this test the metal specimen is totally immersed in a corrosive liquid, where the important factors that influenced the corrosion weight loss are controlled carefully. The total immersion test is mainly used as a control test to determine the corrosion resistance of a new metal or alloy and to assess the quality of any protective coats and other measures.

2) Partial immersion test - In this test the metal specimen is partially immersed in a corrosive liquid to permit corrosion to be evaluated at a liquid-gas interface.

3) Alternative immersion test - In this test the metal specimen is alternatively immersed in a corrosive solution and withdrawn from it in some predetermined cycle. Hence the liquid can be allowed to dry on the sample, showing the effect of the concentration of the liquid, and in addition it permits corrosion products to remain and reach greater concentrations.

4) Spray test - In this test a fog of corrosive liquid comes in contact with the metal test specimen, where the effects of the corrosive liquid and a humid atmosphere are combined.

The total immersion test is selected for this study since this is the only test where the important factors that influence the corrosion weight loss results could be controlled carefully. To aid the experimental study, the important factors influencing the laboratory total-immersion test are discussed briefly.

6.2. Factors Influencing Total Immersion Tests

6.2.1. Specimens and their Preparation

The size and shape of specimen to be selected normally varies with the purpose of the test, the nature of the materials to be tested and the testing apparatus to be used. A proper ratio between the area of the specimen and the volume of the testing solution dominates the size of the specimen to be selected. If the ratio is too large, the corrodent is quickly exhausted and there is a build-up of corrosion products. The corrosion products can either accelerate or inhibit corrosion. The number of specimens is related to the size since increasing the number increases the total area of the specimens. A large number of small specimens is advantageous in that the several replicate specimens can give a more reliable measure of corrosion than a single larger one. Also it would provide the opportunity for removal of specimens at intervals over a period of time. Hence it enables the investigator to determine any relationship of the corrosion rate as a function of time.

It has been shown by many investigators that to obtain more uniform results the surface finish and metallurgical treatment of test samples should be controlled. According to the ASTM Standard[103], a more uniform surface could be obtained either by a preliminary chemical treatment (pickling) or by treatment with a coarse abrasive paper or cloth. The thickness of metal so removed should be at least 0.003 mm or 2 to 3 mg/cm^2 in the case of heavy metals. The final surface and metallurgical treatments are normally varied by investigators to suit their investigations.

6.2.2. Test Solutions

It is recommended by various standards that the test solutions should be made up accurately, using reagents conforming to the appropriate industrial environments. The composition of corrosive solutions can vary from a petroleum fraction to a potable water. Normally the pH is of considerable importance and should be accurately measured and adjusted.

The volume of the test solution should be large enough in comparison with the test specimens to be used to avoid any appreciable changes in its corrosiveness either through the exhaustion of corrosive constituents, or the accumulation of corrosion products that might affect further corrosion. A minimum of 250 ml of testing solution for each 6.3 cm^2 of specimen area is recommended[104].

6.2.3. Support of Specimens

Special attention should be given to specimen supports since bimetallic or crevice corrosion could be developed due to the accumulation of reaction products, where specimens are in contact with their supports. The supports and container should not be affected by the corroding agent to an extent that might cause contamination of the testing solution so as to change its corrosiveness. Also the shape and form of the specimen support should be designed in such a way to avoid, as much as possible, any interference with corroding specimens. In some cases it may be desirable

to apply some protective coating to the areas that are in contact with the supporting members.

6.2.4. Tests Conditions

Since the total immersion test is generally used as a control test to evaluate a new metal or alloy and any protective coating it is necessary to control, as much as possible, the testing parameters such as temperature, relative velocity of specimens and corrosive environment, aeration, and test duration.

Temperature is an important factor and should be controlled since a temperature increase usually increases the reaction rate. Also raising the temperature can reduce the solubility of a dissolved corrosive gas or it can form a protective film of corrosion products tending to lower the corrosion rate. The temperature is probably the easiest factor to control and it is normally recommended that the temperature of the corroding solution should be controlled within $\pm 1^{0}$ C.

The relative motion of metal specimens and corrosive environment is another important factor that has to be controlled. The precise control of relative motion and the study of the effects of motion on corrosion are very difficult. The relative motion can be achieved either by having the test-piece move through a presumably stationary liquid or by having a moving liquid come into contact with a stationary test-piece. A velocity of 2.5 to 7.5 cm/s. is recommended to improve reproducibility of the tests. In some cases it may be proper to omit any relative motion, however it should be recognized that the achievement of zero velocity in a test set-up is about as difficult as the accurate control of some high velocity.

Aeration is of importance since in many cases corrosion is theoretically impossible without corrosive gases. Many corrosion mechanisms are controlled by the rate of diffusion of such gases to the metal surface. It is not possible to maintain the degree of aeration by depending on diffusion from the surface of the solution to metal surface. To achieve proper saturation, the solution should be saturated by bubbling through a

sintered glass diffusion disk of medium porosity to break the gas stream up into small bubbles. The rate of gas flow required to maintain the gas saturation will depend on the volume of the testing solution, the area of the test specimens, temperature, and the rate of corrosion.

6.2.5. Methods of Cleaning Specimens After Test

It is essential that corrosion products are removed carefully from specimens if changes in weight are to be used as a measure of corrosion. There are many satisfactory means of cleaning specimens[103-105] after exposure to corrosive environments. The cleaning methods can be divided into three general categories; mechanical, chemical and electrolytic.

Mechanical cleaning includes scrubbing, scraping, brushing, mechanical shocking and ultrasonic procedures. Scrubbing with a bristle brush and mild abrasive is the most popular of these methods. The other methods used are principally as a supplement to remove heavily encrusted corrosion products before scrubbing. These drastic mechanical cleaning methods should not be used when the corroded specimens are small or the amount of weight change expected is slight.

Chemical cleaning implies the removal of corrosion products from the surface of the corroded specimen by dissolution in an appropriate chemical solution. There are a number of solutions developed over the years and recommended by the ASTM Standard and other literature [103,104]. The hot sodium hydride method is the favoured one for cleaning iron and steel both from the point of view of ease of removal of corrosion products and minimum attack on the metal. Other solutions such as Clarke's solution (mixture of HCl, Sb_2O_3 and $SnCl_2$ at room temperature) and sulphuric acid with an organic inhibitor are also recognized as chemical solvents[103].

Electrolytic cleaning is a more appropriate method for many common metals. Electrolytic cleaning is normally preceded by scrubbing to remove loosely attached corrosion products. One method of electrolytic cleaning recommended by the ASTM Standard employs an electrolyte of 5% (by weight) H_2SO_4 with 2 ml organic inhibitor per litre used at a cathodic current density of 20 mA/cm^2. Golden and Mayne[105] employed another electrolytic cleaning system with success. They used saturated aqueous citric acid as an electrolyte and a cathodic current density of 10 mA/cm^2 for 10 min. Also it had been established that, provided that the temperature of the electrolyte was not allowed to rise above 60^0 C, then the loss in weight due to electrolytic attack on the steel was found to be negligible.

6.3 Experimental Procedures

6.3.1. Preparation of Materials

The EN 42 steel in the form of foil was selected for this study. The chemical composition of the steel is given in Table 5.1. The steel foil was cut into coupons of 5 cm x 1 cm by means of a guillotine. They were polished on both sides with 800 grit silicon carbide paper and degreased in acetone ultrasonically for 30 minutes. Two types of samples were prepared. They are, unprotected plain steel coupons, and coupons coated on one side with unball-milled MoS_2/FEP coat. The protective MoS_2/FEP coat was made with catalyst to FEP ratio of 1 : 1.12. The catalyst and FEP mixture was prepared and applied to the steel coupons as detailed in the section 5.4.2.1. The MoS_2/FEP coated steel coupons were cured at 300^0 C for 10 minutes under a stream of argon. The plain coupons were also subjected to the same heat treatment condition. The NACE solution, 5 percent (mass /volume) sodium chloride and 0.5 percent (volume/volume) acetic acid with H_2S bubbling continuously at 1 atmosphere pressure, was selected as a corrosive environment.

6.3.2. Total Immersion Test

A glass desicator, capable of containing 6 litres of corrosive solution was used as a corrosion chamber. By selecting a perspex specimen support system it was ensured that the corrosive environment had very little effect on the support system. Also the specimens were held at least at a distance of 30 mm in the chamber with the help of the support to avoid any interference between the corroding specimens. A water bath was used to maintain the test temperature at 60 ± 1^{0} C. Also the level of the circulating water in the bath was kept at approximately 20 mm above the level of the corrosive solution in the test chamber to ensure uniform heat transfer.

The prepared steel coupons were arranged on the perspex support and placed in the chamber. Then N_2 gas was passed through the container for 15 minutes and followed by H_2S for another 15 minutes to drive out all air from the test chamber. The corrosive solution was separately prepared and N_2 was bubbled through this solution, maintained at 60^{0} C, for 30 minutes followed by H_2S for another 30 minutes to achieve proper saturation. This H_2S saturated solution was transferred to the test chamber, ensuring that no air leaked into the test chamber. Then, H_2S was bubbled continuously at a rate of about 10 ml per minute at atmospheric pressure throughout the duration of the test. The corrosion weight loss test was carried out for time periods of 25, 50, 75, 100, 150 and 200 hours.

6.3.3. Removal of Corrosion Products:

Since the corrosion coupons were small the corroded steel specimens were first scrubbed with a fine abrasive paper to remove loosely attached corrosion products and then the specimens were electrolyzed as follows;

Electrolyte:	Saturated citric acid
Anode :	Platinum foil (3 cm x 2 cm)
Cathode :	Test specimen
Cathodic current density :	100 mA/cm^2
Temperature :	Room temperature
Cleaning time :	20 to 30 min.

Initially the electrolytic cleaning was conducted on a series of typical uncorroded steel coupons to evaluate the effectiveness of the technique. Table 6.1 gives the change in weight when uncorroded steel specimens were subjected to electrolytic cleaning for 30 minutes. The results show

Table 6.1.
Change in weight of uncorroded EN 42 steel coupons when subjected to citric acid electrolytic cleaning for 30 minutes.

Weight of coupon before the cleaning (g)	Weight of coupon after the cleaning (g)	Weight loss (g)
0.6425	0.6420	0.0005
0.6745	0.6735	0.0010
0.6610	0.6605	0.0005
0.6320	0.6310	0.0010
0.6550	0.6540	0.0010

that the loss in weight of the steel specimens due to electrolytic attack are negligible.

The corroded steel coupon was cathodized in the electrolyte for 5 minutes, after the loose corrosion products had been initially removed. After each 5 minutes period the specimen was rinsed in a jet of distilled and deionized water followed by acetone, without breaking the electrical circuit and was dried with a tissue and weighed. The weight

loss due to the electrolytic cleaning was plotted as a function of time for the specimen. A typical plot is given in Figure 6.1. It has been noticed from the plot that it was possible to draw two lines of different slopes corresponding to corrosion products removal and metal removal for the specimen. The weight loss corresponding to the intersection point was taken as the weight loss due to corrosion. This type of plot was established for protected and unprotected coupons to evaluate the actual weight loss due to corrosion.

6.4. Corrosion Products Analysis

Scanning electron microscopic examination of the corroded surfaces of the protected and unprotected specimen was carried out. The specimens were cleaned with a jet of distilled and deionized water followed with acetone after being subjected to the corrosive environment for various periods of time.

X-ray powder diffraction studies of the corrosion products formed on the protected and unprotected specimens, subjected to the corrosive environment for 100 and 200 hours, were carried out using a Phillips Powder Diffraction Camera with Co - K_{α} radiation.

6.5 Results

Corrosion weight loss measurements were carried out on the MoS_2/FEP protected and unprotected EN 42 steel coupons in NACE solution, with H_2S bubbling continuously at 1 atmospheric pressure at 60^{0} C for various periods of exposure. Typical calculations for the protected and unprotected steel coupons are given below:

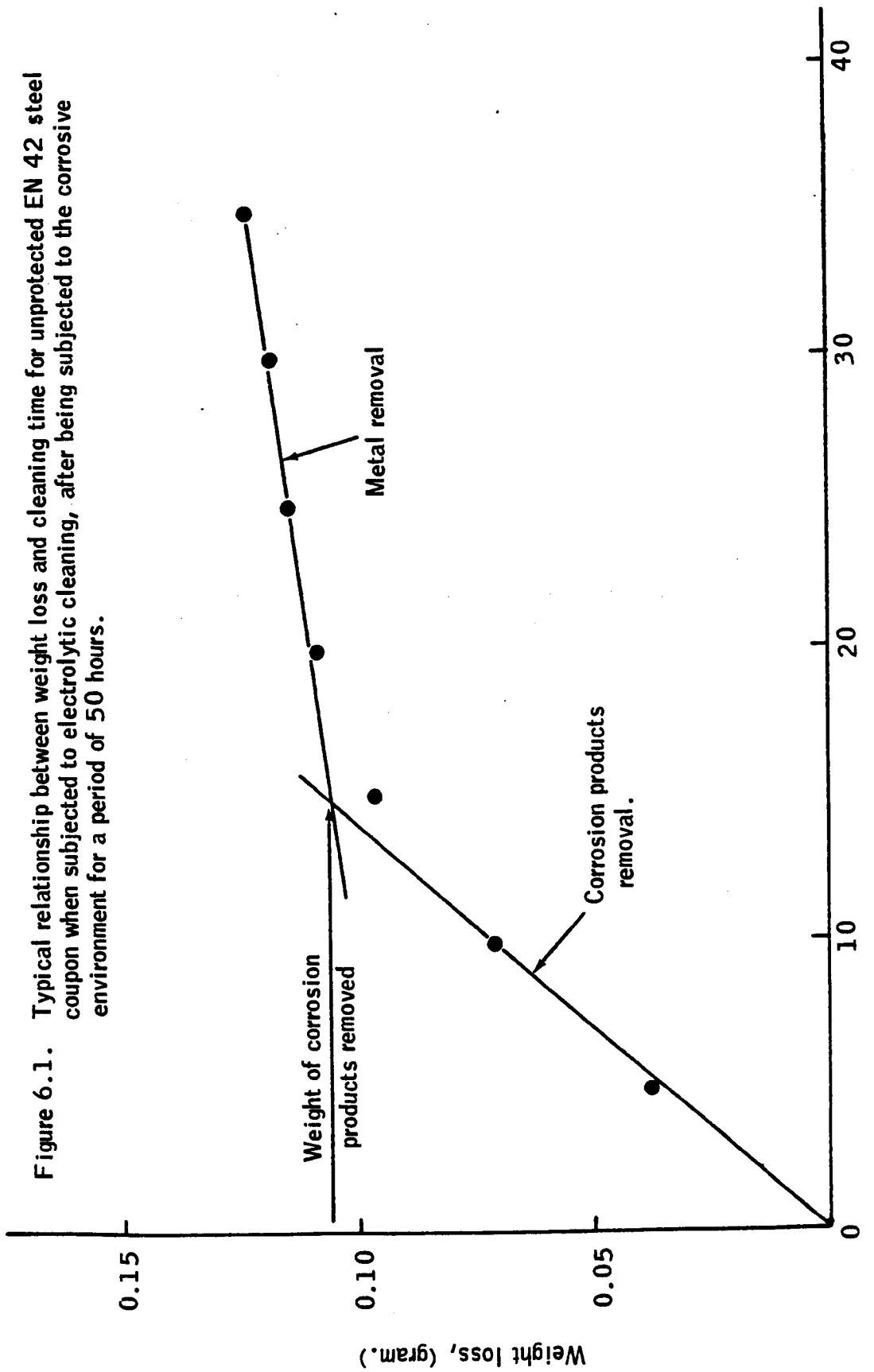

Figure 6.1. Typical relationship between weight loss and cleaning time for unprotected EN 42 steel coupon when subjected to electrolytic cleaning, after being subjected to the corrosive environment for a period of 50 hours.

Unprotected specimen - 25 hours exposure;

Exposed surface area	= 10 cm^2
Weight of the coupon before the test	= 0.6415 g
Weight of the coupon after the corrosion products removed	= 0.5090 g
Weight loss due to corrosion	= 0.1325 g
Weight loss per unit area exposed	= 13.25 mg/cm^2
Corrosion weight loss rate	= 0.53 mg/cm^2/hour.

Protected specimen - 25 hours exposure;

Exposed area	= 5 cm^2
MoS_2/FEP coated area	= 5 cm^2
Weight of coupon before MoS_2/FEP coat applied	= 0.6310 g
Weight of the coupon after the coat applied	= 0.6915 g
Weight of the catalyst/FEP coating	= 0.0605 g
Catalyst loading	= 7.63 mg/cm^2
Weight of the coupon after the corrosion products removed	= 0.5270 g
Weight loss due to corrosion	= 0.1645 g
Weight loss per unit area exposed	= 32.9 mg/cm^2
Corrosion weight loss rate	= 1.316 mg/cm^2/hour.

Table 6.2 gives the average weight loss of the protected and unprotected steel coupons after being subjected to the corrosive environment for periods of 25, 50, 75, 100, 150 and 200 hours. Also it gives the average weight loss ratio of protected and unprotected specimens. The corrosive rates of specimen of both types at various time intervals and their ratio are given in Table 6.3. Figure 6.2 gives a plot of corrosion weight loss versus exposure time. Corrosion weight loss rates at various time intervals are given in Figure 6.3.

Scanning electron microscopic examination carried out on the corroded steel surface of the protected and unprotected steel coupons are given in Plates 1 to 12 as a function of exposure time. X-ray powder diffraction data available in the literature[106] for different iron sulphide compounds are given in Table 6.4. Tables 6.5 and 6.6 give the X-ray powder diffraction data of the corrosion product formed on the protected and unprotected steel coupons when subjected to the corrosive environment for 100 and 200 hours respectively.

Figure 6.2. Effect of MoS_2/FEP coat on weight loss of EN 42 steel in NACE solution with H_2S bubbling continuously at 60^0 C as a funtion of exposure time.

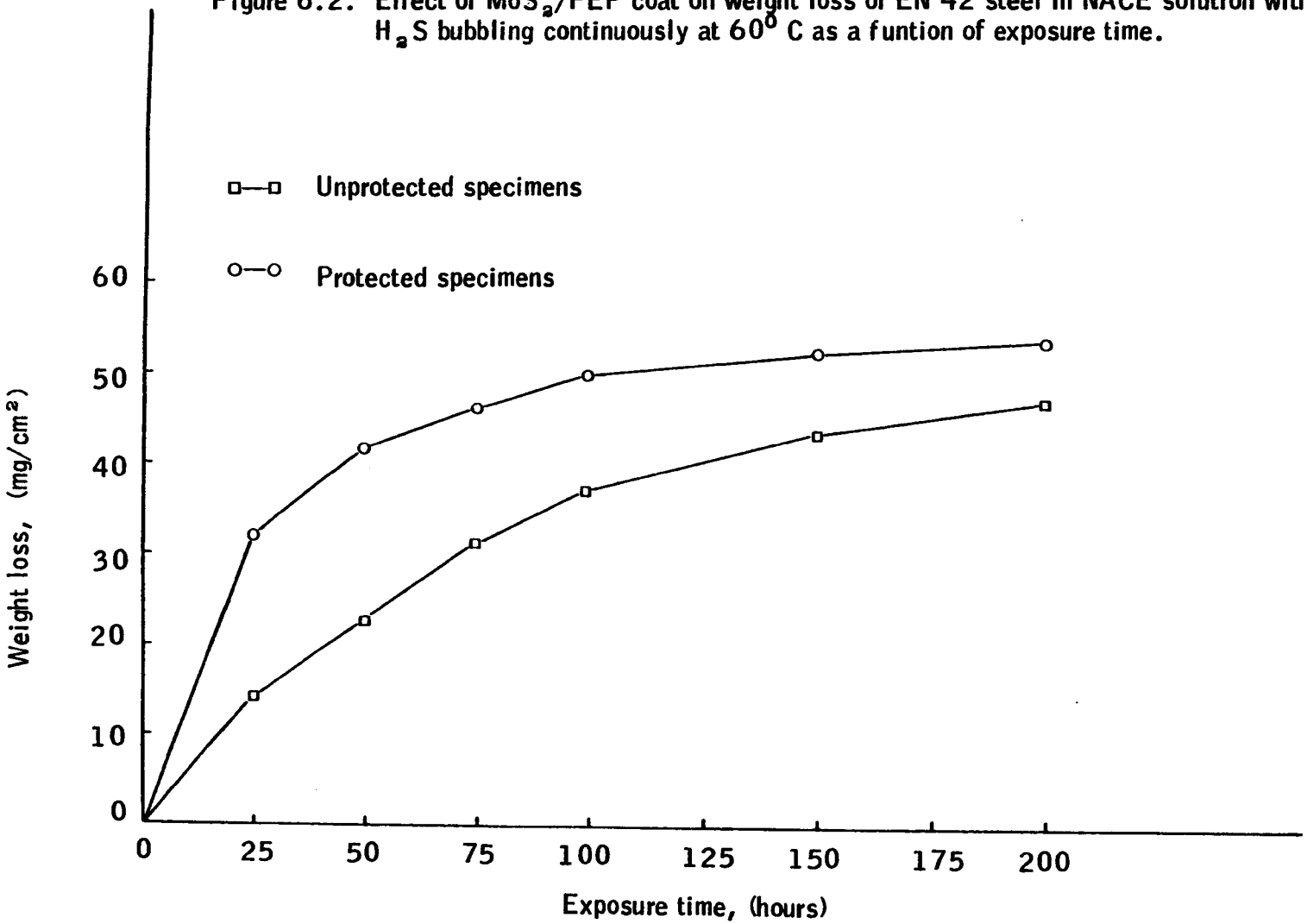

Table 6.2.

Corrosion weight loss of protected and unprotected EN 42 steel coupons when subjected to a corrosive environment, NACE solution with H_2S bubbling continuously at 60° C as a function of exposure time.

Exposure time (hours)	Average catalyst loading of the MoS_2/FEP coat. (mg/cm^2)	Average weight loss of protected coupons. (mg/cm^2)	Average weight loss of unprotected coupons. (mg/cm^2)	Ratio of weight loss (protected/ unprotected)
25	8.07	32.13	14.15	2.27
50	2.05	41.84	22.84	1.83
75	8.30	46.23	31.42	1.47
100	8.19	50.36	37.17	1.35
150	8.70	52.84	43.82	1.21
200	8.45	54.05	47.42	1.14

Table 6.3.

Corrosion weight loss rates at various time intervals for protected and unprotected specimens, when subjected to the corrosive environment, NACE solution with H_2S bubbling continuously at 60° C.

Time (hours)	Corrosion weight loss rate (mg/cm^2/hour)		Ratio of corrosion rate protected/ unprotected.
	Unprotected	Protected	
0 - 25	0.566	1.285	2.27
25 - 50	0.348	0.388	1.12
50 - 75	0.343	0.176	0.51
75 - 100	0.230	0.165	0.72
100 - 150	0.133	0.050	0.37
150 - 200	0.072	0.024	0.34

Figure 6.3. Effect of MoS_2/FEP coat on corrosion weight loss rate of EN 42 steel in NACE solution with H_2S bubbling continuously at 60° C.

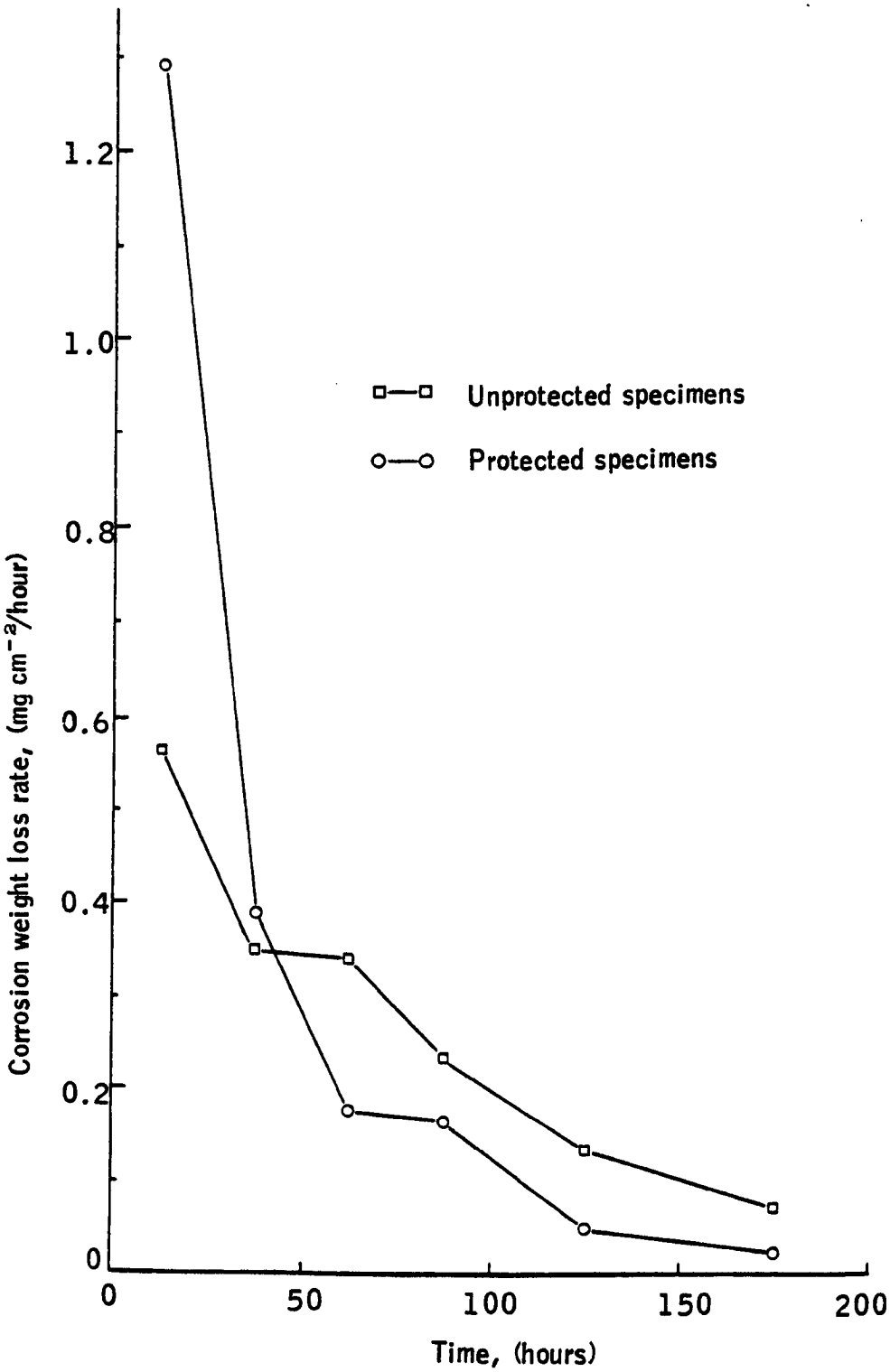

Table 6.4. X-ray powder diffraction data of different Iron sulphides[106].

Compound	d - spacing values							
Pyrite FeS_2	2.71	1.63	2.42	3.13	2.21	1.92	1.04	1.45
rel. intensity	100	70	60	40	40	40	20	10
Marcasite FeS_2	2.69	3.43	1.75	1.76	2.41	2.71	2.31	1.91
rel. intensity	100	70	50	50	40	30	30	30
Troilite FeS	2.09	2.98	2.66	1.72	1.33	2.94	1.12	1.05
rel. intensity	100	60	40	30	10	10	10	10
Pyrrhotite (4C) FeS	2.06	2.97	2.64	2.05	2.62	1.71	2.65	2.04
rel. intensity	100	90	90	90	80	80	30	30
Pyrrhotite (4C mono) Fe_7S_8	2.97	2.05	2.06	2.64	2.63	1.72	2.07	1.72
rel. intensity	100	100	90	60	60	50	50	50
Mackinawite Fe_9S_8	5.05	2.31	1.81	2.97	1.84	1.73	2.60	1.56
rel. intensity	100	80	80	80	40	40	10	10
Smythite Fe_3S_4	2.98	1.75	2.47	3.50	1.90	1.01	1.42	1.29
rel. intensity	100	90	80	70	60	50	30	30

Table 6.5.

X-ray powder diffraction data of the corrosion product formed on the protected and unprotected EN 42 steel coupons when subjected to the corrosive environment for 100 hours.

Unprotected Specimen		Protected Specimen	
measured d - spacing	estimated rel. intensity.	measured d - spacing	estimated rel. intensity.
5.05	100	5.05	100
2.97	80	2.97	80
2.60	10	2.60	10
2.31	80	2.31	80
1.84	30	1.84	30
1.81	70	1.81	80
1.73	40	1.73	30
1.56	10	1.56	10
1.24	10	1.24	10
1.06	10	1.06	10

Table 6.6.

X-ray powder diffraction data of the corrosion product fromed on the protected and unprotected EN 42 steel coupons when subjected to the corrosive environment for 200 hours.

Unprotected Specimen		Protected Specimen	
measured d-spacing	estimated rel. intensity.	measured d-spacing	estimated rel. intensity.
5.05	100	5.05	100
2.97	80	2.97	80
2.60	05	2.60	10
2.31	80	2.31	80
1.84	30	1.84	20
1.81	80	1.81	70
1.73	30	1.73	20
1.56	10	1.56	05
1.24	10	1.24	10
1.06	05	1.06	05

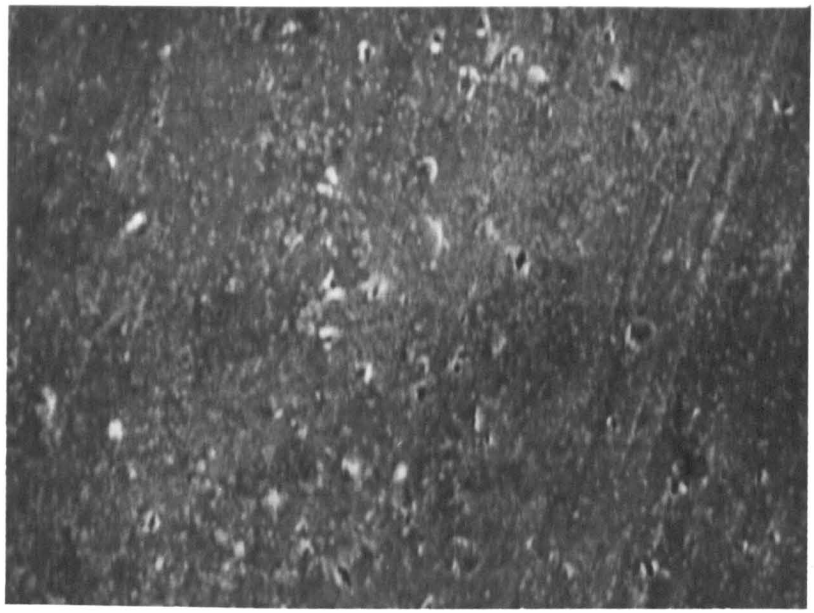

Plate 6.1. SEM micrograph of an unprotected EN 42 steel coupon surface after being subjected to a corrosive environment of NACE solution with H_2S (1 atm.) at 60° C, for 25 hours (0° tilt, 2000 X).

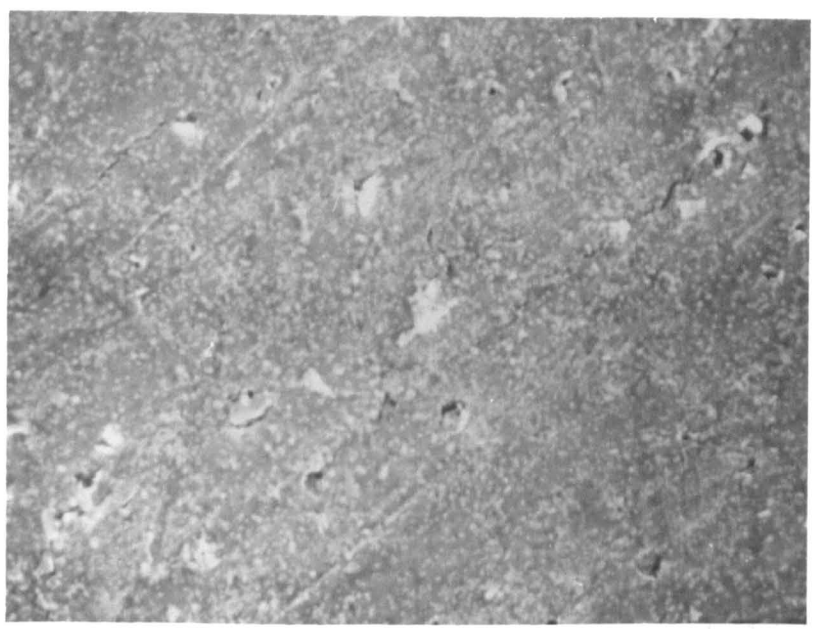

Plate 6.2. SEM micrograph of an uncoated part of a corroded EN 42 steel coupon, with protection (MoS_2/FEP)applied to the other side, after being subjected to a corrosive environment of NACE solution with H_2S (1 atm.) at 60° C, for 25 hours (0° tilt, 2000 X).

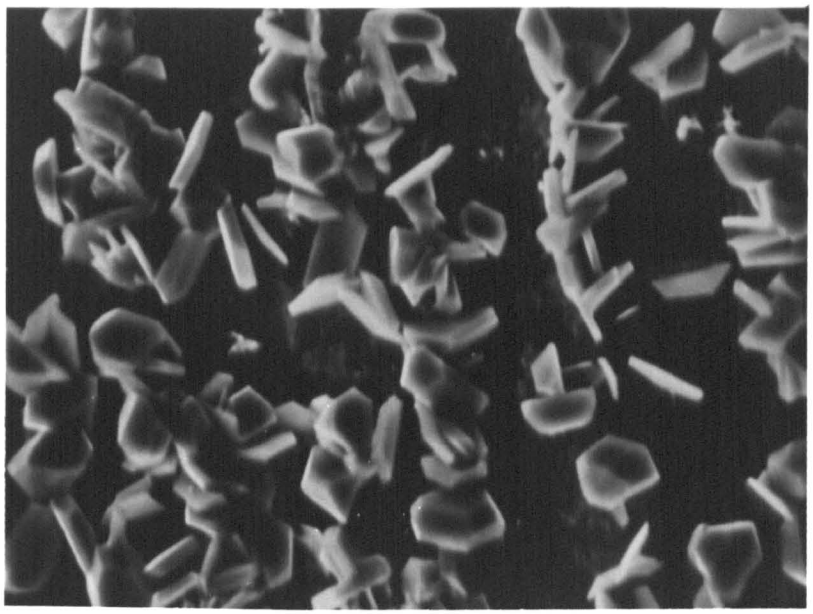

Plate 6.3. SEM micrograph of an unprotected EN 42 steel coupon surface after being subjected to a corrosive environment of NACE solution with H_2S (1 atm.) at 60° C, for 50 hours (0° tilt, 1000 X).

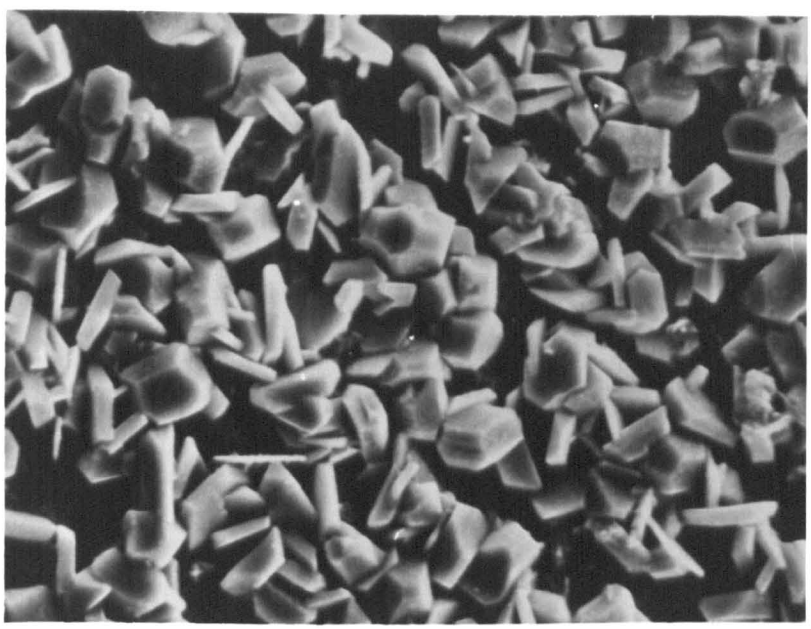

Plate 6.4. SEM micrograph of an uncoated part of a corroded EN 42 steel coupon, with protection (MoS_2/FEP) applied to the other side, after being subjected to a corrosive environment of NACE solution with H_2S (1 atm.) at 60° C, for 50 hours (0° tilt, 1000 X).

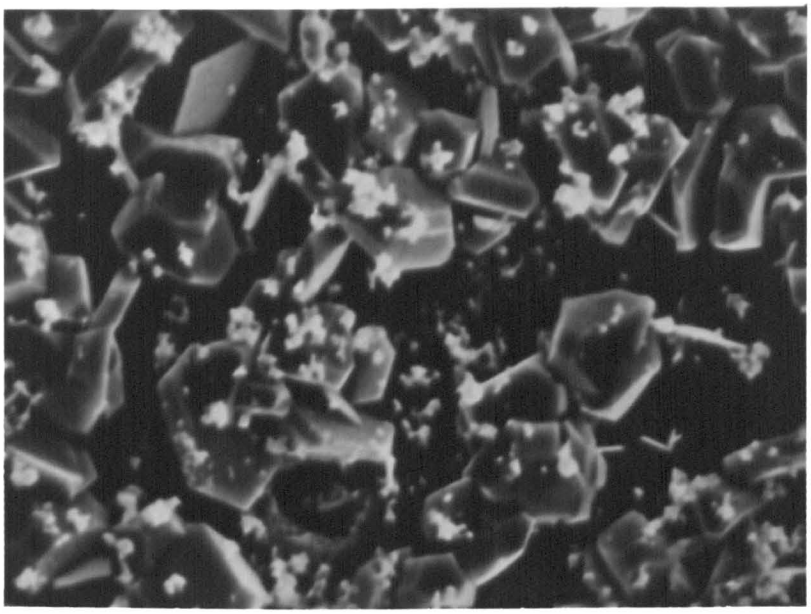

Plate 6.5. SEM micrograph of an unprotected EN 42 steel coupon surface after being subjected to a corrosive environment of NACE solution with H_2S (1 atm.) at 60° C, for 75 hours (0° tilt, 1000 X).

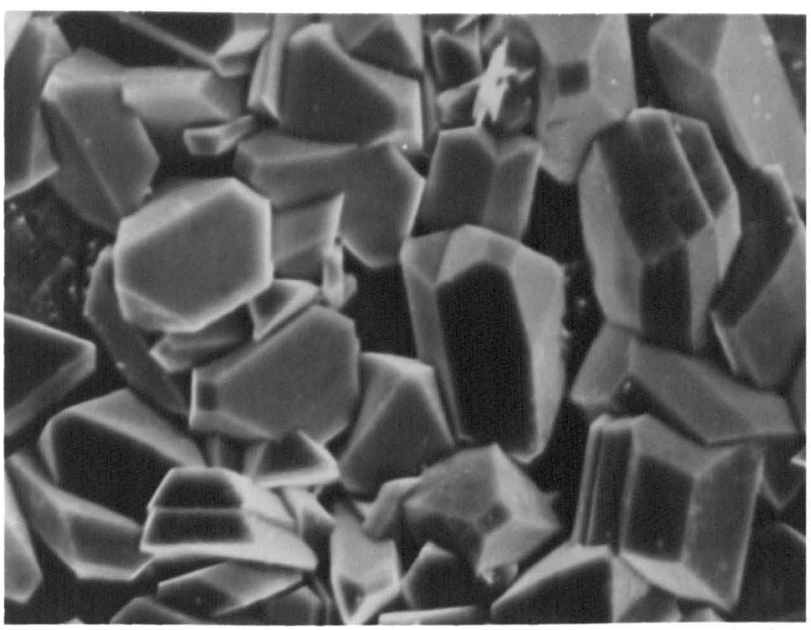

Plate 6.6. SEM micrograph of an uncoated part of a corroded EN 42 steel coupon, with protection (MoS_2/FEP) applied to other side, after being subjected to a corrosive environment of NACE solution with H_2S (1 atm.) at 60° C, for 75 hours, (0° tilt, 1000 X).

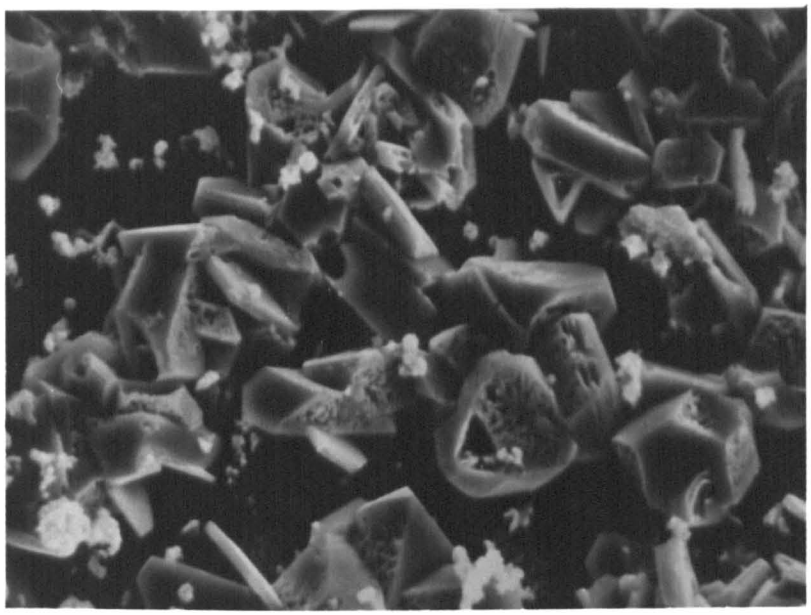

Plate 6.7. SEM micrograph of an unprotected EN 42 steel coupon surface after being subjected to a corrosive environment of NACE solution with H_2S (1 atm.) at 60° C, for 100 hours (0° tilt, 1000 X).

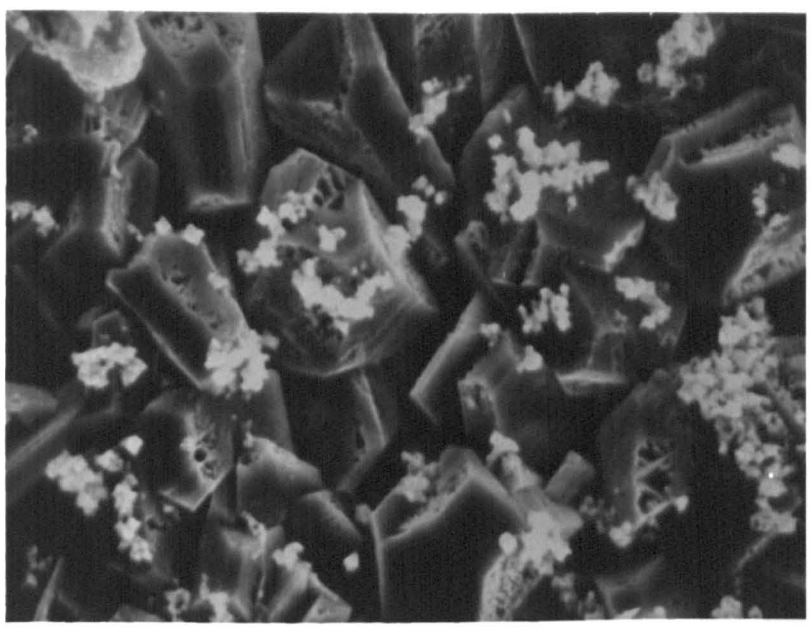

Plate 6.8. SEM micrograph of an uncoated part of a corroded EN 42 steel coupon, with protection (MoS_2/FEP) applied to other side, after being subjected to a corrosive environment of NACE solution with H_2S (1 atm.) at 60° C, for 100 hours (0° tilt, 1000 X).

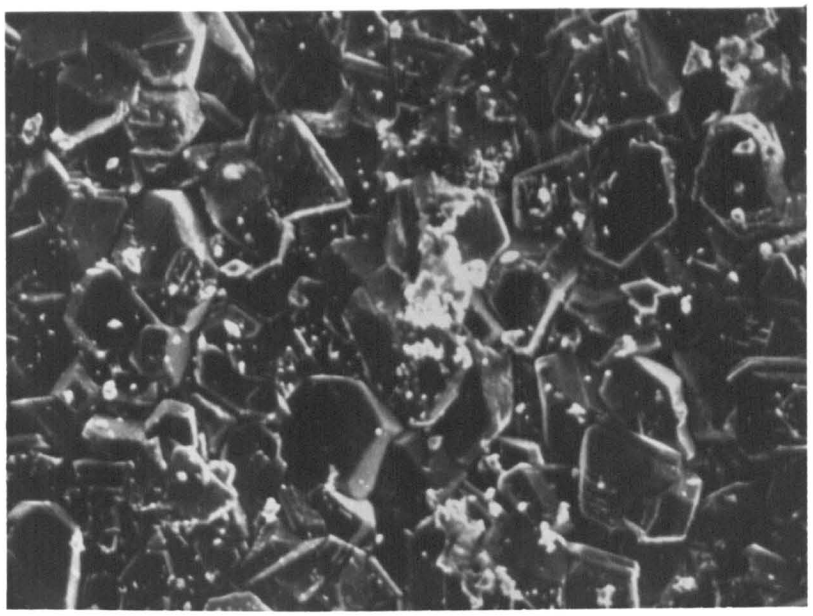

Plate 6.9. SEM micrograph of an unprotected EN 42 steel coupon surface after being subjected to a corrosive environment of NACE solution with H_2S (1 atm.) at 60° C, for 150 hours (0° tilt, 500 X).

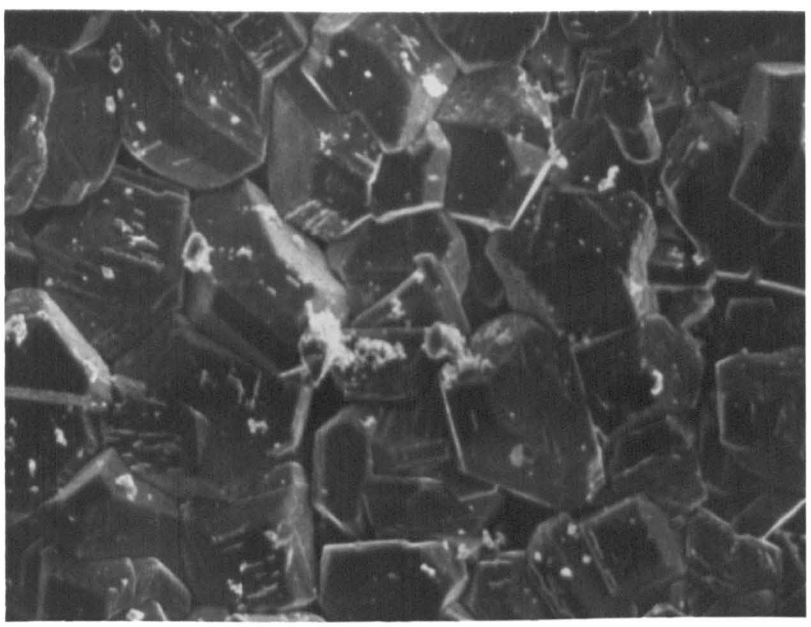

Plate 6.10. SEM micrograph of an uncoated part of a corroded EN 42 steel coupon, with protection (MoS_2/FEP) applied to other side, after being subjected to a corrosive environment of NACE solution with H_2S (1 atm.) at 60° C, for 150 hours (0° tilt, 500 X).

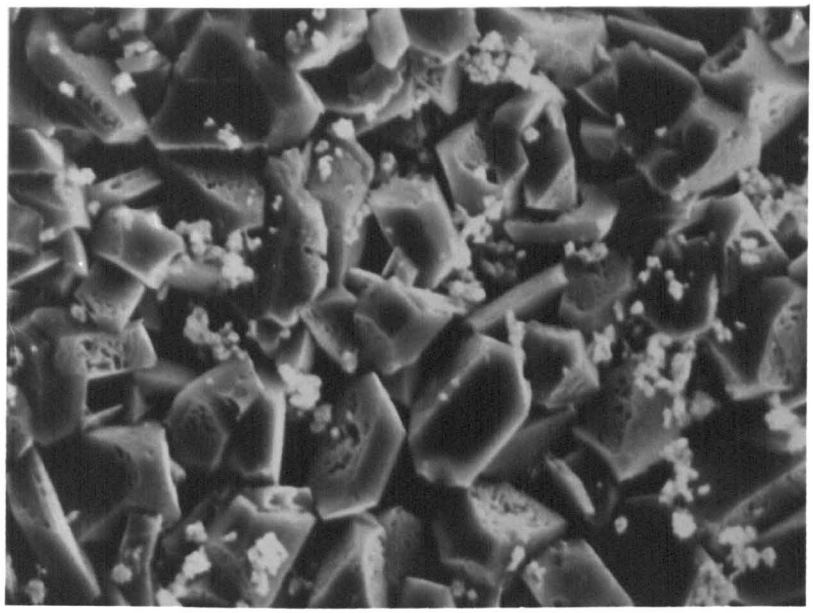

Plate 6.11. SEM micrograph of an unprotected EN 42 steel coupon surface after being subjected to a corrosive environment, NACE solution with H_2S (1 atm.) at 60° C for 200 hours (0° tilt, 500 X).

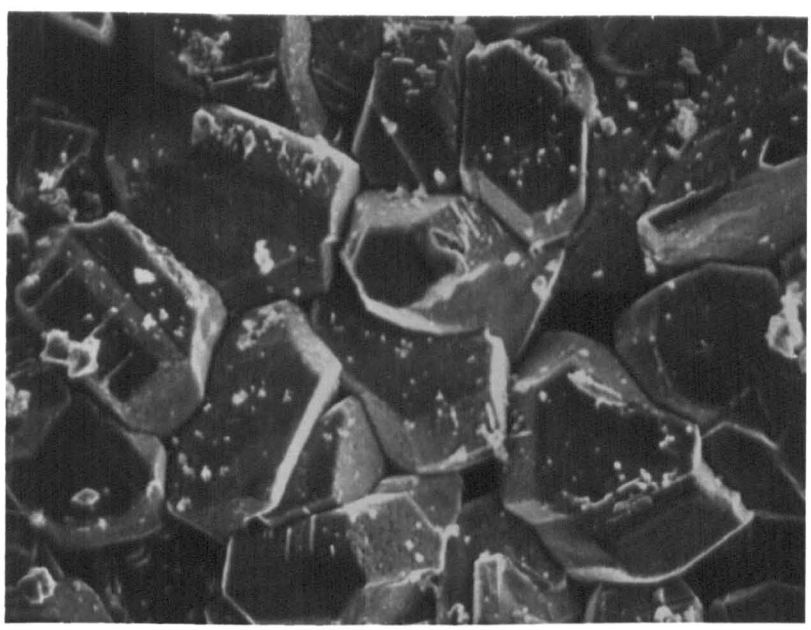

Plate 6.12. SEM micrograph of an uncoated part of a corroded EN 42 steel coupon, with protection (MoS_2/FEP) applied to other side, after being subjected to a corrosive environment, NACE solution with H_2S (1 atm.) at 60° C, for 200 hours (0° tilt, 500 X).

6.6. Discussion:

Weight loss tests on the protected (one side coated with MoS_2/FEP) and unprotected EN 42 steel coupons show (Table 6.2) that the weight loss on the protected specimens were higher than that of unprotected specimens. However, the difference of the weight loss between protected and unprotected specimens decreased with increasing exposure time. This phnomenon is clearly seen from the Figure 6.2. Ratio of weight loss between protected and unprotected specimens shows that at 25 hours of exposure the ratio was 2.27, whereas at 200 hours it was only 1.14. The weight loss ratio of 2.27 after a 25 hour exposure agrees well with the predicted ratio of corrosion currents of 2.82, from the Evans diagram (see Table 5.5). Corrosion weight loss rates calculated for the protected and unprotected specimens at various exposure time intervals indicate (Table 6.3) that for the first 50 hours only the corrosion weight loss rate was higher on the protected specimens. After 50 hours of exposure the weight loss rate on the protected specimens was found to be significantly reduced compared with the unprotected specimens (Figure 6.3). This is very important point to note, i.e., in spite of the presence of a more active hydrogen evolution catalyst coating on the steel, the above observation suggests that the corrosion products formed on the protected specimens were more protective against further corrosion.

The X-ray powder diffraction studies on the corrosion products formed on the protected and unprotected steel coupons suggest (Table 6.4 - 6.6) that the product is mackinwite (Fe_9S_8). It has been reported by Morris et al[107] that mackinawite which is the initial corrosion product of steel in aqueous H_2S environment, enhances the corrosion rate of steel. The weight loss data reported above do not support this view. However the difference between this experimental results and those of Morris et al could be explained as follows; - a dense compact layer of mackinawite drastically reduces the corrosion rate, whereas a porous layer of mackinawite accelerates the corrosion rate because the isolated 'mackinawite' sites on the corroded surface will then act as cathodes. Hence, this argument suggests that although the corrosion products formed on the protected specimens were mackinawite, the products were densely formed on the exposed steel surface as a protective layer. Scanning electron microscopic examination on the corroded steel surfaces confirms the above view. The

corrosion products formed on the protected and unprotected steel coupons, exposed to the corrosive environment for 25 hours, were smooth in nature (Plate 6.1 and 6.2). There was an indication of the formation of very small crystals on the steel surfaces. However, the specimens exposed to the corrosive environment for 50 hours show that the steel surfaces were covered with crystalline product (Plate 6.3 and 6.4). The crystals' have grown considerably larger as a function of time subsequently at 75, 100, 150 and 200 hours, (Plates 6.5 - 6.12). However, it was noticed that the crystalline size of the iron sulphide on the unprotected specimens were always smaller than that on the protected specimens. Furthermore, they were not densely packed as on the protected specimens. In the case of protected steel coupons, the side which is uncoated will act exclusively as an anode, whilst MoS_2/FEP coating acts as the hydrogen evolution cathode. On the other hand in the unprotected steel coupons, the anodic and cathodic sites are very close to one another. The continual evaluation of hydrogen at the cathodic site may prevent the iron sulphide crystals from growing to larger size and thus probably making the iron sulphide layer less dense.

The corrosion weight loss measurement and the corrosion product analysis indicate that the presence of the MoS_2/FEP coat initially enhanced the anodic dissolution, but the corrosion product formed is a much better protective layer and retards corrosion. In the long term, over 50 hours, the presence of MoS_2/FEP coat actually reduces the corrosion rate of the steel, which is a good indication for the viability of the proposed method to inhibit SSCC in steel.

CHAPTER SEVEN

CONCLUSIONS ON PART 1 : THE ELECTROCHEMICAL ASPECTS

CHAPTER 7.

CONCLUSIONS ON PART 1 - THE ELECTROCHEMICAL ASPECTS.

The literature survey on sulphide stress corrosion cracking (SSCC) in steel and its prevention gave a greater understanding on the factors that control SSCC. Also it helped to devise the experimental studies to evaluate the proposed method to inhibit SSCC in steel. The major factors controlling SSCC in steel are summarised below.

- Concentration of H_2S. H_2S concentration of 1 ppm is sufficient enough to produce SSCC in high strength steel.

- pH value. The lower the pH value of the environment, the higher is the susceptibility of the steel to SSCC. However, the susceptibility is independent of pH in the range of 2 to 4.

- Micro-organism. The necessary requirements for growth of micro-organism such as Desulfovibrio (sulphate reducing bacteria) are met when steel structures or pipelines are in contact with the earth or water.

- Temperature. Susceptibility to SSCC is greatly varied with change in temperature. The greatest susceptibility is detected in the temperature range of 15° C to 30° C.

- Sulphide films. The iron sulphide films formed on the surface of the steel during sour corrosion processes, increase the corrosion rate due to the porous nature of the film. The type of film formed and its constituants are dependent on the pH value and concentration of H_2S of the environment.

- Microstructure and heat-treatment. Susceptibility for SSCC varies with microstructure and heat-treatment of steel. Quenched and tempered bainite or martensite gave the best resistance to SSCC.

- Cold work (plastic deformation). Cold work, as little as one percent, can give an adverse resistance to SSCC. There are recommended practices of heat-treatments available in various standards to reduce the susceptibility after cold-working.

- Hardness (strength level). Susceptibility for SSCC increases with increasing hardness value. The maximum hardness value of HRC 22 is recommended by API and ASTM specifications for steels used in the petroleum industry.

The preventive measures to combat SSCC available at present in the petroleum industry are summerised below.

- Inhibition. Addition of corrosion inhibitors is the major prevention step taken in the petroleum industry. There are three types of inhibitors. They are oil soluble, oil soluble-water dispersible and water soluble. These can be used depending on the nature of the fluid or mixture transmitted.

- Protective coatings. Dry powdered thermo-setting epoxy coatings are gaining popularity among the various types of coatings, since they are more economical and have been proved to be reliable.

- Design and operating techniques. Various standards and practices are developed to improve design and operating techniques to combat SSCC.

- Development of new materials. Development of new materials are incorporates with numerous combinations of chemical additives with various heat-treatment and microstructures. However, still there is no single high strength steel that has been proved to be operational in a sour environment where SSCC is eminent.

- Corrosion monitoring. Corrosion monitoring employs various techniques under three categories such as inspection of structure, intermittent testing and cumulative testing. The hydrogen probe technique is most useful since its measurement gives a day-to-day reading to indicate the fluctuation of corrosion in terms of the amount of hydrogen diffused into the steel.

However, all prevention measures indicate that there is no single system which could stop the sour corrosion reaction completely. Therefore SSCC could not be prevented effectively. Hence a novel method is being proposed to inhibit SSCC in steel effectively.

The proposed novel approach is to coat the steel surface with an active hydrogen evolution electro-catalyst, such that the hydrogen evolution will take place on the active catalyst surface, instead of on the corroding steel surface. Hence SSCC in steel will be effectively reduced.

The hydrogen evolution performance of three sulphide electrocatalysts, $NiCo_2S_4$, MoS_2 and WS_2 and EN 42 steel were evaluated in NACE solution both in the presence and absence of H_2S at various temperatures. This evaluation indicated that at the lower potential range, (around -600 mV vs SCE) hydrogen evolution performances were in the following order:

in the absence of H_2S, $NiCo_2S_4 > WS_2 > MoS_2 \gg$ EN 42 steel

in the presence of H_2S, $MoS_2 > WS_2 > NiCo_2S_4 \gg$ EN 42 steel

The pseudo exchange current densities for the sulphide catalysts are 15 to 28 times and 87 to 354 times higher (depending on electrocatalyst loading) than that of EN 42 steel in the presence and in the absence of H_2S respectively at 25° C. The apparent activation energies for hydrogen evolution reaction on the three sulphide electrodes and on EN 42 steel showed the following trend;

$$\text{EN 42 steel} \gg MoS_2 \approx WS_2 > NiCo_2S_4 .$$

However, the $NiCo_2S_4$ electrodes lost more sulphur than the other two electrodes when pre-cathodized either in the presence of H_2S or in the absence of H_2S. Evans diagrams were constructed to predict corrosion rate of the steel when connected with the sulphide electrodes. Also hydrogen diffusion studies were carried out to identify the effectiveness of the three sulphides in the form of separate electrodes and adherent coatings.

The corrosion current of sulphide - EN 42 steel couples were reduced significantly when the catalyst loading was reduced from 17-22 mg/cm^2 to 5-8 mg/cm^2. The corrosion current reduction was not directly proportional to the decrease in catalyst loading. However, the corrosion current ratio of the MoS_2-EN 42 steel couple and EN 42 steel did not change significantly when the catalyst loading was reduced in the presence of H_2S.

Hydrogen diffusion currents through EN 42 steel membranes were significantly reduced from 16 μA/cm^2 to 4 μA/cm^2 when the membranes were protected with higher loading (17 to 22 mg/cm^2) sulphide electrodes. The lower loading (5-8 mg/cm^2) sulphide electrodes also showed the same trend. However, when the membranes were protected with adherent coatings (catalyst to FEP ratios of 1:0.85 for WS_2 and MoS_2 and 1:1 for $NiCo_2S_4$) the maximum diffusion current of 16 μA/cm^2 was reduced to 8 to 9.5 μA/cm^2. There were signs that the adherent coatings were porous and therefore did not protect the substrate effectively against corrosion. A new adherent coating consisting of unball-milled MoS_2 with higher catalyst to FEP ratio was found to be effective in reducing the maximum diffusion current on the level achieved with the connection of separate electrodes. Also the substrates were protected effectively against corrosion. The MoS_2/FEP adherent coat with higher catalyst to FEP ratio was found to be most effective of the three adherent coats.

After full analysis of the experimental results on the three sulphides, the MoS_2/FEP coat with higher FEP content was selected for further weight loss measurement studies.

The corrosion weight loss measurements on EN 42 steel coupons in NACE solution, with H_2S bubbling continuously at 60° C showed that the corrosion rates of the coupons partially coated with MoS_2/FEP coat were higher than those of the uncoated coupons, up to 50 hours. After that the corrosion rate was reduced significantly below that of the uncoated coupons. It has been found that the sulphide film formed on the MoS_2/FEP coated coupons corroded surfaces was more dense. Further, the crystals formed in the sulphide film were bigger than the crystals formed in the sulphide film on uncoated coupons. Subsequent analysis on the corrosion products showed that the product is Mackinawite. The denser film formation and retardation of corrosion rate on the coupons coated with MoS_2/FEP coat improved the viability of the protection method for inhibition of SSCC in steel.

The experimental studies carried out in this electrochemical part helped successfully to select an electrocatalyst, MoS_2, for this novel method and showed that the MoS_2/FEP coat could be used, without enhancing the corrosion rate in the longer term, to inhibit SSCC in Steel. However, the viability of the proposed method should be studied extensively in terms of mechanical properties. Hence, the improvement of the mechanical properties of steels in a sour environment due to the application of this protective coat were extensively evaluated and are reported in Part 2 of this thesis.

PART TWO

THE MECHANICAL ASPECTS

CHAPTER EIGHT

LITERATURE SURVEY ON STRESS CORROSION TESTS METHODS AND INTERPRETATION OF RESULTS

CHAPTER 8.

LITERATURE SURVEY ON STRESS CORROSION TESTS METHODS AND INTERPRETATION OF RESULTS.

8.1 Introduction.

The development of high strength metallic materials to meet the growing industrial demand requires greater understanding of their stress corrosion cracking behaviour. As applications become more sophisticated, complex, and demanding, the need for information on stress corrosion cracking behaviour of metals has become increasingly greater. These have caused problems for the basic material producer, the engineer, the manufacturer, and also the user who must maintain and service the complex structures.

To overcome this problem and to identify the situations, numerous stress corrosion tests have been conducted over the years by the various workers and organizations. The reasons and interests which frequently determine the type of test to be conducted, are the following[108];

(1) to evaluate a metal or alloy, or various heat treatments of one alloy for susceptibility to stress corrosion cracking in certain environments.

(2) to compare stress corrosion cracking susceptibilities of various alloys.

(3) to evaluate environments which might accelerate stress corrosion cracking in various alloys.

(4) to evaluate a specific service requirement with regard to the possibility of stress corrosion cracking.

(5) to evaluate the effectiveness of coatings or other protective measures for reducing stress corrosion cracking of susceptible metals and alloys.

Many different stress corrosion test methods have been developed in the last 40 years to evaluate the above mentioned requirements, but there is no single method that is markedly superior to all others. It is not possible to use the same test method or similar type test in evaluation of all five requirements. An important point to notice in selecting a test method is that it may be possible for one to select a test method, which could be so severe that it leads to the condemnation of a material. However this material could prove adequate for the particular service condition. In contrast the test could permit the use of a material in circumstances where rapid failure would ensue. Recognition of such problems has frequently led to the use of tests that closely simulate a practical situation, especially regarding the structure and composition of the material and usually in relation to environmental aspects, but less frequently in respect of the manner in which the stress has been generated in the test specimen[109].

The type of specimen used in a stress corrosion test depends mainly upon the information sought and time and funds available. In some cases when the purpose of the test is to evaluate the stress corrosion cracking performance of a specific alloy or various heat treatments of one alloy, or to compare the susceptibilities of various alloys, there are no alternatives in the choice of test material. Hence selection of test specimens is confined to a very few types and dimensions and sizes are severely restricted. In other cases, to evaluate the effectiveness of coatings or other protective measures for reducing stress corrosion cracking of susceptible alloys and to study stress corrosion mechanisms, serious consideration should be given to the choice of alloy composition, type of specimen, section thickness, etc. Also in this type of test, specimens taken out in the short-transverse direction are preferable, since this is the direction which shows the greatest susceptibility.

It has been shown[110] clearly that significant susceptibility of a material to stress corrosion cracking (SCC) may escape detection unless pre-cracked specimens are used. If cracks are not intentionally introduced, the test is usually dependent upon the formation of stress concentrators such as fatigue cracks or corrosion pits. Crack development at the bottom of a corrosion pit may not occur if the material does not undergo pitting attack. Furthermore the use of pre-cracked specimens more closely approximate that critical part of a high-strength

structure which contains a crack either built into it or developed during the construction, or in the service, of the structure.

In view of the existence of numerous tests methods, number of test specimens, complexity of the problem and the application of fracture mechanics to stress corrosion cracking, it was decided to carry out a literature survey on stress corrosion test methods. Also it was found that much more understanding was required on specimens geometry and correlations between test results to decide a series of test methods, to evaluate the effectiveness of the proposed novel method, for inhibition of sulphide stress corrosion cracking. Hence this chapter is devoted to a review of the available stress corrosion test methods and interpretation of test results.

8.2 Type of Test Specimens.

8.2.1. Smooth Specimens.

As early as 1944, Madden[111] and Sager, Brown and Mears[112] described specimen types and test methods for determining the susceptibility of materials to stress corrosion cracking at the Symposium on Stress Corrosion of Metals. All the specimens were smooth specimens, as expected, and are (a) two-, three-, and four- point bend specimens, (b) c- ring specimens, (c) cantilever specimens.

The two-, three- and four- point bend specimens are designed for investigating the stress corrosion cracking behaviour of alloy sheets, plates and bars in a variety of environments. Schematic representation of the bend specimens and the configuration of the specimens holder are given in Figure 8.1.

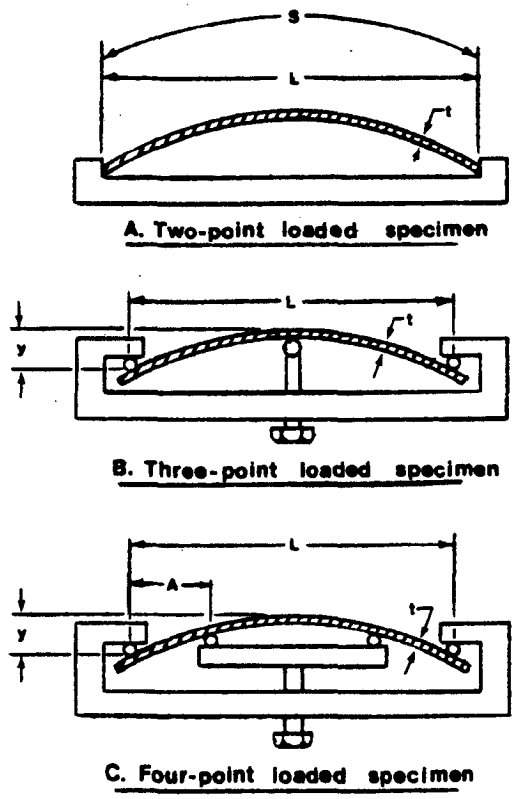

Figure 8.1. Schematic representation of the bend specimens and holder configurations. S-specimen length, L-distance between outer supports, t-thickness of specimen, y-maximum deflection, A-distance between inner and outer supports,[113].

The stress of principal interest in the bend specimens in the longitudinal tension stress on the convex surface. It should be recognized that the stress in the bend specimens, is generally not uniform. First, there is a gradient through the thickness, varying from a maximum tension on the outer surface to a maximum compression on the inner surface. Second, the stress varies from mid-length to the ends, depending on the type of loading, whether two-point, three-point or four-point loading. Finally, the longitudinal stress can vary across the width of the specimen because of transverse stresses, depending on the ratio of width to thickness.

The two-point bend specimens are loaded by holding the ends in a rigid jig to give a required constant deflection. In the two-point bend specimens, the maximum bending stress occurs at midlength of the specimen and decreases to zero at specimen ends. In performing the bending operation, especially with an applied stress approaching the yield stress of the material, overstressing must be avoided to stay within the limitations imposed by the elastic analysis.

The three-point bend specimen has an advantage that a marked localization of the maximum stress exists at the central support. This type of specimen has been employed in an electrolytic test to determine rapidly the susceptibility to stress corrosion cracking of various alloys. The four-point bend specimens are used to produce a uniform bending moment throughout the centre of the specimens. Precautions should be taken in three and four point loading to ensure that no galvanic corrosion can take place between the specimens and the supports. Sager, et al,[112] used glass rods which fit into grooves in the metal specimen supports and loading points.

The C-ring is a versatile, economical specimen for quantitatively determining the susceptibility to stress corrosion cracking of all types of alloys in a wide variety of product forms[113]. It is particularly suitable for testing tubing and for making short transverse tests of various products. Sizes of C-ring may be varied over a wide range, but rings with outer diameter less than about 16 mm are not recommended because of increased difficulties in machining and decreased precision in stressing.

The C-ring specimens are stressed by placing a bolt through holes drilled through the tube walls and drawing up a nut to give the desired stress (Figure 8.2).

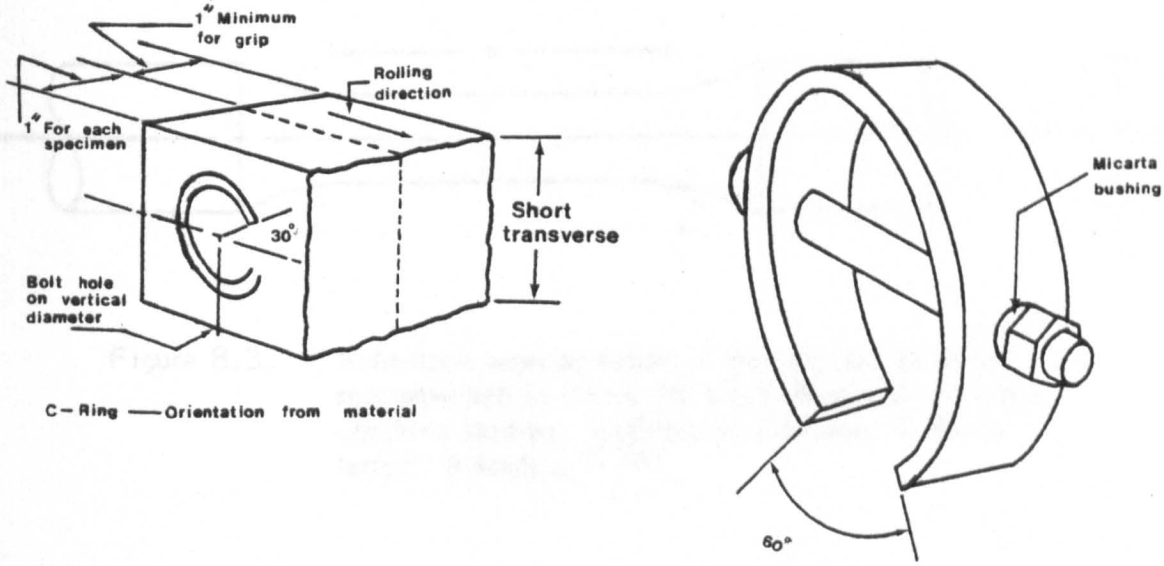

Figure 8.2. Schematic representation of C-ring specimen,[108].

The stress of principal interest in the C-ring specimen is the circumferential stress and it varies around the circumference from zero at each bolt hole to a maximum at the middle of the arc opposite the stressing bolt. The C-rings should be orientated, if possible, in such a way that the direction of maximum tensile stress will be parallel to the short-transverse direction of the piece.

Tensile specimens having a circular cross section are more frequently used for testing small diameter rod material. In some instances flat tensile specimens with rectangular cross section are used if the material to be tested is only available in a flat form. These specimens are normally subjected to a direct loading, which may be accomplished by use of compression springs, lever arms or the tension rings. It is generally accepted that the application of dead load by means of levers is difficult and requires proper placement and alignment. The load to be applied by means of compression springs and tension rings is normally measured either by displacement or strain gauge measurement. Figure 8.3 gives the schematic illustration of the tensile specimen recommended by NACE for sulphide stress corrosion cracking studies.

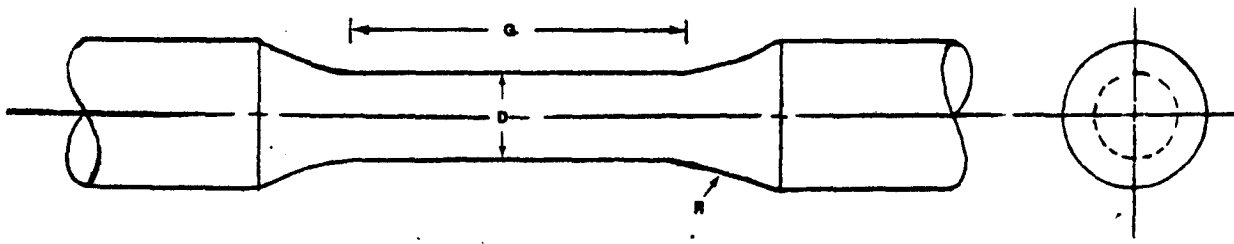

Figure 8.3. Schematic representation of the tensile specimen recommended by NACE for sulphide stress corrosion cracking studies. D:Effective diameter, G:Gauge length, R:Radius,[124].

A new type of tapered tensile specimen is described by O.Jonas[114]. The specimen has a tapered gauge length that provides longitudinal stress distribution with a maximum to minimum stress ratio of 1.85. This specimen is also tested under a constant load, but after the test, the surface of the specimen is inspected and the gauge length is longitudinally sectioned to assess the attack in terms of number and length of cracks.

The smooth specimens described so far have involved stresses in the elastic region. Figure 8.4 illustrates a U-bend specimen, which is formed by plastic deformation of material originally in sheet or plate form. It is

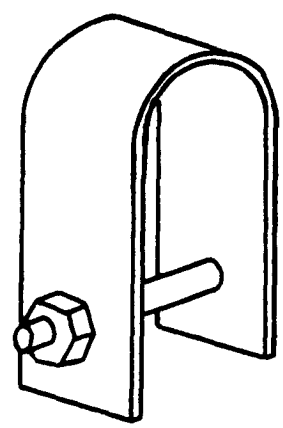

Figure 8.4. Schematic representation of U-bend specimen,[108].

generally considered that the U-bend specimens provide a most severe test condition among the smooth specimens since it contains large amounts of elastic and plastic strain. However, when the tests employ U-bend specimens, they mainly provide a qualitative assessment rather than a quantitative one, since, it combines a relatively unknown stress condition due to an unknown condition of work hardening. In the course of environmental tests, the U-bend specimens frequently crack at some distance from the point of highest load, i.e., the top of the specimen.

The tuning fork specimen is another special purpose specimen that has been used in various modifications. These modified specimens are shown in Figure 8.5. The specimens are used in two ways[113].

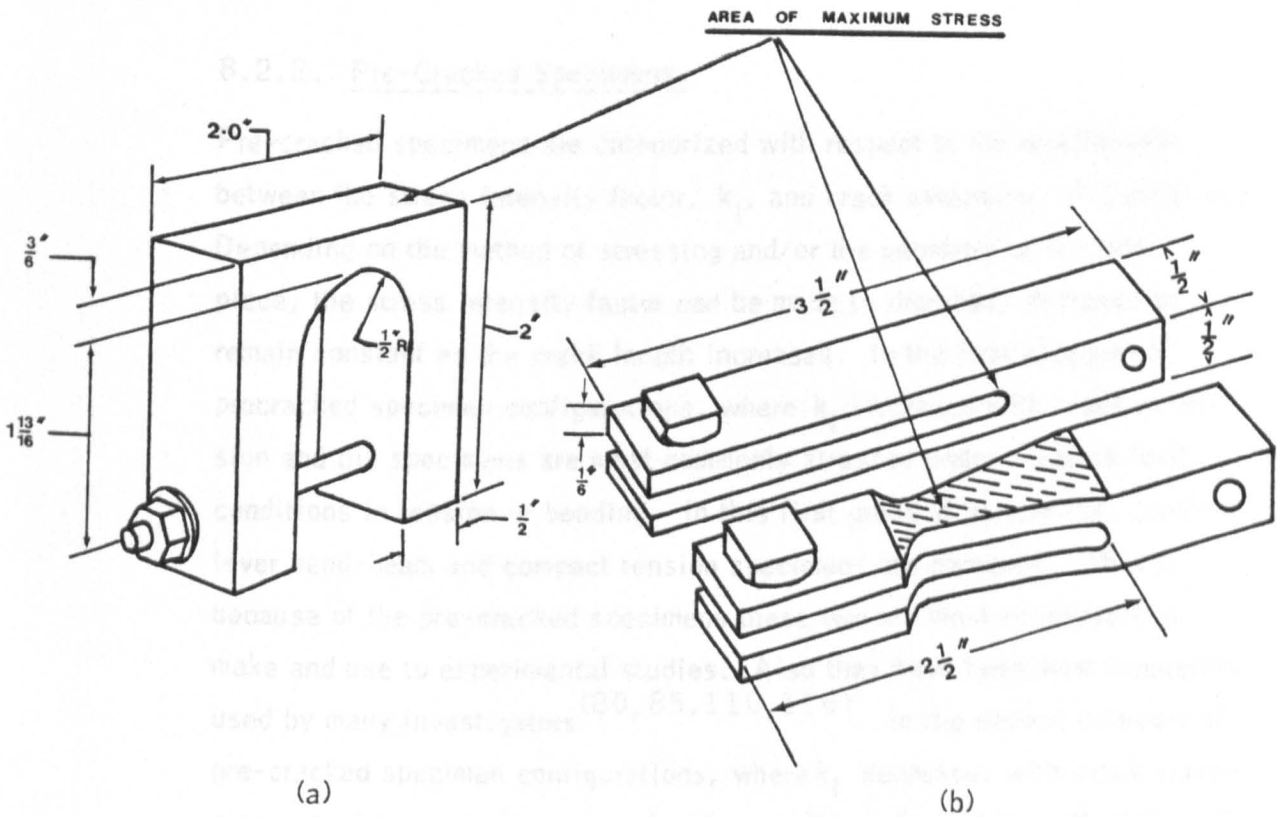

Figure 8.5. Sketches of various types of tuning fork specimens,[115].

In the first way the specimen is strained into the plastic range and stresses and strains are not usually measured, in the second way the specimen is strained within the elastic region and the strain is measured. Loginow[115] reported that specimens such as shown in Figure 8.5b, are convenient to use when a small self-contained specimen is needed that will afford some knowledge of the applied stresses. Such a specimen is particularly suited for testing thin plate material in the longitudinal or long transverse direction. The tuning fork specimens are stressed by closing the specimen tines and restraining them in the closed position with a bolt at the tine ends. The stress on tuning forks with straight tines is a maximum in a small area at the base of the tines. On the tuning forks with tapered tines, the maximum stress extends uniformly along the tapered section.

8.2.2. Pre-Cracked Specimens.

Pre-cracked specimens are categorized with respect to the relationship between the stress intensity factor, k_I, and crack extension, (Figure 8.6). Depending on the method of stressing and/or the geometry of the test piece, the stress intensity factor can be made to increase, decrease or remain constant as the crack length increases. In the first category of precracked specimen configurations, where k_I increases with crack extension and the specimens are most commonly stressed under constant load conditions in tension or bending. In this first group of specimens, cantilever bend-beam and compact tension specimens are dominant. This is because of the pre-cracked specimens these two are most convenient to make and use to experimental studies. Also they have been most frequently used by many investigators[80,85,110,116]. In the second category of pre-cracked specimen configurations, where k_I decreases with crack extension, specimens can be stressed under condition of constant deflection. The most commonly used specimen in this category is the bolt loaded wedge-opening-load (WOL) specimen[117]. Tapered double-cantilever-bend (DCB) specimens[118] gained popularity in the final category of pre-cracked

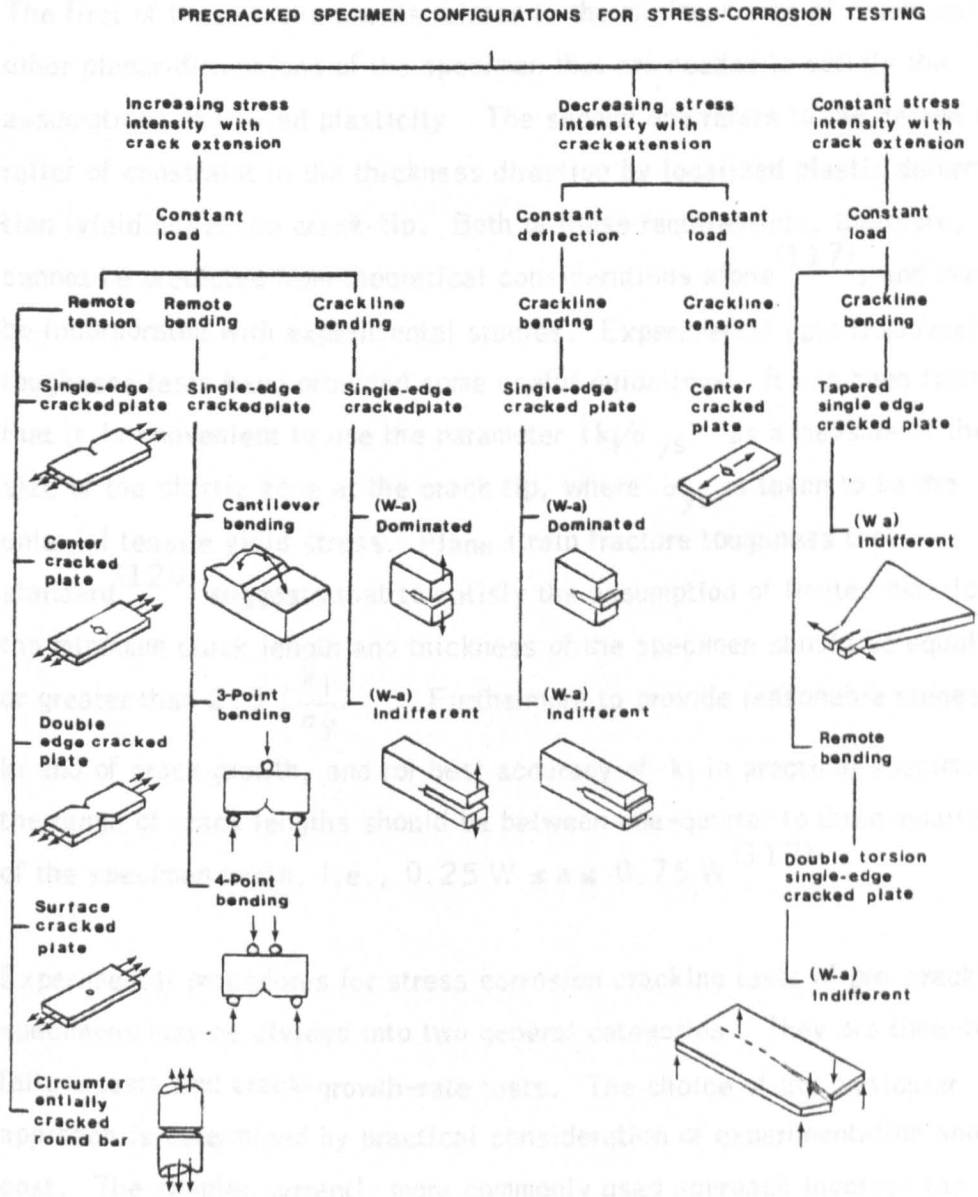

Figure 8.6. Classification of pre-cracked specimens for SSCC testing[113].

specimens, where k_I is constant with crack extension.

There are two distinctly separate requirements that have to be satisfied by the pre-cracked specimens. They are pertaining, one, to the applicability of the linear elastic analysis, and the other with regard to the condition of constraint at the crack tip[119] i.e., plane strain versus plane stress. The first of these requirements relates to the minimum size of crack and of other planar dimensions of the specimen that are needed to satisfy the assumptions of limited plasticity. The second one refers to the degree of relief of constraint in the thickness direction by localized plastic deformation (yielding) at the crack-tip. Both of these requirements, therefore, cannot be predicted from theoretical considerations alone[117], and must be incorporated with experimental studies. Experimental data from fracture toughness tests have provided some useful guidelines. It has been found that it is convenient to use the parameter (k_I/σ_{ys}) as a measure of the size of the plastic zone at the crack tip, where σ_{ys} is taken to be the uniaxial tensile yield stress. Plane strain fracture toughness test standard[120] suggests that to satisfy the assumption of limited plasticity, the minimum crack length and thickness of the specimen should be equal to or greater than $2.5\ (\frac{k_I}{\sigma_y})^2$. Furthermore to provide reasonable ranges of k_I and of crack growth, and for best accuracy of k_I in practical specimens, the range of crack lengths should be between one-quarter to three-quarters of the specimen width, i.e., $0.25\,W \leq a \leq 0.75\,W$[119].

Experimental procedures for stress corrosion cracking tests of pre-cracked specimens may be divided into two general categories. They are time-to-failure tests and crack-growth-rate tests. The choice of the particular approach is determined by practical consideration of experimentation and cost. The simpler, currently more commonly used approach involves the measurement of time-to-failure (or life) for pre-cracked specimens, under different loads (corresponding to different initial k_I), and the determination of threshold stress intensity factor (designated k_{ISCC}) below which, presumably, no failure can occur as a result of stress corrosion cracking[110,116,117]. Figure 8.7 gives a schematic representation of test results which establishes the k_{ISCC} value for a particular material

in a corrosive environment.

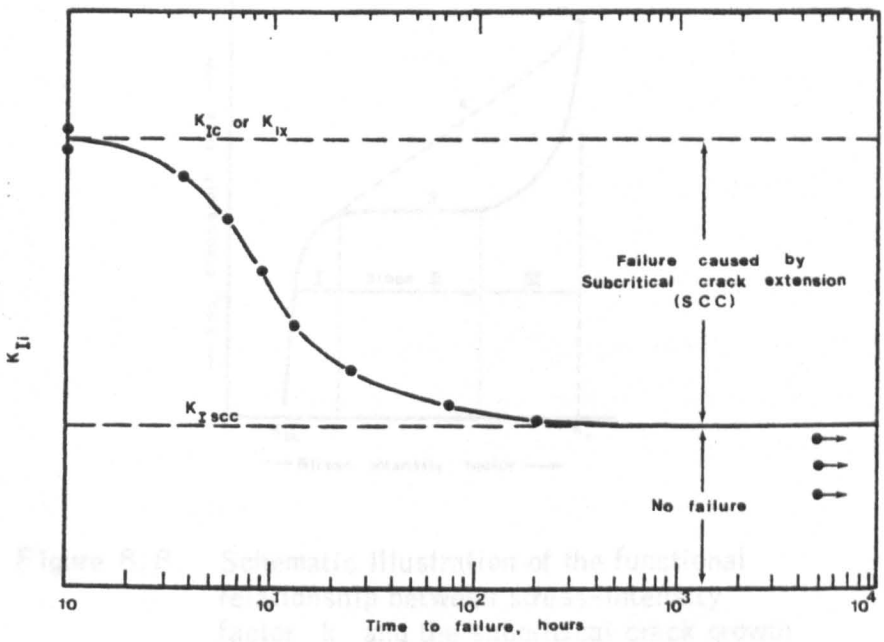

Figure 8.7. Establishment of k_{ISCC} with precracked cantilever-beam specimens test results.

The crack-growth-rate tests are more complex and require more sophisticated instruments than the time-to-failure tests. However, data, obtained by using crack-growth-rate tests should provide information necessary to enhance the understanding of the kinetics, i.e., measurements of the rate of crack growth, $^{da}/_{dt}$, as a function of the mechanical driving force, characterized by k_I, under controlled conditions. Figure 8.8 gives a schematic illustration of the functional relationship between the stress intensity factor (k_I) and the subcritical crack growth rate, $^{da}/_{dt}$. The results suggest that in region I, the rate of stress corrosion crack growth is strongly dependent on the magnitude of the stress intensity factor k_I, such that a small change in the magnitude of k_I results in a large change in the rate of crack growth. Type A behaviour in region II shows that the rate of stress corrosion cracking for many materials is partially dependent on the

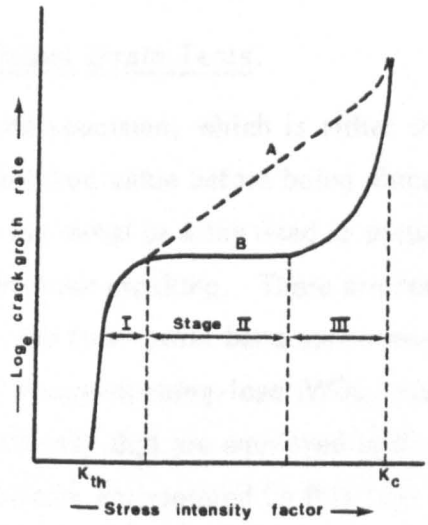

Figure 8.8. Schematic illustration of the functional relationship between stress-intensity factor k and the subcritical crack growth rate $\frac{da}{dt}$.

magnitude of k_I and the environmental conditions. Crack-growth rates in region II for high-strength steels in gaseous hydrogen as well as in other materials - environment systems appear to be independent of the magnitude of the stress intensity factor, (type B behaviour). In such cases, the primary driving force of the crack is not mechanical in nature but is related to other processes occurring at the crack tip such as chemical and electrochemical, (mass-transport, adsorption, diffusion, etc.) processes. The crack growth rate in region III increases rapidly with k_I as the value of k_I approaches k_{IC} for the material. All the three regions are not generally seen for certain environmental alloy systems.

8.3 Method of Stressing.

8.3.1. Constant Strain Tests.

In this test the specimen, which is either smooth or precracked is strained to a pre-determined value before being placed in to the corrosive environment, where the metal or alloy used to prepare the specimens is susceptible to stress corrosion cracking. There are number of specimens, particularly two-, three- and four- point bend specimens in the smooth specimens category and wedge-opening-load (WOL) specimen in the category of precracked specimens, that are employed in this constant strain test. One of the major problems encountered by this type of loading test is that when the smooth specimens are used the initial elastic strain in the specimen is converted into plastic strain as the crack propagates. This is due to the fact that as the crack propagates the stress increases on the remaining uncracked part of the section and eventually reaches the effective yield stress. Then the crack will propagate under yielding and a sharp drop in load would occur. This phenomenon is sometimes mistaken as an indication of the crack having advanced by a burst of brittle fracture. The behaviour of load relaxation on smooth specimens could vary from specimen to specimen depending on the number of cracks developing in a specimen. This behaviour can influence the time to failure because the number of cracks in a specimen can influence the size of the crack that is eventually associated with total failure and the load immediately prior to complete failure[109].

In the case of the precracked WOL specimen used in this constant strain test, the stress intensity factor at the crack-tip will be reduced as the crack propagates and the propagation of the crack will be arrested with time. Hence the specimen will not fail and the test has to be terminated at a convenient time. If the test is stopped at a shorter time than the required time, (the required time sometimes exceed more than 1000 hours) the test could give a misleading result. Furthermore, the propagating crack will become blunt and could branch depending on the material and the environment studied. This could add more uncertainty to the test results. Priest and McIntyre[121] have used EN 30B steel specimens, in which the stress

corrosion crack path was intergranular, to demonstrate the crack blunting effect on the k_{ISCC} value. The results show that as the stress corrosion crack propagates, the crack-tip becomes progressively less sharp due to the formation of an "Intergranular zone" of incompletely separated grains resulting from multiple scale branching around individual grains. Therefore the k_{ISCC} value measured in such a material by an arrest technique, i.e. constant strain test, is expected to be greater than if measured by a constant load test.

Normally when larger specimens are tested under constant strain, the load is applied by a conventional testing machine or a similar device initially, to achieve the required strain, then a restraining frame is fixed to the specimen while maintaining the load. Thereafter the load applied by the testing machine is removed progressively while the restraining frame holds the specimen under a constant strain. In this technique, it is assumed that the strain in the specimen remains constant as the restraint is transferred from the testing machine to the frame. This implies a similar stiffness in the testing machine and frame, which is likely to be so only if the frame is relatively massive compared to the specimen. This point has not always been appreciated since the liaterature shows many examples of soft or relatively small stressing frames having been used in stress corrosion testing[109].

8.3.2. Constant Load Tests.

In this test the specimen which is either smooth or precracked, is loaded with a desired constant load and left until failure occurs in a selected corrosive environment. In this type test, when subjected to a constant load a crack initiates on the specimen and propagates, the applied stress on the remaining part of the cracked specimen will increase while the effective cross-section reduces. Consequently the specimen when subjected to a constant load test is more likely to lead to early failure or total failure than a constant strain test.

Figure 8.9 gives a schematic comparison of results on the two types of test where precracked cantilever-beam specimens developed by Brown[110] are tested under constant load and precracked modified WOL specimens[117]

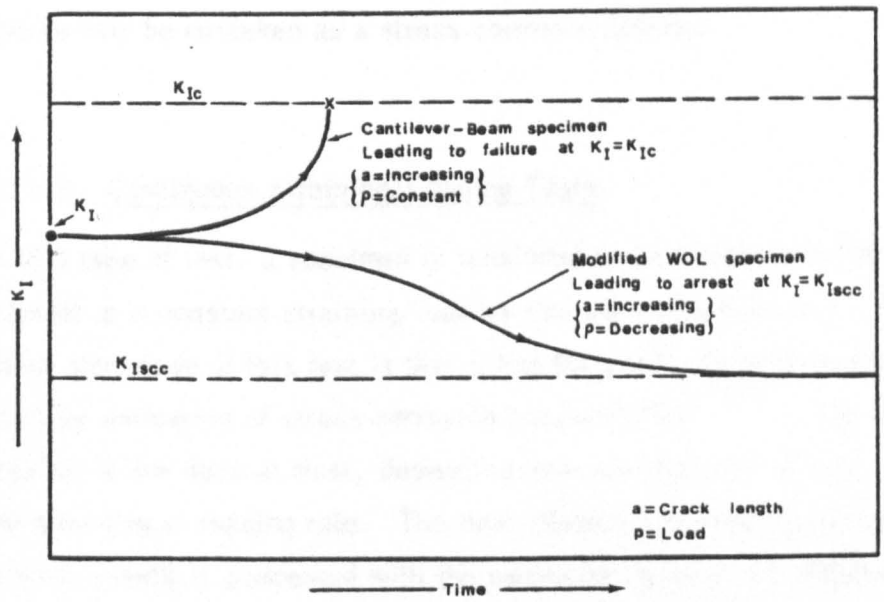

Figure 8.9. Difference in behaviour of modified WOL and cantilever-beam specimens.

are tested under constant strain. In the cantilever-beam testing, the value of the stress intensity factor, k_I, increases as the crack length increases under constant load, which leads to fracture for each specimen. In contrast, for the WOL specimen, the k_I value decreases as the crack length increases under a decreasing load. The decrease in load more than compensates for the increase in crack length and leads to crack arrest, presumably at k_{ISCC}.

Sometimes, smooth tensile specimens of relatively large cross-section are tested under constant load. In this case, a heavy load or a lever system is used. In addition, in some corrosive environments the effective stress required to initiate a failure would be in the region of yield tensile stress. Furthermore, it may be necessary to keep the system on test for a very

long period. Hence a constant load test on a smooth tensile specimen is discouraged due to these difficulties. The difficulties are sometimes avoided by the use of thin wire specimens. But it may be necessary to bear in mind that thin wire specimens could fail due to normal corrosion or by pitting attack where the effective cross-section is reduced. Hence the failure may be mistaken as a stress corrosion failure.

8.3.3. Continuous Straining/Loading Tests.

In this type of test, a specimen is tensioned in a corrosive environment of interest at a constant straining/loading rate until failure occurs. The major advantage of this test is that it has the ability to produce rapid, positive indication of stress corrosion susceptibility[122]. The test requires a few days at most, depending upon the ductility of the alloy and the straining or loading rate. The most important feature of continuous straining tests is concerned with the particular value of the strain rate employed. If the continuous straining rate is too high then ductile fracture will ensue before the necessary corrosion reactions can take place. In contrast, in some cases if the straining rate is too low, then a completely protected film can be formed and cracking would be inhibited. Figure 8.10 illustrates this point schematically. Also it has been established that the

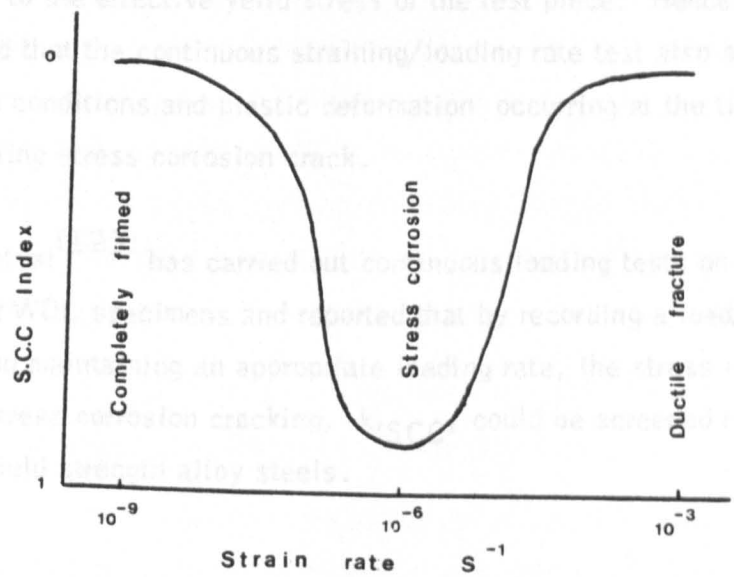

Figure 8.10. Effect of straining rate on the susceptibility of stress corrosion cracking index,[109].

most appropriate straining rate for producing stress corrosion cracking can vary from system to system and will mainly depend on the type of metal and environmental conditions. Although the continuous straining test on a smooth tensile specimen could not give a quantifiable result, the stress corrosion cracking susceptibility may be classified by comparing the time to failure, percentage of reduction in area, percentage of elongation, and plastic strain to fracture. Additional information such as energy absorbed prior to fracture, fracture stress, ultimate tensile stress, etc. could be obtained by recording load versus time curves. In some cases where susceptibility is doubtful because of only slight changes in ductility and time to failure, etc., it is useful to examine the fracture surfaces of a specimen with a microscope to determine the presence of small cracks. Scanning electron microscopic examination could be carried out to confirm the susceptibility of the specimen to SCC.

It may be argued that pulling a specimen to failure at a slower continuous straining/loading rate with failure occurring after considerable plastic deformation, bears little similarity to actual stress corrosion failures. But it has been pointed out[122] that also in constant strain test and constant load test, crack propagation occurs under conditions of slow dynamic strain to a greater or lesser extent depending upon the initial value of stress in relation to the effective yeild stress of the test piece. Hence it may be accepted that the continuous straining/loading rate test also simulates the dynamic conditions and plastic deformation occurring at the tip of a propagating stress corrosion crack.

Clark, et.al[123] has carried out continuous loading tests on precracked modified WOL specimens and reported that by recording a load/displacement curve and maintaining an appropriate loading rate, the stress intensity factor for stress corrosion cracking, k_{ISCC}, could be screened rapidly for higher yield strength alloy steels.

8.4 Interpretation of Test Results.

In view of the existence of numerous experimental studies, where artificial environments have been used to investigate susceptibility to stress corrosion cracking, an adequate analysis of test results and their interpretation are of very great importance. The first problem is to determine the most useful measure of the magnitude of stress corrosion cracking. The second problem is to compare the susceptibility of one material with another for SCC or the efficiency of one protective measure with another. For this a representative value must be selected. Finally, the test results have to be translated into engineering parameters that could be used directly in actual design.

Specimen-life is more frequently used in stress corrosion testing as a parameter which could detect the SCC susceptibility of a material or alloy in a corrosive environment. It is well known that considerable scatter in specimen-life results occurs, and it is often found that the majority of specimens in a test, particularly at higher loads, fail rapidly, however, a few which are loaded at lower loads fail at much longer times, or even do not fail at all before the test is discontinued. The scatter in experimental results has been demonstrated by NACE TASK GROUP T-IF-13[124]. The task group conducted a core program based on four alloy steels among eighteen laboratories and employed a recommended test method for "evaluation of metals for resistance to sulphide stress cracking at ambient temperatures", (NACE T-IF-9). The tests were conducted on smooth tensile specimens under a constant load and on notched bend specimens under a constant deflection. Results on tensile specimen exhibited a certain amount of scatter, however this was accepted, as the scatter lies within the stipulated limits. But the results on the constant deflection notched beam specimens were inconsistant and therefore not acceptable. Some causes for the scatter were found to be the following:

Equipment - stress calibration, internal friction, vibration from outside sources and also when another specimen breaks.

Environment - ratio of specimen area to volume of corrosive liquid, H_2S bubbling rate, depletion of acetic acid, hence pH, intermittent H_2S bubbling and oxygen contamination causing accelerated corrosion.

Materials - inhomogeneities in materials, particularly after heat treatment.

Various criteria of the time-to-failure have been used depending upon the test procedure and type of loading system employed. Under constant load test, the initiation of a stress corrosion crack in high strength alloy steels generally results in rapid fracture of the specimen and the specimen life is easily determined. Frequently, however, with lower-strength alloy or more resistant alloy or with relatively low applied stress, cracking is initiated slowly and is difficult to detect. Further, cracks may initiate at multiple sites, thus, causing problems in deciding when to consider the specimen has failed and when to terminate the test.

A Stress-Life curve could be established to assess the resistance to stress corrosion cracking of a material. This type of curve provides more information when the stress level is varied over a range that changes the life of the specimen. The primary interest is generally in the long-life portion of the curve (stress corrosion threshold). Therefore more tests should be made in this vicinity. Hence, the problem of when to terminate the test could be faced again. To overcome this problem it is suggested to construct a percentage survival curve or a percentage failure curve. These curves provide one of the most significant comparisons of materials that have different degrees of susceptibility to stress corrosion cracking. Also, it is sometimes much more useful to establish the percentage of survival stress with another variable for a constant period of time. Kane and Greer reported[125] their test results in a form of survival stress against another variable which is either temperature or concentration of H_2S and kept the exposure time constant. They have found excellent correlation between SSCC data from tests conducted in actual field environments and laboratory NACE solution environments.

The application of linear elastic fracture mechanics to stress corrosion cracking experimental studies has given a greater hope that the laboratory experimental data could be used directly in engineering design. The determination of threshold stress intensity factor, k_{ISCC}, below which no failure can occur as a result of stress corrosion cracking, could be used directly to calculate the allowable stress and tolerable crack sizes in a particular member of a structure. But it has been

shown that there are some limitations applicable to these results. The time-to-failure on a pre-cracked specimen is quite dependent on the loading condition, specimen size and geometry and environmental conditions, hence it can lead to serious errors in the estimation of k_{ISCC}. For example, by increasing the cut-off time from 100 to 10,000 hours, the apparent k_{ISCC} value is decreased from 187 to 27.5 MN $m^{-3\,2}$ for a high strength alloy steel tested in synthetic sea water at room temperature[119]. Furthermore McIntyre has demonstrated[121] that the threshold value k_{ISCC} could be influenced by stretch zone formation, measurement technique, accuracy of stress intensity measurement and prior history of the specimen. Thus substantial error can be introduced by any of the factors to the k_{ISCC} value. Hence the application of k_{ISCC} value directly to engineering design is discouraged.

The kinetic studies such as crack growth rate measurement using the fracture mechanic concepts could allow calculation of service life of a structure when loaded above the threshold stress intensity factor, k_{ISCC}. Unfortunately the crack growth rate measurement is also influenced by various factors, namely, failure to attain equilibrium, crack branching, crack curvature, and crack blunting[121]. Failure to attain equilibrium for crack growth in a stress corrosion test is demonstrated clearly in Figure 8.11. It shows that the crack

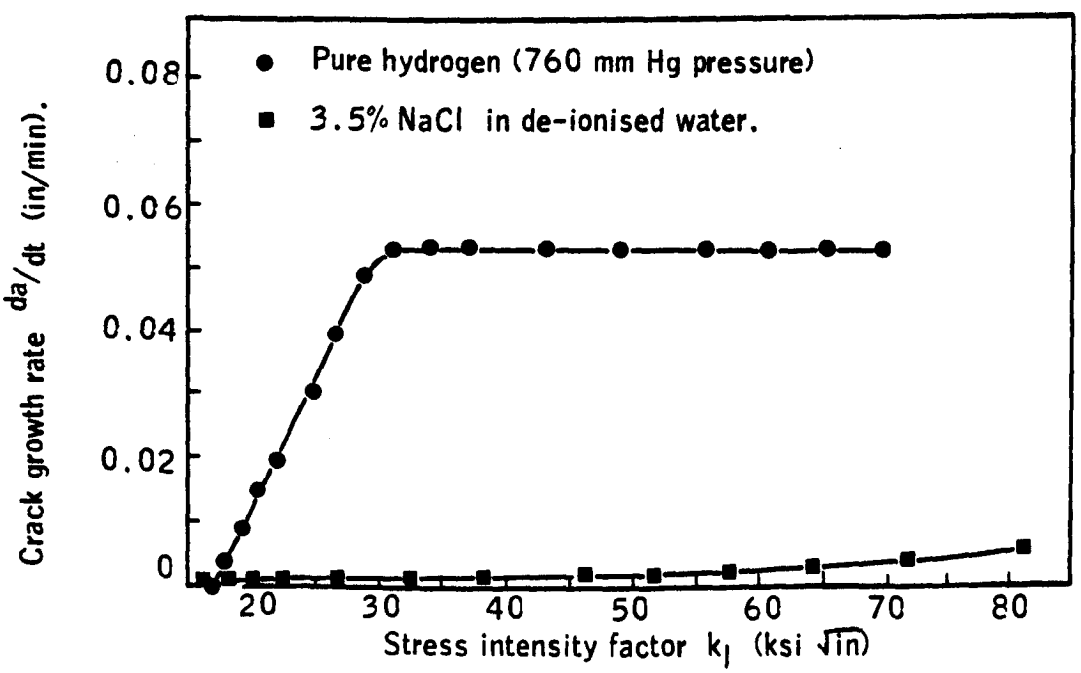

Figure 8.11. Crack growth rate of EN 30B steel as a function of stress intensity factor and environment,[121].

growth rates for EN 30B steel in purified hydrogen and 3.5% sodium chloride in deionized water differs markedly. In the case of hydrogen environment an equilibrium crack growth rate is rapidly attained, whereas the crack grown in sodium chloride environment propagates at a much slower rate which increases progressively during a test but never attained equilibrium.

The difficulties encountered in laboratory stress corrosion test methods, such as, differences in manner of loading, variations among test specimens, differences in environmental severity between laboratory and field conditions and significant scale factor between specimens and members of a structure, make very doubtful to apply the tests data directly to engineering design. There is an indirect method used in the petroleum industry to select new material from laboratory experimental studies to industrial application. The method is summarized as follows[2];

A laboratory test environment is selected which is slightly more severe than could be expected during the service life of the structure, and the threshold stress for failure (or alternative, the critical stress Sc value) is determined for the material being evaluated. This is compared on a rank order basis with other materials, including those known to have failed in service and those known to have proved satisfactory. To allow for differences in strength among the materials being evaluated some investigators have expressed threshold stress for failure as a percentage of the yield stress. For evaluating oil field materials the two reference points most generally used are; API Grade J-55 tubing and casing which have been substantially free of embrittlement failures, and API Grade P-105 tubing which has failed in sour gas service. An acceptability limit would lie between these two materials.

It is clearly seen from the interpretation of the results that there is no one stress corrosion test capable of providing a quantitative parameter which could be applied directly to engineering design or be used to evaluate any protective measures developed to combat stress corrosion cracking. Hence, it is common practice among researchers to select a particular test method and specimen type to suit the facilities available in their laboratories and the funds provided for the research.

CHAPTER NINE

CONTINUOUS SLOWER STRAINING/LOADING RATE TEST ON COMPACT TENSION SPECIMEN, (CTS)

CHAPTER 9.

CONTINUOUS SLOWER STRAINING/LOADING RATE TEST ON COMPACT TENSION SPECIMEN, (CTS).

9.1 Introduction.

The continuous slower straining/loading rate test is one of the stress corrosion test methods which could be used successfully within a limited period time to screen the effectiveness of the proposed protective measure to inhibit sulphide stress corrosion cracking in steel. The test method has some limitations over its advantages as discussed in the previous chapter. The most important feature of the continuous straining/loading test is concerned with the selection of the particular value of strain rate that is to be employed. Clearly, if this rate is too high ductile fracture will ensue before the necessary corrosion reaction takes place. Hence it is of utmost importance to select a strain rate, which could clearly show the sulphide stress corrosion attack in the environment to be studied, to evaluate the proposed technique.

In the earlier experimental studies, i.e., the hydrogen diffusion and corrosion weight loss measurement studies, the proposed protective coating, MoS_2/FEP, was used as an adherent coat to the steel membranes or steel coupons. In those studies the dimension of the protective coat and distance between the coating and exposed steel were not critical, simply because the specimens were in the form of flat pieces of steel. But in this case the proper control of the application of the protective coating is vital since this continuous slower straining/loading rate test employs precracked thicker compact tension specimens. Also the application of the protective coat could give a unfair advantage over the unprotected specimen. Therefore it is important to study how and where to apply the protective coating on the compact tension tension specimens and to select a coating pattern which could be used in further experimental studies.

It has been accepted generally that temperature is one of the important factors which could control the susceptibility of steel to sulphide stress corrosion cracking. Also most of the oil and gas wells operate at elevated temperatures up to 80° C and in some cases even higher. Hence the proposed technique to inhibit

sulphide stress corrosion cracking in steel should be studied as a function of temperature.

Based on the above facts the continuous slower straining/loading rate tests on compact tension specimens are sub-divided into three groups. These are:

(a) Studies on the effect of various straining/loading rate on CTS fracture toughness in air and corrosive environment, which would help to select a straining/loading rate.

(b) Studies on the effect of application of the protective coating at various dimensions and position, which would facilitate the selection of a pattern of the protective coating on CTS.

(c) Studies on the effectiveness of the proposed technique as a function of temperature, taking advantage of straining/loading rate and coating pattern to be selected from the above mentioned two groups (a) and (b).

9.2 Experimental Procedures.

9.2.1. Materials Preparation.

G1 Special steel equivalent to EN 30B steel, in the form of a strip and API 5LX 65 steel in the form of a pipe were supplied by Caxton Steel Company, London, and the Welding Institute, Abingdon, respectively. The chemical composition of the steels are given in Table 9.1. The steels were machined in the longitudinal direction to produce compact tension specimens as shown schematically in Figure 9.1. The notch was machined to a depth of 18 mm and 1.5 mm wide with a root radius not exceeding 0.01 mm from which a fatigue crack not greater than 2.5 mm would be developed. The G1 Special steel specimens were heat treated at a temperature of 830° C in an argon environment for one hour. This was followed by oil quenching at room temperature. It was then tempered at 200° C for 1 hour and cooled at room temperature in air. The heat-

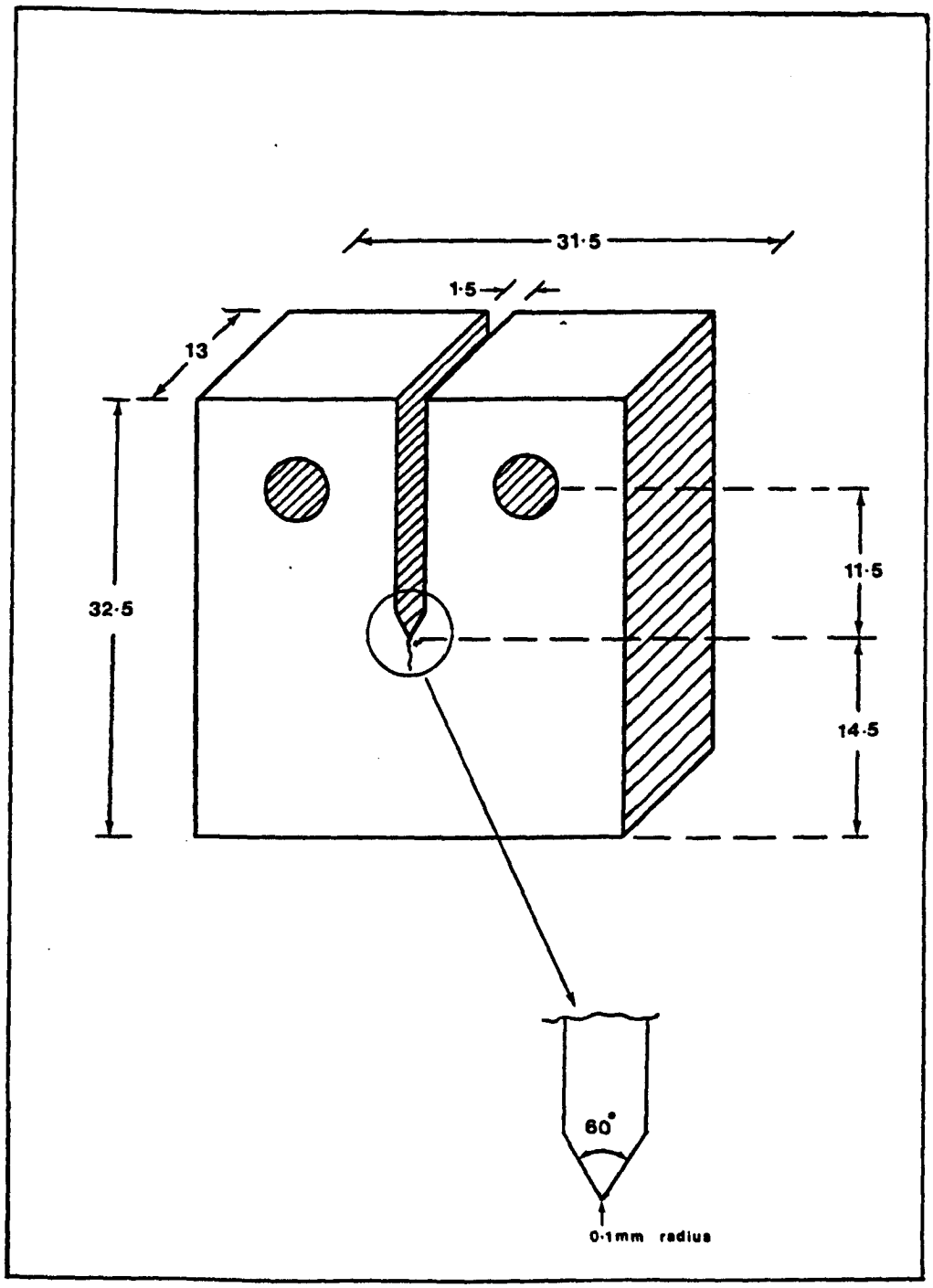

Figure 9.1. Schematic illustration of compact tension specimen, (CTS). Dimensions are in mm.

treated G1 Special steel and un-heat-treated API 5LX 65 steel specimens were polished with 600 grade silicon carbide paper in a direction that could not interfere with the observation of the fatigue crack to be initiated at the V-notch tip.

A fatigue crack was developed from the starter notch by the application of cyclic load. A Losenhousen fatigue testing machine was used to develop the tension-tension cyclic loading. The fatigue crack was initiated on the G1 special steel specimen by maintaining the maximum load at 8 kN and minimum load at 0.8 kN at a frequency of 10 Hz. This laoding value kept the maximum stress intensity factor developed at the V-notch tip to less than 50 percent of the fracture toughness value. Once the crack was initiated, the maximum load was gradually reduced to 2.0 kN, while maintaining the ratio minimum load/maximum load R at the value of 0.1. It was also ensured that the stress intensity factor at the growing fatigue crack tip was less than 75 percent of k_{ISCC}. The same procedure was adopted for the API 5LX 65 steel, except that the maximum load at final stages was reduced to 3.5 kN instead of 2.0 kN. Thus the cyclic loading was reduced another level while the frequency was maintained at 10 Hz and the crack was closely watched to grow between 1.5 and 2.0 mm. Initially the fatigue crack lengths on the specimens were measured using the metallurgical microscope at magnification of 100. Finally a correction was made to the measured fatigue crack value when the test specimens were split into two pieces and the crack measured after each experiment.

The mechanical properties of both types of steel are given in Table 9.2.

Ball-milled and unball-milled MoS_2 and FEP protective coatings were used with the catalyst to FEP ratios of 1:0.85 and 1:1.12 respectively in this study. The mixtures of the appropriate coat were prepared as outlined in the section 4.3.1.3. The unball-milled MoS_2 and FEP mixture was coated in three different patterns shown schematically in Figures 9.2 to 9.4. Unprotected specimens were coated with Lacomit Varnish G 371, obtained from Agar Aids, Stansted, Essex, England. This coating helped to insulate the unprotected specimen substrate from any

TABLE 9.1. Percentage chemical composition of the steels used.

Steel / Elements	GI Special	API 5LX 65	Mild Steel	EN 8
C	0.25	0.14	0.77	0.38
Mn	0.54	1.33	0.58	0.56
Si	0.33	0.25	0.13	0.27
S	0.008	0.005	0.025	0.036
P	0.014	0.020	0.018	0.20
Ni	4.0	0.10	0.17	-
Cr	1.35	0.02	0.09	-
Mo	0.25	0.01	0.03	-
Nb	0.01	0.03	0.01	-
Al	0.008	0.025	0.025	0.015
Ti	0.009	0.008	0.003	0.01
Cu	0.21	0.30	0.24	0.002
Co	0.07	0.02	0.02	-
Zr	0.01	0.01	0.01	-
V	0.01	0.08	0.01	0.01
Sn	0.01	0.01	0.02	0.01
B	0.005	0.005	0.005	0.005

TABLE 9.2. Mechanical properties of the GI Special and API 5LX 65 steels.

Steel	Yield Stress (σ_y N/mm^2)	Ultimate Tensile Stress (σ_{UTS} N/mm^2)	Elongation (percent)	Area of Reduction (percent)
GI Special	1094	1336	27	66
API 5LX 65	515	606	38	50

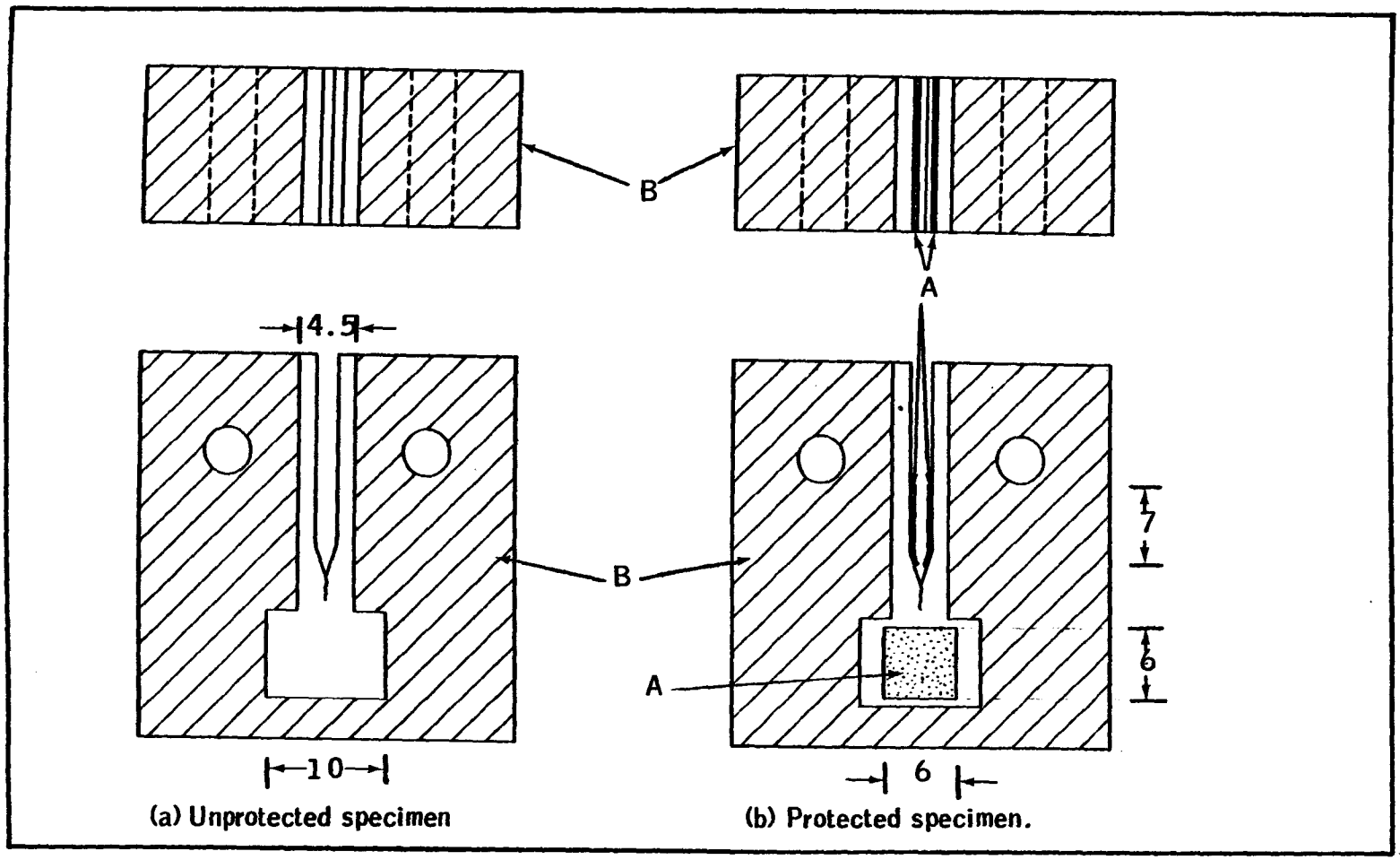

Figure 9.2. Pattern 1 of MoS_2/FEP and lacomit varnish coats on compact tension specimens A) MoS_2/FEP coat, B) Lacomit varnish coat. Dimensions are in mm.

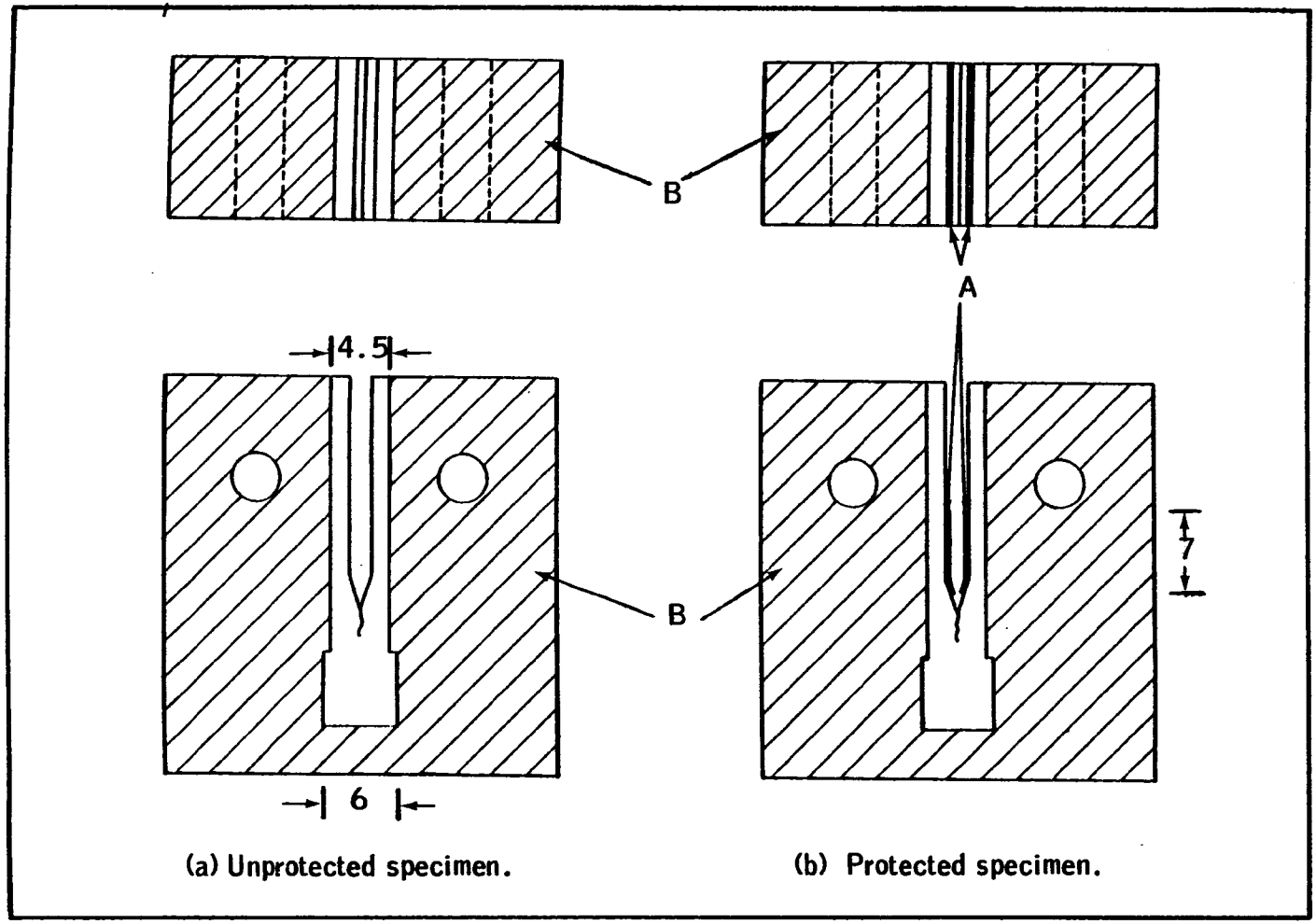

Figure 9.3. Pattern 2 of MoS_2/FEP and lacomit varnish coats on compact tension specimens. A) MoS_2/FEP coat, B) Lacomit varnish coat. Dimensions are in mm.

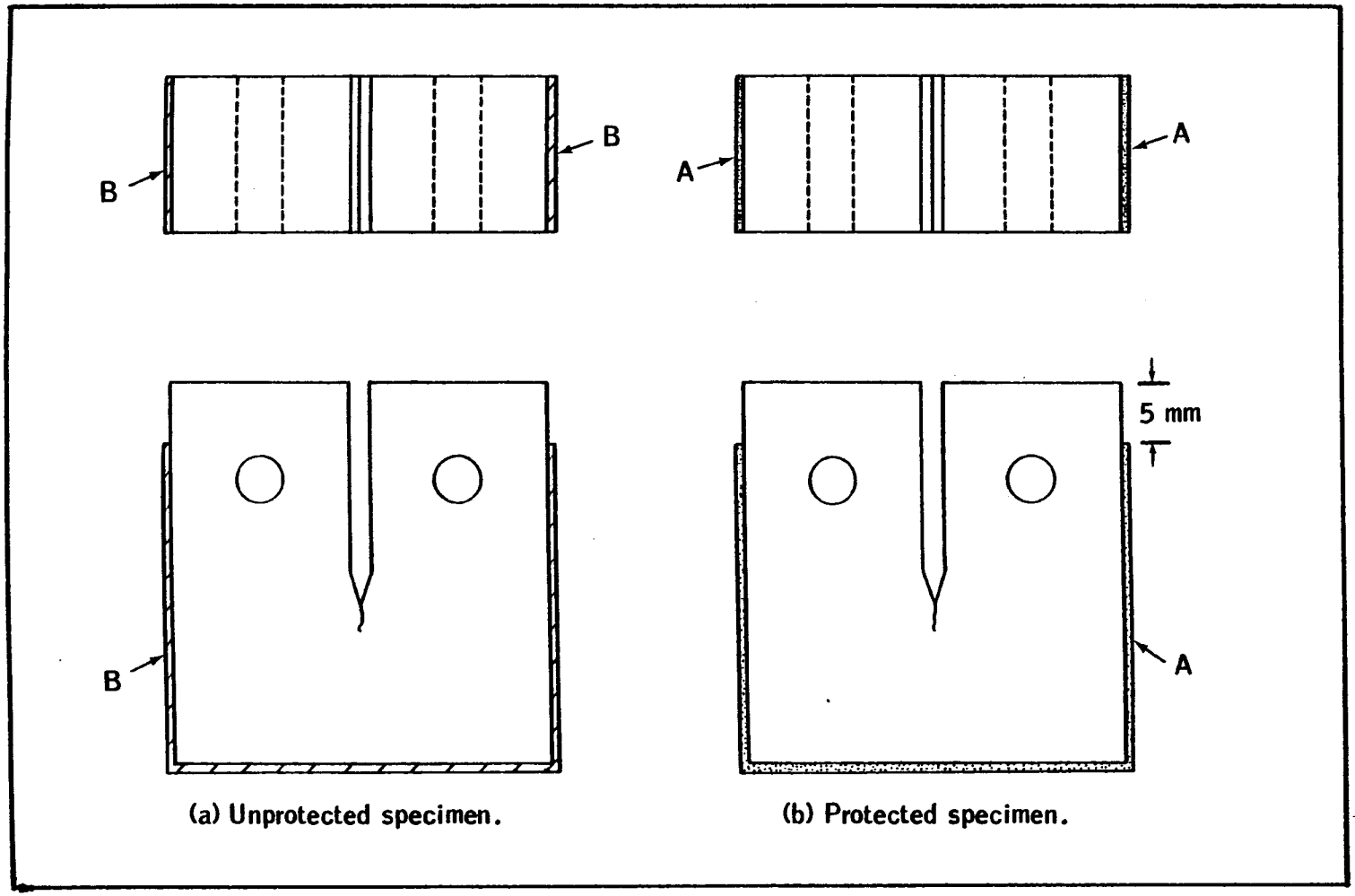

Figure 9.4. Pattern 3 of MoS_2/FEP and lacomit varnish coats on compact tension specimens. A) MoS_2/FEP coat, B) Lacomit varnish coat.

electrochemical reaction and to keep an effective comparison between protected and unprotected specimens.

NACE solution (5 percent sodium chloride by mass and 0.5 percent acetic acid by volume) saturated with H_2S was selected for this study instead of continuous bubbling of H_2S at 1 atmospheric pressure, because the testing system employed, Plate 9.1, dictated the selection of corrosive environment.

9.2.2. Test Cell

A perspex cell was made to contain 500 ml of corrosive solution and it had a provision for a thermometer and a heating tape to be wrapped around to maintain required temperature. Also it had an inlet and an outlet to facilitate proper drainage and to give a path for any gas pressure developed to escape during the test without any air getting into the test cell. Plate 9.1 shows the test cell and the facilities of the testing machine employed in this continuous slower straining/loading rate test. Teflon sleeves were used with loading pins to prevent any galvanostatic corrosion between the test specimen and attachment. A schematic representation of the attachment with a specimen is given in Figure 9.5. Furthermore the attachment was coated with Lacomit Varnish to prevent any electrochemical reaction which might take place on the attachment surface and change the composition of the corrosive environment.

9.2.3. Test Procedure.

The appropriately coated specimen was fixed to the attachment and placed in the test cell then connected to the Mayes testing machine with the help of extension bars. The NACE solution was purged with N_2 for 30 minutes followed by H_2S for another 30 minutes to ensure proper saturation before it was placed in the cell. The 500 ml wash bottle used to purge the gases was kept in a water bath while purging with the gases to achieve the required temperature. Also it was necessary to keep the temperature

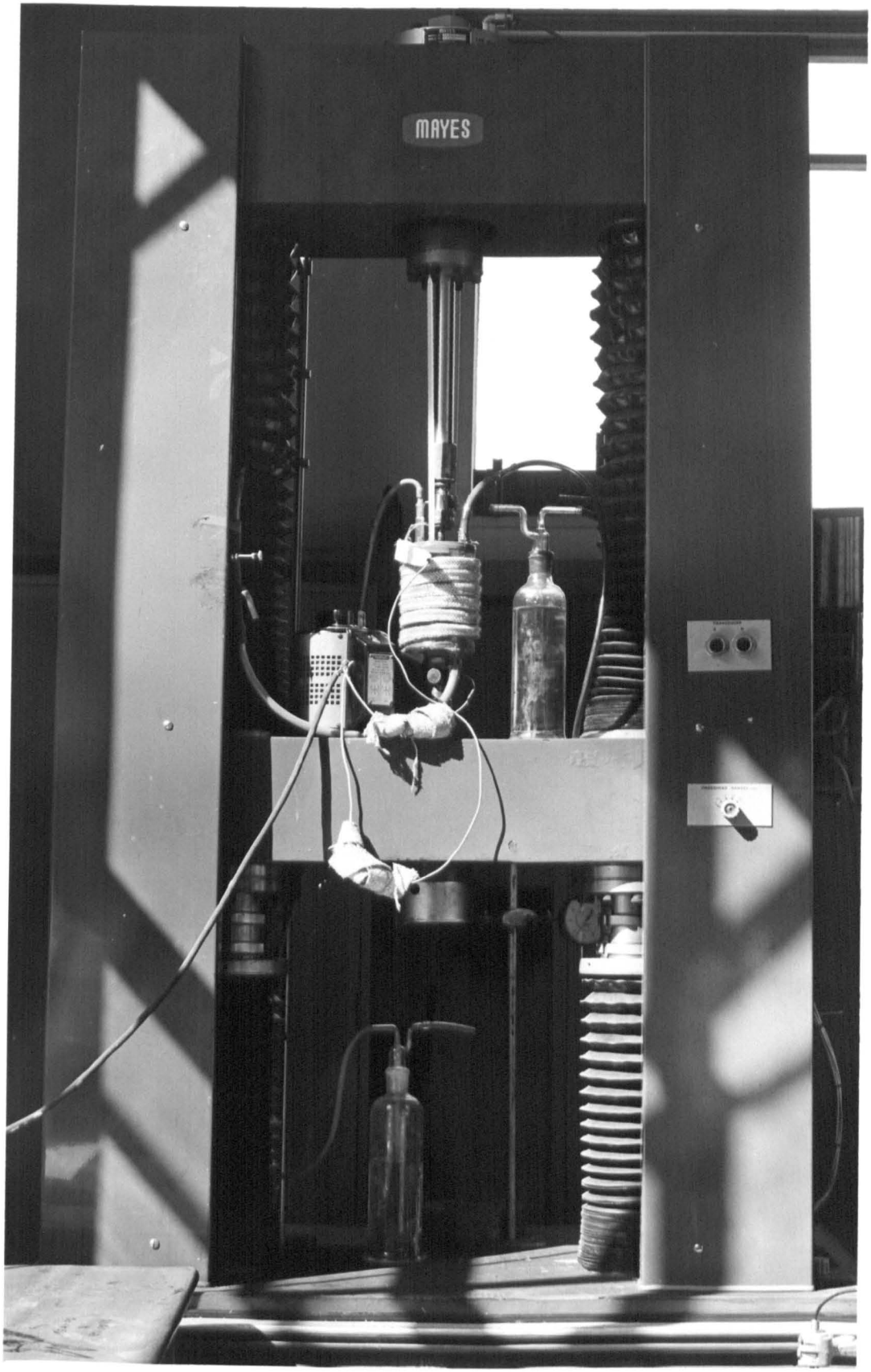

Plate 9.1. The set-up of continuous slower straining/loading rate test on the Mayes machine for compact tension specimen, (CTS).

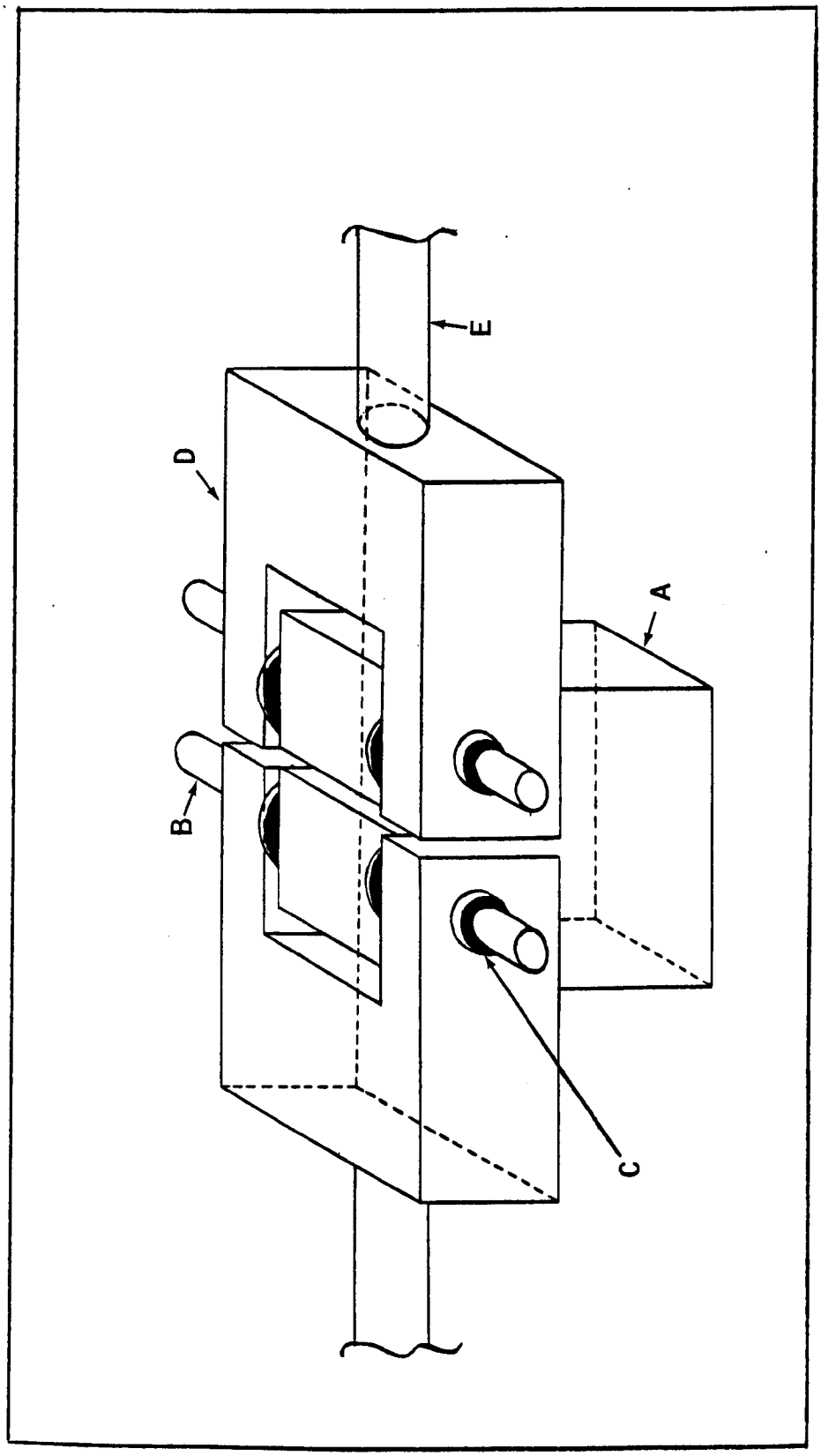

Figure 9.5. Schematic illustration of the attachment with a specimen.
A) Compact tension specimen, B) Loading pin, C) Teflon sleeves,
D) Steel attachment, E) Part of extension rod.

constant during the H_2S purging because the amount of H_2S required to achieve saturation varies with temperature. The prepared corrosive solution was placed in the test cell and the appropriate temperature was maintained with the aid of heating tape. After filling the test cell with the corrosive solution, the specimen was subjected to a pre-selected straining/loading rate until the specimen failed completely. The Mayes testing machine had a facility to pre-select any straining/loading rate that was required in this series of tests and recorded the load-displacement curves automatically from which the parameters: stress intensity factor at failure, and total energy for fracturing the specimen, were calculated. When the compact tension specimens were tested in air, a clip gauge (satisfied to BS-.5447 Plane Strain Fracture Toughness Testing) was fixed to the specimen which facilitates the recording of a separate load-displacement curve simultaneously with the curve recorded by the Mayes machine.

9.2.4. Determination of H_2S Concentration.

Due to the nature of the testing system used for this study it was found that it was essential to use H_2S saturated NACE solution instead of continuous bubbling H_2S at 1 atmospheric pressure. Hence the H_2S concentration in the corrosive solution was reduced to an unknown level at the end of test depending on the duration and the temperature of the test. Furthermore it is generally accepted that the concentration of H_2S in a corrosive environment is one of the important factors which control sulphide stress corrosion cracking. Hence it is of utmost importance to determine the H_2S concentration at the beginning and at the end of test, particularly when the test temperature changes. For this purpose a standard iodimetric titration technique was employed. In this test a known volume corrosive solution was taken and diluted with distilled and deionized water to prevent any escape of H_2S during the titration. A known concentration and excessive volume of iodine solution was added to the diluted H_2S corrosive solution to facilitate the following reaction.

$$H_2S + I_2 \rightarrow S + 2H^+ + 2I^-$$

The amount of iodine consumed, hence the concentration of H_2S, was determined by back titrating the iodine solution against a standard sodium thio-sulphate solution according to the equation:

$$2\,S_2O_3^{2-} + I_2 \rightarrow 2I^- + S_4O_6^{2-}$$

A freshly prepared starch solution was used as an indicator.

9.3 Scanning Electron Microscopic Examination of Fracture Surfaces.

It has been recognised that scanning electron microscopic examination of a fracture surface is probably the most important diagnostic tool available to identify the sulphide stress corrosion cracking failures. Hence in this study scanning electron microscopic examination on fracture surfaces were carried out when ever possible.

Since the corrosive environment employed in this study was saturated with H_2S, it has been found that the fracture surface became contaminated with sulphides. Hence it was found that the fracture surfaces had to be cleaned to obtain more clear fractographs. Initially the fracture surfaces were cleaned ultrasonically in acetone for 30 minutes. However, when the test was carried out more than 10 hours or was left to run overnight it was found that an electrolytic cleaning was required. Therefore the fracture surfaces were electrolyized at a cathodic current density of 100 mA/cm^2 for 5 minutes in saturated citric acid and rinsed with a jet of distilled and deionized water without breaking the electric circuit. This treatment was found to be quite adequate and satisfactory, whenever required.

9.4. Results.

9.4.1. Various Straining/Loading Rate Tests.

G1 special steel specimens were employed in this study at different straining/loading rate varying from 7680 to 2.65 MN $m^{-3/2}$/hour in air

and in NACE solution saturated with H_2S at $20^0 \pm 2^0$ C. Fracture toughness was calculated from the load versus clip gauge displacement curve according to the BS 5447, when the specimens were tested in air. This calculation and load-displacement curves were compared with the curve obtained autographically by the testing machine. It had been established that there were no variations in identifying the onset of a crack or selecting the maximum load used to calculate the fracture toughness. Therefore when the tests were conducted in the corrosive environment without the clip gauge displacement measurements it was ensured that still valid stress intensity factors at failure were calculated from the automatically recorded load versus displacement curves.

Figure 9.6 gives the plot of loading rate versus stress intensity factor at fracture in air and the corrosive environment. Plates 9.2 to 9.5 give the scanning electron microscopic fractographs for the specimens tested in air at various rates. The similar fractographs for the specimens tested in H_2S saturated NACE solution are given in Plates 9.6 to 9.9.

9.4.2. Different Pattern of Protective Coating tests.

The effect of various patterns of the protective coatings on the compact tension specimens were studied on API 5LX 65 steel. The specimens coated in three different patterns were tested at a loading rate lower than 7 MN $m^{-3/2}$/hour in NACE solution saturated with H_2S at $20^0 \pm 2^0$ C. The protective coating used in this study was ball-milled MoS_2/FEP coat with the catalyst to FEP ratio of 1:0.85. The stress intensity factor, k_{IQ} at failure was calculated from the peak load, dimensions of the specimen and the initial crack length. The size of the specimen and low yield stress of the API 5LX 65 steel does not satisfy the requirements for a valid linear elastic fracture mechanics stress intensity factor calculation. Therefore the k_{IQ} can only be considered as a qualitative indicator. The total energy required for fracturing the specimen was calculated from the area of load-displacement curve. This quantity divided by the distance from the fatigue crack tip to the edge of the specimen gave the average energy required for unit length of crack extension.

Figure 9.6. Effect of loading rate on GI Special compact tension specimens fracture toughness in air and in a corrosive environment, NACE solution saturated with H_2S at 20° C.

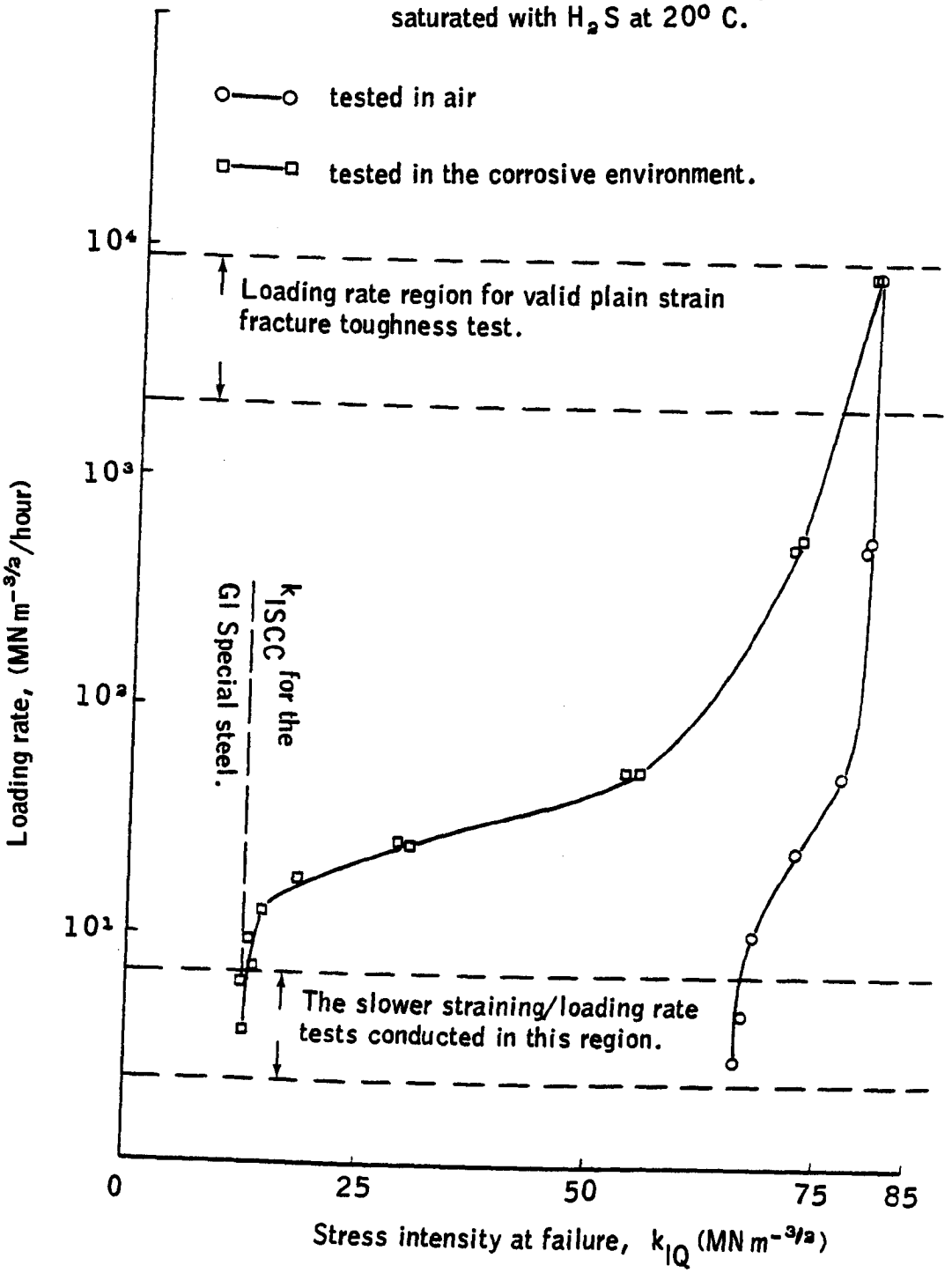

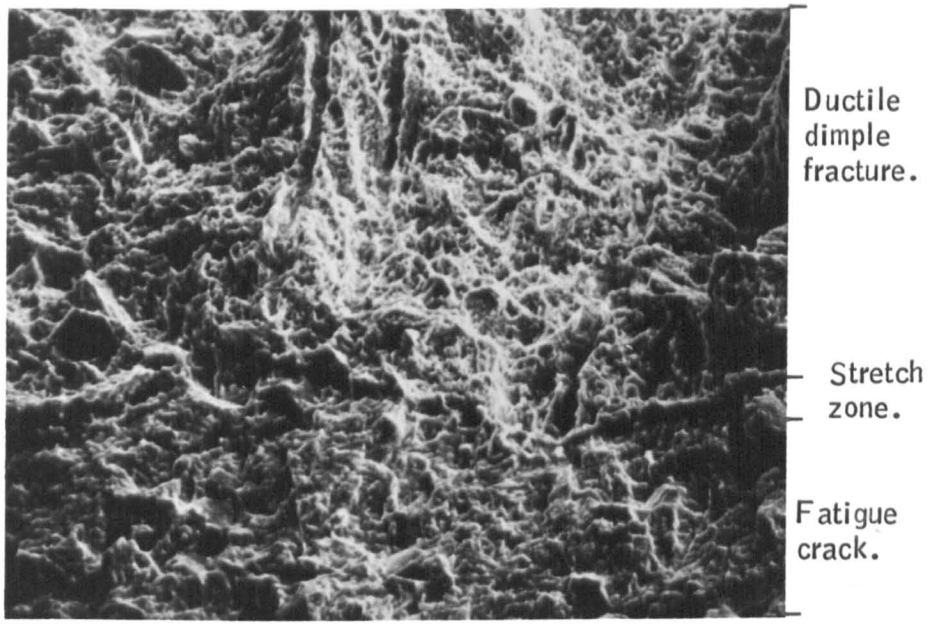

Plate 9.2. SEM fractograph of the G1 special steel CTS tested under a loading rate of 7680 MN $m^{-3/2}$/hour, in air at 20 ± 2° C, (45° tilt, 440 X).

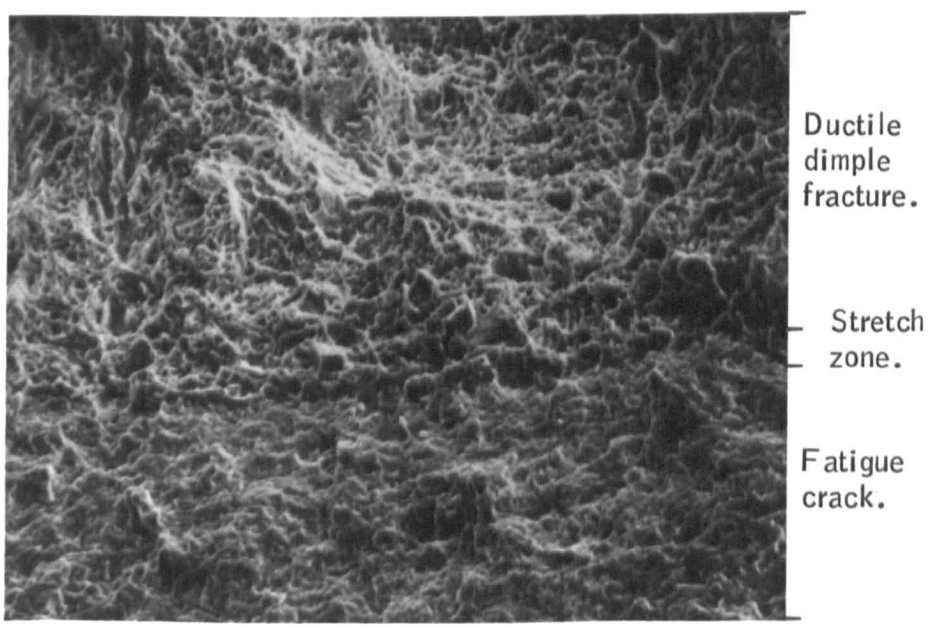

Plate 9.3. SEM fractograph of the G1 specail steel CTS tested under a loading rate of 528 MN $m^{-3/2}$/hour, in air at 20 ± 2° C, (45° tilt, 440 X).

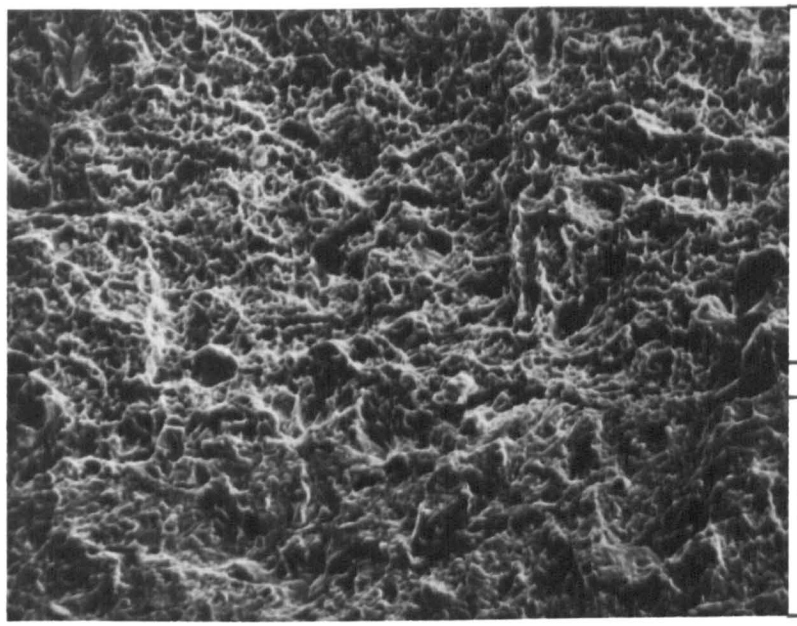

Plate 9.4. SEM fractograph of the G1 Special steel CTS tested under a loading rate of 46.8 MN $m^{-3/2}$/hour, in air at 20 ± 2° C, (45° tilt, 450 X).

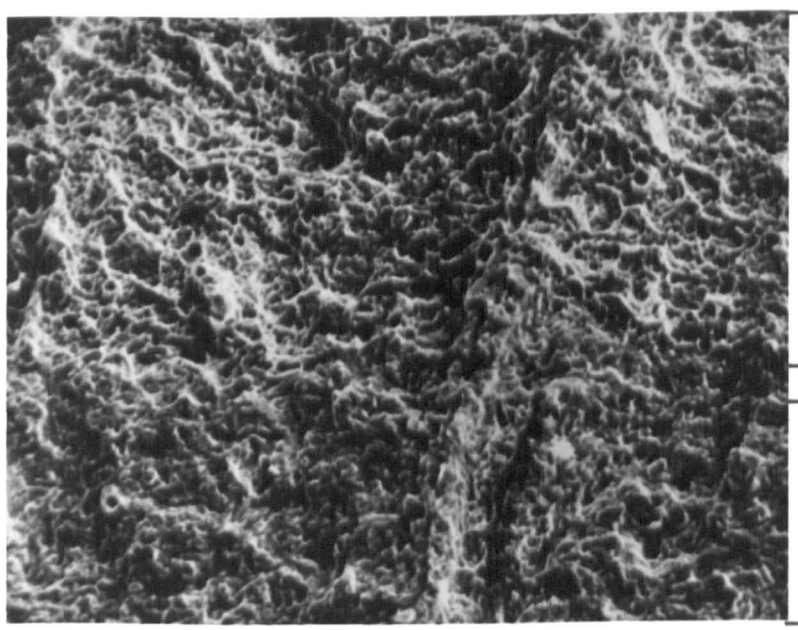

Plate 9.5. SEM fractograph of the G1 Special steel CTS tested under a loading rate of 3.2 MN $m^{-3/2}$/hour, in air at 20 ± 2° C, (45° tilt, 450 X).

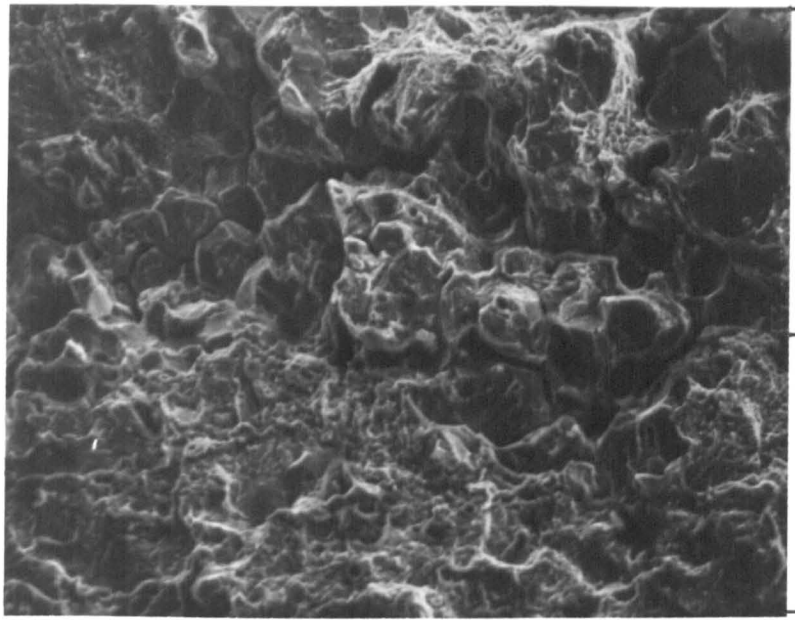

Plate 9.6. SEM fractograph of the G1 Special steel CTS tested under a loading rate of 55.2 MN $m^{-3/2}$/hour, in a corrosive environment, NACE solution saturated with H_2S, at 20 ± 2° C (45° tilt, 440 X).

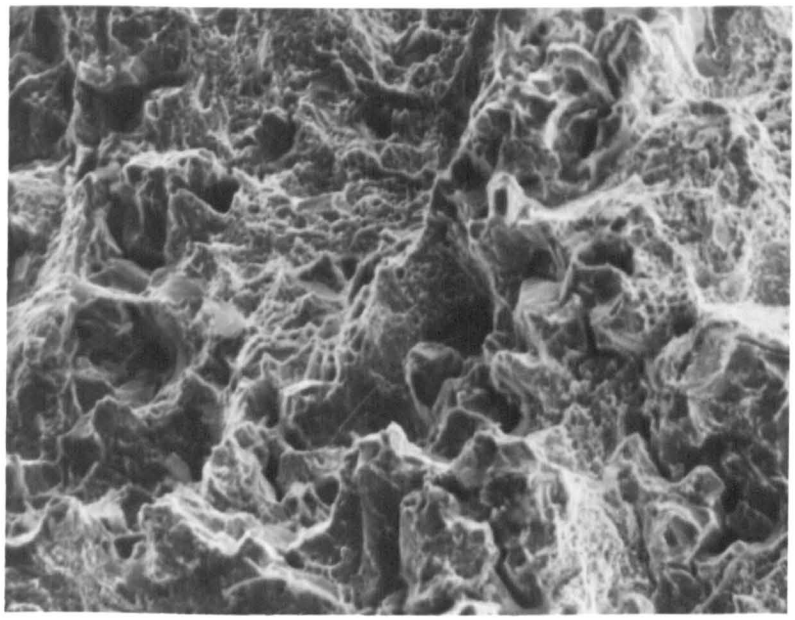

Plate 9.7. This SEM fractograph is taken further down the fracture surface of the specimen illustrated in Plate 9.4, (45° tilt, 440 X). It shows a transition region where intergranular fracture changes to ductile dimple.

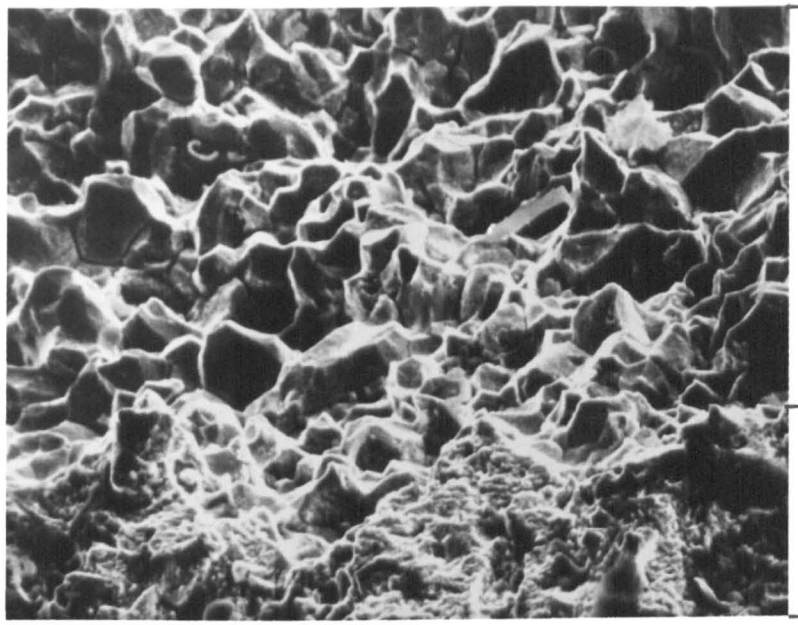

Plate 9.8. SEM fractograph of the G1 Special steel CTS, tested under a loading rate of 25.2 MN $m^{-3/2}$/hour, in a corrosive environment, NACE solution saturated with H_2S at 20 ± 2° C (45° tilt, 440 X).

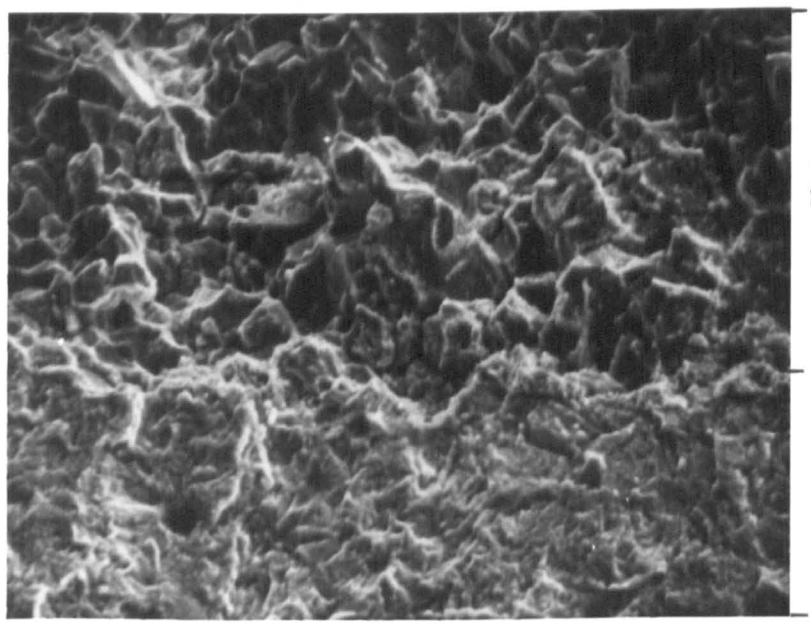

Plate 9.9. SEM fractograph of the G1 Special steel CTS, tested under a loading rate of 3.3 MN $m^{-3/2}$/hour, in a corrosive environment, NACE solution saturated with H_2S at 20 ± 2° C (45° tilt, 440 X).

This is a qualitative indicator of the toughness of the material. Tables 9.3 to 9.5 give the results of the specimens coated with various patterns of the protective coating as shown in Figures 9.2 to 9.4 respectively.

9.4.3. Continuous Slower Straining/Loading Rate Tests as a Function of Temperature.

G1 Special and API 5LX 65 steels compact tension specimens were tested with the loading rates less than 7 MN $m^{-3/2}$/hour as a function of temperature ranging from 10 to 60° C in NACE solution saturated with H_2S. Two types of the protective coating with different compositions were used in this study.

(a) Ball-milled MoS_2/FEP coat with the catalyst to FEP ratio of 1:0.85.

(b) Unball-milled MoS_2/FEP coat with the catalyst to FEP ratio of 1:1.12.

Both protective coatings were applied in the pattern as shown in Figure 9.4. The stress intensity at failure, k_{IQ}, the total energy required for fracturing the specimen and the average energy consumed per unit length of crack extension were calculated for both steels. For the API 5LX 65 steel specimens the calculated k_{IQ} parameter is not valid since the requirements for linear elastic fracture mechanics were not met.

Table 9.6 gives the results of the API 5LX 65 steel specimens protected with ball-milled MoS_2/FEP coat and unprotected specimens tested at 20, 40 and 60° C. Table 9.7 gives the corresponding results of the specimens protected with unball-milled MoS_2/FEP coat. Table 9.8 gives the results of the G1 Special steel specimens protected with unball-milled MoS_2/FEP coat and unprotected specimens tested at 10, 20 and 40° C. Table 9.9 gives the typical concentrations of H_2S in the corrosive solutions before and after the tests conducted at temperatures 10, 20, 40 and 60° C.

TABLE 9.3. Continuous slower straining/loading rate test results on API 5LX 65 CTS coated as shown in Figure 9.2 (ball-milled MoS_2/FEP coat used) and tested in NACE solution saturated with H_2S at 20 ± 2° C.

Loading rate ($MN\,m^{-3/2}$/hour)	k_{IQ} ($MN\,m^{-3/2}$)	Total fracture energy (joules)	Average energy consumed for unit length of crack extension. (J/mm)
Protected:			
4.91	53.00	15.13	1.178
Unprotected:			
4.25	43.64	10.8	0.818

TABLE 9.4. Continuous slower straining/loading rate test results on API 5LX 65 CTS coated as shown in Figure 9.3 (ball-milled MoS_2/FEP coat used) and tested in NACE solution saturated with H_2S at 20 ± 2° C.

Loading rate ($MN\,m^{-3/2}$/hour)	k_{IQ} ($MN\,m^{-3/2}$)	Total fracture energy (joules)	Average energy consumed for unit length of crack extension (J/mm)
Protected;			
5.71	50.08	9.90	0.842
6.84	54.50	14.51	1.155
5.05	50.08	12.67	0.986
	$\bar{x}$ = 51.55	$\bar{x}$ = 12.36	$\bar{x}$ = 0.994
Unprotected;			
4.56	47.45	8.81	0.713
3.31	46.73	7.70	0.640
6.25	48.12	8.24	0.654
	$\bar{x}$ = 47.43	$\bar{x}$ = 8.25	$\bar{x}$ = 0.669

TABLE 9.5.

Continuous slower straining/loading rate test results on API 5LX 65 CTS coated as shown in Figure 9.4, (ball-milled MoS_2/FEP coat used) and tested in NACE solution saturated with H_2S at 20 ± 2^0 C.

Loading rate ($MN\,m^{-3/2}$/hour)	k_{IQ} ($MN\,m^{-3/2}$)	Total fracture energy (joules)	Average energy consumed for unit length of crack extension. (J/mm)
Protected;			
3.41	51.42	13.92	1.074
3.12	50.24	13.47	1.055
	$\bar{x} = 50.83$	$\bar{x} = 13.70$	$\bar{x} = 1.065$
Unprotected;			
5.12	47.84	10.20	0.801
4.67	47.13	10.01	0.774
4.49	46.91	10.78	0.818
	$\bar{x} = 47.29$	$\bar{x} = 10.33$	$\bar{x} = 0.798$

TABLE 9.6.

Continuous slower straining/loading rate test results on API 5LX 65 CTS coated as shown in Figure 9.4 (ball-milled MoS_2/FEP coat used) and tested in NACE solution saturated with H_2S at various temperatures.

Temperature (° C)	Loading rate ($MN\,m^{-3/2}$/hour)	k_{IQ} ($MN\,m^{-3/2}$)	Total fracture energy (joules)	Average energy consumed for unit length of crack extension. (J/mm)
Protected;				
20	3.41	51.42	13.92	1.074
20	3.12	50.24	13.47	1.055
		$\bar{x}$=50.83	$\bar{x}$=13.70	$\bar{x}$ =1.065
40	3.76	53.83	13.72	1.070
40	3.06	52.26	12.30	0.951
		$\bar{x}$=52.94	$\bar{x}$=13.01	$\bar{x}$ = 1.011
60	3.98	54.60	13.66	1.034
60	2.53	57.09	14.00	1.083
		$\bar{x}$=55.85	$\bar{x}$=13.83	$\bar{x}$ = 1.059
Unprotected;				
20	5.12	47.84	10.20	0.801
20	4.62	47.13	10.01	0.774
20	4.49	46.91	10.78	0.818
		$\bar{x}$=47.29	$\bar{x}$=10.33	$\bar{x}$ = 0.798
40	3.70	49.30	9.72	0.755
40	5.70	48.86	9.80	0.764
40	6.11	46.38	11.53	0.864
		$\bar{x}$=48.18	$\bar{x}$=10.35	$\bar{x}$ = 0.795
60	4.10	49.96	9.86	0.754
60	3.01	50.07	8.64	0.694
60	5.92	50.18	11.66	0.867
		$\bar{x}$ = 50.07	$\bar{x}$=10.05	$\bar{x}$ = 0.772

TABLE 9.7.

Continuous slower straining/loading rate test results on API 5LX 65 CTS, coated as shown in Figure 9.4 (unball-milled MoS_2 /FEP coat used) and tested in NACE solution saturated with H_2S at various temperatures.

Temperature (^{0} C)	Loading rate ($MN\ m^{-3/2}$/hour)	k_{IQ} ($MN\ m^{-3/2}$)	Total fracture energy (joules)	Average energy consumed for unit length of crack extension. (J/mm)
Protected:				
20	4.12	52.34	14.32	1.084
20	6.14	54.43	16.00	1.200
20	3.96	51.72	14.04	1.078
		$\bar{x}$=52.83	$\bar{x}$=14.79	$\bar{x}$ = 1.121
40	3.88	51.02	13.02	0.974
40	5.91	54.90	13.00	0.988
40	4.88	54.25	13.88	1.062
		$\bar{x}$=53.39	$\bar{x}$=13.30	$\bar{x}$ = 1.008
60	5.45	55.78	14.20	1.079
60	5.20	58.14	12.88	1.096
60	4.59	58.19	13.82	1.037
		$\bar{x}$=57.37	$\bar{x}$=13.63	$\bar{x}$ = 1.071
Unprotected:				
20	5.12	47.84	10.20	0.801
20	4.62	47.13	10.01	0.774
20	4.49	46.91	10.78	0.818
		$\bar{x}$=47.29	$\bar{x}$=10.33	$\bar{x}$ = 0.798
40	3.70	49.30	9.72	0.755
40	5.70	48.86	9.80	0.764
40	6.11	46.38	11.53	0.865
		$\bar{x}$=48.18	$\bar{x}$=10.35	$\bar{x}$ = 0.795
60	4.10	49.96	9.86	0.754
60	3.01	50.07	8.64	0.694
60	5.92	50.18	11.66	0.867
		$\bar{x}$=50.07	$\bar{x}$=10.05	$\bar{x}$ = 0.772

TABLE 9.8.

Continuous slower straining/loading rate test results on GI Special CTS coated as shown in Figure 9.4 (unball-milled MoS_2 /FEP coat used) and tested in NACE solution saturated with H_2S at various temperatures.

Temperature (°C)	Loading rate ($MN\,m^{-3/2}$/hour)	k_{IQ} ($MN\,m^{-3/2}$)	Total fracture energy (joules)	Average energy consumed for unit length of crack extension. (J/mm)
Protected:				
10	2.49	33.32	7.09	0.530
10	2.22	27.40	6.52	0.517
10	2.34	30.74	6.17	0.492
		$\bar{x}$=30.49	$\bar{x}$=6.59	$\bar{x}$ = 0.513
20	2.30	18.27	2.74	0.212
20	2.42	15.25	2.82	0.213
20	2.28	16.37	2.64	0.203
		$\bar{x}$=16.63	$\bar{x}$=2.73	$\bar{x}$ = 0.209
40	2.07	17.33	2.07	0.162
40	3.98	18.87	2.29	0.175
40	3.06	16.05	2.54	0.190
		$\bar{x}$=17.42	$\bar{x}$=2.30	$\bar{x}$ = 0.176
Unprotected:				
10	2.36	28.40	5.63	0.420
10	3.40	25.59	5.03	0.382
10	2.75	27.04	5.10	0.383
		$\bar{x}$=27.01	$\bar{x}$=5.25	$\bar{x}$ = 0.395
20	2.24	13.56	1.67	0.127
20	2.46	12.97	1.38	0.109
20	2.34	13.67	1.42	0.110
		$\bar{x}$=13.40	$\bar{x}$=1.49	$\bar{x}$ = 0.115
40	3.04	14.31	1.80	0.134
40	2.81	12.43	1.31	0.097
40	2.87	13.52	1.51	0.119
		$\bar{x}$=13.42	$\bar{x}$=1.54	$\bar{x}$ = 0.117

TABLE 9.9.

Typical H_2S concentration of the NACE solution saturated with H_2S used for the continuous slower straining/loading rate tests at various temperatures.

Temperature (^oC)	Duration of the test (hours)	Concentration of H_2S before the test (ppm)	Concentration of H_2S after the test (ppm)
10	14	3329	2456
20	9	2712	1444
40	10	1613	306
60	10	950	191

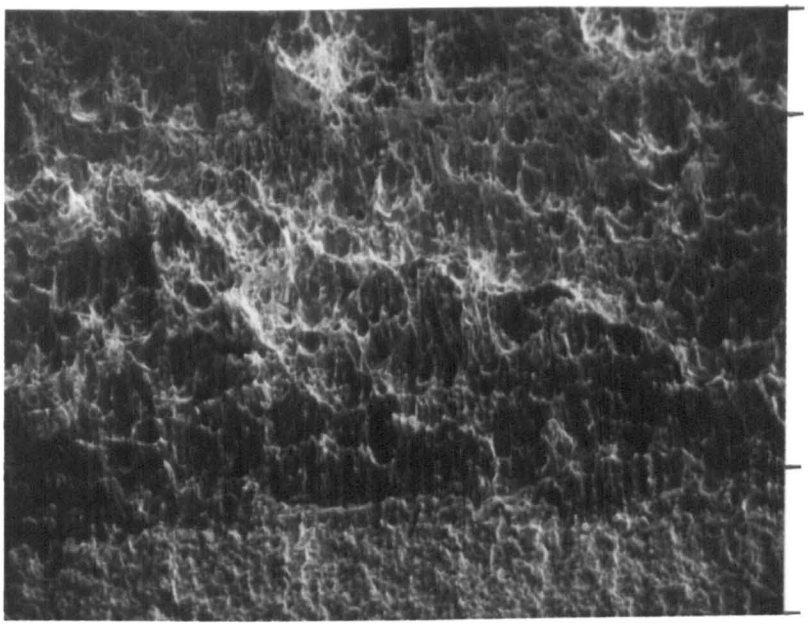

Plate 9.10. SEM fractograph of the API 5LX 65 pipe-steel CTS, tested under a loading rate of 6.08 MN $m^{-3/2}$/hour, in air at 20 ± 2° C (45° tilt, 100 X).

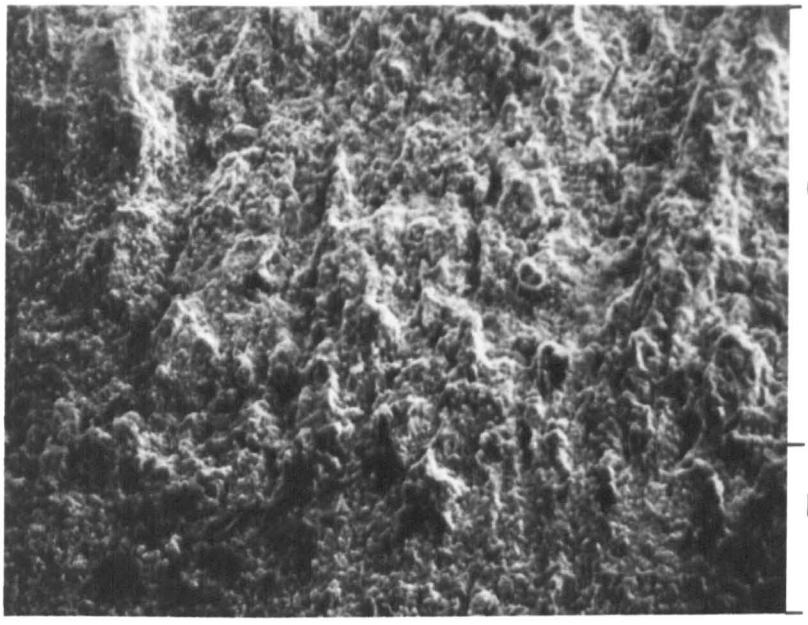

Plate 9.11. SEM fractograph of the API 5LX 65 pipe-steel CTS, tested under a loading rate of 6.14 MN $m^{-3/2}$/hour, with a protectec coating (un-ball milled MoS_2 used), in a corrosive environment, NACE solution saturated with H_2S at 20 ± 2° C (45° tilt, 100 X).

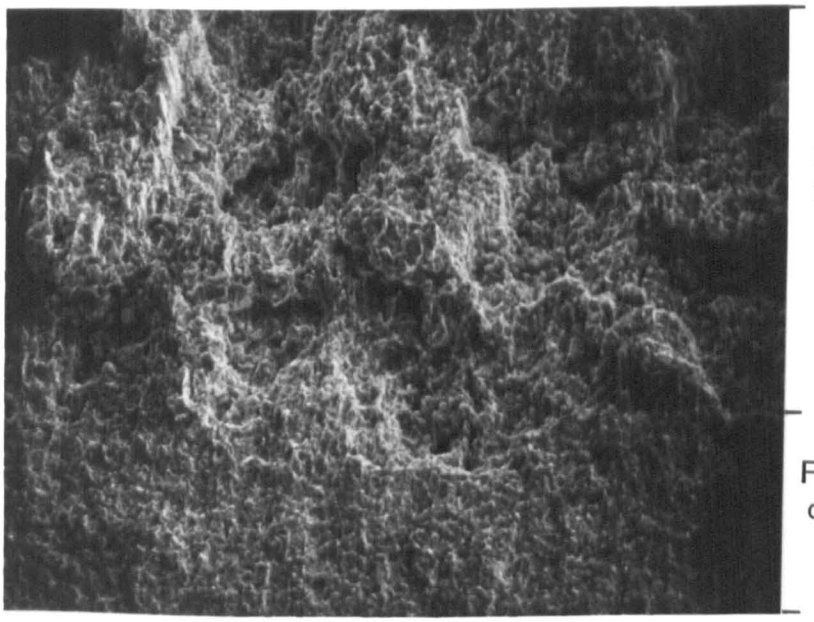

Plate 9.12. SEM fractograph of the API 5LX 65 pipe-steel CTS, (unprotected), tested under a loading rate of 5.12 MN $m^{-3/2}$/ hour, in a corrosive environment NACE solution saturated with H_2S at 20 ± 2° C (45° tilt, 100 X).

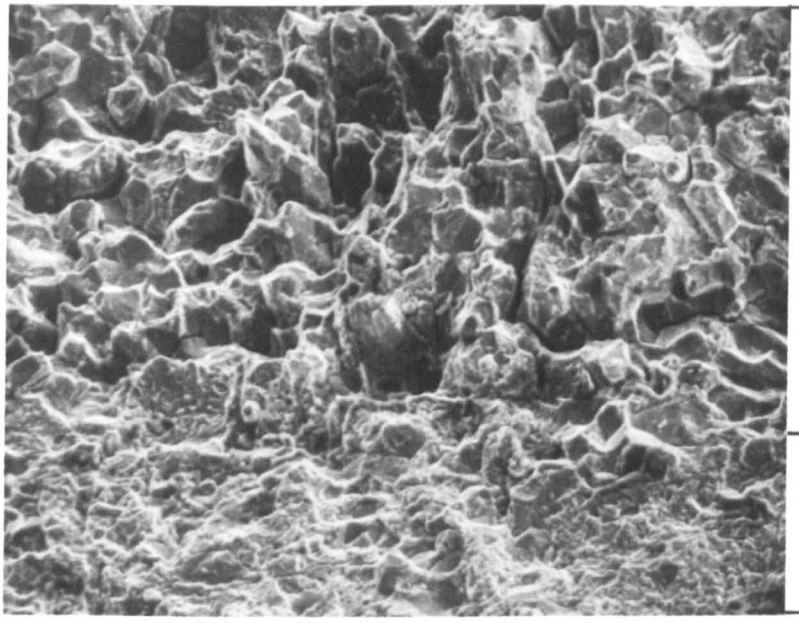

Plate 9.13. SEM fractograph of the G1 Special steel CTS tested under a loading rate of 2.49 MN $m^{-3/2}$/hour, with a protected coating (un-ball milled MoS_2 used) in a corrosive environment, NACE solution saturated with H_2S at $10 \pm 2°$ C (45° tilt, 440 X).

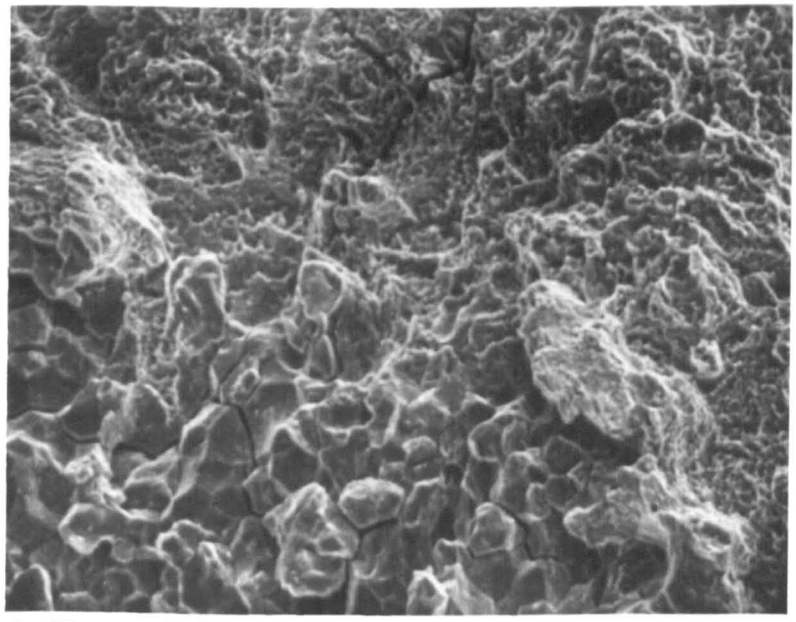

Plate 9.14. This SEM fractograph is taken further down the fracture surface of the specimen illustrated in Plate 9.13, (45° tilt, 440 X). It shows a transition region where intergranular fracture changes to ductile dimple.

9.5 Discussion.

The results on the G1 Special steel compact tension specimens tested as a function of loading rate shows (Figure 9. 6) that when the loading rate was reduced, the stress intensity factor k_{IQ} for failure also reduced in both air and the corrosive environment. The reduction in k_{IQ} was very much greater in the corrosive environment than in the air. An important point noticed in this result is that the k_{IQ} for failure in the corrosive environment approached a constant value of 12 MN $m^{-3/2}$ as the loading rate approached about 10 MN $m^{-3/2}$/hour. This constant value seems to be the threshold value of stress intensity, designated k_{ISCC}, below which stress corrosion cracking would not occur. Furthermore this value 12 MN $m^{-3/2}$ is in good agreement with the literature data[80]. McIntyre[116] reported that for similar EN 30B steel (G1 special is the new steel equivalent to the EN 30B steel available in the market) the threshold stress intensity for stress corrosion cracking, k_{ISCC}, in H_2S media was 12.1 ± 1.1 MN $m^{-3/2}$. Further this value was also confirmed for this steel in artificial sea water by Onuchukuwa[80].

Scanning electron microscopic fractographs on the fracture surfaces of the G1 special steel CTS tested at various loading rate from 7680 to 3 MN $m^{-3/2}$/hour range in air at 20 ± 2^0 C show (Plates 9.2 to 9.5) that the major fracture mode did not change even at the two extreme loading rates. The fracture mode was an equiaxial dimple indicating the ductibility of the specimen. It was noticed that the width of the stretch zone, which very frequently correlated with k_{ISCC}[80,116], was decreased with the reduction in loading rate. The specimen tested with the loading rate of 3.0 MN $m^{-3/2}$/hour indicated that there was only a very narrow stretch zone formed. This may be an indication for the steep reduction observed in fracture toughness when the loading rate was reduced from about 47 to 3 MN $m^{-3/2}$/hour.

The SEM fractographs (Plates 9.6 and 9.7 taken from the G1 Special steel CTS tested in the corrosive environment with the loading rate of 55.2 MN $m^{-3/2}$/hour reveals an interesting mode of fracture. The fractograph on the region just ahead of the pre-fatigue-cracked surface (Plate 9.6) shows that the fracture progressed with a complete intergranular fracture mode with some secondary crack-

ing confirming the hydrogen attack. The fractograph taken further down the fracture surface of the specimen shows (Plate 9.7) a transition region where the intergranular fracture mode changed to ductile dimple mode. This observation shows that at the loading of 55.2 MN $m^{-3/2}$/hour although the fracture was initiated and gorwn for a distance under the sulphide stress corrosion attack, the final fracture was ductile mode. The fractographs taken on the specimens tested at the loading rates of 25.2 and 3.3 MN $m^{-3/2}$/hour show that the fracture was a complete intergranular fracture mode and there was no transition region, such as shown in Plate 9.7. Also it may be seen that there was no stretch zone formed when the specimens were tested in the corrosive environment at the loading rate 55.2 MN $m^{-3/2}$/hour or below.

The above discussion confirms two points;

(1) When the G1 Special CTS were tested in the corrosive environment with the loading rate of 25.2 MN $m^{-3/2}$/hour or below, the fracture surface was completely intergranular cracking indicating that the failure was dominated by sulphide stress corrosion cracking.

(2) When the G1 Special CTS were tested in the corrosive environment with the loading rate of 10 MN $m^{-3/2}$/hour or below, the stress intensity factor at failure became equivalent to k_{ISCC} for the material.

Hence it was decided to employ a loading rate below 10 MN $m^{-3/2}$/hour in the continuous slower straining/loading rate tests to evaluate the effectiveness of the proposed technique.

There were three different patterns of protective coatings used on the API 5LX 65 steel compact tension specimens to evaluate the effect of different patterns of the coating on the mechanical properties of the specimens and to compare with unprotected specimens.

It can be seen from the results (Table 9.3) on the specimens coated as shown in Figure 9.2 that the resistance to fracture of the specimen provided with the MoS_2 coating was better than that of the comparison specimen (unprotected),

in terms of stress intensity factor at failure, k_{IQ}, the total energy required for fracturing the specimens and the average fracture energy consumed for unit length of crack extension. It was thought that the presence of the active sulphide coating in front of the crack might physically inhibit the crack from extending. Hence an unfair advantage was given to the protected specimen compared to the unprotected specimen. Therefore the pattern of coating shown on Figure 9.2 was abandoned. Thereafter a set of experiments were carried on the specimens coated as shown on Figure 9.3, where no protective coating was applied in front of the crack tip. The results on such specimens given in Table 9.4 again show that the specimens provided with the MoS_2 coating had improved in fracture resistance as compared with the unprotected specimens. In carrying out the above tests it was observed that hydrogen gas evolved on the protective coating tends to become trapped in the notch thus preventing the corrosive solution from reaching the crack front. Another difficulty was that it was difficult to ensure constant quality and thickness of the coatings on the inner walls of the notch. Hence it was found that the specimens coated as shown in Figure 9.3 were also not satisfactory.

Further tests were carried out on the specimens coated as shown in Figure 9.4 where it was ensured that no coating was present on either major surfaces of each specimen nor on the inner walls of the notch. The preparation of the protective coating and the quality control of the coating were found to be much easier since the protective coating was applied on extreme faces of the specimens. The results on the specimens show (Table 9.5) that the MoS_2 coating was still effective to inhibit SSCC in comparison with the unprotected specimens even when situated away from the crack. Hence it was decided to employ the coating pattern shown in Figure 9.4 for further evaluation of the proposed novel method.

Effectiveness of the proposed technique for the inhibition of sulphide stress corrosion cracking in steel was studied as a function of temperature. The protective ball-milled and unball-milled MoS_2/FEP coatings were used on compact tension specimens of API 5LX 65 and G1 Special steels and tested in H_2S saturated NACE solution. The coatings for the specimens were applied as shown in Figure 9.4 and the loading rate of the tests were kept below 7 MN $m^{-3/2}$/hour.

The results given in the Tables 9.6 and 9.7 in terms of the stress intensity factor at failure, the total energy for fracturing the specimen and the average energy required for unit length of crack extension show that there was no significant difference found between both types of coatings, ball-milled and unball-milled MoS_2/FEP coat, when the API 5LX 65 steel CTS were employed. But hydrogen diffusion studies (Chapter 5) indicated that the unball-milled MoS_2 coat with higher FEP content was better than the ball-milled MoS_2 coat. This could be due to the fact that the compact tension specimens were very much thicker and bigger than the hydrogen diffusion membranes. Also the parameters calculated from the continuous slower straining/loading rate tests could not indicate the smaller differences and the effectiveness between the coatings as hydrogen diffusion current.

The results on the specimens show that the total fracture energy required for fracturing the specimen was significantly greater for the protected than the unprotected specimen. The total fracture energy for the protected specimens were improved about 32, 26 and 38 percent over the unprotected specimen at 20, 40 and 60° C respectively when the ball-milled MoS_2/FEP coating were applied on the API 5LX 65 steel specimens. Whereas the unball-milled MoS_2/FEP coated specimens gave 43, 28 and 36 percent improvement at 20, 40 and 60° C respectively. It was noted on the API 5LX 65 steel specimens that the change in test temperature did not give any significance change in performance in any of the three groups of specimens, i.e. the two protected groups and the other unprotected group. High resistance for SSCC could be the reason for the very little change between the parameters measured in the tests with various temperatures. However the results on the protected and unprotected specimens at each temperature confirm that the both protective coatings gave an average of 30 percent improvement over the total fracture energy required for fracturing the specimens and the energy required for unit length of crack extension. Furthermore, although the stress intensity factor calculated at failure for the specimens were not valid due to low yield strength of the steel and due to the dimension of the specimens, it shows about 10 to 15 percent improvement for the protected specimens when compared with the unprotected specimens.

Scanning electron microscopic fractograph on the API 5LX 65 CTS tested under the loading rate of 6.08 MN $m^{-3/2}$/hour in air at 20 ± 2° C shows (Plate 9.10) that the fracture was completed in two steps, namely sub-critical and critical fracture. The sub-critical crack growth seems to be dominated by elongated dimple fracture. The critical fracture exhibits uniaxial dimple. The fractographs on the specimens tested with and without protection in the corrosive environment at 20 ± 2°C show (Plates 9.11 and 9.12) that there were no signs of sub-critical crack growth. It seems that both specimens were fractured in a mixed mode indicating ductile dimple fracture with some local cleavage. The unprotected specimen tested in the corrosive environment exhibits severe secondary cracking and this confirms the hydrogen attack. These fractographs strongly support the improvement in the mechanical properties of the API 5LX 65 steel specimens when they were coated with the protective MoS_2/FEP coat and tested in the corrosive environment.

The H_2S concentration analysis of the NACE solution before and after the tests at 10, 20, 40 and 60° C shows (Table 9.9) that at the end of tests there were H_2S concentrations of 74, 53, 19 and 20 percent concentration respectively compared to the saturated level. It has been shown in the literature[1,2] that less than 1 percent concentration of H_2S could course damage to the steels in a form of sulphide stress corrosion cracking. Hence it is fully justified that the environment employed in this study had enough concentration of H_2S to promote SSCC.

The studies of the G1 Special compact tension specimens also show that the unball-milled MoS_2/FEP protective coat applied specimens performed significantly better than the unprotected specimens in the corrosive environment at various temperatures. There were improvement of 26, 83 and 49 percent in terms of total energy required for fracturing the specimens at 10, 20 and 40° C respectively, when the specimens were coated with the protective MoS_2/FEP, coat as shown in Figure 9.4. The stress intensity factors at failure of the protected specimens also show the same trend and gave an improvement of 13, 24 and 30 percent at 10, 20 and 40 °C respectively.

The G1 Special steel specimens showed a greater variation in the fracture resis-

tance parameters within the protected and unprotected groups when they were tested as a function of temperature in the corrosive environment. In the protected specimens, the total fracture energy for fracturing the specimens was reduced from 6.59 to 2.30 joules when the temperature increased from 10 to 40° C. Whereas in the unprotected specimens group the energy reduced from 5.25 to 1.54 joules at the same conditions. The comparison of stress intensity factor at failure within the groups also reveal the same trend. In the protected specimens the, k_{IQ} at failure was reduced from 30.49 to 17.42 Mn $m^{-3/2}$ when the temperature increased from 10 to 40° C, whereas in the unprotected specimens it was reduced from 27.01 to 13.42 Mn $m^{-3/2}$ at the same conditions. This results indicate that the G1 Special steel is much more susceptible for sulphide stress corrosion cracking than the API 5LX 65 steel.

The SEM fractograph taken on the protected G1 Special steel CTS tested under a loading rate of 2.49 Mn $m^{-3/2}$/hour, in the corrosive environment at 10 ± 2° C shows (Plate 9.13) that the fracture mode ahead of the pre-fatigue-cracked surface was an intergranular fracture. The fractograph taken further down on the protected specimen shows (Plate 9.14) that there was a transition region where the intergranular cracking changed to ductile dimple fracture. This type of transition mode of fracture was also monitored, on the unprotected specimens, when they were tested under the same experimental conditions. The assessment of the ductile fracture area on the protected and unprotected specimens shows that when the specimens were protected with the MoS_2/FEP coat the ductile fracture area varied between 55 and 65 percent while on the unprotected specimens it varied between 10 and 20 percent. The increase in ductile fracture area on the protected specimens was another indication of the improvement against SSCC. This type of transition region was not seen when the specimens either protected or unprotected were tested at 20° C or above. This behaviour supports the earlier observation that when the temperature was increased there was a greater variation in the mechanical properties of the specimens.

However, the results for both steels indicate the same trend, i.e., the application of MoS_2/FEP coat gave a significant improvement in SSCC resistance although the steels studied were shown to have a greater variation between each other in the parameters calculated as a function of temperature.

CHAPTER TEN

SUSTAINED LOAD TEST ON G1 SPECIAL STEEL COMPACT TENSION SPECIMEN, (CTS)

CHAPTER 10.

SUSTAINED LOAD TEST ON GI SPECIAL STEEL COMPACT TENSION SPECIMEN, (CTS).

10.1 Introduction.

The experimental procedures for stress corrosion cracking tests on precracked specimens could be divided into two general categories. They are;

1) establishment of time to failure curve for an environment - alloy system, from which threshold stress intensity for stress corrosion cracking, k_{ISCC}, could be calculated.

2) measurement of crack growth rate which could provide information necessary to enhance the understanding of the kinetics of stress corrosion cracking.

These two parameters, could be used successfully as measures to evaluate the effectiveness of the proposed MoS_2/FEP coat to inhibit SSCC in steel.

It was clearly shown in Chapter 8 that there are numerous precracked specimens and test methods that could be used in stress corrosion studies. In view of the knowledge gained in the continuous, slower straining/loading rate test and specimens preparation facilities available, compact tension specimens of GI Special steel were selected for these sustained load tests. The sustained load tests were carried out for protected and unprotected compact tension specimens, (CTS) in a corrosive environment, NACE solution continuously bubbled with H_2S at $20 \pm 2^{\circ}$ C. The MoS_2/FEP coat protection was applied to the specimens in two different ways;

(a) Separate MoS_2 electrodes were made and connected to the specimens electrically.

(b) The protective coating applied to the specimen itself.

Time to failure curves were established on the specimens that were protected with FEP bonded MoS_2 electrodes and adherent MoS_2/FEP coat. The crack growth rate measurements were carried out on the specimens which were protected with an adherent MoS_2/FEP coat. One of the problems faced in the crack growth rate measurement test was the determination of growing-crack-length at various time intervals without interrupting the test. To overcome this problem a crack length calibration curve was established using the facilities available in the Unisteel Stress Corrosion Testing machine.

10.2. Experimental Procedures.

10.2.1. Materials Preparation.

G1 Special steel CTS were prepared as detailed in the section 9.2.1. The specimens were coated with the unball-milled MoS_2/FEP coat with the catalyst to FEP ratio of 1:1.12. The MoS_2/FEP coat and Lacomit varnish coat were applied to the protected and unprotected specimens respectively, in the pattern given in Figure 9.4. MoS_2 electrodes with a dimension of 2.5 cm x 4 cm were prepared as outlined in the section 4.3.1.3. The electrodes were made with ball-milled MoS_2/FEP coat with the catalyst to FEP ratio of 1:0.85 and the loading of 5-6 mg/cm^2. A Unisteel Stress Corrosion Testing machine was used in these studies with adequate facilities to control the temperature. The NACE solution continuously bubbled with H_2S at 1 atmospheric pressure was selected for this study.

10.2.2. Crack Length Calibration.

A number of G1 Special steel CTS were prepared with equal length of fatigue cracks, (1.5 ± 0.2 mm). The specimen was fixed to the attachment, which had Teflon sleeve insulations to separate electrically the

specimen and attachment. Figure 9.5 gives a schematic illustration of the attachment. The specimen was placed in a cell made of perspex and connected to the testing machine as shown in Plate 10.1. The specimen was subjected to a constant load of 3.29 kN with the help of a loading arm, built in the machine. The loading arm displacement against time was recorded with the help of a displacement transducer and an X-Y plotter. The loaded system was left for 20 minutes to avoid any initial settlement which could be taken misleadingly as the displacement produced due to crack growth. The NACE solution first purged with N_2 for 30 minutes followed by H_2S for another 30 minutes at 20° C was added to the test cell when the loading system achieved a steady state. Then the H_2S was continuously bubbled and the temperature was maintained at $20 \pm 2^{\circ}$ C throughout the experiment. After a certain period of time, when a length of crack growth was ensured, the specimen was taken-out and dried before being broken in air to measure the length of crack. The grown crack length was estimated by taking the average of five readings at equal distance through the thickness. The corresponding loading-arm displacement was measured from the displacement-time curve recorded autographically. Figure 10.1 gives the calibration curve for measurements of growing-crack-length obtained by this technique.

10.2.3. Tests Procedure.

Initially the prepared specimen was fixed to the attachment as shown in Figure 9.5 and placed in the test cell and connected to the Unisteel Stress Corrosion Testing machine. In the case of specimens protected with separate MoS_2 electrodes, the electrodes were precathodized at a current density of 30 mA/cm^2 for two hours before being connected to the specimen electrically. Two 10 cm^2 MoS_2 electrodes were used for each specimen. The electrical connections were made on the top face of the specimen and they were coated with Lacomit varnish to prevent any galvanostatic corrosion. Then the pre-calculated load was added to the loading-arm and left for 20 minutes to avoid any discrepancies to the results which might be caused due to the initial settlement. The NACE

Figure 10.1. Calibration curve for the calculation of growing-crack-length in GI Special steel CTS subjected to the sustained load test.

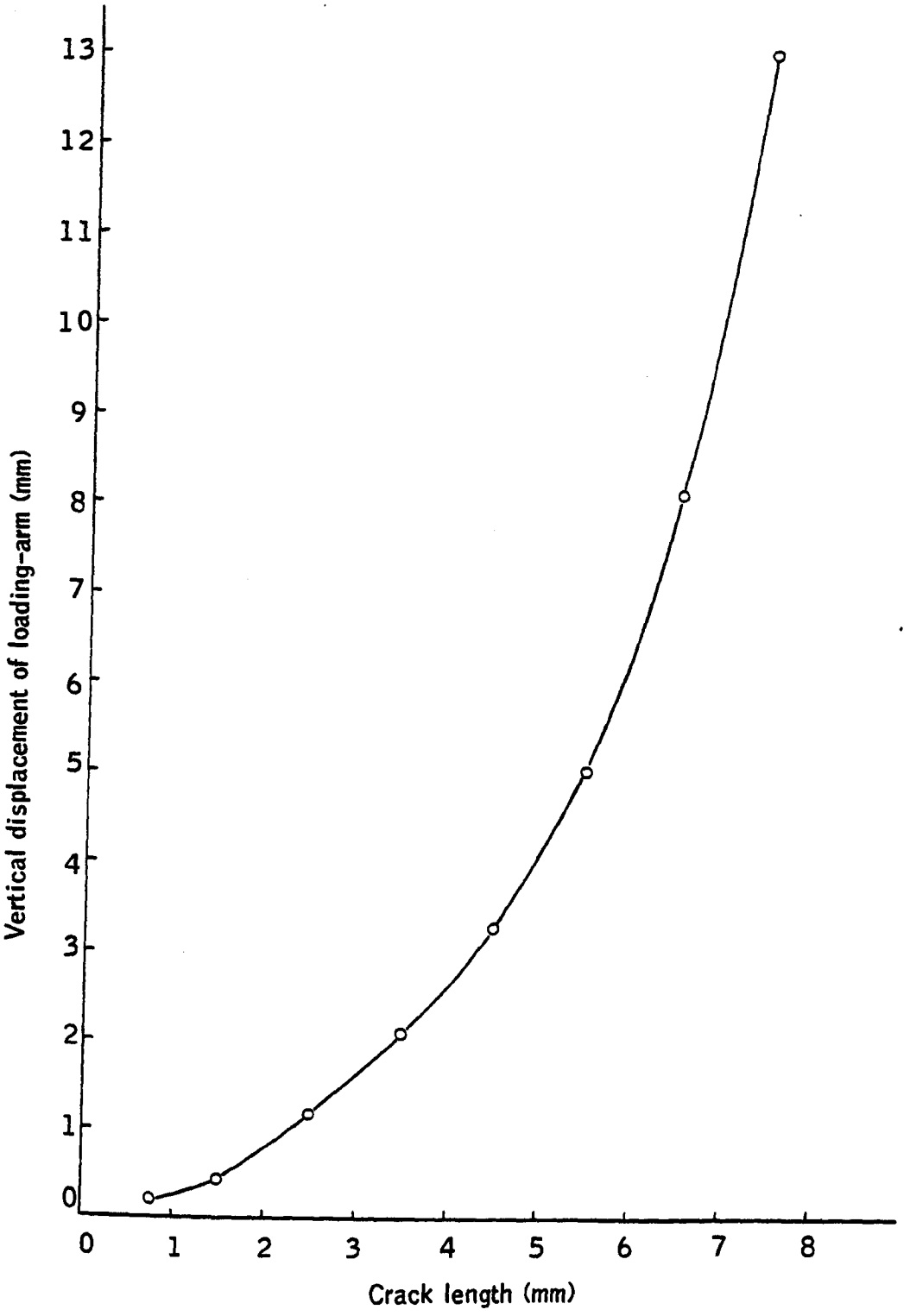

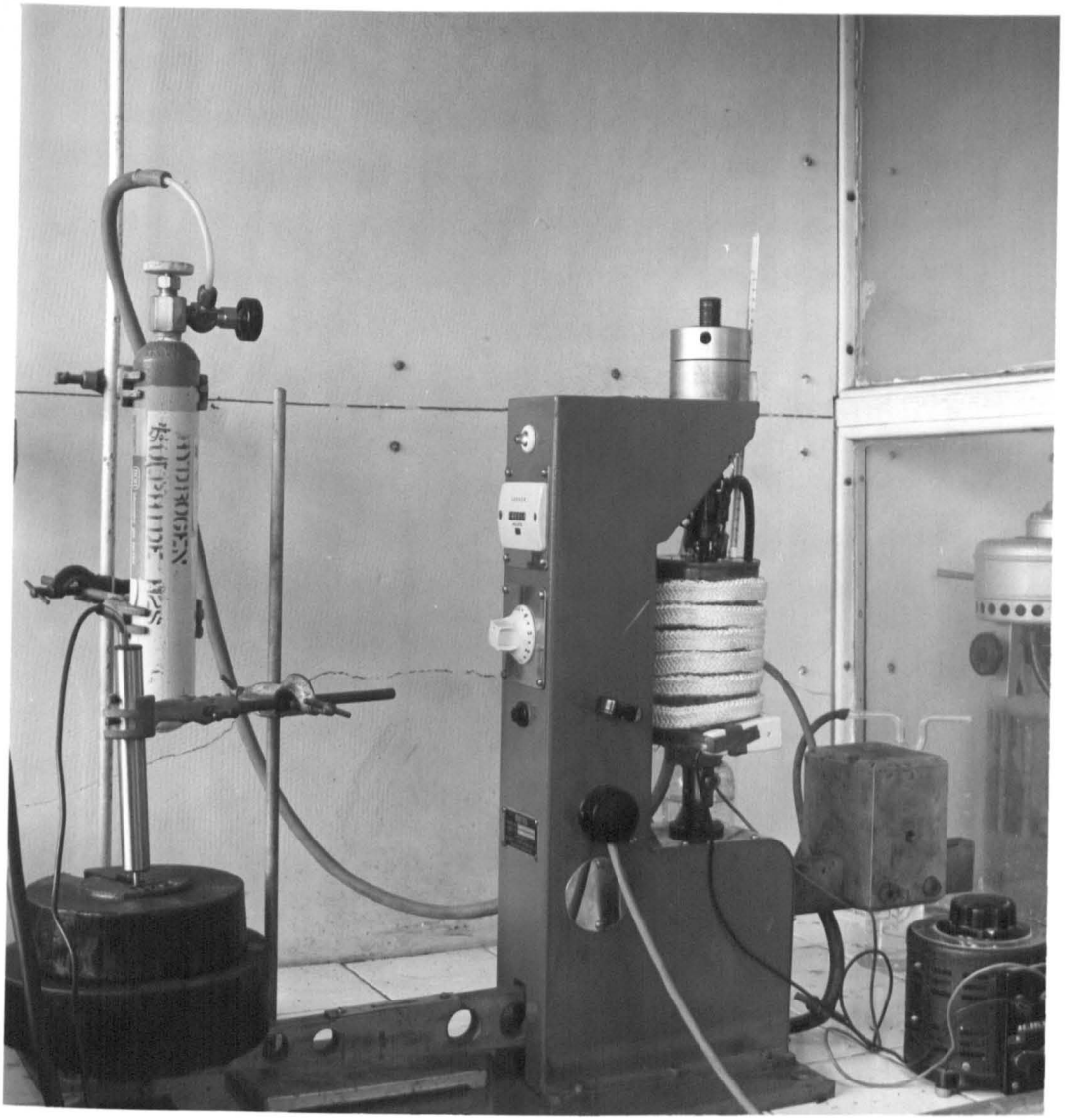

Plate 10.1. Photograph of a sustained load test set-up.

solution first purged with N_2 for 30 minutes followed by H_2S for another 30 minutes at 20° C and was added to the test cell. The temperature was controlled at 20 ± 2° C throughout the tests with the help of heating tape. The time to failure was recorded by a built-in electric clock. In the case of the crack growth rate measurement test a displacement transducer was fixed to the loading-arm and the loading-arm displacement versus time was recorded autographically.

Scanning electron microscopic examination was carried out on the fracture surfaces of the specimen. The fracture surfaces were cleaned ultrasonically in acetone for 30 minutes. Sometimes it was necessary to clean the fracture surfaces electrolytically. The technique is described in section 9.3.

10.3. Results.

The initial stress intensity factor, k_{Ii} of the CTS in the sustained load test was calculated from the load applied, the length of fatigue crack and planar dimensions of the specimen, using linear elastic fracture mechanics[120]. Time to failure curves for the GI Special steel CTS were constructed using the failure time recorded automatically by the clock built in the testing machine and the initial stress intensity factor calculated for the specimen. The effect of connecting the FEP bonded MoS_2 electrodes on the CTS time to failure curve in NACE solution, with continuously bubbling H_2S at 20 ± 2° C, is given in Figure 10.2. Figure 10.3 gives the corresponding time to failure curves for the specimens coated with MoS_2/FEP protective coat as shown in Figure 9.4.

The scanning electron microscopic fractographs of the protected GI Special CTS (protection applied as adherent coat) tested with an initial stress intensity factor of 15.70 MN $m^{-3/2}$ in the corrosive environment, are given in Plates 10.2 and 10.3. The corresponding fractograph for the unprotected specimen, tested with initial stress intensity factor of 16.06 MN $m^{-3/2}$ is given in Plate 10.4.

Figure 10.2. Effects of connecting MoS_2 electrodes on the failure time of precracked G1 Special steel compact tension specimens in NACE solution continuously bubbling with H_2S at room temperature.

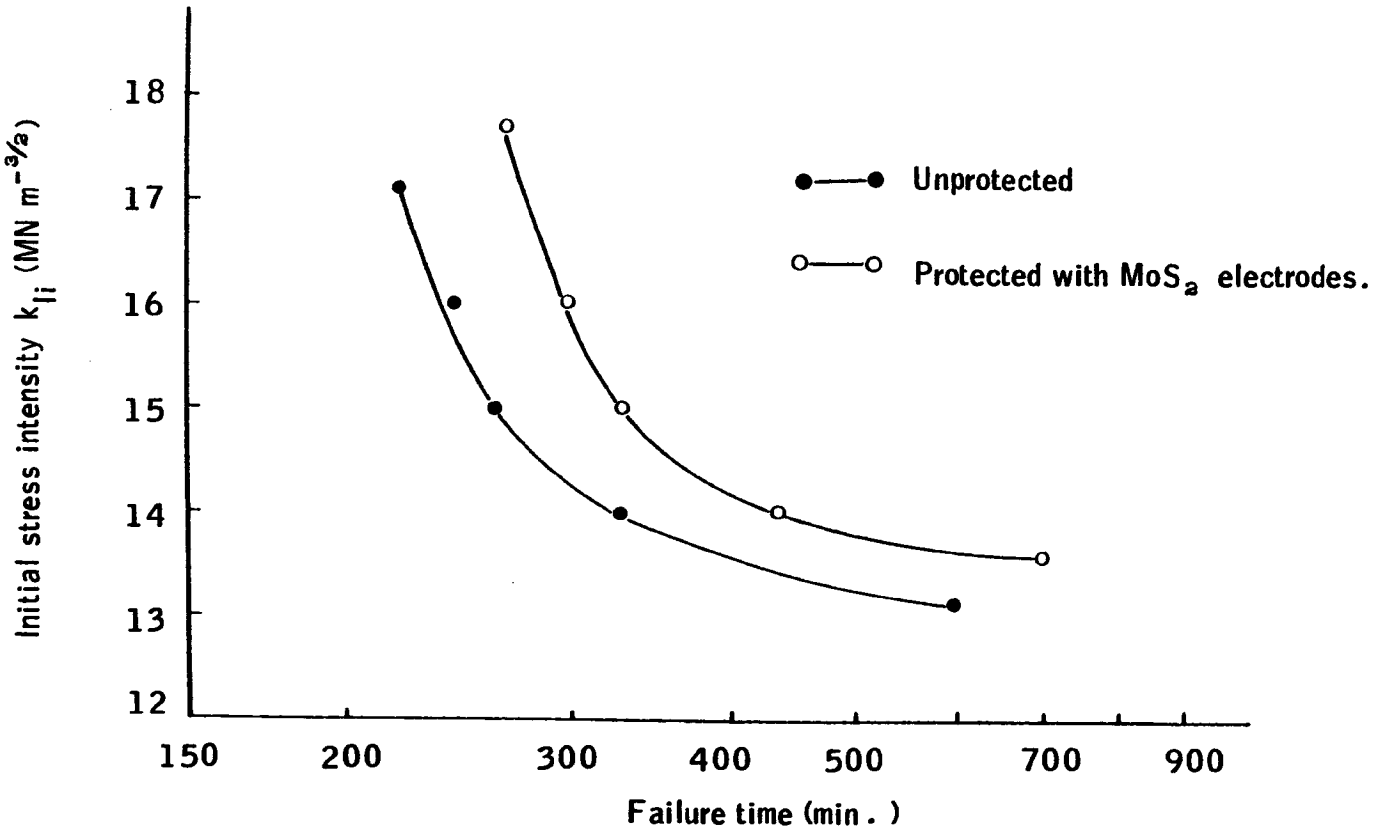

Figure 10.3. Effect of adherent MoS_2/FEP coat on the failure time of precracked G1 Special steel compact tension specimens in NACE solution with H_2S bubbling continuously at 20^0 C.

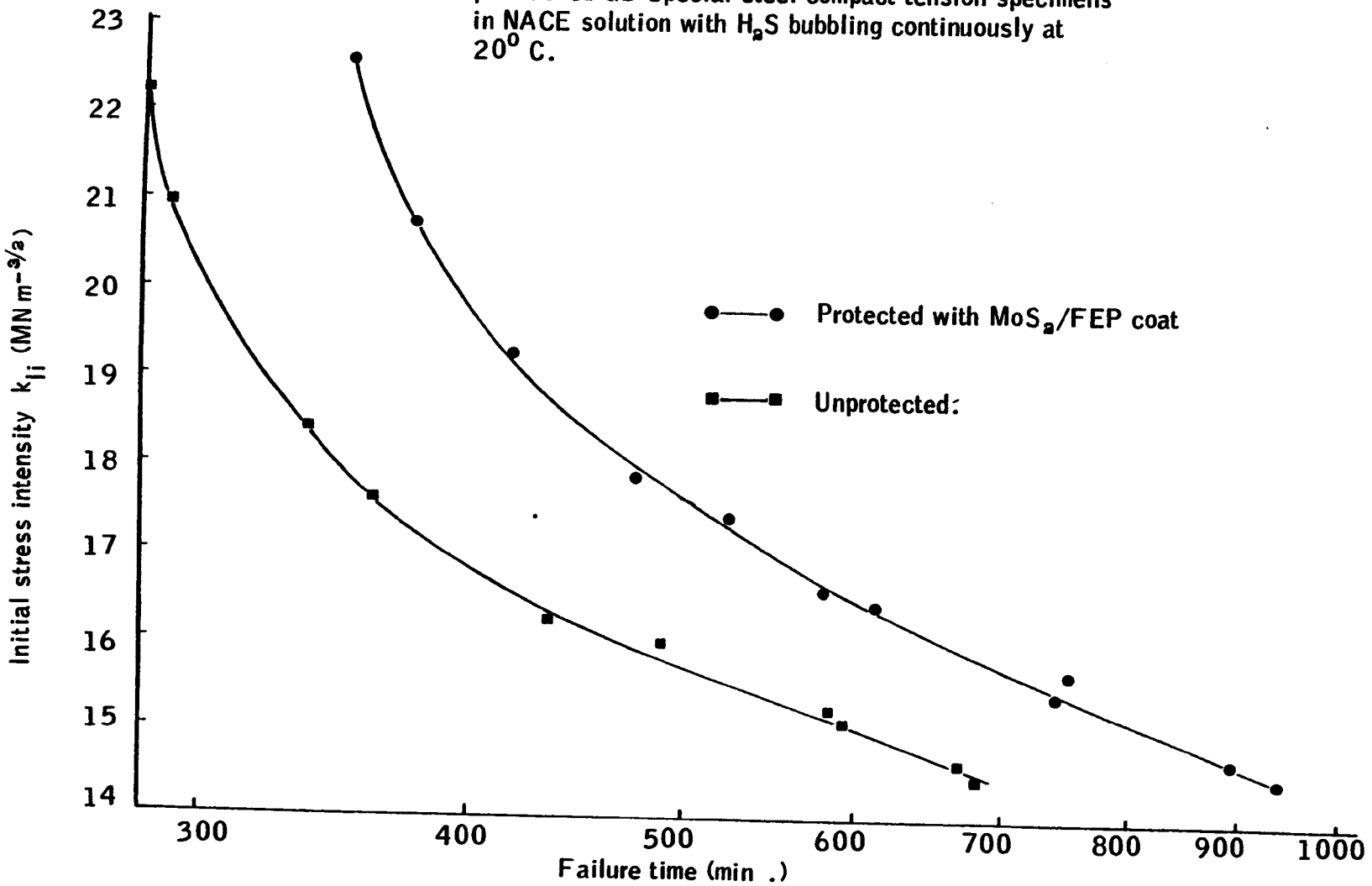

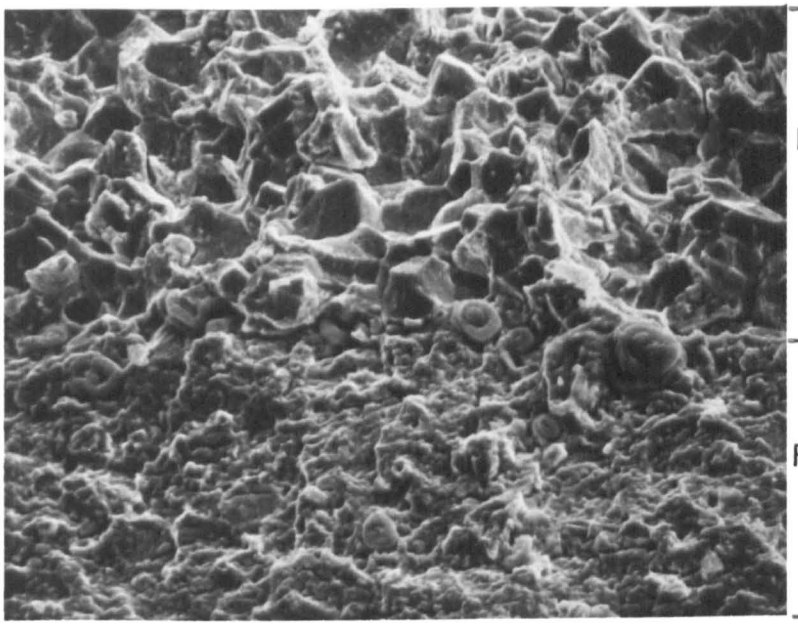

Plate 10.2. SEM fractograph of the GI Special steel CTS, tested under a sustained load ($K_{Ii} = 15.70$ MN $m^{-3/2}$) with a protected coating (un-ball milled MoS_2 used) applied as shown in Fig. 9.4, in a corrosive environment, NACE solution with H_2S (1 atm.) at 20 ± 2^{o} C, (45^{o} tilt, 440 X).

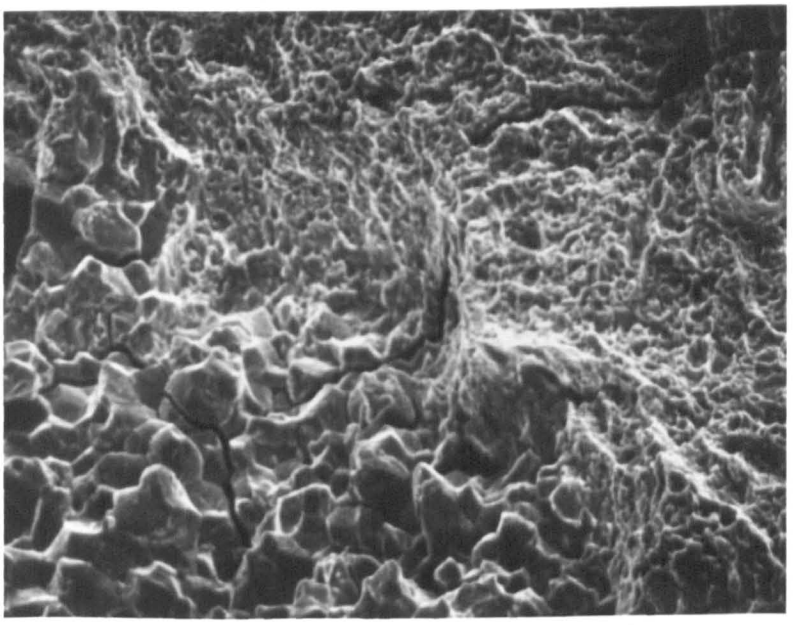

Plate 10.3. This SEM fractograph is taken further down the fracture surface of the specimen illustrated in Plate 10.1, (45^{o} tilt, 440 X). It shows a transition region where intergranular fracture changes to a ductile dimple.

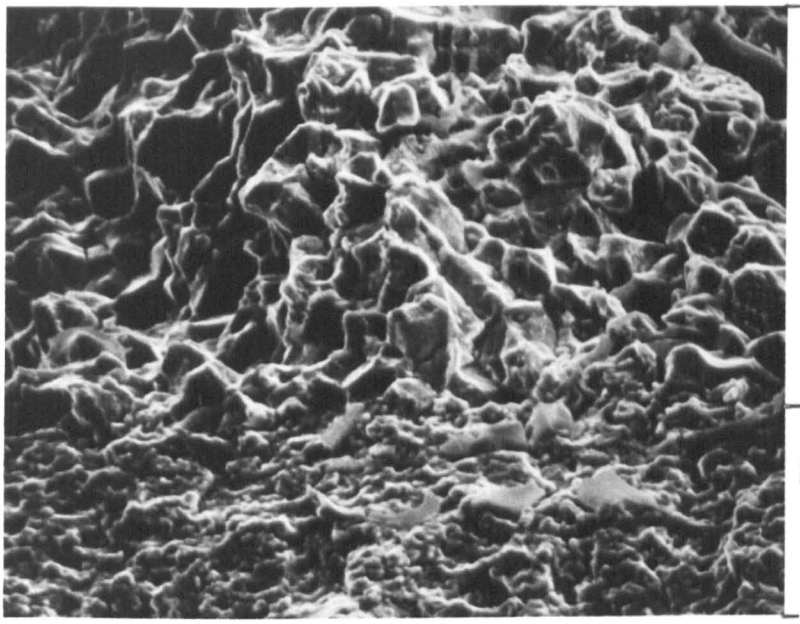

Plate 10.4. SEM fractograph of the GI Special steel CTS, tested under a sustained load ($K_{Ii} = 16.06$ MN $m^{-3/2}$) without protection applied, in a corrosive environment, NACE solution with H_2S (1 atm.), at 20 ± 2^{o} C, (45° tilt, 420 X).

In the crack growth rate measurement tests, the length of the growing-crack was calculated at various time intervals by using time versus loading-arm displacement curve of each test and the calibration curve established, (Figure 10.1). Figures 10.4 to 10.6 give the curves of crack growth versus time for the protected and unprotected specimens tested with various initial stress intensity factors in NACE solution with H_2S continuously bubbled at $20 \pm 2^{\circ}$ C. The instantaneous stress intensity factors of the specimen at various times were calculated using the crack length measured at the corresponding time, the load applied and the planar dimensions of the specimen. Figures 10.7 to 10.9 give the curves of crack growth rate versus time for the protected and unprotected specimens tested with various initial stress intensity factors. Figures 10.10 to 10.12 give the curves of crack growth rate versus instantaneous stress intensity factors for the specimens .

10.4. Discussion.

Time to failure curves for the GI Special steel CTS protected with separate electrodes (Figure 10.2) and protected with adherent coating (Figure 10.3) show that the proposed protection technique gave a considerable amount of improvement in failure time for protected specimens over unprotected specimens. For example, the curves indicate that if specimens were tested with initial stress intensity of 15 MN $m^{-3/2}$ the life would be increased from 260 minutes to 330 minutes (i.e., an increase of 27 percent) when protected with seperate electrodes; whereas if the specimens protected with adherent coating and tested with the same initial stress intensity factor, the life would be increased from 610 minutes to 840 minutes (i.e., an increase of 38 percent). Although the accelerated tests could not predict actual service-life of a structure quantitatively, the improvement on the failure time of the protected specimens certainly exhibit the effectiveness of the proposed technique to inhibit SSCC in steel.

The scanning electron microscopic fractograph of the protected (protection applied with adherent coating) G I Special steel CTS shows (Plate 10.2) that the fracture area just ahead of pre-fatigue-cracked area propagated in an

Figure 10.4. Crack growth as a function of time for protected and unprotected GI Special steel CTS in NACE solution with H_2S bubbling continuously at 20° C. The specimens were tested with initial stress intensity factor of 14.5 ± 0.2 MN m$^{-3/2}$.

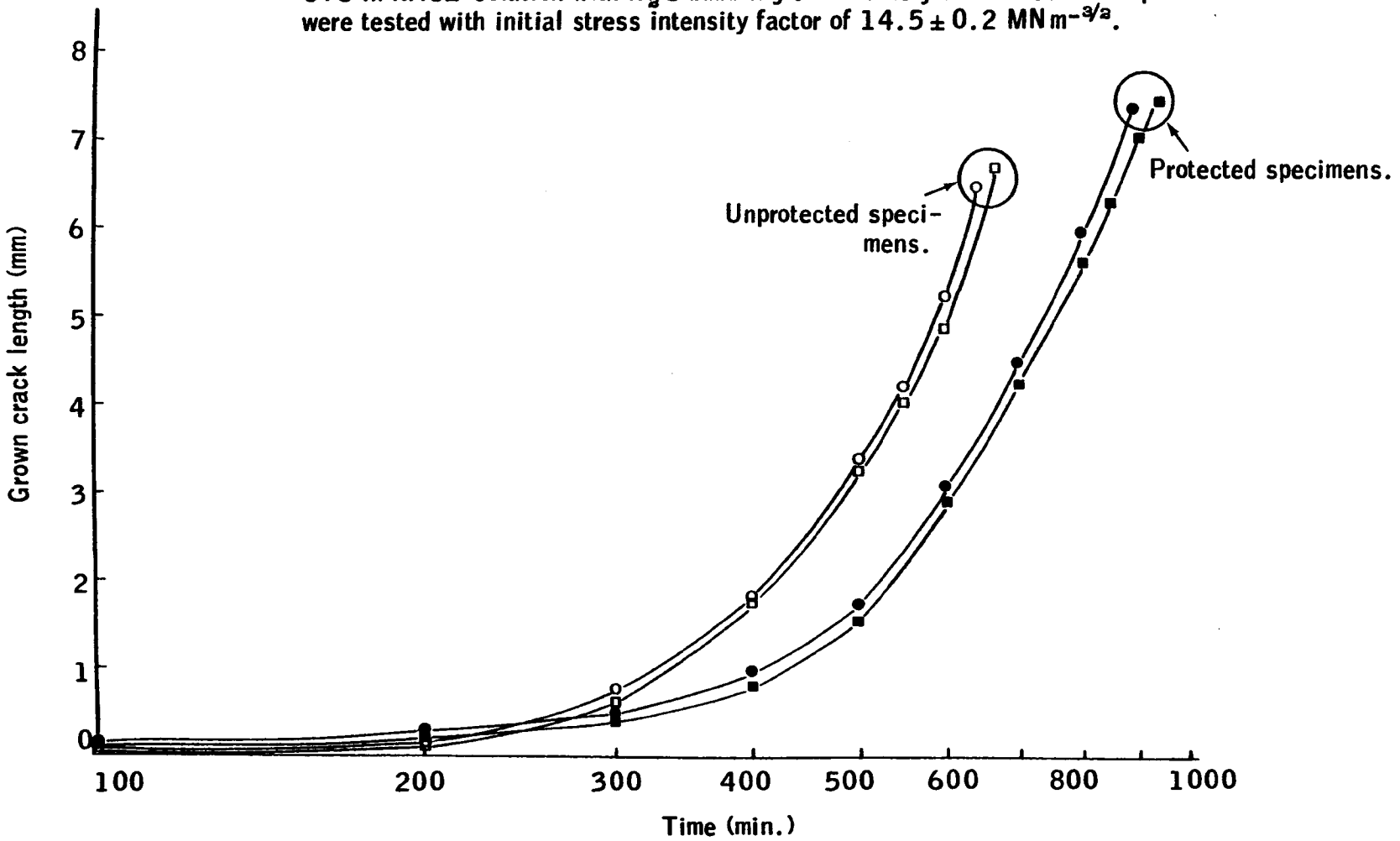

Figure 10.5. Crack growth as a function of time for protected and unprotected GI Special steel CTS in NACE solution with H_2S bubbling continuously at 20° C. The specimens were tested with initial stress intensity factor of 16.0 ± 0.2 MN $m^{-3/2}$.

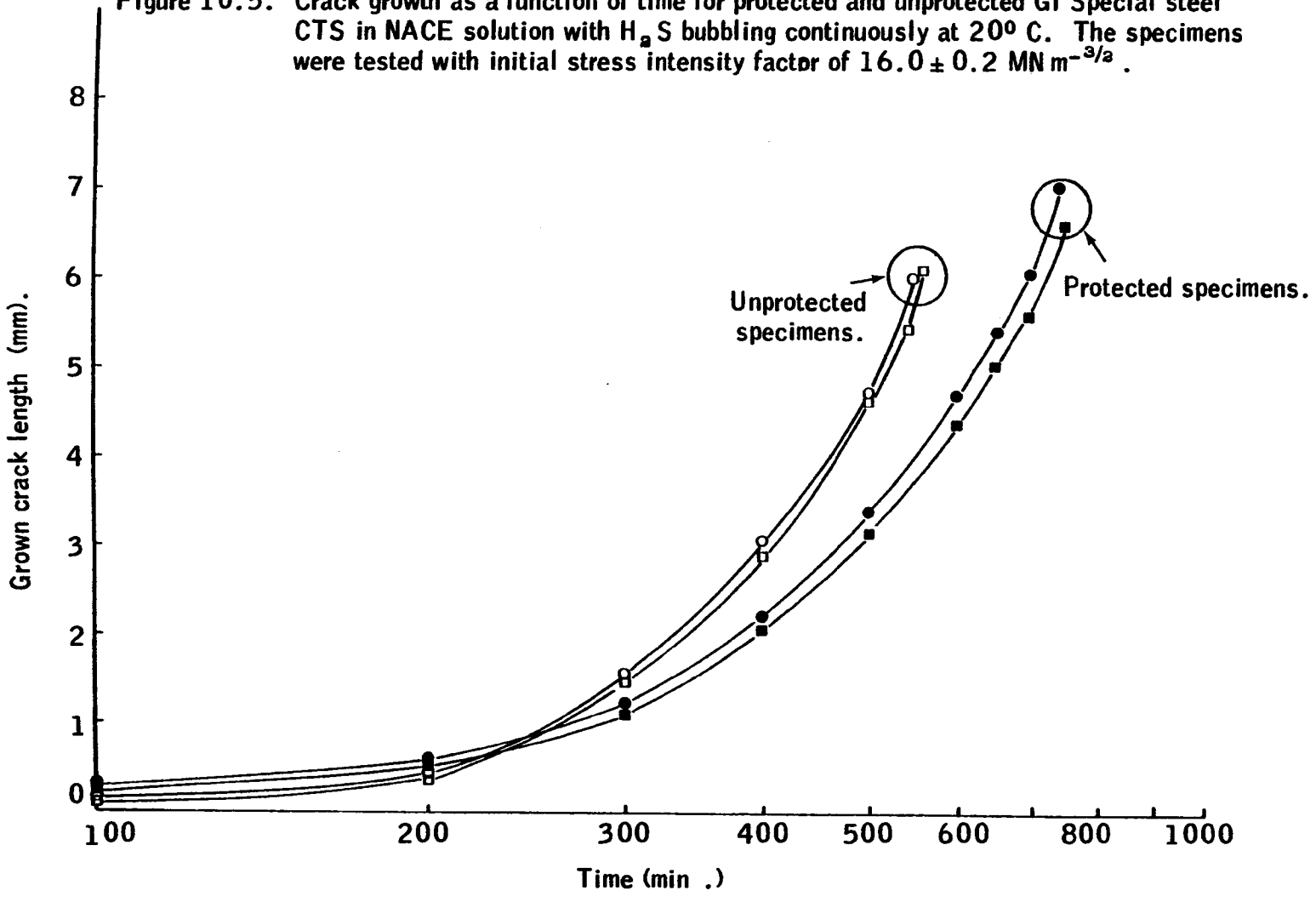

Figure 10.6. Crack growth as a function of time for protected and unprotected GI Special steel CTS in NACE solution with H_2S bubbling continuously at 20° C. The specimens were tested with initial stress intensity factor of 21.5 ± 0.3 MN $m^{-3/2}$.

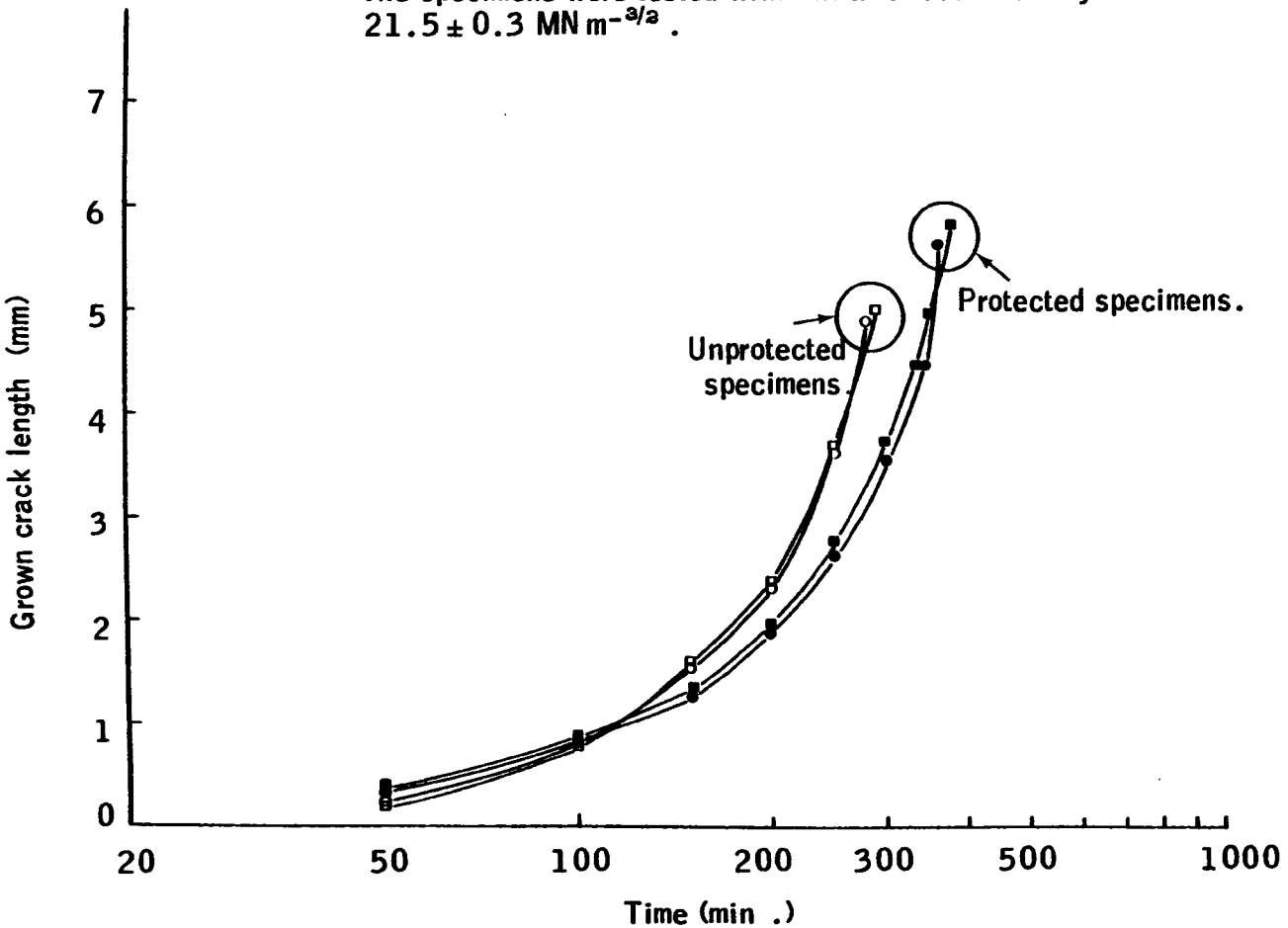

Figure 10.7. Plots of crack growth rate as a function of time for protected and unprotected GI Special steel CTS in NACE solution with H_2S bubbling continuously at 20^0 C. The specimens were tested with initial stress intensity factor of 14.5 ± 0.2 MN m$^{-3/2}$.

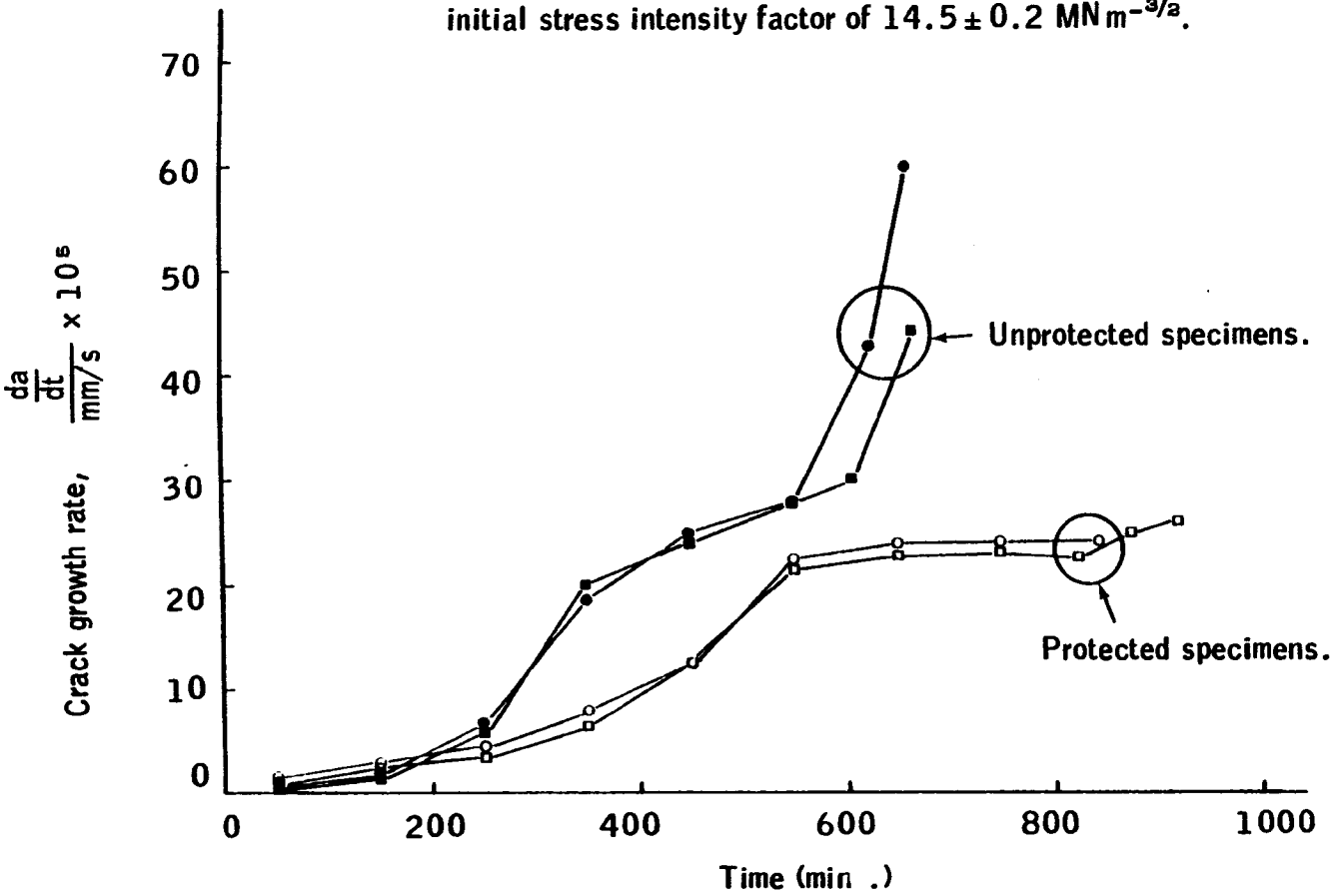

Figure 10.8. Plots of crack growth rate as a function of time for protected and unprotected GI Special steel CTS in NACE solution with H_2S bubbling continuously at 20° C. The specimens were tested with initial stress intensity factor of 16.0 ± 0.2 MN m$^{-3/2}$.

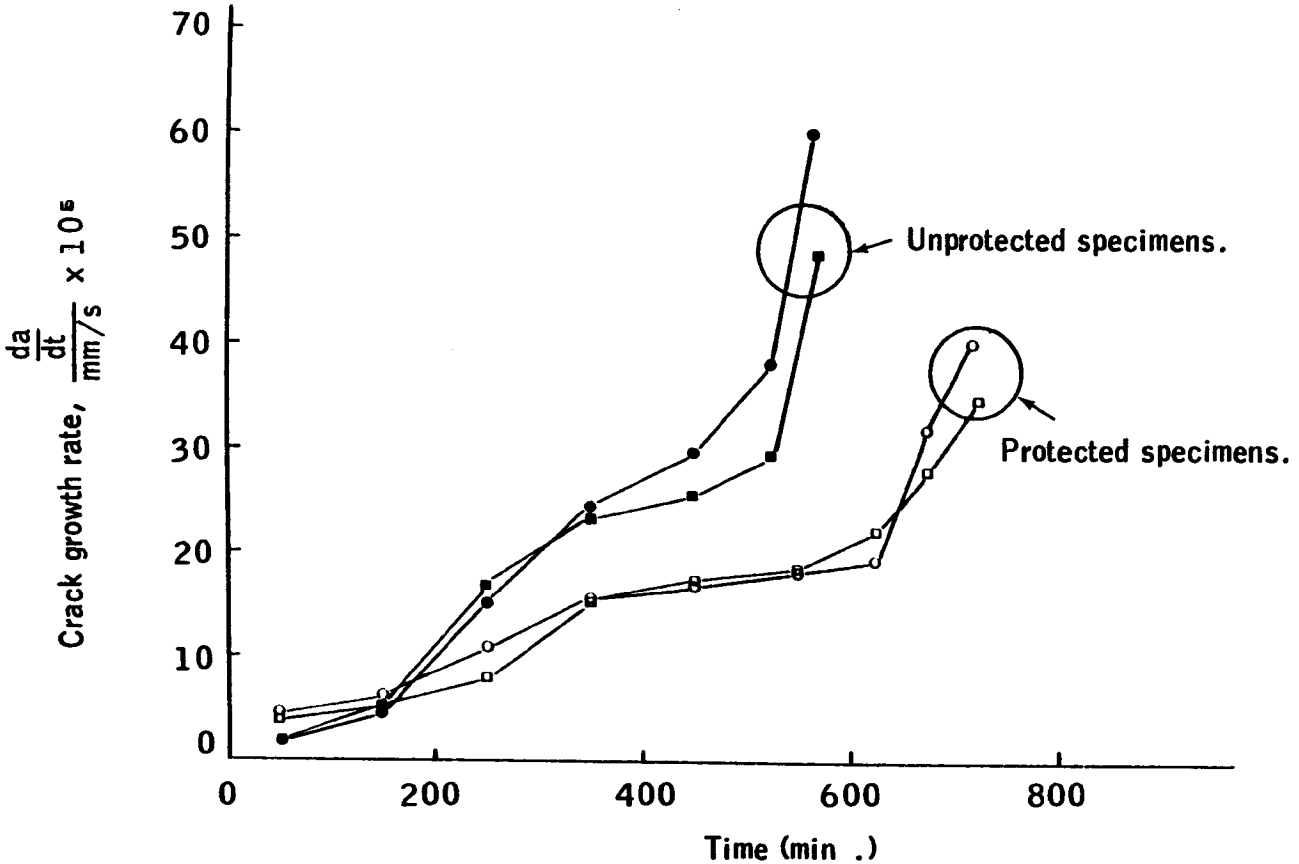

Figure 10.9. Plots of crack growth rate as a function of time for protected and unprotected GI Special steel CTS in NACE solution with H_2S bubbling continuously at 20° C. The specimens were tested with initial stress intensity factor of 21.5 ± 0.3 MN $m^{-3/2}$.

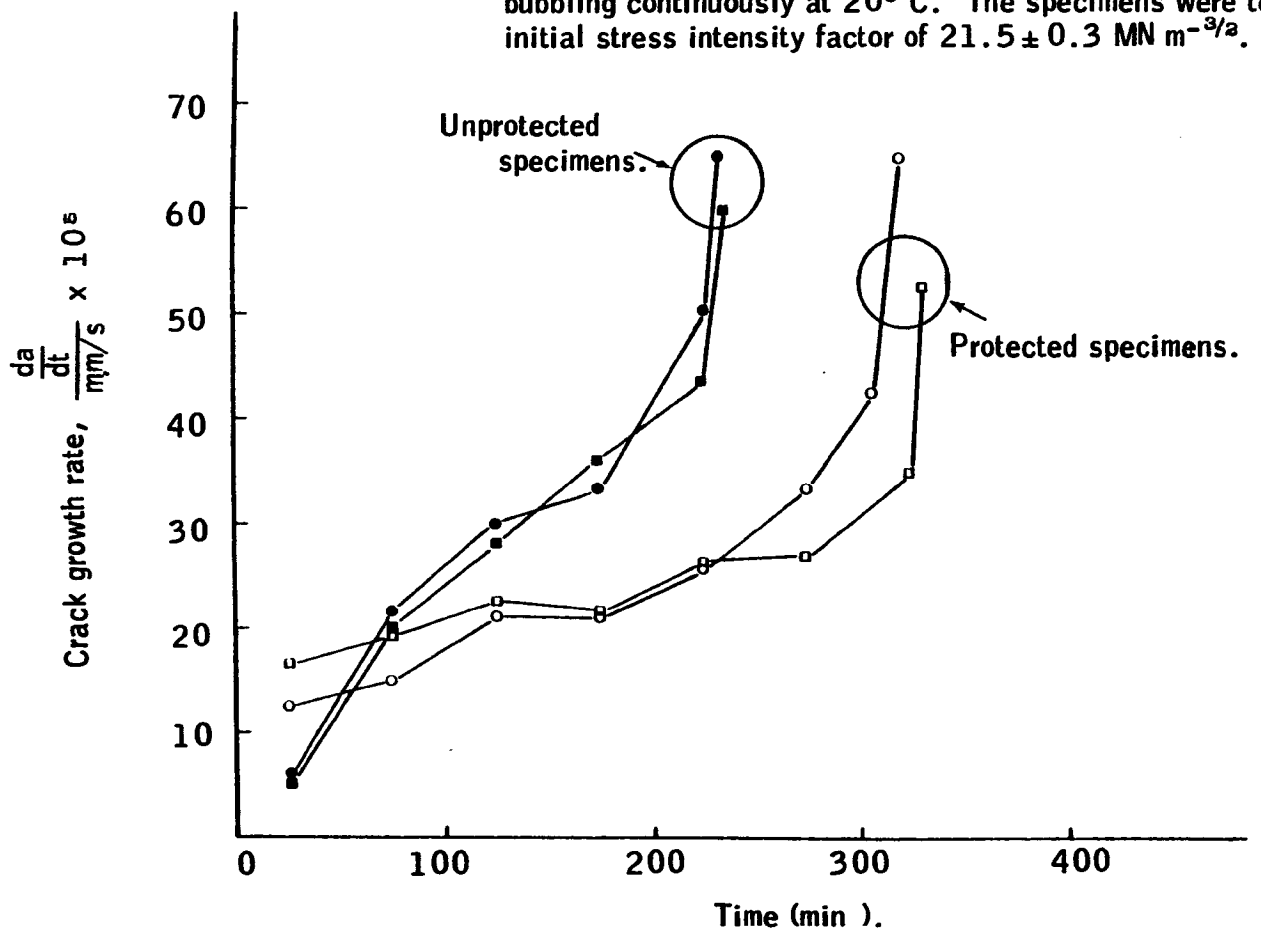

Figure 10.10. Crack growth rate for protected and unprotected GI Special CTS as a function of stress intensity factor in NACE solution with H_2S bubbling continuously at 20° C. The specimens were tested with initial stress intensity factor of 14.5 ± 0.2 MNm$^{-3/2}$.

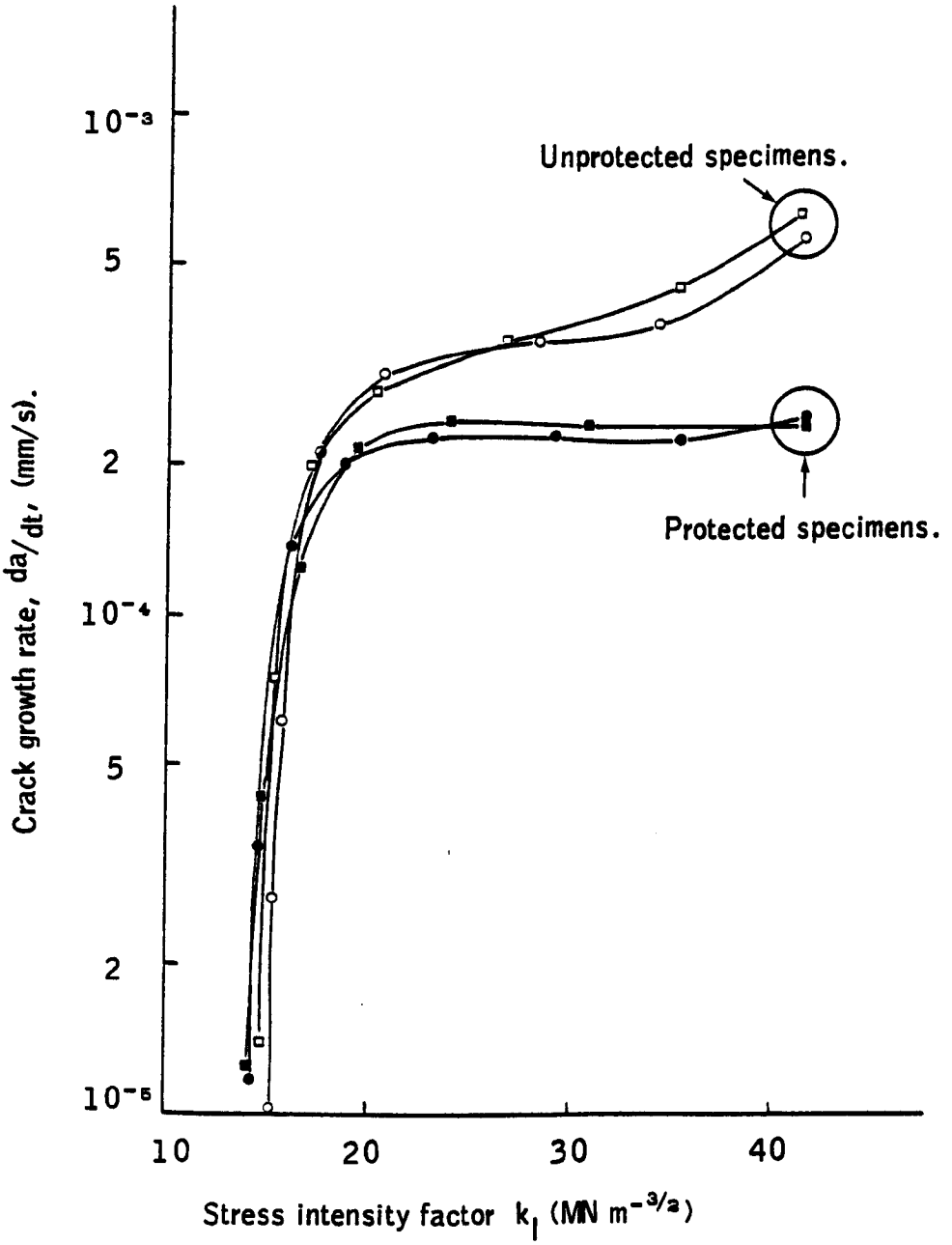

Figure 10.11. Crack growth rate for protected and unprotected GI Special CTS as a function of stress intensity factor in NACE solution with H_2S bubbling continuously at 20° C. The specimens were tested with initial stress intensity factor of 16.0 ± 0.2 MN $m^{-3/2}$.

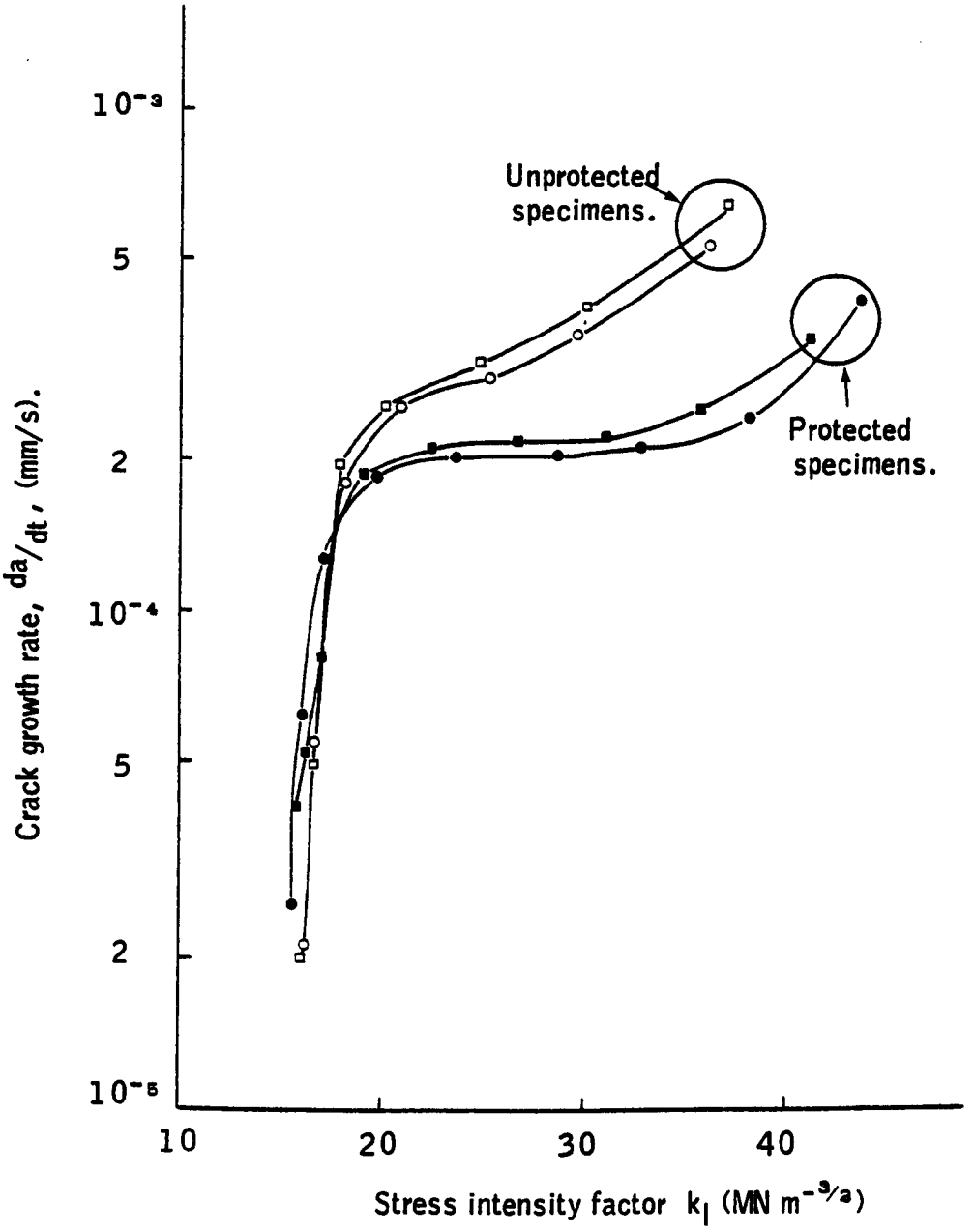

Figure 10.12. Crack growth rate for protected and unprotected GI Special CTS as a function of stress intensity factor in NACE solution with H_2S bubbling continuously at 20° C. The specimens were tested with initial stress intensity factor of 21.5 ± 0.3 MN $m^{-3/2}$.

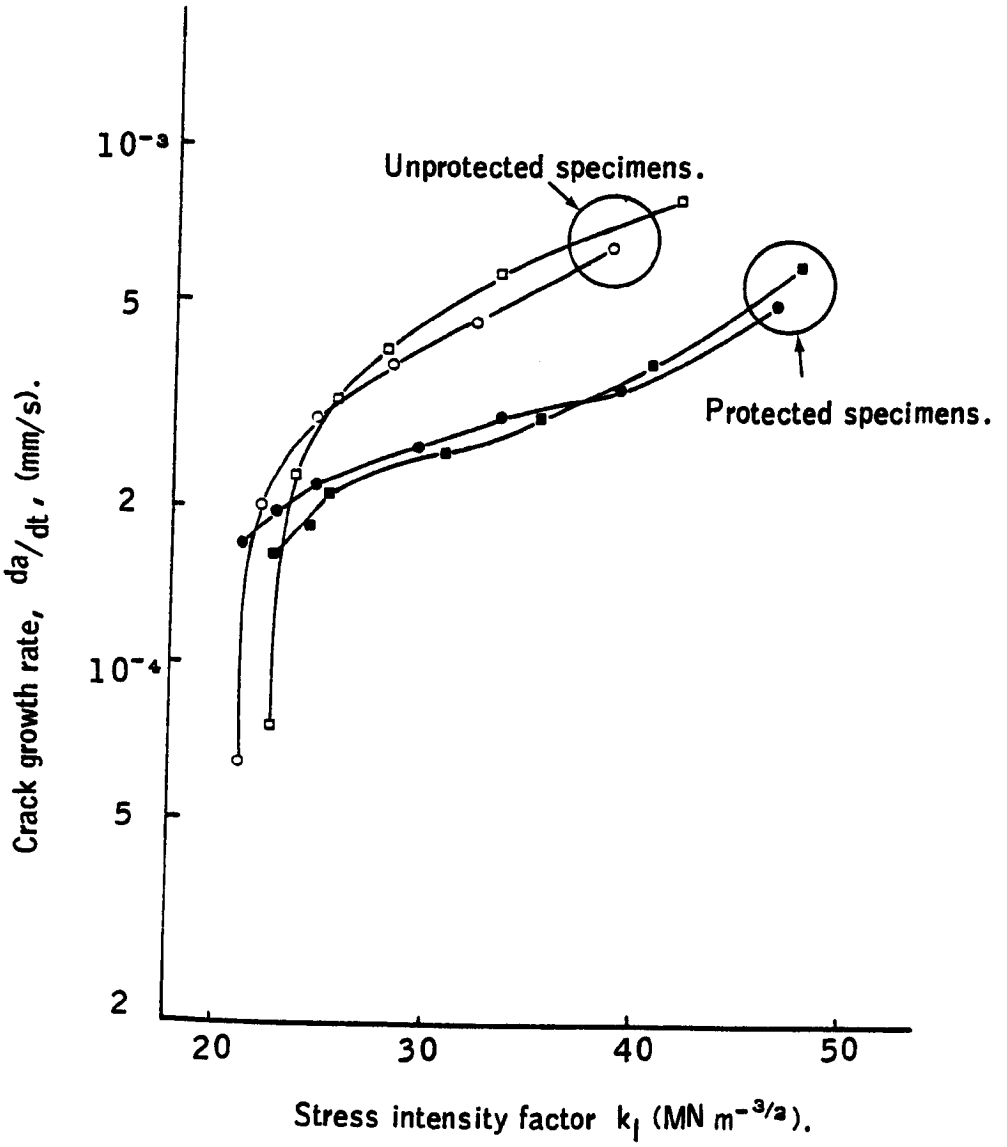

intergranular fracture mode. Examination further down the fracture surface of the protected specimen (Plate 10.3) shows a transition region where the intergranular fracture changes to the ductile dimple fracture mode and this mode followed throughout. The SEM fractograph of the unprotected specimen (Plate 10.4) shows an intergranular fracture ahead of the pre-fatigue-cracked area and it followed throughout without any change in fracture mode. The SEM fractographs clearly indicate that the protected specimens absorbed only a small amount of hydrogen compared to the unprotected specimens, during the sustained load test in the sour corrosion environment.

The curves of crack growth versus time (Figures 10.4 - 10.6) on the protected and unprotected specimens tested at various initial stress intensity factors indicate that the cracks grew slower on the protected specimens than the unprotected specimens. Also it shows that on the protected specimens the cracks grew longer before the specimens failed completely. This shows that the protected specimens had a higher fracture toughness value than the unprotected specimens, in the corrosive environment. These two observations indicate that the MoS_2/FEP coat gave a significant resistance to SSCC in steel. It may be noticed that initially the length of crack-grown was higher on the protected specimens than on the unprotected specimens. However, it should be emphazied that the variation in crack-growth was less than 0.2 mm within the first mm length of crack. Two reasons could be given for this variation;

1) the sulphide stress corrosion crack growth at early stages could have been assisted by anodic dissolution rather than hydrogen embrittlement due to the application of the MoS_2/FEP protective coat,

2) errors that may be due to crack length calculations at early stages could have contributed. This is because, the crack lengths were obtained from the calibration cruve in the region (at the lower end) where the loading-arm displacement was very sensitive to the crack length.

The first explanation is supported by the corrosion weight loss measurement studies reported in Chapter 6, where at the early stages of the corrosion weight loss tests it was noticed that the protected specimens lost more weight than the

unprotected specimens. However, the anodic dissolution at the early stages cannot override the viability of the application of the MoS_2/FEP coat protective method since the early enhanced crack growth only represents less than 3 percent of the total length of crack grown in the specimens.

The curves of crack growth rate versus time (Figures 10.7 to 10.9) on the protected and unprotected specimens indicate that the crack growth rate was considerably lower on the protected specimens than on the unprotected specimens. It may be seen from the curves that the useful life-time of the specimens were improved when they were protected with adherent MoS_2/FEP coat and tested at various initial stress intensity factors. Improvement of 55, 37 and 50 percent in useful life-time of the specimens were noted when they were tested at initial stress intensity factors of ≈ 14.5, ≈ 16.0 and ≈ 21.0 MN $m^{-3/2}$ respectively.

The curves of crack growth rate versus instantaneous stress intensity factor (Figures 10.10 to 10.12) confirmed the general view of the stress corrosion crack growth rate behaviour as a function of stress intensity factor which can be divided into three regions. In region I , the rate of growth was strongly dependent on the magnitude of the stress intensity factor, such that a small change in magnitude of k_I resulted in a large change in crack growth. In region II where the crack growth was strongly dependent on the corrosive environment and on the electrochemical or other physical processes taking place on the specimen and the crack-tip. In region III the crack growth rate increased rapidly when the stress intensity factor values approached the critical value k_{IC}. It is clearly seen from the curves that the proposed MoS_2/FEP protective coat gave a considerable amount of protection against the crack growth in the region II, where the growth rate was controlled by electrochemical or other physical processes such as formation of hydrogen due to corrosion, hydrogen adsorption on the metal surface, absorption by the metal, diffusion to the crack tip area, etc. In this region II, the crack growth rates on the unprotected specimens were increased between 1.7 to 2.0 times than the protected specimens.

All the parameters measured in this sustained load test clearly show the effectiveness of the proposed technique to inhibit SSCC in steel.

CHAPTER ELEVEN

LONG-TERM SOUR CORROSION EFFECTS ON MECHANICAL PROPERTIES OF STEELS PROTECTED WITH THE PROPOSED MoS_2/FEP COAT

CHAPTER 11.

LONG-TERM SOUR CORROSION EFFECTS ON MECHANICAL PROPERTIES OF STEELS PROTECTED WITH THE PROPOSED MoS_2/FEP COAT.

11.1 Introduction.

Although the mechanical tests reported on the previous chapters demonstrated clearly the effectiveness of the proposed technique to inhibit SSCC in steel, it is necessary to evaluate the technique against long-term sour corrosion effects for the following reason. The MoS_2/FEP coat and top layer of non-conducting coat protecting a pipeline in service condition could be damaged any time of the pipeline-life period. If the coatings of the pipeline are damaged in the early part of the life-period the MoS_2/FEP coat must provide longer period of protection. Hence it is of utmost importance to evaluate the proposed technique for long-term sour corrosion effects.

A comprehensive test program was established to study the sour corrosion effects on mechanical properties of steels protected with MoS_2/FEP coat. Four different steels, namely API 5LX 65, GI Special, EN 8 and mild steel were selected for this study. They were used to produce various types of specimens and the mechanical parameters of these specimens were measured. The parameters measured on the specimens are:

(a) for compact tension specimens (CTS);
- stress intensity factor at failure
- total energy required for fracturing the specimen
- average energy consumed for unit length of crack extension
- crack opening displacement (COD).

(b) for three-point bend specimens;
- crack opening displacement, (COD).

(c) for Charpy V-notch impact test specimens;

- fracture energy.

The specimens were coated appropriately and placed in a corrosive environment, i.e., NACE solution with H_2S continuously bubbling at 60^0 C for various periods of time. After the exposure to the corrosive environment corresponding mechanical tests were carried-out. Scanning electron microscopic examinations were carried out on the fracture surfaces to identify the mode of fracture.

The mechanical tests could be divided into three groups;

(1) Continuous slower straining/loading rate test on GI Special and API 5LX 65 steels CTS.

(2) Crack opening displacement measurements on three-point-bend specimens of API 5LX 65 steel.

(3) Charpy V-notch impact fracture toughness test on API 5LX 65, EN 8 and mild steel specimens.

11.2 Crack Opening Displacement (COD) Test.

Linear elastic fracture mechanics facilitates the measurement of the plane strain fracture toughness (k_{IC}) of the structural steels. To obtain valid plane strain fracture toughness data for low strength structural steels, it is important to ensure plane strain conditions, hence it is necessary to use (a) large test pieces, (b) increased rate of loading, and (c) low testing temperature. However, it is generally found that the temperature conditions and material thickness used for any practical applications of structural steel are such that large amounts of plastic deformation occur prior to fracture, hence, invalidating the use of linear elastic fracture mechanics. One approach to this problem is to measure the COD parameter. Furthermore, the advantage of the COD approach is that COD values

can be measured throughout the entire plane-strain, elastic-plastic, and fully plastic behaviour regions, whereas k_{IC} values can be measured only in the plane-strain region or approximated in the early portions of the elastic-plastic region.

The concept of COD parameter measurement can be readily appreciated by considering the process occurring when a pre-cracked specimen is tested under a continuous loading. As the applied load increases on a precracked specimen plastic yielding occurs at the crack-tip resulting in separation of the crack faces without any increase in the length of the crack. This separation of the two faces is referred to as the crack opening displacement. In such a test a stage is reached at a particular load when the material in the vicinity of the crack-tip fractures. This depends upon the extent of plastic deformation and hence the load required for failure. The fracture may proceed in a cleavage or shear mode depending on other parameters such as heat-treatment, type of alloy, maximum load achieved etc. The specific value of COD obtained at the crack tip at the instant of fracture is considered to be a measure of the fracture toughness of the material under examination.

There are various geometrical parameters that may affect the result of a COD test. These are, the crack size ($^{a}/_{W}$), test piece thickness, notch acuity, and testing machine stiffness. After considerable study of various methods to measure COD, the British Standard Institution has published a method for measuring the COD parameter of metallic materials[126]. Basically,a precracked, three-point bend specimen (Figure 11.1) is used to measure the COD parameter. Test results are recorded by plotting autographically the applied force against the clip gauge-displacement measured at the test piece surface across knife edges located on opposite sides of the notch. A variety of load-clip gauge displacement records can be obtained depending on the test material, rate of loading, test temperature, etc. There are five types of load-clip gauge displacement graphs given in the British Standard for calculation of COD. If onset of crack growth cannot be established to calculate the COD for fracture initiation, from any of the load-

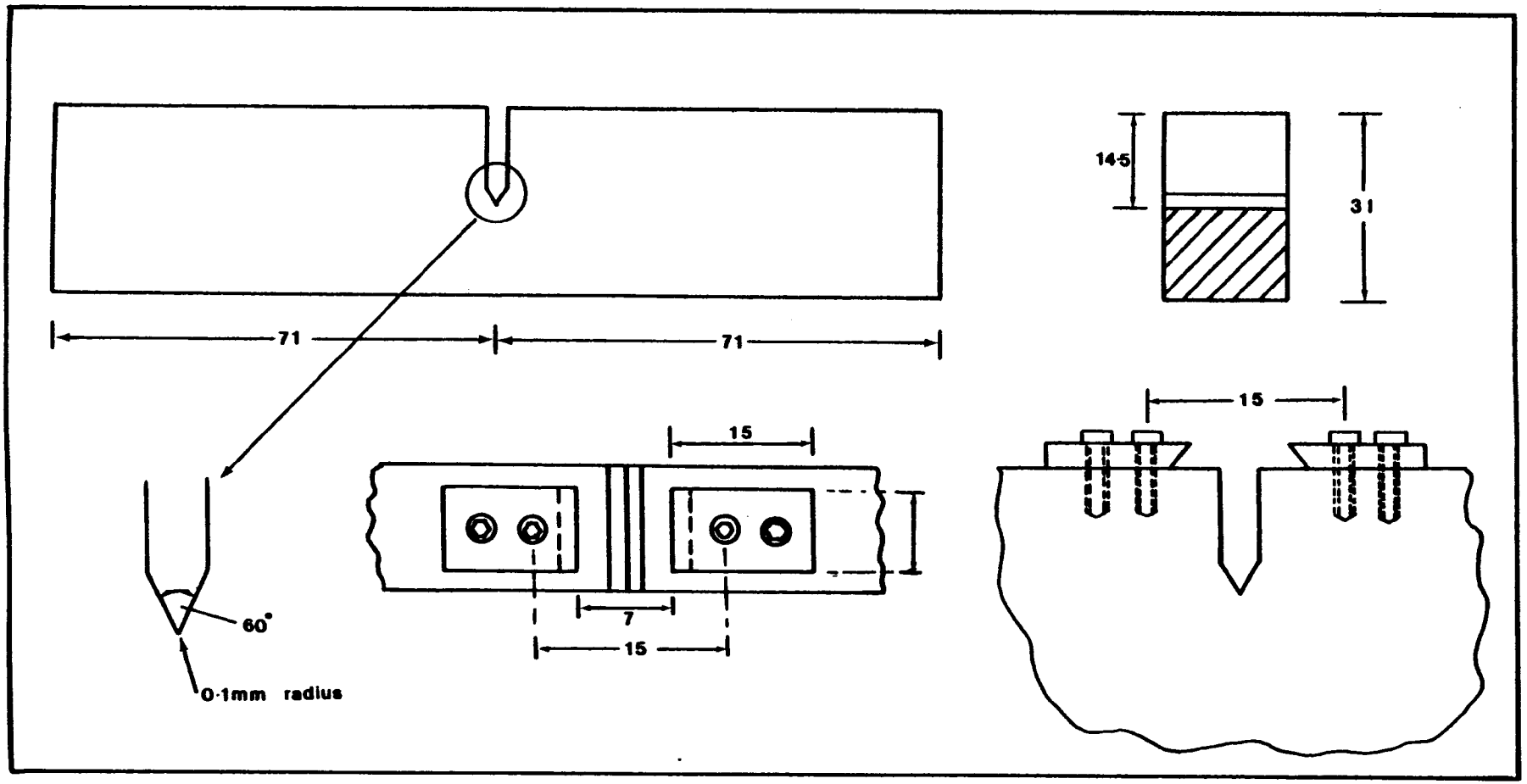

Figure 11.1. Schematic illustration of three-point-bend specimen and knife edges for location of clip gauge. Dimensions are in mm.

displacement curves it is recommended to use a multiple specimen technique for determining COD at initiation of slow crack growth. For material comparison purposes a maximum COD could be calculated from the clip gauge displacement measurement at the first attainment of a maximum load.

Having obtained the critical or maximum value of the clip gauge displacement, it is necessary to convert this to the relevant crack tip opening displacement value. The recommended method assumes deformation to occur by a hinge mechanism about a center of rotation at a depth of $\frac{1}{n}(w - a)$ below the crack tip (Figure 11.2).

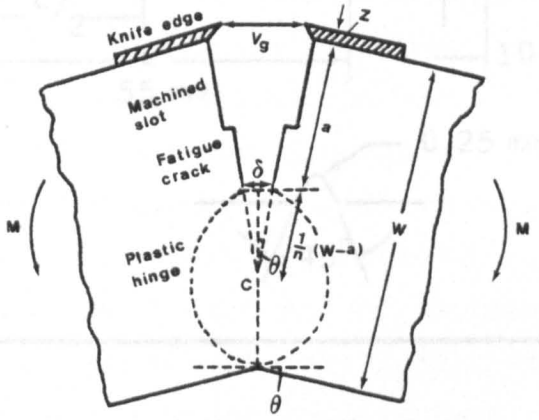

Figure 11.2. Schematic illustration of relationship between crack-tip opening displacement, δ, and knife-edge displacement, V_g, (129).

11.3 Charpy V-Notch Impact Test.

The Charpy V-notch impact fracture toughness test is the most widely used test to determine the toughness behaviour of structural materials, prior to the development of fracture mechanics. Even today after two decades of development on fracture mechanic specimens and concepts, the Charpy impact test is widely used throughout the world, not only as a general reference test but in many actual toughness specification.

The Charpy impact test specimen is a bar 55 mm in length with a square cross section having sides of 10 mm. It has a V-shaped notch machined midway along the length of the specimen. Figure 11.3 gives a schematic illustration of the specimen. There are three parameters reported from Charpy impact tests in the

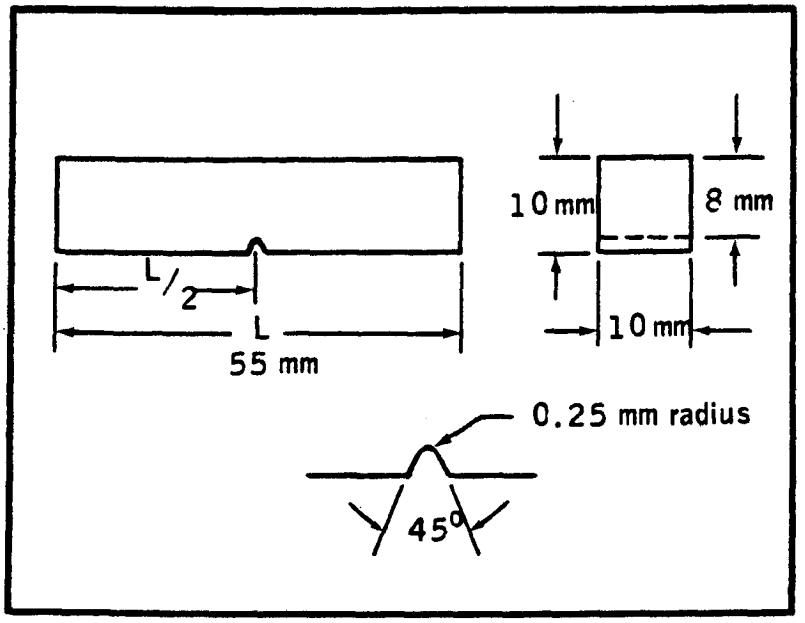

Figure 11.3. Charpy V-notch impact test specimen.

form of transition curves. They are the following;

(1) energy absorbed for fracture.

(2) fracture surface appearance.

(3) lateral expansion at the compression side directly opposite the notch.

From the transition curves, a ductile/brittle transition temperature (T_T) can then be determined for many metallic materials. Above this transition temperature the absorbed energy is large (e.g. greater than 15 ft.lbf. or 20 J), where fracture occurs at nominal stresses exceeding the yield stress. At temperatures lower than T_T, the energy absorbed by the specimen is small and fracture occurs at

norminal stresses below the yield stress. The energy absorption during the impact test is controlled by two factors. One is the strength of the steel, which regulates the force required to deform the Charpy specimen and the other is the ductility of the steel, which determines the distance through which the force acts during testing. It is widely recognized that loss of fracture toughness is due to loss in ductility rather than strength where the Charpy specimens are tested over a range of temperatures. Hence the measurement of lateral expansion of the specimen at the compression side directly opposite the notch is more significant than the energy absorbed in establishing the transition temperature.

There are some valid criticisms applicable to the Charpy impact test. The absorbed energy measured cannot be related directly to structural design parameters. The tests are conducted on small specimens (10 mm square, rectangular bars) at extremely high strain rates (impact loading) and involve fracture ahead of shallow, rounded notches (root radius of 0.25 mm) where the energy absorbed in crack initiation and crack propagation cannot be readily distinguished. Despite criticisms the Charpy impact test is used widely throughout the world because it is quick to conduct, inexpensive and simple to use. Furthermore it has many years of correlation with service performance and there are several empirical correlations between the charpy V-notch impact test results and the plane strain fracture toughness k_{Ic} (static) and k_{Id} (dynamic) characterized by linear elastic fracture mechanics[127].

11.4 Experimental Procedures.

11.4.1. Materials Preparation.

GI Special steel and API 5LX 65 steel were the two types of steels selected to make compact tension specimens. The percentage chemical composition of the steels and the specimen dimensions are given in Table 9.1 and Figure 9.1 respectively. The preparatory method for the CTS is detailed in the section 9.2.1. However a provision was made for the testing of CTS of API 5LX 65 steel, to fix knife edges as shown in

Plate 11.1. Ball-milled MoS_2/FEP protective coating was prepared with the catalyst to FEP ratio of 1:0.85 as detailed in the section 4.3.1.3 and applied to the GI Special CTS in a pattern given in Figure 9.4. In a similar manner unball-milled MoS_2/FEP protective coating with the catalyst to FEP ratio of 1:1.12 was applied to API 5LX 65 steel CTS. Lacomit-Varnish coat was applied to the unprotected CTS as shown in Figure 9.4 to maintain the same condition.

Three-point bend COD specimens of the preferred B x 2B geometry specified in British Standard 5762[126] were prepared from the API 5LX 65 steel. The specimens were machined from a pipe in longtitudinal direction and notched in the direction of the circumference of the pipe. Schematic illustration of the specimen is given in Figure 11.1. Although the standard recommends to test the specimen with full thickness, about $\frac{1}{4}$ to $\frac{1}{2}$ mm thickness of scale was removed on both sides of the pipe wall to enable the corrosion reaction to take place without any barrier when the specimens were placed in the corrosive environment. The prepared specimens were polished with 600 grit silicon carbide paper in a direction that could not interfere with the observation of the fatigue crack to be initiated at the V-notch tip. After degreasing the specimens with acetone in an ultrasonic bath, unball-milled MoS_2/FEP protected coating prepared as detailed in the section 4.3.1.3, with the catalyst to FEP ratio of 1:1.12 was applied to the specimen. Plate 11.2 shows the specimens with the MoS_2/FEP protective coating and with the Laconit varnish coating. A fatigue crack was initiated from the V-notch tip by the application of cyclic loading. The crack was initiated by maintaining the maximum load at 10 kN and the minimum load at 1 kN at a frequency of 10 Hz. Once the fatigue crack was initiated, the loads were reduced gradually to a maximum of 5 kN and minimum of 0.5 kN while maintaining the frequency at 10 Hz. Finally the fatigue crack was closely watched as it grew between 1.5 and 2.0 mm.

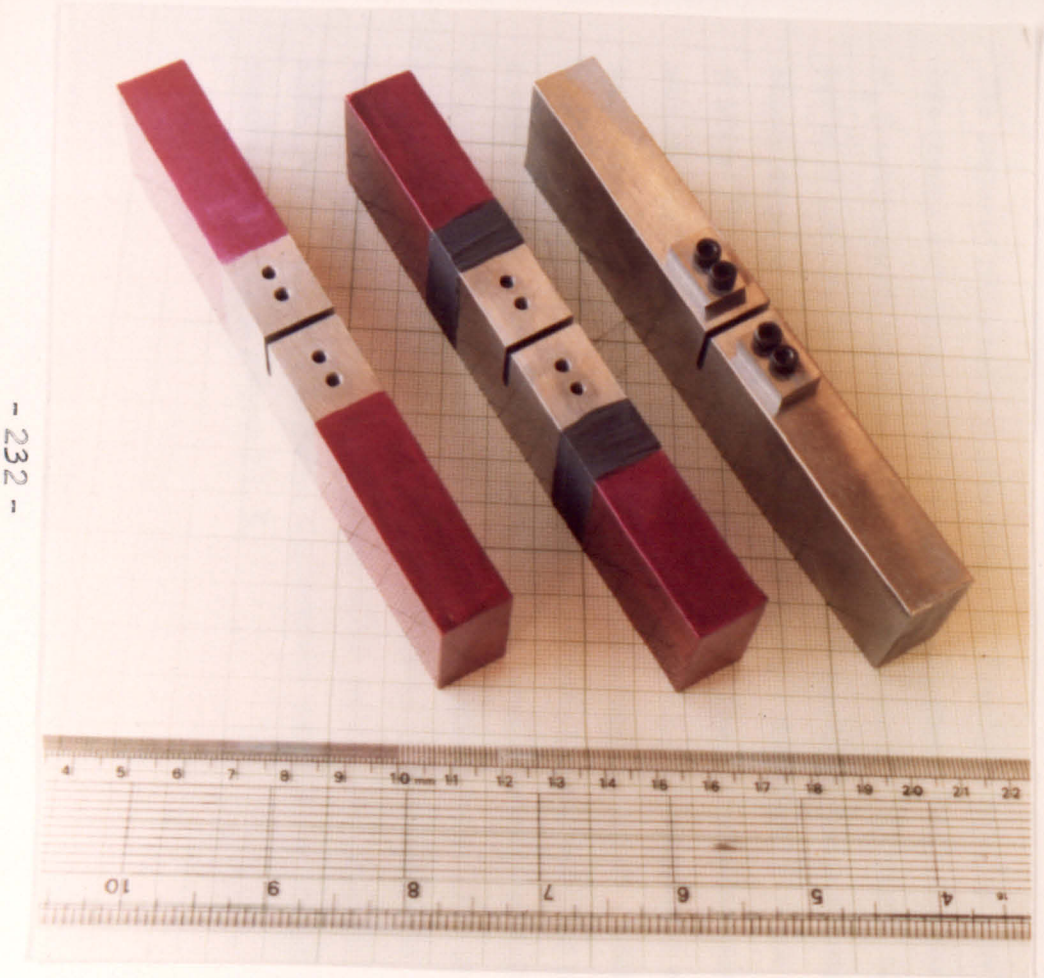

Plate 11.2. Photograph illustrates the coatings applied to the protected and unprotected three-point bend test specimens.

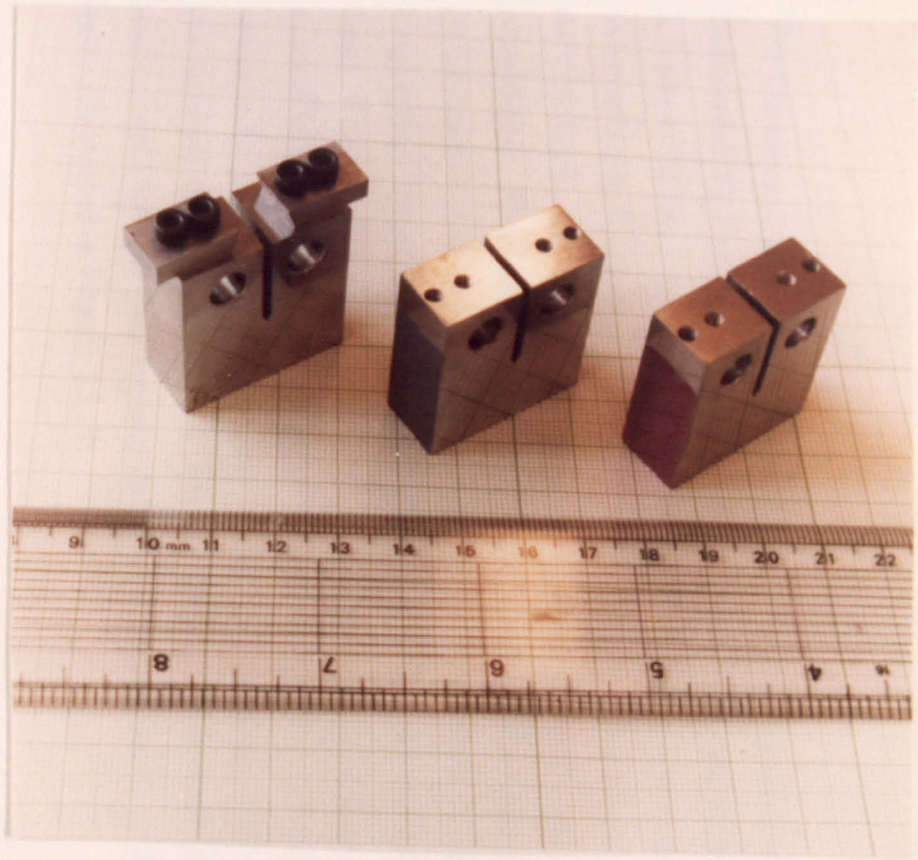

Plate 11.1. Photograph illustrates the coatings applied to the protected and unprotected compact tension specimens.

The Charpy test specimens were prepared in accordance with the British Standard 131 Part 2[128]. The Charpy specimens were of the standard 10 mm x 10 mm x 55 mm diamensions. The specimen and its notch are schematically illustrated in Figure 11.3. Three different steels, API 5LX 65, EN 8 and Mild Steel, were used to prepare the Charpy test specimens. The chemical composition of the steels are given in Table 9.1. In the case of API 5LX 65 pipe-steel the specimens were taken in the longitudinal direction of the pipe and notched in the circumferential direction. Further, for pipe-steel Charpy specimens, unball-milled MoS_2/FEP protective coating with the catalyst to FEP ratio of 1:1.12 was applied, whereas for the other steel specimens, ball-milled MoS_2/FEP coating with the catalyst to FEP ratio of 1:0.85 was applied. The MoS_2/FEP coat and Lacomit varnish coat regions on the Charpy specimens are schematically illustrated in Figure 11.4.

11.4.2. Test Procedures.

The prepared protected and unprotected GI Special steel CTS were divided into groups and placed in the corrosive environment, NACE solution with H_2S continuously bubbling at 60 °C for a period of 750 hours. After this period of time the corroded GI Special CTS was taken-out and tested on the Mayes machine under a loading rate of either 40 MN $m^{-3/2}$/hour or 5 MN $m^{-3/2}$/hour in air at room temperature. The load-displacement curve was recorded autographically. The API 5LX 65 CTS specimens were also subjected to similar treatment and tested at a loading rate of 5 MN $m^{-3/2}$/hour. An additional load-clip gauge displacement curve was also recorded autographically in the case of API 5LX 65 steel specimens with the help of a separate system incorporated with the Mayes machine. The separate system employed an X-Y recorder (2900 series, Bryans Southern Instruments Limited) and a transducer meter (C52 series, Boulton Paul Aircraft Ltd). A typical load-clip gauge displacement curve for the compact tension specimen is given in Figure 11.5.

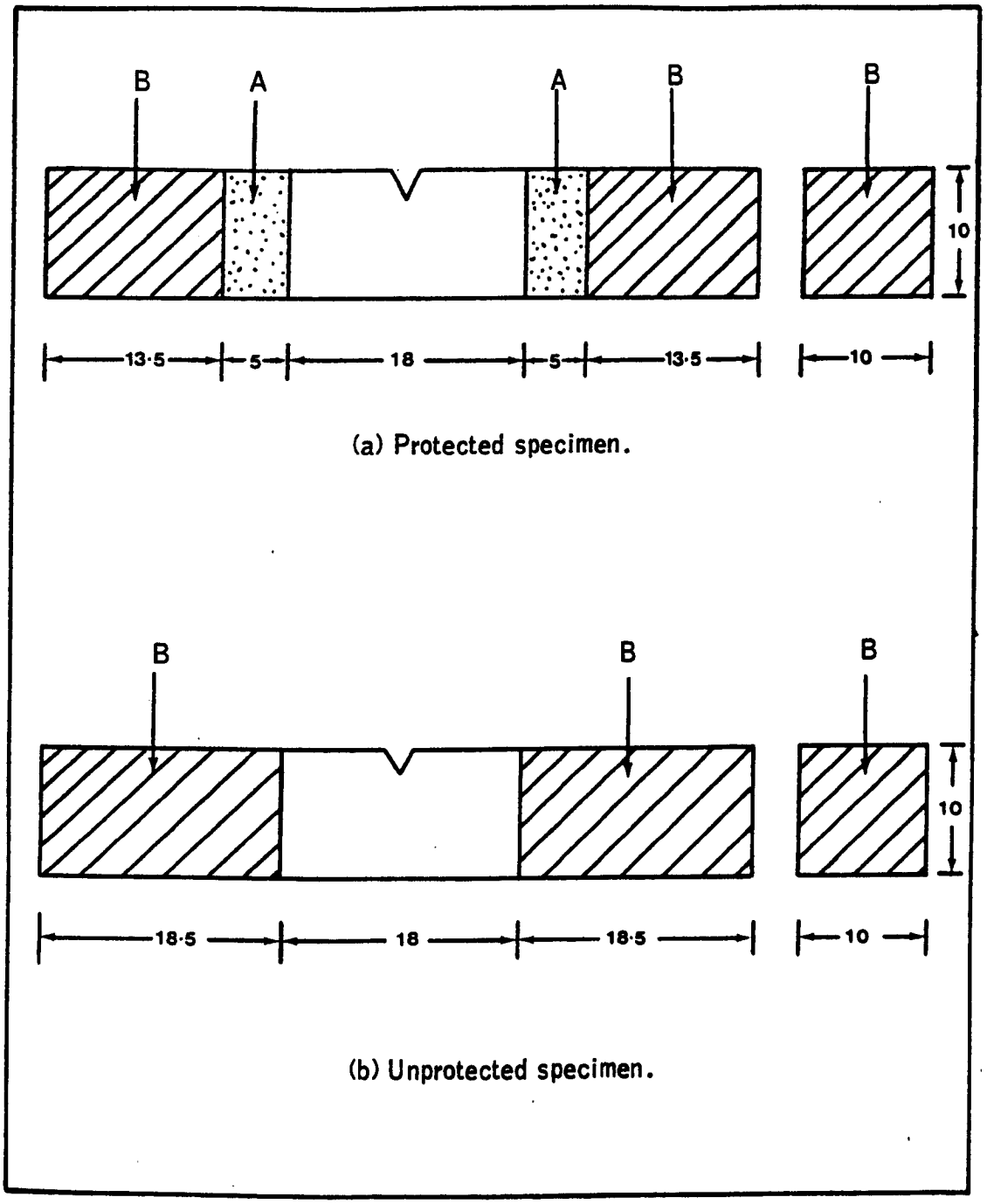

Figure 11.4. Pattern of MoS_2/FEP and Lacomit varnish coats on Charpy impact test specimens. (A) MoS_2/FEP coat, (B) Lacomit varnish coat. Dimensions are in mm.

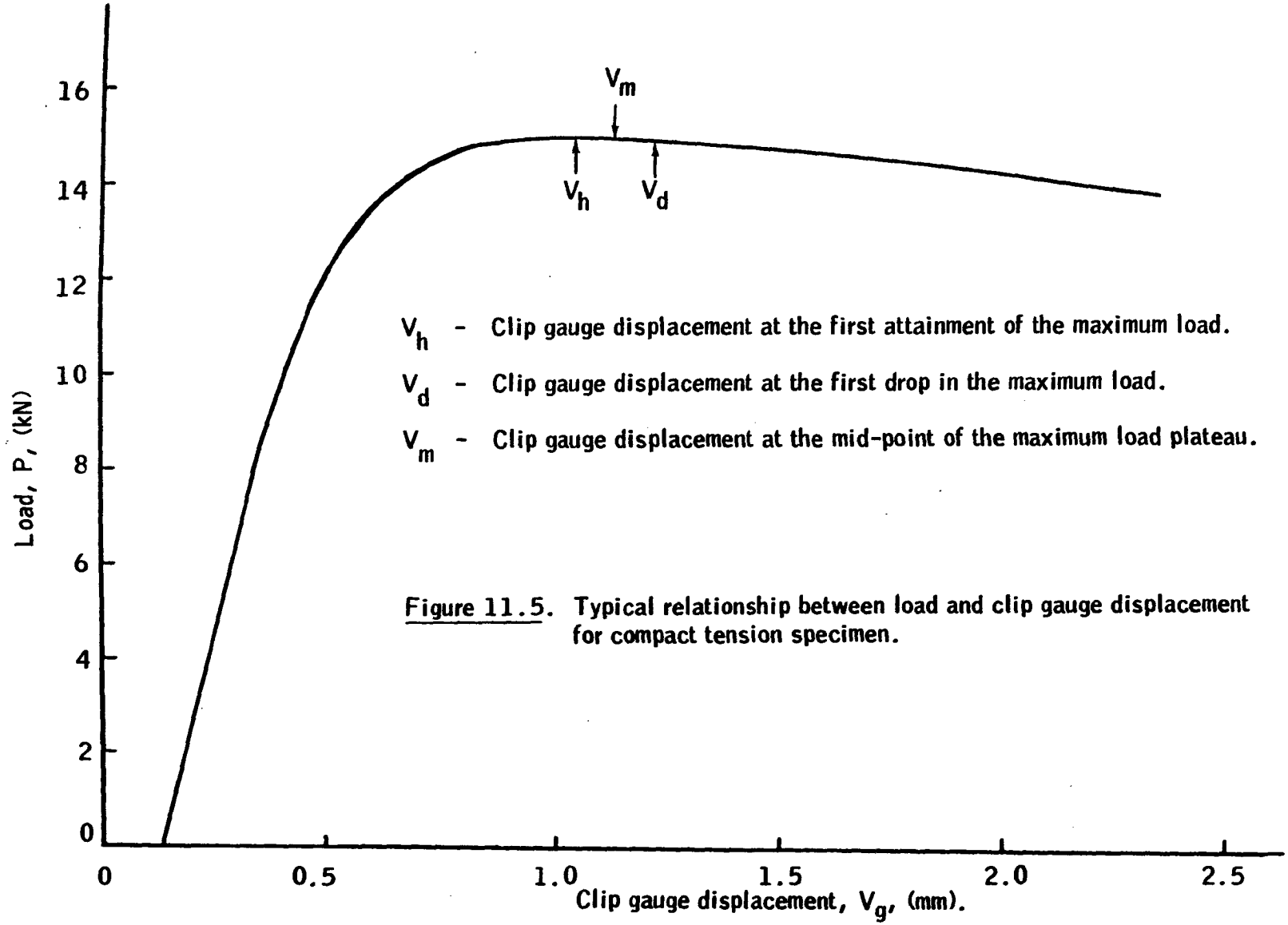

V_h - Clip gauge displacement at the first attainment of the maximum load.

V_d - Clip gauge displacement at the first drop in the maximum load.

V_m - Clip gauge displacement at the mid-point of the maximum load plateau.

Figure 11.5. Typical relationship between load and clip gauge displacement for compact tension specimen.

The prepared three-point bend specimens were placed in the corrosive environment at 60° C for a period of 750 hours. The corroded specimens were removed from the corrosive environment and the COD parameter was measured as specified in the British Standard 5762, under the displacement control Mayes testing machine. Plate 11.3 gives the general arrangement and the equipment, (clip gauge, Mayes machine, X-Y recorder and transducer meter) used for this test. Plate 11.4 gives a close-up view of the three-point bend specimen's loading arrangement with the clip gauge attached to the Specimen. The COD tests were conducted at two different loading rates, of 3425 MN $m^{-3/2}$/hour (as recommended in the standard) and ≈ 47 MN $m^{-3/2}$/hour. The load-clip gauge displacement curves were recorded autographically. A typical load-clip gauge displacement curve for the three-point-bend specimen is given in Figure 11.6.

Two groups each consisting of 10 protected and 10 unprotected Charpy specimens of API 5LX 65 steel were placed in the corrosive environment for a period of 350 and 850 hours at 60° C. The same number of protected and unprotected Charpy specimens of mild steel and EN 8 Steel were placed in the corrosive environment for periods of 350 and 750 hours respectively. The corroded specimens were removed and tested on a Charpy testing machine which consists of a rigid frame with a swinging pendulum. The specimens were placed on anvils solidly attached to the frame. Then the pendulum was released at the start of the test and a striker built into the base of the pendulum broke the specimen on impact. The kinetic energy of the moving pendulum was known at the point of impact on the specimen. The machine incorporates a device for measuring the difference in pendulum energies before and after it fractured the specimen. Hence the energy absorbed during the fracture was read-out directly.

Plate 11.3. Photograph gives the general arrangement and the equipment used for the three-point bend test with COD measurement.

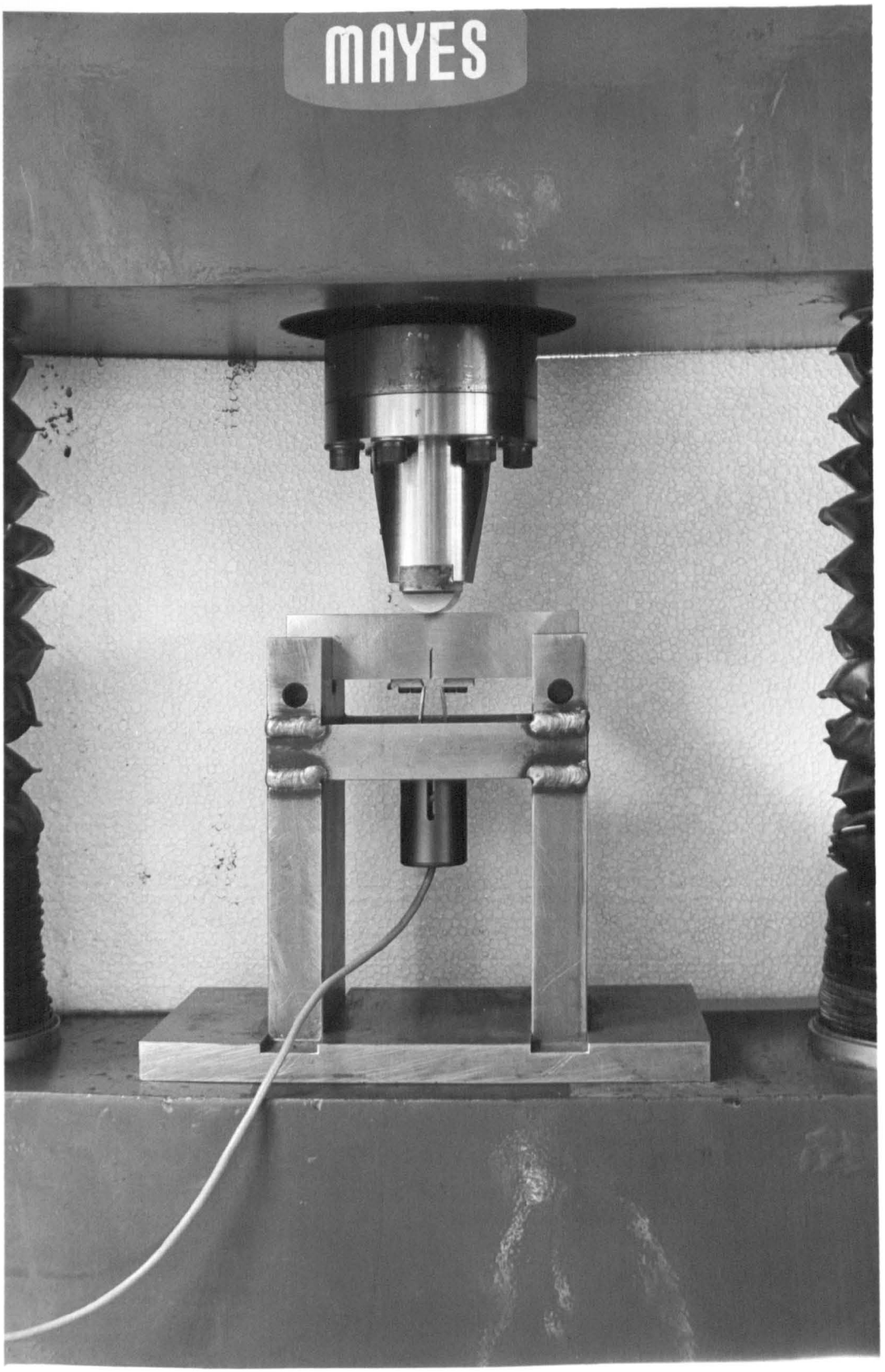

Plate 11.4. Photograph gives a close-up view of the three-point bend specimen with the clip gauge used to measure the displacement.

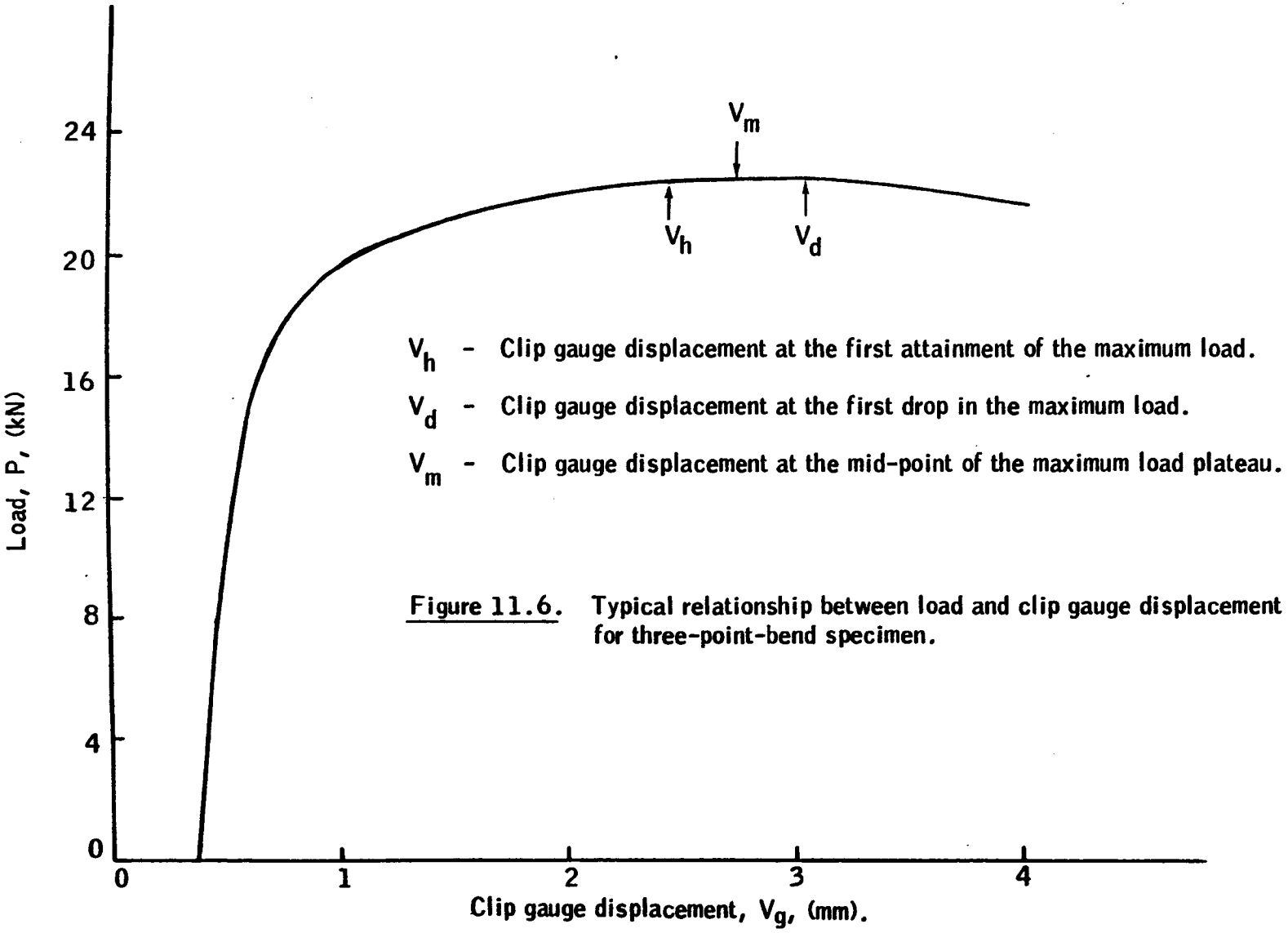

V_h - Clip gauge displacement at the first attainment of the maximum load.

V_d - Clip gauge displacement at the first drop in the maximum load.

V_m - Clip gauge displacement at the mid-point of the maximum load plateau.

Figure 11.6. Typical relationship between load and clip gauge displacement for three-point-bend specimen.

11.4.3. Fracture Surfaces Examination.

Scanning electron microscopic examinations were carried-out on the fracture surfaces of the corroded CTS and Charpy V-notch impact test specimens. Since all the specimens were tested in air, after the treatment in the corrosive environment, the fracture surfaces were not contaminated with sulphides. Light fractographs were taken on the API 5LX 65 steel and EN 8 steel Charpy specimens fracture surfaces to demonstrate the lateral expansion of the specimen at the compression side directly opposite the notch.

11.5 Results.

Table 11.1 shows the results for the protected and unprotected GI Special steel CTS in terms of (1) stress intensity factor at failure, k_{IQ}, (2) total energy required for fracturing the specimen and (3) the average energy consumed for unit length of crack extension. The critical stress intensity factor was calculated from the peak load, planar dimensions of the specimen and the initial crack length using linear elastic fracture mechanics[120]. The total work required to fracture the specimen was calculated from the area of the load displacement curve. This quantity divided by the distance from the fatigue crack tip to the edge of the specimen gave the average energy consumed for unit length of crack extension. Scanning electron microscopic fractograph of the unprotected G1 Special steel CTS tested after being subjected to corrosion at a loading rate of 40 MN $m^{-3/2}$/ hour is given in Plate 11.5. SEM fractograph of the protected (ball-milled MoS_2 used) G1 Special steel CTS tested as illustrated above is given in Plate 11.6.

For the API 5LX 65 Steel CTS the crack opening displacements were also calculated in addition to the parameters calculated for GI Special steel CTS. In the crack opening displacement calculation for the CTS it was assumed that the deformation occurs by a hinge mechanism about a center of rotation at a depth of $\frac{1}{n}(W-a)$ below the crack tip (Figure 11.2). A value of 2.5 was selected[129]

TABLE 11.1.

Longterm sour corrosion effect on the mechanical properties of GI Special steel CTS. The specimens were placed in a corrosive environment, NACE solution with H_2S continuously bubbling at 60° C for 750 hours and tested in air under slower straining/loading at room temperature.

Loading rate ($MN\,m^{-3/2}$/hour)	k_{IQ} at failure ($MN\,m^{-3/2}$)	Total work done for fracturing the specimen (joules)	Work done for unit length of crack extension (J/mm)
Control:			
41.28	76.85	18.42	1.423
40.27	76.42	17.85	1.371
43.58	77.63	18.63	1.460
	$\bar{x}$= 76.97	$\bar{x}$ = 18.30	$\bar{x}$=1.418
5.70	67.58	16.42	1.266
5.14	68.41	16.63	1.291
4.94	66.42	16.25	1.247
	$\bar{x}$= 67.47	$\bar{x}$ = 16.43	$\bar{x}$=1.268
Protected:			
40.11	65.68	12.35	0.979
38.76	66.03	12.52	0.982
41.24	64.87	12.45	0.980
	$\bar{x}$= 65.53	$\bar{x}$ = 12.44	$\bar{x}$=0.980
5.40	30.07	5.22	0.392
4.82	28.01	5.08	0.381
5.13	29.87	4.96	0.387
	$\bar{x}$= 29.32	$\bar{x}$ = 5.09	$\bar{x}$=0.387
Unprotected:			
43.23	56.12	8.21	0.618
40.25	53.68	7.98	0.602
39.27	54.12	8.14	0.611
	$\bar{x}$= 54.64	$\bar{x}$ = 8.11	$\bar{x}$=0.610
4.96	21.14	2.80	0.227
5.18	19.81	2.93	0.261
4.59	20.05	3.18	0.264
	$\bar{x}$= 20.33	$\bar{x}$ = 2.97	$\bar{x}$=0.251

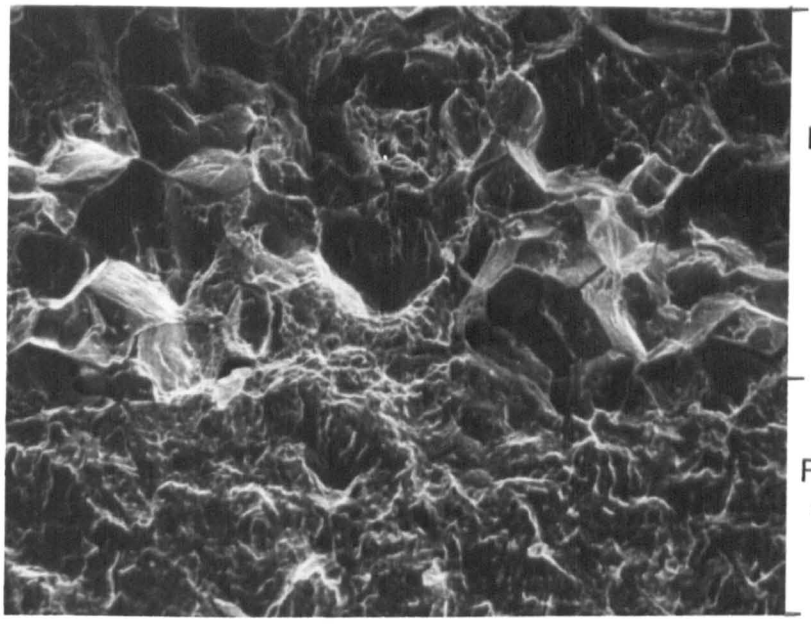

Plate 11.5. SEM fractograph of the unprotected GI Special steel CTS placed in a corrosive environment, NACE solution with H_2S (1 atm.) at 60° C for 350 hours, and tested under a loading rate of 41.2 MN $m^{-3/2}$/hour, in air at room temperature, (30° tilt, 520 X).

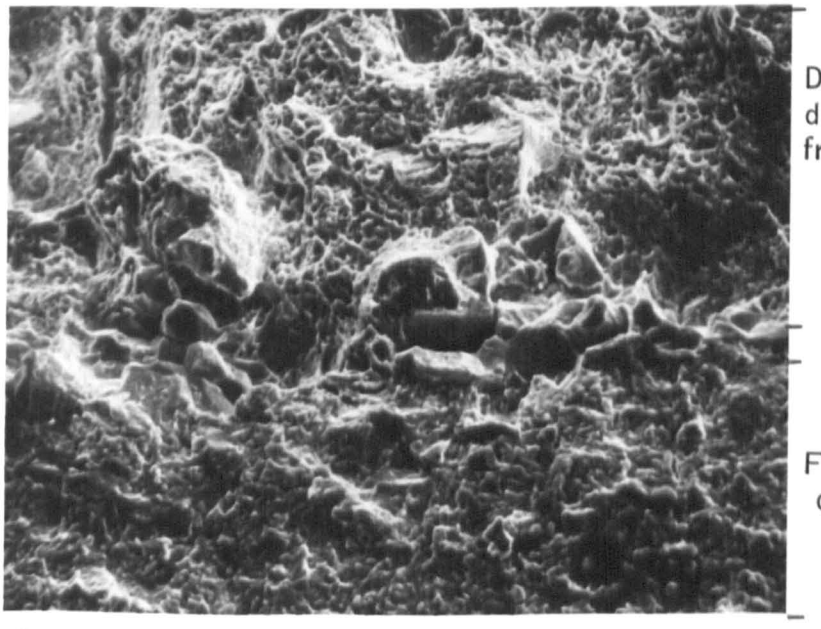

Plate 11.6. SEM fractograph of the GI Special steel CTS with protection applied (ball-milled MoS_2 used) as shown in Fig. 9.4, placed in a corrosive environment, NACE solution with H_2S (1 atm.) at 60° C for 350 hours, and tested under a loading rate of 40.3 MN $m^{-3/2}$/hour, in air at room temperature, (30° tilt, 520 X).

Plate 11.7. SEM fractograph of the unprotected API 5LX 65 pipe-steel CTS, placed in a corrosive environment, NACE solution with H_2S (1 atm.) at 60° C for 750 hours and tested under a loading rate of 5.67 MN $m^{-3/2}$/hour, in air at room temperature (45° tilt, 100 X).

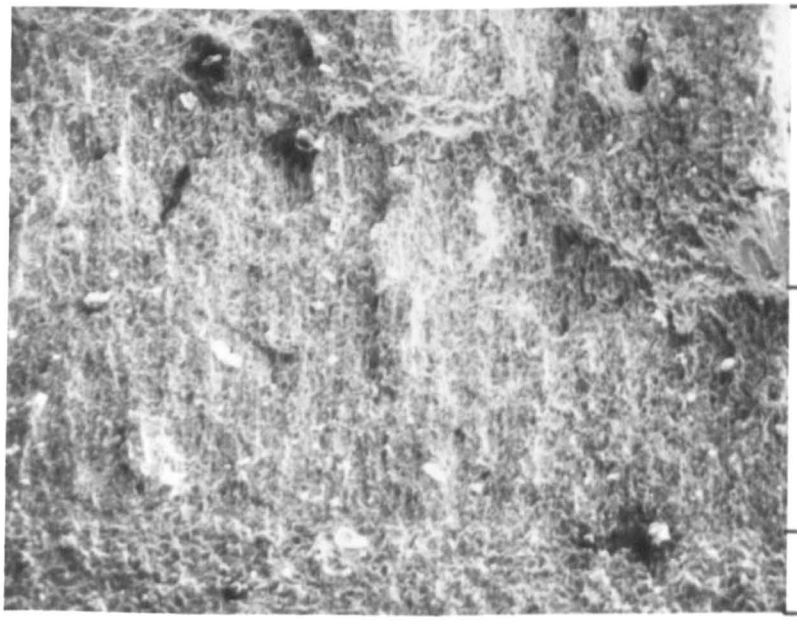

Plate 11.8. SEM fractograph of the API 5LX 65 pipe-steel CTS, with protection (un-ball-milled MoS_2 used) applied as shown in Fig. 9.4, placed in a corrosive environment, NACE solution with H_2S (1 atm.) at 60° C for 750 hours and tested under a loading rate of 5.58 MN $m^{-3/2}$/hour, in air at room temperature (45° tilt, 100 X).

for the term 'n' and the COD was calculated from the following equation;

$$\delta = \frac{V_g}{1 + \frac{n(a+z)}{(W-a)}}$$

where, δ, is the crack opening displacement value.

V_g, is the plastic displacement measured by the clip gauge.

a, is the initial crack length.

W, is the width of the specimen.

z, is the thickness of the knife-edge.

Table 11.2 gives the results of the corroded API 5LX 65 steel CTS both protected and unprotected and tested at a loading rate of 5 MN $m^{-3/2}$/hour. SEM fractographs of the unprotected and protected CTS are given in Plates 11.7 and 11.8 respectively.

The crack opening displacements were calculated for the protected and unprotected three-point bend specimens according to the British Standard 5762[126]. The standard recommends the following relationships for the calculation of COD, when the a/W ratio of the specimen lies, $0.15 \leq a/W \leq 0.7$;

$$\delta = \frac{K(1-\nu^2)}{2\sigma_y E} + \frac{0.4(W-a)V_p}{0.4W + 0.6a + z}$$

where $K = \frac{YP}{BW^{\frac{1}{2}}}$

P and V_p are the force and plastic component of the clip gauge opening displacement respectively.

Y is the compliance function corresponding to crack length/test piece width ratios (a/W).

Table 11.3 gives the crack opening displacement results for the control, protected and unprotected three-point bend specimens tested at two different loading rates of $\approx$3425 MN $m^{-3/2}$/hour and $\approx$ 47 MN $m^{-3/2}$/hour.

TABLE 11.2. Longterm sour corrosion effect on the mechanical properties of API 5LX 65 steel CTS. The specimens were placed in a corrosive environment, NACE solution with H_2S continuously bubbling at 60° C for 750 hours and tested under slower straining/loading with COD measurement at room temperature.

Loading rate ($MNm^{-3/2}$/hour)	k_{IQ} at failure ($MN\,m^{-3/2}$)	Total work done for fracturing the specimen. (joules)	Work done for unit length of crack extension. (J/mm)	Crack opening displacement, δ_{max}. (mm).
Control:				
6.33	91.92	162.73	12.45	0.596
5.86	89.89	166.34	13.35	0.569
6.08	93.65	155.78	12.31	0.561
5.22	93.55	174.53	13.49	0.625
	$\bar{x}$=92.25	$\bar{x}$ = 164.85	$\bar{x}$ = 12.90	$\bar{x}$ = 0.588
Protected:				
5.58	73.83	79.77	6.21	0.251
6.04	76.64	83.28	6.37	0.264
5.74	73.49	66.35	5.34	0.232
4.93	72.24	67.01	5.27	0.253
	$\bar{x}$=74.05	$\bar{x}$ = 74.10	$\bar{x}$ = 5.80	$\bar{x}$ = 0.250
Unprotected:				
5.67	69.19	46.88	3.64	0.111
6.17	67.69	53.96	4.61	0.216
5.39	67.76	56.81	4.32	0.192
4.81	66.06	48.65	3.66	0.141
	$\bar{x}$= 67.68	$\bar{x}$ = 51.58	$\bar{x}$ = 4.06	$\bar{x}$ = 0.165

TABLE 11.3.

Longterm sour corrosion effect on the maximum crack opening displacement value of API 5LX 65 steel three-point-bend specimens. The specimens were placed in a corrosive environment, NACE solution with H_2S continuously bubbling at 60° C for 750 hours and tested in air with different loading rate at room temperature.

Loading rate ($MN\,m^{-3/2}$/hour)	k_{IQ} at failure ($MN\,m^{-3/2}$)	Maximum displacement measured, V_{max} (mm)	Crack opening displacement δ_{max}, (mm).
Control:			
3426	108.37	2.540	0.629
3429	108.82	3.438	0.832
3423	111.01	3.061	0.744
3424	100.50	3.128	0.754
			$\bar{x}$=0.740
46.44	100.01	2.462	0.588
47.52	104.99	2.683	0.644
			$\bar{x}$=0.616
Protected:			
3428	91.52	2.345	0.522
3426	92.05	2.788	0.605
3429	93.34	2.136	0.529
			$\bar{x}$=0.552
47.16	96.86	1.485	0.376
47.88	97.10	1.316	0.340
			$\bar{x}$=0.358
Unprotected:			
3426	89.97	2.183	0.517
3428	89.54	2.217	0.520
3425	88.97	1.980	0.510
			$\bar{x}$=0.516
46.80	85.91	0.899	0.238
47.52	90.85	1.042	0.279
			$\bar{x}$=0.259

Fracture energies of the mild steel control, protected and unprotected Charpy V-notch impact test specimens tested in air at 25 °C after being subjected to the corrosive environment at 60 °C for 350 hours are given in Table 11.4. Table 11.5 gives the fracture energies of the EN 8 steel specimens after being subjected to the corrosive environment at 60 °C for 750 hours and tested in air at 25 °C. The fracture energies of the API 5LX 65 steel Charpy specimens tested in air at 20 °C after being subjected to the corrosive environment for 350 and 750 hours are given in Tables 11.6 and 11.7 respectively. Plate 11.9 gives a light fractograph of the EN 8 steel Charpy impact specimens tested in air at 25 °C, after a period of 750 hours exposure to the corrosive environment. A scanning electron microscopic fractograph of the control EN 8 steel Charpy specimen is given in Plate 11.10. Plates 11.11 and 11.12 give the SEM fractographs of the protected and unprotected EN 8 steel Charpy specimens respectively. Plates 11.13 and 11.14 give the light fractographs of the API 5LX 65 steel Charpy test specimens tested in air at 20 °C, after being subjected to the corrosive environment at 60 °C for 350 and 750 hours respectively. SEM fractographs of the control API 5LX 65 steel Charpy specimens tested in air at 20 °C, are given on Plates 11.15 to 11.17. The SEM fractographs taken on the protected API 5LX 65 steel specimens are given on Plates 11.18 and 11.19. Plate 11.20 gives the corresponding fractograph of the unprotected Charpy specimen.

11.6 Discussion.

The slower straining/loading rate test on the corroded GI Special steel CTS indicates (Table 11.1) that the proposed technique gave a considerable amount of protection for the steel against SSCC. All three parameters, viz. the stress intensity factor at failure, the total work done for fracturing the specimens and the average energy consumed for unit length of crack extension, confirmed the effectiveness of the protective method. It can be seen from the results that with each group either protected or unprotected GI Special CTS the change in loading rate from 40 to 5 MN $m^{-3/2}$/hour exhibited a greater variation in the mechanical propertes. However the reduction in the mechanical properties were

TABLE 11.4.

Fracture energies of mild-steel Charpy impact test specimens tested in air at 25° C after being subjected to a corrosive environment, NACE solution with H_2S bubbling continuously at 60° C for 350 hours. Protected coating; ball-milled MoS_2 with catalyst to FEP ratio of 1 : 0.85.

Control specimens (joules)	Protected specimens (joules)	Unprotected specimens (joules)
32.5	32.5	28.5
27.1	27.8	23.7
28.5	31.2	28.5
32.5	28.5	28.5
36.6	35.3	27.1
33.2	27.1	27.1
34.6	25.8	23.0
36.6	32.5	28.5
$\bar{X} = 32.7$	$\bar{X} = 30.1$	$\bar{X} = 26.9$
$\sigma_{n-1} = 3.5$	$\sigma_{n-1} = 3.3$	$\sigma_{n-1} = 2.2$

TABLE 11.5.

Fracture energies of EN 8 steel Charpy impact test specimens tested in air at 25° C, after being subjected to a corrosive environment, NACE solution with H_2S bubbling continuously at 60° C, for 750 hours. Protected coating; ball-milled MoS_2, with catalyst to FEP ratio of 1 : 0.85.

Control specimens (joules)	Protected specimens (joules)	Unprotected specimens (joules)
29.8	24.4	21.7
27.1	24.4	16.3
27.1	23.0	17.6
25.8	24.4	21.7
24.4	24.4	21.0
30.5	24.4	24.4
29.8	24.4	24.4
25.7	24.4	21.7
29.8	21.7	21.7
29.8	23.0	17.6
$\bar{x} = 28.0$	$\bar{x} = 23.9$	$\bar{x} = 21.3$
$\sigma_{n-1} = 2.2$	$\sigma_{n-1} = 0.9$	$\sigma_{n-1} = 2.3$

TABLE 11.6.

Fracture energies of API 5LX 65 steel Charpy impact test specimens tested in air at 20° C, after being subjected to a corrosive environment, NACE solution with H_2S continuously bubbling at 60° C, for 350 hours. Protected coating; unball-milled MoS_2, with catalyst to FEP ratio of 1:1.12.

Control specimens (joules)	Protected specimens (joules)	Unprotected specimens (joules)
203	160	163
193	179	157
184	190	171
206	179	165
198	168	171
188	176	146
218	165	176
203	190	179
213	190	171
194	198	155
$\bar{x}$ = 200	$\bar{x}$ = 179.5	$\bar{x}$ = 165.4
σ_{n-1} = 10.7	σ_{n-1} = 12.5	σ_{n-1} = 10.3

TABLE 11.7.

Fracture energies of API 5LX 65 steel Charpy impact test specimens tested in air at 20° C, after being subjected to a corrosive environment, NACE solution with H_2S bubbling continuously at 60° C for 850 hours. Protected coating; unball-milled MoS_2, with catalyst to FEP ratio of 1:1.12.

Control specimens (joules)	Protected specimens (joules)	Unprotected specimens (joules)
203	146	130
193	161	159
184	155	149
206	144	152
198	160	146
188	133	125
218	171	160
203	163	122
213	157	141
194	174	145
$\bar{x}$ = 200	$\bar{x}$ = 156.4	$\bar{x}$ = 142.9
σ_{n-1} = 10.7	σ_{n-1} = 12.5	σ_{n-1} = 13.4

Plate 11.9. Light fractograph of the EN 8 steel Charpy impact test specimens, placed in a corrosive environment, NACE solution with H_2S (1 atm.) at 60° C, for 750 hours and tested in air at room temperature 25 ± 2° C. It shows much coarser fracture surface and very little deformation in all the specimens.

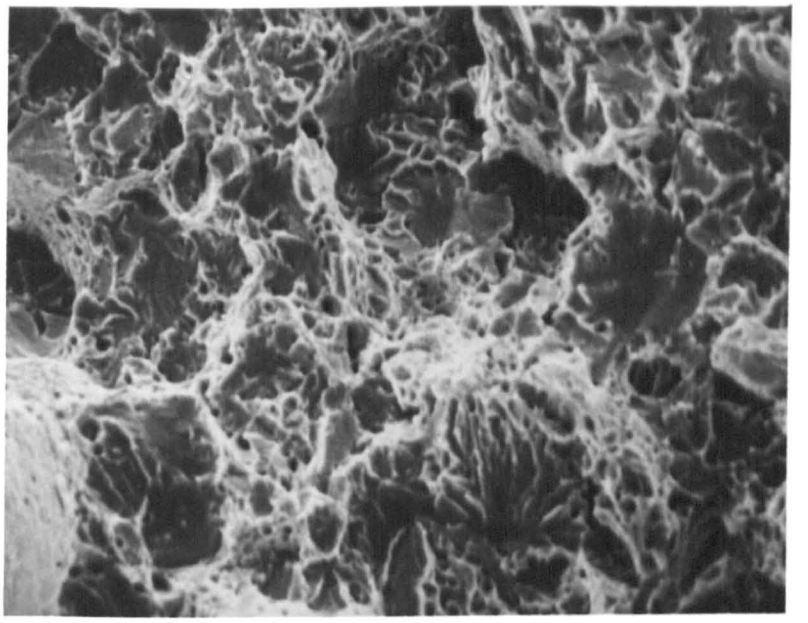

Plate 11.10. SEM fractograph of the control EN 8 steel Charpy impact test specimen tested in air at 25 ± 2° C (45° tilt, 620 X). It shows a quasicleavage fracture with some indication of dimples.

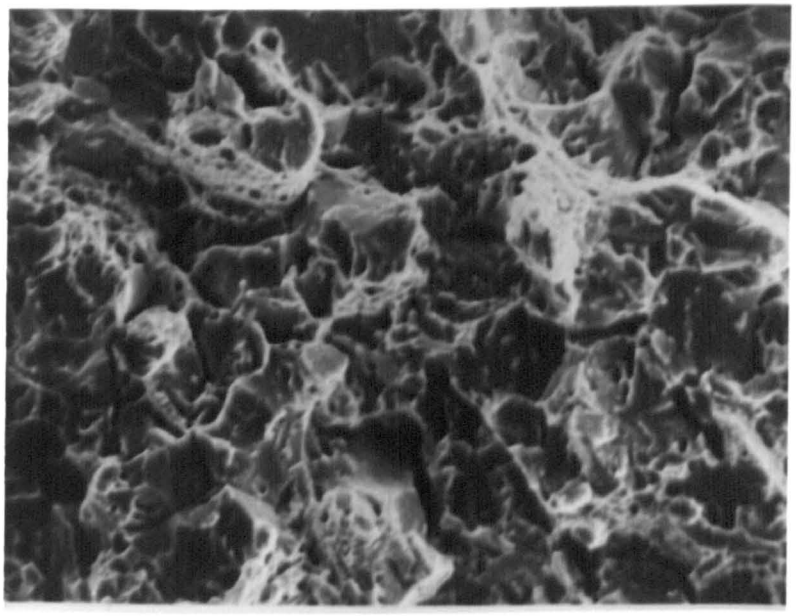

Plate 11.11. SEM fractograph of the EN 8 steel Charpy impact test specimen, with protection applied (un-ball-milled MoS_2 used), placed in a corrosive environment, NACE solution with H_2S (1 atm.) at 60° C for 750 hours and tested in air at 25 ± 2° C, (45° tilt, 620 X). This exhibits mixture of cleavage facets and short, deep intergranular crack, yet shows indication of some dimples.

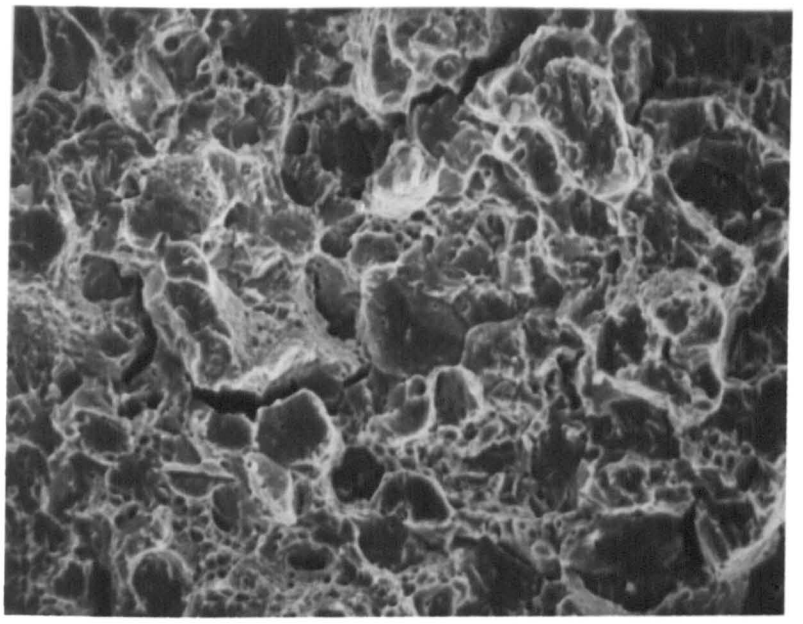

Plate 11.12. SEM fractograph of the unprotected EN 8 steel Charpy impact test specimen, placed in a corrosive environment, NACE solution with H_2S (1 atm.) at 60^0 C for 750 hours and tested in air at 25 ± 2^0 C, (45^0 tilt, 620 X). It exhibits mixture of cleavage facets and short, deep intergranular cracks, yet with indication of some dimples. Also note the deep secondary intergranular cracks, which may be demonstrating the sevior hydrogen attack.

Plate 11.13. Light fractograph of the API 5LX 65 pipe-steel Charpy impact tests specimens, placed in a corrosive environment, NACE solution with H_2S (1 atm.) at 60° C for 350 hours and tested in air at 20 ± 2° C. It shows some blister type attack on unprotected specimens and a comparison of specimens' deformation among the three types.

Plate 11.14. Light fractograph of the API 5LX 65 pipe-steel Charpy impact test specimens, placed in a corrosive environment, NACE solution with H_2S (1 atm.) at 60° C for 850 hours and tested in air at 20 ± 2° C. It shows some blister type attack on unprotected specimens and a comparison of specimens' deformation among the three types.

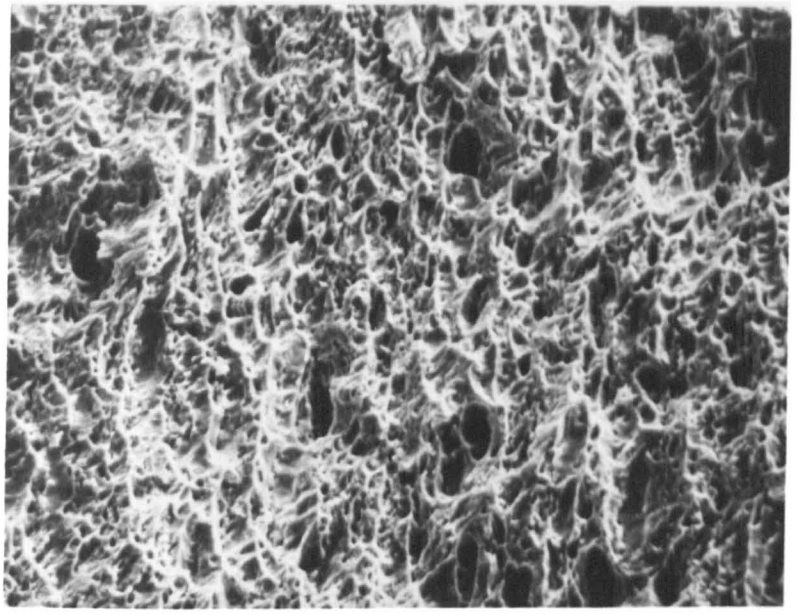

Plate 11.15. SEM fractograph of the control API 5LX 65 pipe-steel Charpy impact test specimens, tested in air at 20 ± 2° C. It shows a complete dimple fracture, (0° tilt, 500 X).

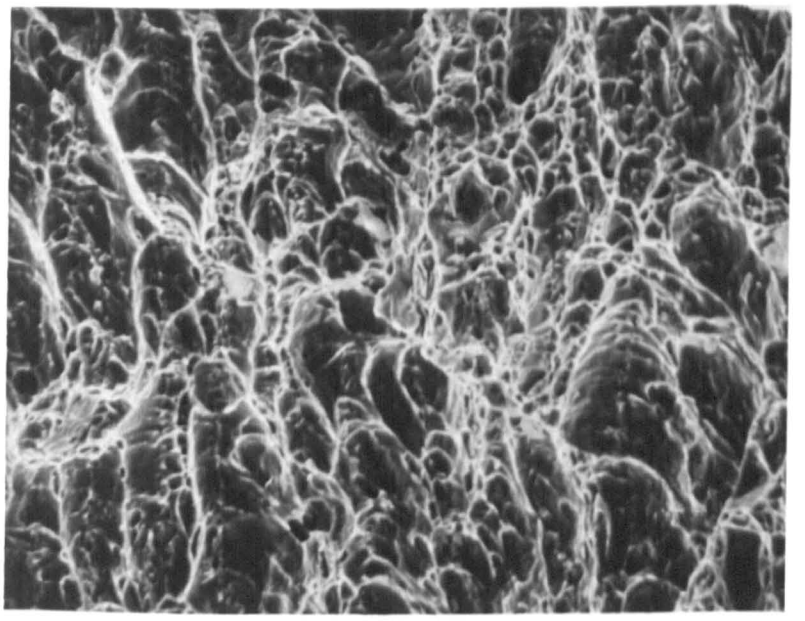

Plate 11.16. This SEM fractograph is taken on the middle of the specimen illustrated in Plate 11.15 (0° tilt, 500 X). It shows a quasicleavage fracture and very little dimple.

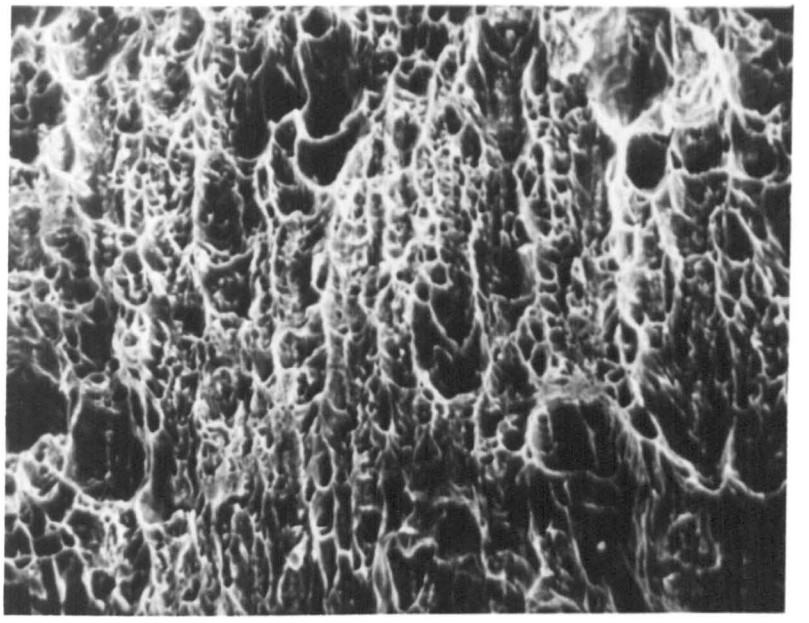

Plate 11.17. This SEM fractograph is taken about $\frac{3}{4}$-way-down the fracture surface of the specimen illustrated in Plate 11.15, (0° tilt, 500 X). It shows mostly shear dimples with a quasicleavage fracture.

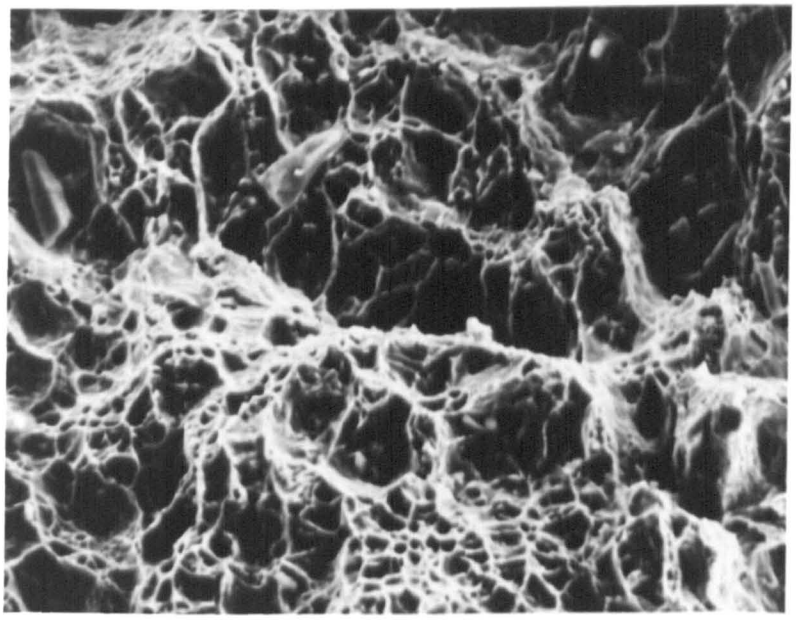

Plate 11.18. SEM fractograph of the API 5LX 65 pipe-steel Charpy impact test specimen, with protection applied (un-ball-milled MoS_2 used), placed in a corrosive environment, NACE solution with H_2S (1 atm.) at 60° C for 350 hours and tested in air at 20 ± 2° C, (0° tilt, 500 X). It shows a mixture of quasicleavage and dimple fracture.

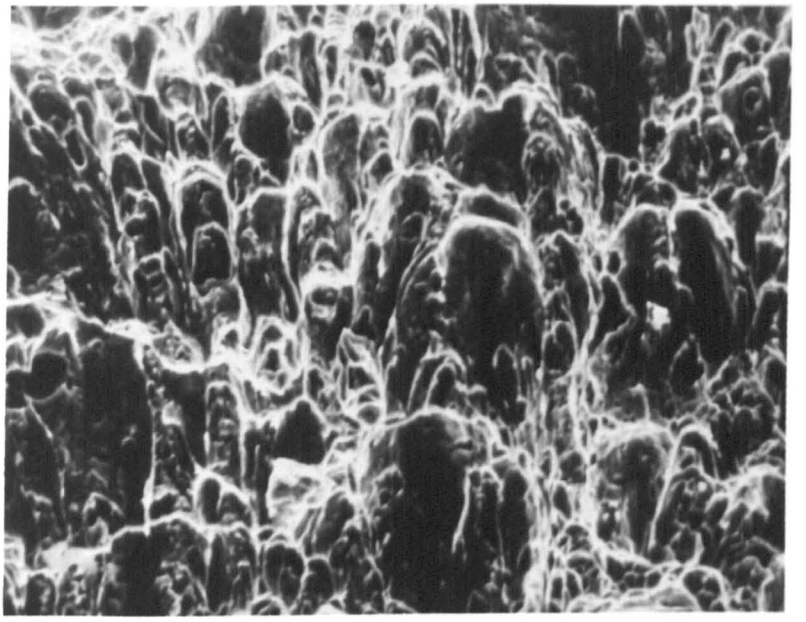

Plate 11.19. This SEM fractograph is taken about $\frac{1}{2}$-way-down the fracture surface of the specimen illustrated in Plate 11.18, (0° tilt, 500 X). It shows a complete quasicleavage fracture.

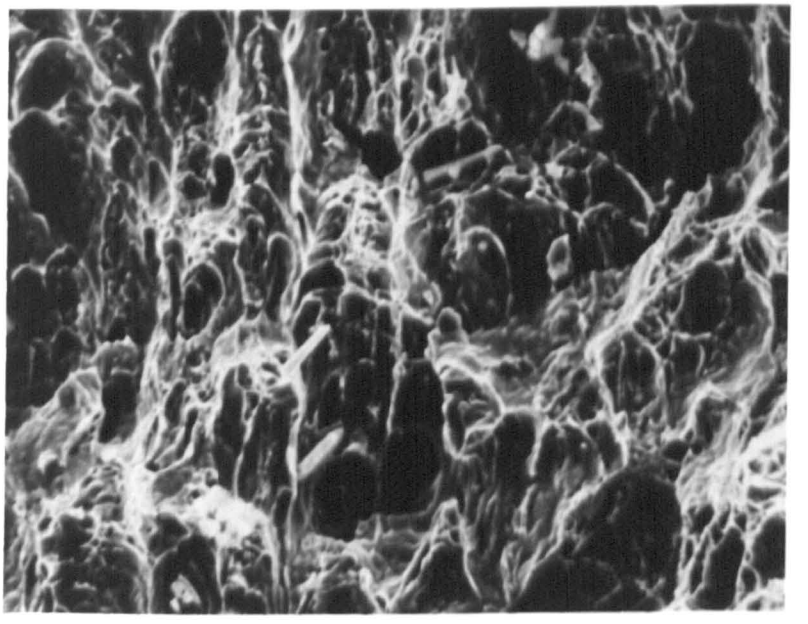

Plate 11.20. SEM fractograph of the API 5LX 65 pipe-steel Charpy impact test specimen without protection applied, placed in a corrosive environment, NACE solution with H_2S (1 atm.) at 60° C for 350 hours and tested in air at 20 ± 2° C, (0° tilt, 500 X). This shows a complete quasicleavage fracture and cavities which may be an indication for sevior hydrogen attack.

far more greater in the case of unprotected specimen than the protected specimen. The total energy required for fracturing the specimen was reduced from 12.44 to 5.09 joules in the group of protected specimens, whereas in the unprotected group it was reduced from 8.11 to 2.97 Joules.

The scanning electron microscopic fractograph (Plate 11.5) taken from the unprotected GI Special CTS and tested at the loading rate of 40 MN $m^{-3/2}$/hour shows that the fracture surface just ahead of the prefatigued-crack was dominated by intergranular fracture. Further SEM examination on the specimen's fracture surface indicated that the mode of fracture was completely intergranular throughout. The SEM examination (Plate 11.6) on the protected GI Special CTS, tested at the same loading rate, shows that the fracture just ahead of the prefatigued-crack has progressed about 2 to 3 grain distances under intergranular fracture mode. Then the fracture mode changed to complete ductile dimple and followed this mode throughout. The change in the mode of fracture indicates that when the GI Special CTS were placed in the corrosive environment, the protected specimens picked-up far less hydrogen than the unprotected specimens. Hence it confirms that the proposed technique gave a considerable amount of protection against SSCC over a period of time in the corrosive environment.

The corroded API 5LX 65 steel CTS tested with and without applied protection, at a loading rate of $\approx$ 5.5 MN $m^{-3/2}$/hour, showed (Table 11.2) that there was a significant improvement in the mechanical properties of protected specimens compared to the unprotected specimens. Furthermore the COD calculated for the compact tension specimens showed that the protected specimens exhibited higher values of δ_{max}, (maximum COD value) than the unprotected specimens. Hence it confirms that the protected specimens were more ductile and absorbed far less hydrogen than the unprotected specimens. The SEM fractographs (Plates 11.7 and 11.8) on the protected and unprotected API 5LX 65 steel CTS show that there was a sub-critical crack growth prior to critical fracture in both cases. Both, sub-critical and critical fractures would seem to be of mixed mode, ductile dimple with some local cleavage.

The crack opening displacement calculated, (Table 11.3) from the corroded three-point-bend specimens with and without the applied protection, indicates that there was an improvement in the COD obtained for the protected specimens over the unprotected ones, when they were tested at a loading rate of ≈ 47 MN $m^{-3/2}$/hour. However, when the specimens were tested at a higher loading rate of ≈ 3425 MN $m^{-3/2}$/hour there was a very little change in the claculated COD values. This may be due to the fact that the hydrogen embrittlement or susceptibility to sulphide stress corrosion cracking could only be detected when the loading/straining rates were very much lower. However, the crack opening displacement measurements on both types of specimens confirm that when the loading rate was significantly lower, the proposed technique exhibited an appreciable improvement in terms of COD values.

The energy absorbed by Charpy V-notch specimens of three different steels (API 5LX 65, EN 8 and Mild steel) also indicates (Tables 11.4 to 11.7) that the protected specimens consumed more energy in comparison with the unprotected specimens in all cases. The API 5LX 65 steel Charpy specimens tested in air at 20 °C after, being exposed to the corrosive environment for 350 and 750 hours, indicate that the longer exposure of the specimens in the corrosive environment the higher the intake of hydrogen and hence increased susceptibility for SSCC.

The light fractograph (Plate 11.9) of the EN8 Charpy impact specimens shows that there was very little deformation of the specimens at the compression side directly opposite the notch in all the cases. This may be due to the fact that the EN 8 steel exhibited a low impact energy of 30 joules. The scanning electron microscopic fractograph on the control EN 8 steel Charpy specimen shows (Plate 11.10) that the fracture was a quasicleavage fracture with some indication of dimples. The SEM fractograph of the corroded EN 8 steel Charpy specimen shows (Plate 11.11) that the fracture surface was a mixture of cleavage facets and short, deep intergranular cracking, yet shows indication of some dimples. The SEM fractograph (Plate 11.12) of the unprotected specimen demonstrates that the fracture surface was similar to the one reported to the protected specimen. But it can also be seen that there are some deep intergranular cracks in the unprotected specimen fracture surface, which is an indication

of severe hydrogen attack on the unprotected specimens. Hence, the SEM fractographs confirm that the proposed technique gave a considerable amount of protection.

The light fractographs (Plates 11.13 and 11.14) of the API 5LX 65 steel Charpy specimens indicate that there was a blister type attack on the unprotected specimens when exposed to the corrosive environment for 350 and 850 hours. Furthermore it may be seen that the blister type attack was increased with time. The lateral deformation of the specimens at the compression side directly opposite the notch shows that the unprotected specimens' were deformed less in comparison with the protected specimens. There was very little deformation observed when the unprotected specimens were exposed to the environment for 850 hours. This observation also confirms that there had been a severe hydrogen attack on the unprotected specimens.

The scanning electron microscopic fractographs taken of the control API 5LX 65 steel Charpy specimens show that there were three types of fracture zones. These zones are shown in Plates 8.15, 8.16 and 8.17. The Plate 8.15 exhibits a complete dimple fracture; Plate 8.16 shows a quasicleavage fracture with little appearance of dimples; and Plate 8.17 indicates more dimple fracture than the quasicleavage. The SEM fractographs (Plates 11.18 and 11.19) of the protected specimens show that two types of fracture surface exist, one a mixture of quasicleavage and dimple fracture, the other a complete quasicleavage fracture. The SEM fractograph on the unprotected specimen indicates that there was only one type of fracture, a complete quasicleavage with some cavities, which is an indication for the severe hydrogen attack.

The above discussion on the SEM fractographs of the specimens add its confirmation that the proposed MoS_2/FEP coat gave a considerable protection to the steels against SSCC, when subjected to a sour corrosive environment for various periods of time.

CHAPTER TWELVE

EVALUATION OF THE PROPOSED METHOD UNDER SOUR-CORROSION-FATIGUE CONDITION

CHAPTER 12.

EVALUATION OF THE PROPOSED METHOD UNDER SOUR-CORROSION-FATIGUE CONDITION.

12.1. Introduction.

Although the effectiveness of the proposed technique to inhibit the SSCC in steel has been demonstrated clearly in the previous chapters, it is necessary to study the effect of the MoS_2/FEP coat on corrosion fatigue crack growth of steel in a sour environment. This is because pipelines protected with the MoS_2/FEP coat have to operate in sour corrosive environments where the corrosion fatigue problem is unavoidable. Furthermore, in recent years, several failures have been reported in large diameter crude oil transmission pipelines and it was identified that the failures were due to the extension of small cracks (developed due to weld defects) on the inner side of pipe structures by corrosion fatigue[130]. Moreover Vosikowsky[131] reported that fatigue crack growth in pipeline steel in crude oil saturated with hydrogen sulphide, ($\approx$ 5000 ppm) was substantially increased, by up to 20 times, compared with the crack growth in air. Due to this increase of corrosion fatigue crack growth rate in a sour environment it was decided to carry-out corrosion fatigue tests on API 5LX 65 steel compact tension specimens (CTS) both with and without the proposed MoS_2/FEP coat applied.

One of the major problems faced in this study is the measurement of growing fatigue crack length in the corrosive environment without interrupting the test. To overcome this problem, the crack lengths were calculated by using changes in total system compliance in a calibration curve.

12.2. Experimental Procedures.

12.2.1. Materials Preparation.

API 5LX 65 steel compact tension specimens (CTS) were used for this study. The chemical composition and mechanical properties of the steel are given in Tables 9.1 and 9.2 respectively. The CTS were prepared as detailed in the section 9.2.1. The protected and unprotected specimens were coated with MoS_2/FEP and Lacomat varnish respectively as shown in Figure 9.4. Unball-milled MoS_2/FEP protective coat with catalyst to FEP ratio of 1:1.12 was prepared as outlined in the section 5.4.1.1. NACE solution saturated with H_2S was used as the sour corrosive environment.

12.2.2. Crack Length Calibration Using Total System Compliance.

It has been demonstrated by Duggan and Proctor[132] that growing crack lengths may be measured from changes in specimen compliance. Normally the load-displacement curve is recorded for a specimen with the help of a clip gauge or a displacement transducer positioned conveniently on the specimen depending on its type. The autographically recorded load-displacement curve facilitates the calculation of the specimen's compliance at a particular value of crack length. Furthermore a series of measurements at various crack length, on the same type of specimens would help to construct a calibration curve and subsequently it could be used to measure growing crack length in fatigue tests without interruption.

In this corrosion fatigue study it was found difficult to construct a compartment to separate the corrosive environment at the crack tip area and the V-notch area where the clip gauge should be placed. This is because of the small dimensions of the CTS determined by the thickness of the parent material. Therefore it was decided to use total system (specimens and attachment) compliances at various crack lengths to establish a calibration curve. The experimental procedures adopted to construct the calibration curve are outlined below.

Fatigue cracks of different lengths ranging from 1 to 8 mm were made on a series of API 5LX 65 steel CTS as detailed in the section 9.2.1. The specimen was fixed to the attachments as illustrated in Figure 9.5. then placed in the test cell and connected to the testing machine with the help of extension rods as shown in Plate 9.1. When the specimen was fixed to the Mayes testing machine, 3 cycles of cyclic load (maximum of 7 kN and minimum 0.7 kN), with a frequency of 10 cycles/min. was applied before the corrosive solution was placed in the test cell. The load-displacement (crosshead) curve was recorded autographically by an X-Y plotter built into the Mayes machine. Then the test cell was filled with NACE solution saturated with H_2S at 20^0 C and maintained at a temperature of 20 ± 2^0 C during the course of the experiment. As soon as the corrosive solution was added to the test cell, 3 cycles of cyclic load with the same characteristic was applied to the specimen and load-displacement curves were recorded. This process was repeated every hour for six hours continuously. The specimen was taken out at the end of the 6 hour period and dried before being broken in air to identify any subsequent crack growth.

It was found from the calibration test results that there was hardly any change in the total system compliance value between the test in air and in the corrosive environment at different periods of time, when the initial fatigue crack on the specimens were below 5.5 mm in length. At higher values of initial fatigue crack length, above 5.5 mm, changes in the compliance with time were noted. Subsequent microscopic examination of such fracture surfaces revealed that there was a growth in the initial crack due to the application of even a few cycles. Also it was found that the change in compliance values agreed well with the length of the crack grown. Furthermore the results confirmed that the compliance values were not changed due to an embrittlement effect. The calibration curve established from the results is given in Figure 12.1.

Figure 12.1. The calibration curve used in the calculation of growing-corrosion-fatigue-crack length.

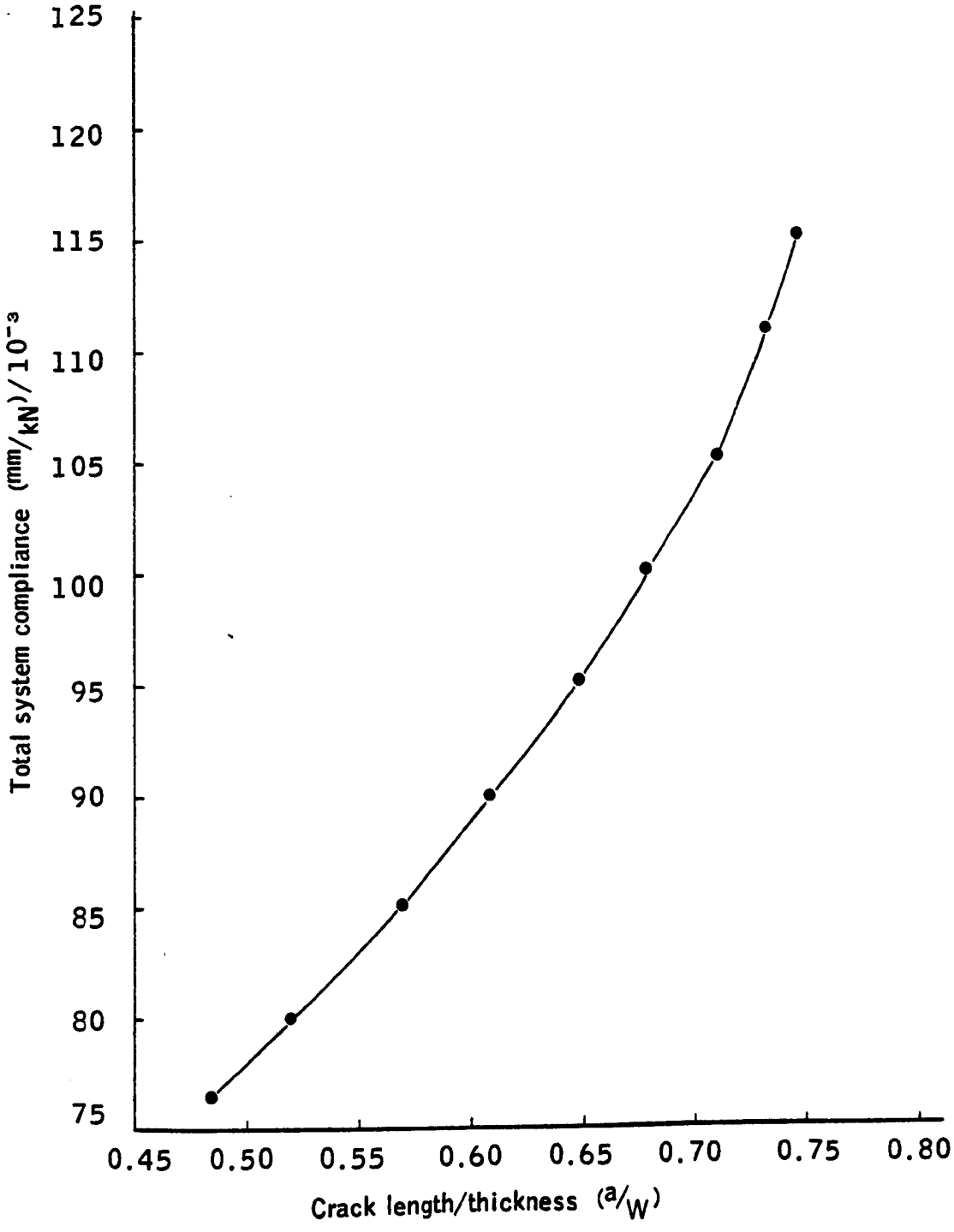

12.2.3. Test Procedure.

The coated CTS was placed in the test cell and connected to the Mayes testing machine as detailed in the previous section. The NACE solution was first purged with N_2 for 30 minutes followed by H_2S for another 30 minutes while maintaining the temperature at 20^0 C, to ensure proper saturation. The test cell was filled with the corrosive solution and the temperature was maintained at 20 ± 2^0 C throughout the experiment with the help of heating tape. The preselected cyclic load with a frequency of 10 cycles/min. and R value (minimum load/maximum load) of 0.1 was applied. The load-displacement curve was recorded autographically at the beginning of the test and continued at specific time intervals. Typical load displacement curves at a series of time for an unprotected specimen is given in Figure 12.2.

12.3. Results.

Using the load-displacement curves recorded with the function of time the corresponding compliance values were calculated. The calculated compliance values were used to read-off the crack lengths from the calibration curve. Then the stress intensity factors ($k_{Imin.}$ and $k_{Imax.}$) at a particular instance were calculated from the maximum and minimum loads, the calculated crack length at that instant and dimensions of specimens, using the principles of linear elastic fracture mechanics[120].

Figure 12.3 gives the curves of corrosion fatigue crack length, a, versus total number of elapsed load cycles 'N' on the protected and unprotected specimens when tested under the cyclic load range of 5 kN and 0.5 kN, in NACE solution saturated with H_2S at 20 ± 2^0 C. The corresponding curves for the specimens when tested under the cyclic load range of 7 kN and 0.7 kN are given in Figure 12.4. The corrosion fatigue crack growth rate versus stress intensity factor plots for the protected and unprotected specimens, tested in the corrosive environment at the two ranges of cyclic loading are given in Figures 12.5 and 12.6 respectively.

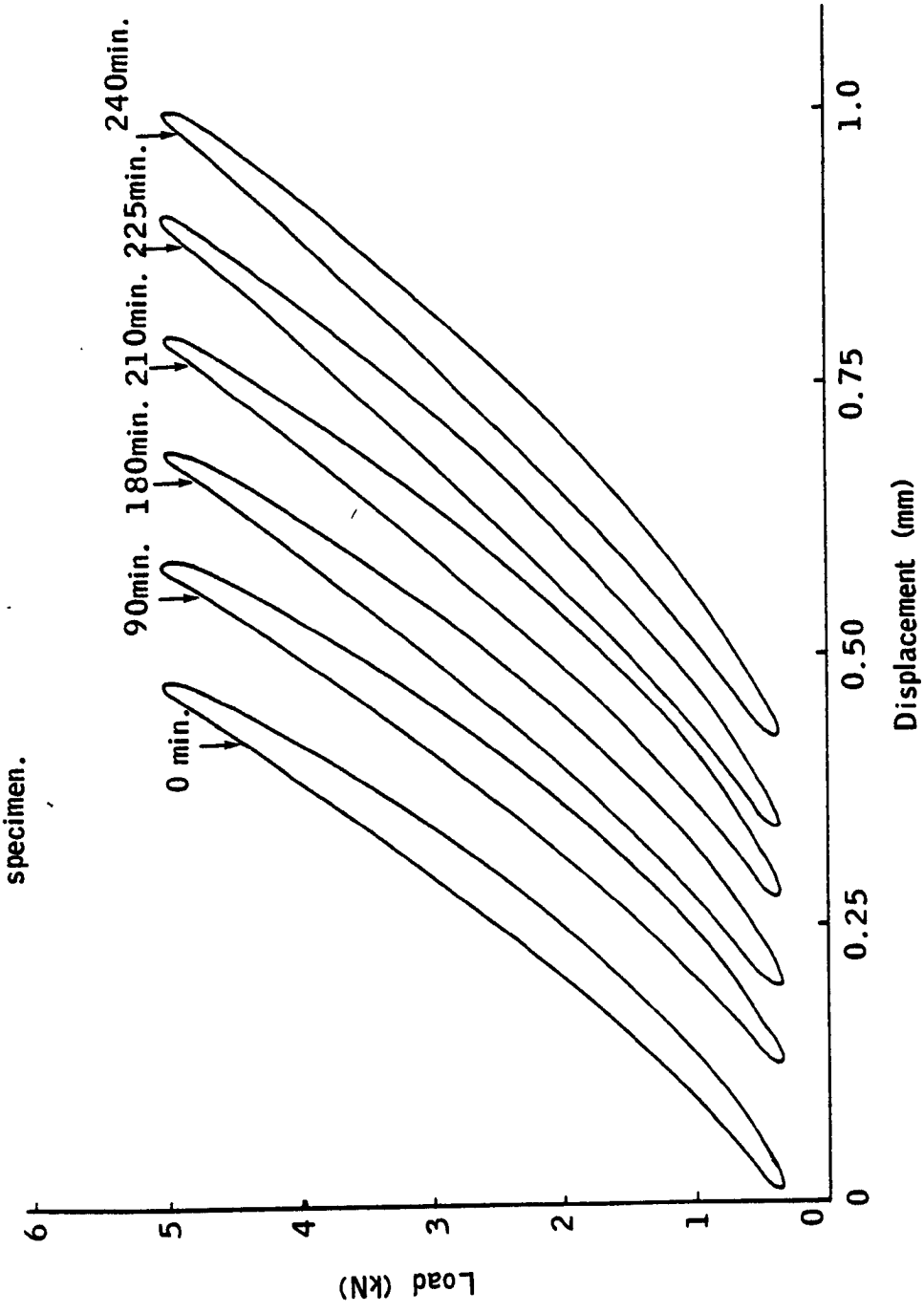

Figure 12.2. Typical corrosion fatigue cyclic load-displacement curves recorded autographically at various times for an unprotected specimen.

Figure 12.3. Corrosion fatigue crack growth as a function of elapsed load cycles for protected and unprotected API 5LX 65 steel CTS tested under a loading range of 5 kN to 0.5 kN in NACE solution with H_2S saturated at 20^0 C.

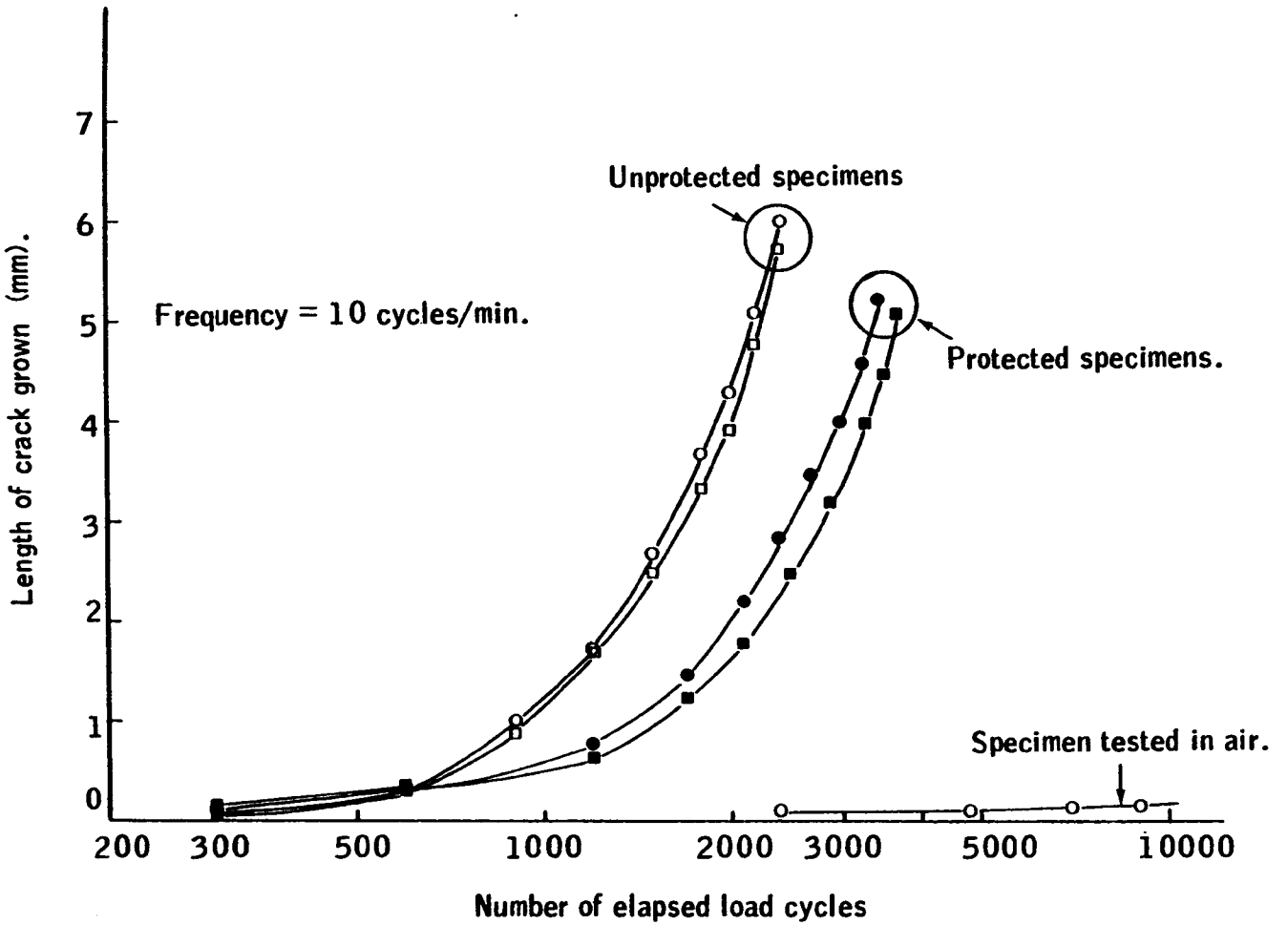

Figure 12.4. Corrosion fatigue crack growth as a function of elapsed load cycles for protected and unprotected API 5LX 65 steel CTS tested under a cyclic loading range of 7 kN to 0.7 kN in NACE solution saturated with H_2S at 20^0 C.

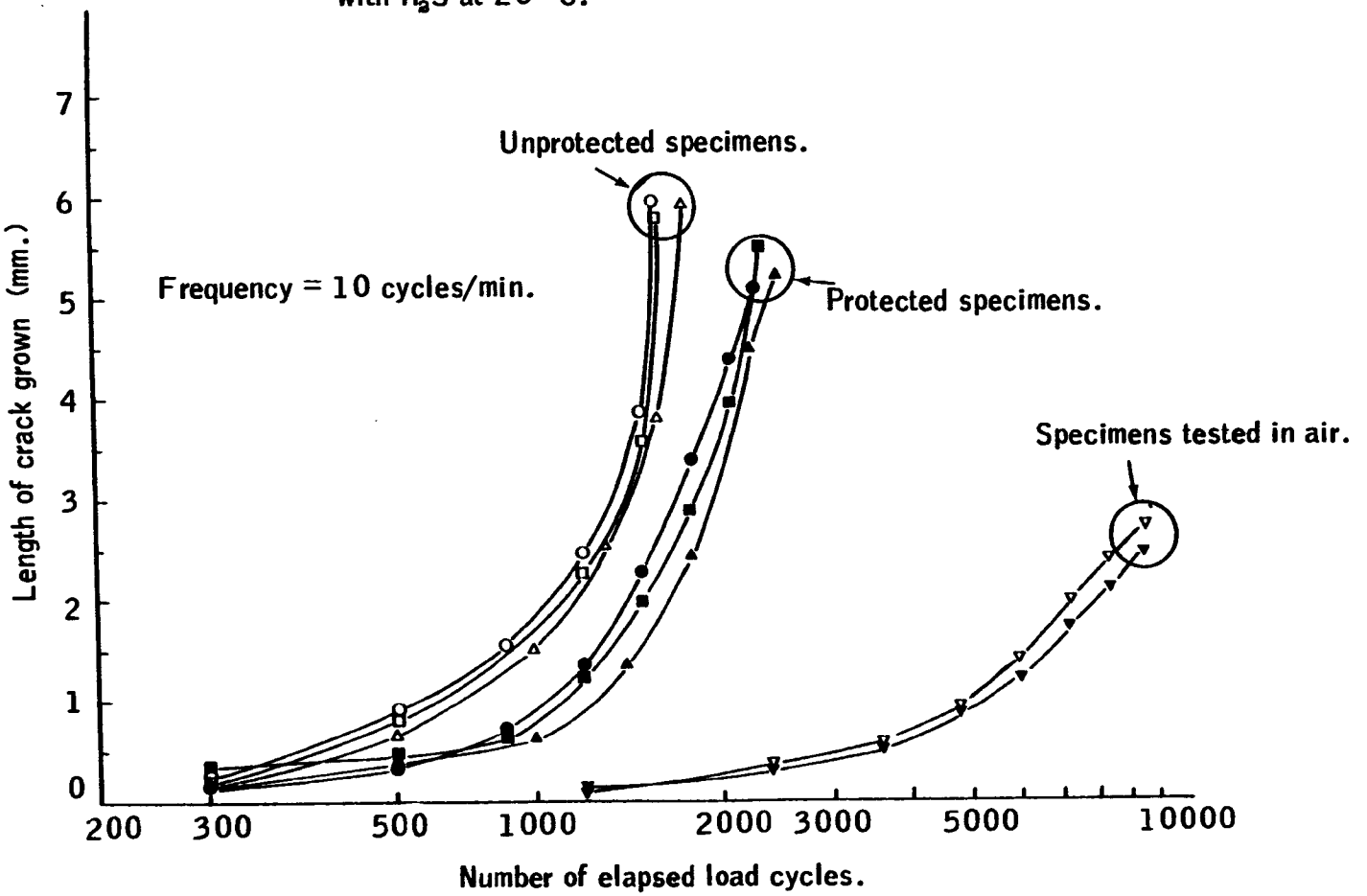

Figure 12.5. Corrosion fatigue crack growth rate for API 5LX 65 steel CTS as a function of stress intensity factor. The specimens were tested with a load range of 5 kN to 0.5 kN in NACE solution saturated with H_2S at 20° C.

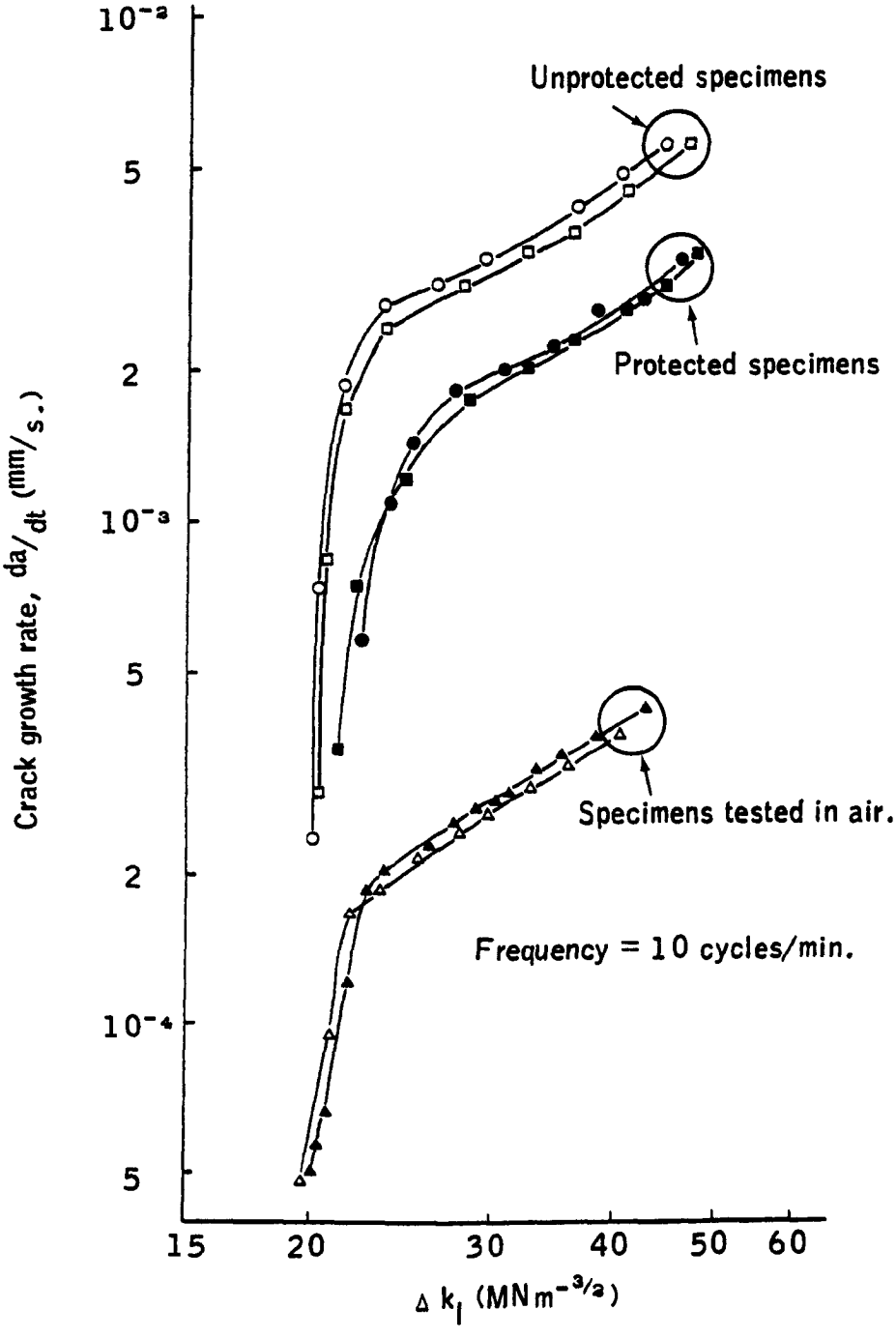

Figure 12.6. Corrosion fatigue crack growth rate for API 5LX 65 steel CTS as a function of stress intensity factor. The specimens were tested with a load range of 7 kN to 0.7 kN in NACE solution saturated with H_2S at 20° C.

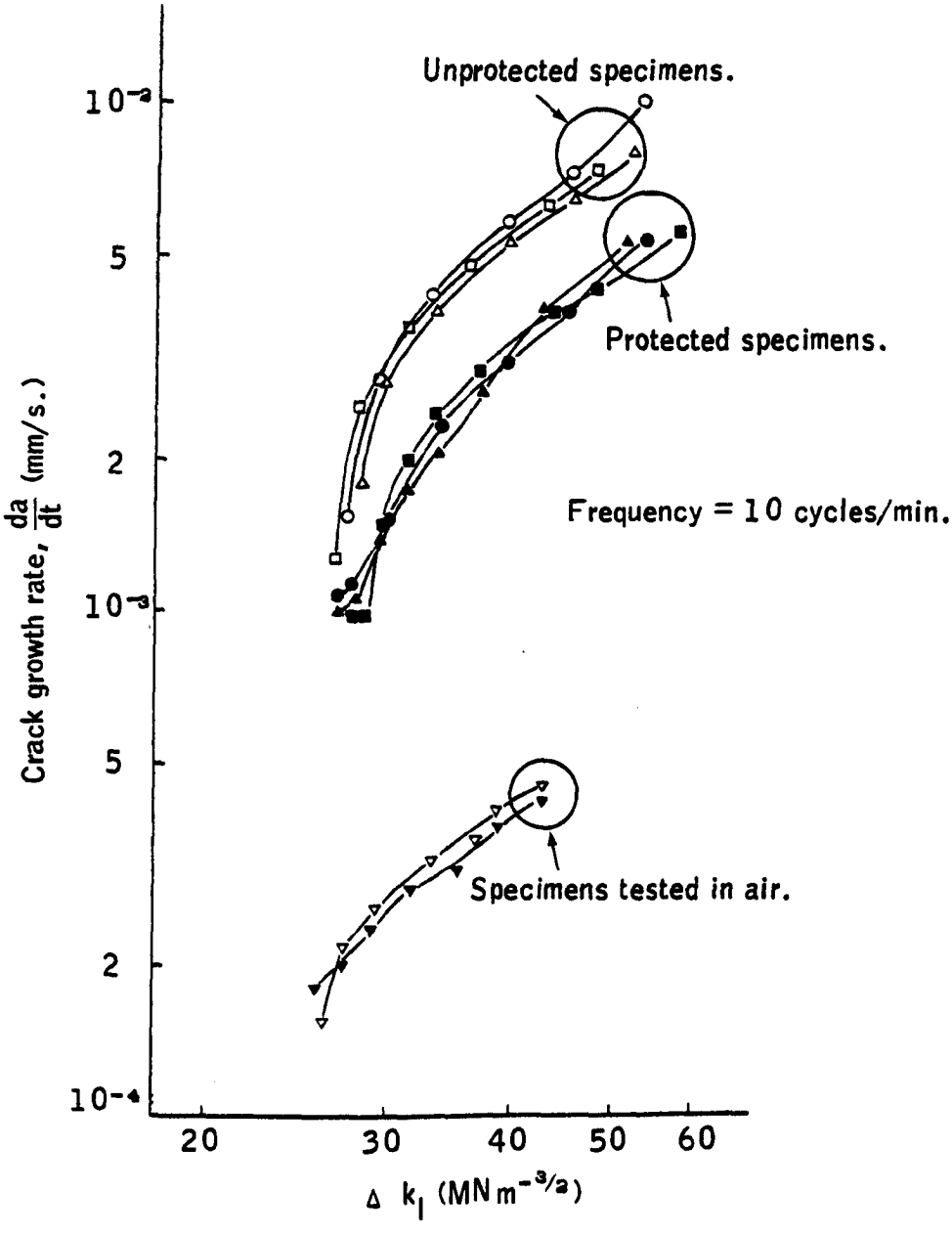

12.4. Discussion.

The data presented on the curves of crack length versus total number of elapsed load cycles (Figure 8.3 and 8.4) indicates that the corrosion fatigue life of the protected specimens increased considerably compared to the unprotected specimens. In the case when 5 kN was the maximum load maintained in the cyclic loading, the corrosion fatigue life of the protected specimens improved by about 60 percent compared to the unprotected specimens. Furthermore, in the case of the 7 kN maximum load experiments the life of the protected specimens increased by about 45 percent.

The measured corrosion fatigue crack growth rates in H_2S saturated NACE solution at a low cyclic frequency of 10 cycles/min as a function of stress intensity factor, indicate that the crack growth rates on the unprotected specimens were considerably higher than the protected specimens. In the case of the 5 kN maximum cyclic load the crack growth rate in unprotected specimens in the corrosive environment increased up to 13 times compared with the crack growth in air. At the same conditions, the crack growth rate in the protected specimens increased by only up to 7 times compared to the results in air. Hence the corrosion fatigue crack growth rate in unprotected specimen was increased about 85 percent compared to the protected specimen in the sour environmental condition. The same amount of crack growth rate increase was found in the unprotected specimens when the specimens were tested under the maximum load of 7 kN.

The results on the corrosion fatigue tests clearly indicate that the MoS_2/FEP protective coat gave a considerable amount of improvement in the corrosion fatigue life of the API 5LX 65 steel. This confirms positively that the proposed method for inhibition of SSCC in steel could be used successfully in a sour corrosive environment where the corrosion fatigue problem is unavoidable.

CHAPTER THIRTEEN

CONCLUSIONS ON PART 2 : THE MECHANICAL ASPECTS

CHAPTER 13.

CONCLUSIONS ON PART 2 - THE MECHANICAL ASPECTS.

The mechanical studies carried out to evaluate the effectiveness of the proposed novel method to inhibit sulphide stress corrosion cracking (SSCC) in steel were greatly helped by the literature survey on stress corrosion test methods and interpretation of results. No single stress corrosion test method that was superior to all others was found in the literature. It has been clearly shown that susceptibility of a material for stress corrosion cracking (SCC) could escape detection unless pre-cracked specimens are used. There are many types of pre-cracked specimens described in the literature. However, compact tension-, cantilever beam- and double cantilever tapered-specimens are the most commonly used pre-cracked specimens. The pre-cracked specimens are tested under three different loading conditions, which are constant strain, constant load and continuous straining/loading. Two parameters, threshold stress intensity factor for SCC, i.e. k_{ISCC}, (presumably no stress corrosion crack grows below this stress intensity factor) and crack growth rate above the k_{ISCC} value are measured on these pre-cracked specimens. Although the application of fracture mechanics facilities understanding more about SCC, in terms of k_{ISCC} and crack growth rate, the experimental results could not be used directly for engineering design. This is because the parameters measured in experimental studies are dependent on various other parameters, which could give misleading values. Therefore, the petroleum industry uses an indirect method to evaluate new materials and protective measures developed to combat SSCC.

Continuous slower straining/loading rate tests using compact tension specimens made of G1 Special steel (equivalent to EN 30B steel available in the market) and API 5LX 65 steel were mainly selected to evaluate the proposed method in terms of mechanical properties. The tests on the G1 Special steel CTS with various loading rates indicated that when the loading rate was reduced from 7680 MN $m^{-3/2}$/hour to 10 MN $m^{-3/2}$/hour or below, the stress intensity factor at failure reduced from 76 ± 2 MN $m^{-3/2}$ to 12.5 ± 0.5 MN $m^{-3/2}$ in NACE

solution saturated with H_2S at 20 ± 2° C. This susceptibility to SSCC measured in terms of stress intensity factor was firmly supported by the scanning electron microscopic (SEM) examination studies of the fracture surfaces of the specimens. The SEM fractographs of the specimens tested at a loading rate of 55.2 MN $m^{-3/2}$/hour showed that the fracture had progressed with an intergranular fracture mode then changed to ductile dimple mode. This ductile dimple fracture mode is the fracture mode generally observed on the GI Special CTS when tested in air with various loading rates ranging from lowest of 3.3 MN $m^{-3/2}$ /hour to highest of 7680 MN $m^{-3/2}$/hour. The SEM fractographs of the specimens tested at a loading rate of 25.2 MN $m^{-3/2}$/hour showed that the fracture was completely of intergranular fracture mode. This mode of fracture demonstrates that the crack has grown fully under the influence of SSCC. But, the stress intensity factor at failure at this loading rate did not approach a constant value. However, when the GI Special CTS were tested at or below 10 MN $m^{-3/2}$ /hour loading rate, the fracture mode was completely intergranular as noticed at the loading rate of 25.2 MN $m^{-3/2}$/hour and the stress intensity factor value at failure approached a constant value of 12.5 ± 0.5 MN $m^{-3/2}$. Furthermore this value agreed well with the k_{ISCC} value given in the literature for this material. This shows that when high strength steels pre-cracked CTS are tested with a loading rate of 10 MN $m^{-3/2}$/hour or less in NACE solution saturated with H_2S at 20 ± 2° C, the susceptibility to SSCC could be detected. Hence the loading rate of less than 10 MN $m^{-3/2}$/hour was used in the continuous slower straining/loading rate tests and three parameters, viz., stress intensity factor at failure, energy required for fracturing the specimens and average energy consumed for unit length of crack extension were measured.

The continuous slower straining/loading rate tests on API 5LX 65 steel CTS protected with ball-milled MoS_2/FEP coat showed a significant improvement of the mechanical parameters measured over the unprotected specimens. The specimens protected with unball-milled MoS_2/FEP coat with higher FEP content also gave a significant improvement over the unprotected specimens, but there was very little difference between each type of coats. However the unball-milled MoS_2/FEP coated specimens gave marginally better results than the

specimens coated with ball-milled MoS_2/FEP coat. Table 13.1 shows the percentage improvement in the measured mechanical properties on the API 5LX 65 steel CTS coated with both types of coat and tested under the same experimental conditions. From Table 13.1 it is clearly seen that both

Table 13.1.

The percentage improvement in the measured mechanical properties on the API 5LX 65 steel CTS coated with both types of coat and tested with a loading rate of ≈ 5 MN $m^{-3/2}$/hour in NACE solution saturated with H_2S as a function of temperature.

Temperature (° C)	k_{IQ} at failure (percent)		Total fracture energy (percent)		Average energy consumed for unit length of crack extension (percent)	
	ball-milled	unball-milled	ball-milled	unball-milled	ball-milled	unball-milled.
20	7.5	11.7	32.6	43.2	33.5	40.5
40	9.9	10.8	25.7	28.5	27.2	26.8
60	11.5	14.6	37.6	35.6	37.2	38.6

coats gave 11, 33 and 34 percent improvement on the parameters, k_{IQ} at failure, total energy consumed for fracturing the specimen and average energy consumed for unit length of crack extension respectively. The slower straining/loading rate tests on the GI Special steel CTS gave significant improvement in mechanical properties over unprotected specimens, when protected with ball-milled MoS_2/FEP coat. The percentage improvements are given in Table 13.2 in terms of the mechanical parameters measured as a function of temperature.

Table 13.2.

The percentage improvements in the measured mechanical properties on the G1 Special steel CTS protected with ball-milled MoS_2/FEP coat and tested with loading rates ≈ 5 MN $m^{-3/2}$/hour in NACE solution saturated with H_2S as a function of temperature.

Temperature (° C)	k_{IQ} at failure (percent)	Total fracture energy (percent)	Average energy consumed for unit length crack extension. (percent)
10	12.9	25.5	29.9
20	24.1	83.2	81.7
40	29.8	89.4	50.4

The results given in Tables 13.1 and 13.2 show that the effectiveness of the protective coat improved more in the case of G1 Special steel CTS (about 80 percent in terms of energy terms) than in the API 5LX 65 steel CTS when tested at temperatures of 20 and 40° C. This was attributed to the fact that the G1 Special steel is more susceptible to the SSCC than the API 5LX 65 steel. Further, effectiveness of the proposed method to inhibit SSCC in the G1 Special steel CTS was supported by the SEM studies on the fracture surfaces of the specimens. The assessment of the ductile fracture area on the protected and unprotected specimens' fracture surfaces, tested in the corrosive environment at $10 \pm 2^{\circ}$ C showed that there were about 55 to 65 percent ductile fracture area noticed on the protected specimens whereas on the unprotected specimens the ductile fracture area was only 10 to 20 percent.

The sustained load tests carried out on the G1 Special steel CTS showed that the proposed method gave a considerable amount of improvement in the failure time when protected with either separate electrodes or with an adherent coat (unball-milled MoS_2/FEP coat), in NACE solution with H_2S bubbling continuously at $20 \pm 2^{\circ}$ C. The crack growth rate measurement studies indicated that the specimens protected with adherent coat and tested at initial stress intensity factors of 14.5, 16.0 and 21.0 MN $m^{-3/2}$ improved in useful life time by 55, 37 and 50 percent respectively. The crack growth rates measurement showed that in the region II where the crack growth rate was controlled by an electro-chemical or physical process, the growth rates on the unprotected specimens were increased between 1.7 and 2.0 times those on the specimens protected with the adherent coat.

Slower straining/loading rate tests on the G1 Special steel CTS after being subjected to the corrosive environment of NACE solution continuously bubbling with H_2S at 60° C for 750 hours showed that the adherent protective coat gave a significant improvement to the protected specimens in terms of the mechanical parameters measured. Table 13.3 gives the percentage improvement of the mechanical properties when the specimens were protected with the ball-milled MoS_2/FEP coat. The effectiveness of the proposed protective coat was

Table 13.3.

The percentage improvements of the mechanical properties measured on the GI Special steel CTS protected with ball-milled MoS_2/FEP coat tested under slower straining/loading rate in air at room temperature after being subjected to the corrosive environment of NACE solution,continuously bubbling with H_2S,at 60° C for 750 hours.

Loading rate (MN $m^{-3/2}$/hour)	k_{IQ} at failure (percent).	Total fracture energy (percent).	Average energy consumed for unit length of crack extension (percent)
40	19.9	53.4	60.6
5	44.2	71.4	54.2

clearly shown at the loading rates of 40 and 5 MN $m^{-3/2}$/hour. However, the percentage improvement of the mechanical properties were higher when the loading rate was reduced from 40 to 5 MN $m^{-3/2}$. This is due to the fact that the susceptibility to SSCC is enhanced when the specimens are tested at significantly lower straining/loading rates.

The API 5LX 65 steel CTS tested with a loading rate of $\approx$ 5 MN $m^{-3/2}$ after being subjected to the corrosive environment of NACE solution,continuously bubbling with H_2S,at 60° C for 750 hours showed that the specimens coated with unball-milled MoS_2/FEP coat, improved significantly in the measured mechanical parameters over the unprotected specimens. There were 9.4,43.7, 42.9 and 51.5 percent improvements noticed in the mechanical parameters of stress intensity factor at failure, total energy consumed for fracturing the specimen, average energy consumed for unit length of crack extension and maximum value of crack opening displacement (COD) respectively. The three-point bend specimens made of API 5LX 65 steel and protected with unball-milled MoS_2/ FEP coat after being subjected to the corrosive environment also exhibited significant improvement on the COD value over the unprotected specimens when tested with a lower loading rate of 47 MN $m^{-3/2}$/hour. However,at the higher loading rate of 3425 MN $m^{-3/2}$ the COD values of the protected and the unprotected specimens did not differ significantly though they exhibited higher values than of the lower loading rate. This is due to the fact that the susceptibility to SSCC or delayed failure in terms of the COD values could be only

detected when the specimens are tested at significantly lower straining/loading rates.

The Charpy impact test on the API 5LX 65 steel, EN 8 steel and mild steel specimens after being subjected to the corrosive environment of NACE solution continuously bubbling with H_2S at 60^0 C for various periods of time indicated an improvement of between 10 and 15 percent in terms of fracture energy. The light fractograph of the EN 8 specimens indicated very little deformation on the compression side directly opposite the notch. However, the SEM fractographs of the specimens showed that there were deep secondary intergranular cracks in the unprotected specimens surface, which is an indication of severe hydrogen attack. The light fractographs of the API 5LX 65 Charpy specimens indicated that there was a blister type attack on the unprotected specimens which increased with time. Also the SEM fractographs of the specimens indicated that there were some cavities in the unprotected specimen. This shows that the unprotected specimens picked up more hydrogen when subjected to the corrosive environment.

The corrosion fatigue crack growth studies on the API 5LX 65 steel CTS in the corrosive environment of NACE solution saturated with H_2S at 20 ± 2^0 C indicated that the fatigue life of the protected specimens improved by 60 and 45 percent when tested with the maximum value of 7 kN and 5kN cycles respectively. The corrosion fatigue crack growth rates studies on the specimens indicated that the crack growth rates in the unprotected specimens were about twice the rate in the specimens coated with the unball-milled MoS_2/FEP coat.

Therefore all the mechanical parameters measured in this part 2 of the experimental sutdies clearly show that the proposed protective coat of MoS_2/FEP inhibited the SSCC in the steels studied to an appreciable level. Also these studies effectively show the viability of the protective method. Thus this protective method has a great potential for industrial application.

CHAPTER FOURTEEN

CONCLUSIONS AND SUGGESTIONS FOR FURTHER WORK

CHAPTER 14.

CONCLUSIONS AND SUGGESTIONS FOR FURTHER WORK.

14.1. Conclusions

The internal sour corrosion which brings about sulphide stress corrosion cracking, SSCC, in hot risers carrying crude oil and gas mixtures from the geological strata to production platforms and the pipelines carrying these products to refineries is one of the major problems faced by the petroleum industry throughout the world. This SSCC is likely to increase in severity for the North Sea oil and gas industry as the fields get older and platforms are moved to deeper waters. This is because hydrogen sulphide concentration increases as the fields get older and deeper water explorations require high strength steels. Prevention measures taken at present are not adequate to prevent SSCC effectively. Therefore extensive research has been carried out to find suitable methods to prevent SSCC in the petroleum industry. A novel method has been found and evaluated for its effectiveness to inhibit SSCC in steel. The novel method is based on using an active hydrogen evolution sulphide electro-catalyst, more active than steel, as a coat on steel surface, such that the hydrogen evolution will take place on the catalyst surface, instead of on the corroding steel surface. Therefore the amount of atomic hydrogen diffusing through the steel is greatly reduced. Hence, SSCC in steel is effectively inhibited.

A computer-aided literature survey supplemented with a manual search on SSCC in steel and its prevention, with particular reference to the oil and gas industry, was carried out to understand the problem and to devise experimental studies to evaluate the method. According to the literature survey there are 8 major factors via., concentration of H_2S, pH value, micro-organisms, temperature, sulphide film, microstructure and heat-treatment, cold work and strength level that are found to dominate the level of susceptibility of steels to SSCC.

The electrochemical aspects of the three sulphide electro-catalysts were evaluated in the various experimental studies, viz., electrochemical polarization, hydrogen diffusion and corrosion weight loss measurements. The MoS_2/FEP electro-catalyst coat was selected for further studies and it is found to possess, three major characteristics that are summarised below.

1. The coat is stable without any deterioration due to the sour corrosive environmental attack.

2. The coat is active enough to reduce the diffusion of atomic hydrogen through steel, which is formed on the steel surface due to sour corrosion.

3. The coat provides as little as possible enhancement of normal corrosion, when partially coated on to the steel coupons. It also helps to form a protective sulphide film which inhibits the sour corrosion in the longer term.

An understanding of the mechanical aspects of the experimental studies was aided by the literature survey on stress corrosion test methods and the interpretation of results. No single stress corrosion test method, that was superior to all others, was found in the literature. However, slower straining/loading rate tests, and sustained load tests were selected to study the changes in various mechanical parameters on different types of specimens when protected with MoS_2/FEP coat. In addition to these tests, Charpy impact tests were also carried out. The mechanical parameters measured on the specimens are;

a) for compact tension specimens
   - stress intensity factor at failure
   - total energy required for fracturing the specimen
   - average energy consumed per unit length of crack extension
   - crack opening displacement
   - crack growth rate
   - time to failure.

b) for three-point bend specimens
   - crack opening displacement.

c) for Charpy V-notch impact test specimens
   - fracture energy.

All these mechanical parameters clearly exhibited the viability and effectiveness of the MoS_2/FEP coat to inhibit SSCC in steel. Furthermore, the significant improvement in the mechanical parameters were confirmed by scanning electron microscopic studies.

The sour-corrosion-fatigue studies on compact tension specimens confirmed that the MoS_2/FEP protective coat to inhibit SSCC in steel could be used effectively in environments where the cyclic loading pattern is unavoidable. Thus, it was proved without any doubt that the protective MoS_2/FEP coat possess a great potential to inhibit SSCC.

14.2 Suggestions for Further Work

The method of using MoS_2/FEP coat to inhibit SSCC in steel has been extensively evaluated from electrochemical and mechanical points of view. It has been proved that the technique possess a great potential to inhibit SSCC in steel for a significant level which is considered to be a breakthrough [133]. However, it is of utmost importance to evaluate the method further before it could become a major technique to prevent SSCC of steels in the petroleum industry. Further work should be concentrated in four areas which are outlined below.

1. Investigation of the sulphide film.
2. Study of the mechanical and physical properties of MoS_2/FEP coat.
3. Development of a non-conducting top coat.
4. Full scale testing.

The first three areas are closely inter-related and should be investigated concurrently, before full scale testing.

1. Investigation of the sulphide film.

   It has been found during corrosion weight loss measurement studies that the sulphide film formed on the MoS_2/FEP partially coated coupons corroded surface was dense and protected the substrate against further corrosion. This study was only carried out up to 200 hours. Hence it is necessary to study the sulphide film formation for longer periods in more detail. The mechanism of its formation, stability as a function of time, electrochemical characteristics and effect of other species on the film such as CO_2 and O_2 should be evaluated.

2. Study of mechanical and physical properties of MoS_2/FEP coat.

   Although the electrochemical characteristics of the MoS_2/FEP coat are the most important for the novel method of preventing SSCC in steel, the mechanical and physical properties of the coat are equally important for its application in the actual working environment. Hence, it is necessary to study its mechanical properties such as thickness, strength and toughness, and physical properties such as thermal conductivity, coefficient of expansion, bonding strength, and effect of contamination. Furthermore, in the experimental studies reported in this thesis, the MoS_2/FEP coat was prepared in very small quantities and applied with a paint brush on small test pieces. This practice cannot be used in the industrial situation. Hence, it is necessary to develop a new technique to apply the MoS_2/FEP mixture.

3. Development of non-conducting top coat for MoS_2/FEP coat:

   The development of the technique to inhibit SSCC in steel in the petroleum industry is coupled with the evaluation of a non-conducting topcoat for the MoS_2/FEP coat. No effort has been made to evaluate this non-conducting coat in the experimental studies reported in this thesis due to lack of time. However, it requires urgent attention and

evaluation, because industrial application is heavily dependent on the successful development of this non-conducting top coat.

4. Full scale testing:

Although the effectiveness of the MoS_2/FEP coat has been evaluated in great detail in the experimental studies from the electrochemical and mechanical points of view, it is necessary to evaluate its effectiveness in actual working conditions. Hence, tests have to be carried out in an industrial environment using various specimens and full scale pipes, coated with the MoS_2/FEP and the top non-conducting coats.

REFERENCES

REFERENCES.

1. Book 2 of The Vocational Training Series, "Corrosion of Oil- and Gal-Well Equipment", Production Department, American Petroleum Institute, 1958.

2. R.S. Treseder and T.M. Swanson, "Factors in Sulphide Corrosion Cracking of High Strength Steels", Corrosion. Vol.24, pp.31-37, Feb. 1968.

3. C.J. Biefer, "The Environmental Cracking of Line Pipe Steels: A Short Review", Mines Branch Information Circular IC 295, Physical Metallurgy Division, Mines and Resources, Department of Energy, Canada, November, 1972.

4. R.S. Treseder, "Oil Industry Experience with Hydrogen Embrittlement and Stress Corrosion Cracking", Proceedings of Stress Corrosion Cracking and Hydrogen Embrittlement of Iron Base Alloys Conference, Unieux-Firminy, France, June 12-16, 1973.

5. G.E. Kerns, M.T. Wang and R.W. Staehle, "Stress Corrosion Cracking and Hydrogen Embrittlement in High Strength Steels", Proceedings of Stress Corrosion Cracking and Hydrogen Embrittlement of Iron Base Alloys Conference, Unieux-Firminy, France, June 12-16, 1973.

6. P.R. Fessler, T.P. Greeneveld and A.R. Elsea, "Stress-Corrosion and Hydrogen-Stress Cracking in Buried Pipelines", Proceedings of Stress Corrosion Cracking and Hydrogen Embirttlement of Iron Base Alloys Conference, Unieux-Firminy, France, June 12-16, 1973.

7. S.A. Golovamenko, V.N. Zikeev, E.B. Serebryanaya and L.V. Popova, "Effect of Alloying Elements and Structure on the Resistance of Structural Steels to Hydrogen Embrittlement", Metallurgical Science Heat-Treatment, Vol.20, pp.3-14, Jan-Feb. 1978.

8. A.C.C. Tseung, P.Russ, H.C. Chan and A.I. Onuchukwu, "Prevention of Hydrogen Embrittlement in Hot, Sour Oil and Gas Pipelines", Research Report, The City University, London 1980.

9. J.M. West, "Electrodeposition and Corrosion Processes", Pub. Van Nostrand, N.Y.81, 1961.

10. J.O.M. Bockris, J. McBreen,, L.Nanis, "The Hydrogen Evolution Kinetics and Hydrogen Entry into α-Iron", J.Electrochm. Soc., Vol. 112, pp.1025-1031, 1965.

11. M.A.V. Devanathan, Z. Stachurski and W. Beck, "A Technique for the Evaluation of Hydrogen Embrittlement Characteristics of Electroplating Baths", J. Electrochem. Soc., Vol. III, pp.886-890, 1963.

12. D.A. Vaughan and Phaless, "Reactions Contributing to the Formation of Susceptible Paths for Stress Corrosion Cracking", ASTM STP 425, pp.209-227, 1967.

13. W. Becks, J. O'M. Bockris, J. McBreen and L.Nanis, "Hydrogen Permeation in Metals as a Function of Stress, Temperature and Dissolved Hydrogen Concentration", Proc. Roy. Soc., Vol.290 A, pp. 220-235, 1966.

14. W.Beck, A.L. Galss and E. Taylor, "The Role of Adsorbed CN Groups in the Hydrogen Embrittlement of Steel", J. Electrochem. Soc., Vol.112, pp.53-59, 1965.

15. W. Kabozer and V. Montblanova, Zhur.Fiz. Kim., Vol.6, p.38, 1952.

16. M. Pourbaix, "Atlas of Potential/pH Diagrams", Pergamon, Oxford, 1962.

17. M. Pourbaix, "Lectures on Electrochemical Corrosion", Pub. Plenum Press, New York, London, 1973.

18. E. French, "Corrosion and Hydrogen Blistering Control in Sour Water Systems", Materials Performance, pp.20-25, Vol.20, March 1978.

19. P. McIntyre and E.F. Walker, "The Influence of Applied Polarization on the Corrosion Properties of a High Strength Steel", 3E4, Proceedings of Second International Congress on Hydrogen in Metals, 6-11 July, 1977.

20. B.F. Brown, "Stress Corrosion Cracking of High Strength Steels", Proceedings of NATO Science Committee, Research Evolution Conference, Brussels, 1971.

21. H.E. Townsend, Jr., "Hydrogen Sulphide Stress Corrosion Cracking of High Strength Steel Wire", Corrosion, Vol.28, No.2, pp.39-46, Feb. 1972.

22. C.F. Booth, E.A. Steigerwald and A.R. Troiano, "Hydrogen Permeability and Delayed Failure of Polarized Martenstic Steels", Corrosion, Vol. 25, No.9, pp.353-358, Sept. 1969.

23. A.R. Troiano and J.P. Fidelle, "Hydrogen Embrittlement in Stress Corrosion Cracking", Proceedings of Hydrogen in Metals Conference, The International Conference held in Paris, May-June, 1972.

24. B.F. Brown, J.A. Smith and M.H. Peterson, "Electrochemical Conditions at the Tip Advancing Stress Corrosion Crack in AISI 4340 Steel", Corrosion, Vol.26, No.12, pp.539-542, 1970.

25. F.E. Blount, B.C. Arnivine and R.J. Chandler, "Results of a Field Study to Select a Tubing Program for Ellenberger Gas", Materials Protection, Vol.1, No.12, pp.24-26, Dec.1962.

26. C.M. Hudgins, R.L. McGlasson, P. Mehdizadeh and W.M.Rosborough, "Hydrogen Sulphide Cracking of Carbon and Alloy Steels", Corrosion, Vol.22, pp.238-251, 1966.

27. P.E. Hudson, E.E. Snavely, Jr., J.S. Payne, L.D. Fiel , and N. Hackerman, "Absorption of Hydrogen by Cathodically Protected Steel", Corrosion, Vol.24, pp.189-196, July, 1968.

28. E.C. Greco and W.F. Brickell, "SAE 1020 Steel Exposed to H_2S-CO_2-H_2O-Hydrogen", Materials Protection, Vol.5, pp.29-33, Oct. 1966.

29. E.C. Greco and W.B. Wright, "Corrosion of Iron in an H_2S-CO_2-H_2O System", Corrosion, Vol.18, pp.119t-124t, March 1962.

30. L.M. Dvoracek, "Sulphide Stress Cracking of Steels", Corrosion, Vol. 26, pp.177-188, May, 1970.

31. C.M. Hudgins, "A Review of Sulphide Corrosion Problems in the Petrolium Industry", Materials Protection, Vol.8, pp.41-47, Jan. 1969.

32. T. Skei, A. Wachter, W.A. Bonner and H.D. Burnham, "Hydorgen Blistering of Steel in Hydrogen Sulphide Solutions", Corrosion, Vol.9, pp.163-172, May 1953.

33. G.H. Booth and F. Wormwell, "Corrosion of Mild Steel by Sulphate-Reducing Bacteria, Effect of Different Strains of Organisms", First International Congress on Metalic Corrosion, London, 10-15 April, 1961.

34. J.N. Wanklyn and C.J.P. Spruit, "Influence of Sulphate-Reducing Bacteria on the Corrosion Potential of Iron", Nature, Vol.169, pp.928-929, May 1952.

35. G.H. Booth and A.K. Tiller, "Polarization Studies of Mild Steel in Cultures of Sulphate-Reudcing Bacteria", Trans. Faraday Soc., Vol.56, pp.1689-1696, 1960.

36. J.B. Greer, "Factors Affecting the Sulphide Stress Cracking Performance of High Strength Steels", Materials Performance, pp.11-22, March, 1975.

37. H.E. Townsend, "Hydrogen Sulphide Stress Corrosion Cracking of High Strength Steel Wire", Corrosion, Vol.28, pp.39-46, 1972.

38. J.B. Greer, "Metal Thickness and Temperature Effects in Casing and Tubing Design for Deep Sour Wells", SPE 3968 Paper Presented at the 47th Annual Fall Meeting of the Society of Petroleum Engineers of the AIME, San Antonio, Texas, 1972.

39. J.B. Greer, E.L. Von Rosenberg, and J. Martinez, "Effect of Temperature and State of Stress on Hydrogen Embrittlement of High Strength Steel", Corrosion, Vol.28, pp.378-384, October 1972.

40. D.W. Sharnon and J.E. Boggs, "Factors Affecting the Corrosion of Steel by Oil-Brine-Hydrogen Sulphide Mixtures", Corrosion, Vol.15, pp.299t-302t, June 1959.

41. S.P. Ewing, "Electrochemical Studies of the Hydrogen Sulphide Corrosion Mechanism", Corrosion, Vol.11, pp.497t-501t, Nov. 1955.

42. J.B. Sardisco and R.F. Pitts, "Corrosion of Iron in an H_2S-CO_2-H_2O System-Mechanism of Sulphide Film Formation and Kinetics of Corrosion Reaction", Corrosion, Vol.21, pp.245-253, No.8, 1965.

43. F.H. Mayer, O.L. Riggs, R.L. McGlasson and J.D. Sudbury, "Corrosion Products of Mild Steel in Hydrogen Sulphide Environments", Corrosion, Vol.14, pp.109t-115t, Feb.1958.

44. E. Snape, "Roles of Composition and Microstructure in Sulphide Cracking of Steels", Corrosion, Vol.24, pp.261-282, 1968.

45. J.W. Kennedy and J.A. Whittaker, "Review Articale - Stress-Corrosion Cracking of High Strength Steels", Corros.Sci.,, Vol.8, pp.359-375, 1968.

46. M.F. Baldy and R.C. Bowden, "The Effect of Martensite on Sulphide Stress Corrosion Cracking", Corrosion, Vol.11, pp.417t-422t, 1955.

47. R.A. McCoy and W.W. Gerberich, "Hydrogen Embrittlement Studies of a Trip Steel", Met. Trans., Vol.4, pp.539-547, Feb. 1973.

48. R.R. Vandervoost, A.W. Ruotola and E.L. Raymond, "Embrittlement of Trip Steel in High - Pressure Hydrogen Gas", Metallurgical Transection, Vol.4, pp.1175-1178, April 1973.

49. R.T. Ault, K.O. McDowell, P.L. Hendricks, and T.M.F. Ronald, "Increased Reliability of High-Strength Steel Through Thermal-Mechanical Treatments", Trans. ASM, Vol.60, pp.79-87, 1967.

50. M. Henthorne and R.N. Parkins, "Some Aspects of The Influence of Structure Upon Stress-Corrosion Cracking and Grain Boundary Corrosion in Mild Steels", Br. Corros. J., Vol.2, pp.186-192, Sept. 1967.

51. Advances in Corrosion Science and Technology, Vol.7, Edited by M.G. Footand and R.W. Staehle, Plenum Press, 1980.

52. R. Hausler, L. Goeller and R. Rosenwald, "Contribution to the Mechanism of Hydrogen Sulphide Corrosion Inhibition", 3rd Eur. Symp. on Corrosion Inhibitor, Ferrara, Italy, pp.399-420, 14-17th Sept. 1970.

53. G.M. Waid and R.J. Stiglitz, "The Development of High Strength Casing Steels with Improved Hydrogen Sulphide Cracking Resistance for Sour Service", Proceedings of the 11th Offshore Technology Conference, pp.1317-1330, April 30th-May 3rd, 1979, Houston, Texas.

54. K. Masamiti, et al, "New Steel for Oil Pipe with High Resistance to Corrosion Cracking in Sulphide Environments", Sumitomo Kindzoku, Vol.24, No.3, p.38, 1972.

55. K.I. Vereshchagin, Yu. I. Rubenchik and G.V. Karpenko, "Effect of Alloying and Microalloying on Resistance of Steels to Cracking", Fiz-Khim, Mekh. Mater., No.5, pp.15-23, 1971.

56. P. Grobner, D. Sponseller and W. Gias, "Development of Higher Strength H_2S - Resistant Steels for Oil Field Applications", Mater. Perform., Vol.14, No.6, pp.35-43, June 1975.

57. "Sulphide Cracking Resistant Metallic Materials for Values for Production and Pipeline Service, NACE Publication IF 166", Materials Protection, Vol.5, pp.81-82, Sept.1966.

58. M.F. Baldy, "Sulphide Stress Cracking of Steels for API Grade N-80 Tubular Products", Corrosion, Vol.17, pp.509t-513t, November 1961.

59. J.F. Bates, "Sulphide Cracking of High Yield Strength Steels in Sour Crude Oils", Materials Protection, Vol.8, pp.33-40, Jan.1969.

60. M. Hill, E.P. Kaivasaki and G.E. Kronbach, "Oil Well Casing; Evidence of the Sensitivity to Rapid Failure in an H_2S Environment, Materials Protection and Performance, Vol.11, pp.19-22, Jan.1972.

61. NACE Standard RP-06-75, Recommended Practice, "Control of Corrosion on Offshore Steel Pipelines", National Association of Corrosion Engineers - Technical Practices Committee, 1975.

62. P.L. Pettus and L.N. Strickland, "Water Soluble Corrosion Inhibitors Help Solve Internal Corrosion Problems", Pipeline Gas J., Vol.202, N2, pp.27-30, Feb.1975.

63. L.W. Gatlin, "Evalution of Inhibitors for Wet, Sour Gas Gathering Systems", Mat. Per. pp.9-19, May, 1978.

64. V.J. Dijk and A. Capelle, "Combating Corrosion in the Dutch Oil and Casfields with Corrosion Inhibitors", Euro. Corr. 77, p.395, London, 1977.

65. P. Geelan and K. Groenewoud, Euro. Corr. 77, p.403, London, 1977.

66. Jr. F. Lyle, S. Lechler, J. Brandt, F.E. Blount, and E.S. Snavely, "Inhibition of Steel Corrosion in Sour Gas Well Environments Containing Sulphur and Ethylamine", Mat. Per., pp.24-31, Jan. 1978.

67. J. Bregman, "Inhibition in the Petroleum Industry", Proceedings of 3rd Eur. Symp. on Corrosion Inhibitors, Ferrara, Italy, p.364, 14th-17th Sept. 1970.

68. L. Hackl, et al., "Mechanism of the Action of Amine-Type Inhibitors in the Presence of H_2S", 4th Euro. Symp. on Corrosion Inhibitors, Ferrara, Italy, p.212, 1975.

69. S. Kut, "Internal and External Pipe Coatings", Pipes and Pipelines International, pp.12-19, Nov. 1971.

70. S. Kut, "Epoxy Resin Powder Coatings for Pipe", Pipes and Pipelines International, pp.8-12, Feb. 1972.

71. R. Moore, Amer. Gas Asso., "Design and Construction of Sour Gas Gathering Systems", American Gas Association Operating Section Proceedings, Paper Presented at the Transmission Conference, Las Vegas, Nevada, T-135, May 3-5th 1976.

72. J.P. O'Donnall, Offshore Pipeline Internally Coated in Place. The Oil and Gas Journal, pp.93-97, Oct. 22, 1973.

73. R.C. Hearn, "Glass Reinforced Coatings and Lining", The Paper Presented at the First International Symposium on High Performance Reinforced Plastics: New Material for the Petroleum Industry, 1978.

74. G.M. Waid and R.J. Stiglitz, "Tubulars' Metallurgy Advances for Ultradeep Sour Wells", Oil and Gas Journal, pp.72-79, Dec.24, 1979.

75. D.R. Fincher, A.C. Nestle and J.J. Marr, "Coupon Corrosion Rates versus Hydrogen Probe Activity", Materials Performance, pp.34-40, Jan. 1976.

76. F.W. Hewes, "Monitoring Internal Corrosion in Pipelines Transporting Natural Gas Containing CO_2 and H_2S", Proceedings of 5th International Corrosion Congress, pp.953-959, Tokyo, 1975.

77. J. Horrath, L. Hackl, and A. Rauscher, "Investigation of the Possibilities of Corrosion Inhibition in Metal-Sulphur-Water Ternary Systems on the Basis of Potential-pH Equilibrium Diagrams", Proceedings of 2nd Ferrara Symposium on Inhibitors, Italy, pp.477-505, 1965.

78. "Corroion Vol.1 - Metal/Environment Reactions", Edited by L.L. Shreir, Pub. Butterworth & Co. (Publishers) Ltd., London, 1978.

79. R.N. Tuttle, "Deep Drilling - a Materials Engineering Challenge", J. Materials Performance, pp.42-46, Feb. 1974.

80. A.I. Onuchukwu, "A Study of Stress Corrosion of Steel", Ph.D. Thesis, The City University, London, Jan. 1980.

81. A.C.C. Tseung and M.C.M. Man, "Electrocatalyst", British Provisional Patent 44362/7, 25th October 1977.

82. M.C.M. Man, S. Jasem, K.L.K. Yeung and A.C.C. Tseung, "Optimization of Gas Evolving Teflon-Bonded Electrodes", Seminar on Hydrogen as an Energy Vector, its Production, Use and Transportation, 3-4th October 1978, Commission of European Communities, pp.255-275, Edit., B.J. Monnet, Brussels - Luxemburg, 1978.

83. M.C.M. Man, "High Performance Hydrogen Evolution Electrocatalyst in Alkaline Media", Ph.D. Thesis, The City University, March 1978.

84. D.B. Hibbert and A.C.C. Tseung, "A Study of $NiCo_2S_4$ in Chlor-Alkali Environments", Research Report, The City University, London, 1978.

85. A.C.C. Tseung, N.B. Fouzder, H.C. Chan and T. Sriskandarajah, "Prevention of Hydrogen Embrittlement in Hot Sour Oil and Gas Pipelines", Research Report, 1st August, 1980 - 30th November, 1980.

86. A.D.S. Tantram and A.C.C. Tseung, "Structure and Performance of Hydrophobic Gas Electrodes", Nature, Vol. 221, pp.167-168, Jan. 1969.

87. P. Vassie, "A Study of Gas Evolution in Porous Electrodes", Ph.D. Thesis, The City University, London, 1976.

88. J. O'M. Bockris and A.K. N. Reddy, "Modern Electrochemistry", p.1231, Pub. Plenum Press, New York, 1970.

89. J. O'M. Bockris and D.M. Dragic, "Electrochemical Science", p.155, Pub. Taylor & Francis Ltd., London, 1972.

90. J. O'M. Bockris and H. Wroblowa, "Electrocatalysis", J. Electroanal, Chem. Vol.7, pp.428-451, 1964.

91. M.H. Mills and M.A. Thompson, "Periodic Variations of Overvoltages for Water Electrolysis in Acid Solutions from Cyclic Voltametric Studies", J. Electrochem. Soc., Vol.123, pp.1459-1461, Oct. 1976.

92. M. Greeness, M.W. Thompson, and R.W. Khan, "Electrocatalytic Activation of Tungsten and Tungstic Oxide Doped with Platinum by Means of Ion Implantation", J. Apply, Electrochem., Vol.4, pp.211-218, 1974.

93. J. Balej and T.P. Vondrak, "Electrochemical Properties of Tungsten Bronzes - Hydrogen Evolution on Sodium Tungsten Bronzes", Electrochim. Acta., Vol. 20, pp.283-287, 1975.

94. D.E. Brown, M.N. Mahmood, A.K. Turner, S.M. Hall and P.O. Fogarty, "Low Overvoltage Electrocatalysts for Hydrogen Evolving Electrode", Int. J. Hydrogen Energy, Vol.7, No.5, pp.405-410, 1982.

95. E.C. Potter, "Electrochemistry Principles and Applications", Pub. Cleaver-Hume Press Ltd., 1961.

96. A.C.C. Tseung, P. Rasiyah and J. Antonian, "Production of Electrocatalysts", British Patent Application No. 80.36847, 1980.

97. K.R. Williams, "An Introduction to Fuel Cells", Pub. Elsevier, Amsterdam, 1966.

98. U.R. Evans, "The Corrosion and Oxidation of Metals", Pub. Arnold, London, 1961.

99. J. O'M.Bockris, "On Hydrogen Damage and the Electrical Properties of Interfaces", Proceedings of Stress Corrosion Cracking and Hydrogen Embrittlement of Iron Base Alloys, pp.286-305, June 12-16, 1973, Unieux-Firminy, France.

100. T.P. Radhakrishnan and L.L. Shreir, "Permeation of Hydrogen Through Steel by Electrochemical Transfer - 1. Influence of Catalytic Poisons", Electrochemica. Acta, Vol.11, pp.1007-1021, 1966.

101. T. Zakroczymski, Z. Szklanska-Smialowska and M. Smialowski, "Effects of Promoters on the Permeation of Electrolytic Hydrogen Through Steel", Werkstoffe und Korrosion, V.27, pp.625-630, 1976.

102. "Manual of Industrial Corrosion Standards and Control", Edited by F.H. Cocks, STP 534, ASTM, 1973.

103. ASTM Designation G1-72, "Standard Recommended Practice for, Preparing, Cleaning and Evaluating Corrosion Test Specimens", Manual of Industrial Corrosion Standards and Control, Edited by F.H. Cocks, STP 534, ASTM, 1973.

104. "Corrosion Vol.2 - Corrosion Control", Edited by L.L. Shreir, Pub. Butterworth & Co. (Publishers) Ltd., London, 1978.

105. J. Golden and J.E.O. Mayne, "Inhibition of the Corrosion of Mild Steel by Zinc Potassium Chromate", British Corrosion J., No.1, Vol.13, 1978.

106. "X-ray Powder Diffraction File", Pub. JCPDS, International Centre for Diffraction Data, 1601 Park Lane, Pennsylvania 19081, U.S.A., 1978.

107. D.L. Morris, L.P. Sampaleanu and D.N. Veysey, "The Corrosion of Steel by Aqueous Solutions of Hydrogen Sulphide", Electrochem. Soc., Vol.127, No.7, pp.1228-1235, 1980.

108. Report of Task Group 1 on "Stress Corrosion Testing Methods", pp.3-20, ASTM Special Technical Publication No. 425, 1966.

109. R.N. Parkins, "Stress Corrosion Test Methods - the European Federation of Corrosion Contribution", AGARD Conference Proceedings No.98, 1971.

110. B.F. Brown, "A New Stress-Corrosion-Cracking Test for High-Strength Alloys", Materials Research & Standards, Vol.6, No.3, p.129, March 1966.

111. B.C. Madden, Jr., "Test Methods and Progress in the Stress Corrosion Investigation at Wright Field", Symposium on Stress Corrosion Cracking of Metals, ASTM-AIME, Philadelphia, 1944.

112. G.F. Sager, R.H. Brown and R.B. Mears, "Tests for Determining Susceptibility to Stress Corrosion Cracking",Symposium on stress corrosion cracking of metals , ASTM-AIME, Philadelphia, 1944.

113. W.H. Ailor, "Handbook on Corrosion Testing and Evaluation", John Wiley and Sons, Inc. New York - London - Sydney - Toronto, 1971.

114. O. Jonas, "Tapered Tensile Specimen for Stress Corrosion Threshold Stress Testing", J. Testing and Evaluation (ASTM), pp.40-47, Vol.6, Jan. 1978.

115. A.W. Loginow, "Stress Corrosion Testing of Alloys", Mat. Prof., Vol. 5, No.5, pp.33-39, May 1966.

116. P. McIntyre, "Stress Corrosion in Steel",Proceedings of the Practical Implications of Fracture Mechanics , The Institution of Metallurgists, Spring Meeting, 27-29 March 1973.

117. R.P. Wei, "Fundalmental Aspects of Stress Corrosion Cracking", Proceedings of National Association of Corrosion Engineers Conference, 1969.

118. H.L. Marcus and G.C. Sih, "A Crackline-Loaded Edge-Crack Stress Corrosion Specimen", J. Engineering Fracture Mechanics, Vol.3, pp.453-461, 1971.

119. R.P. Wei, "The Fracture Mechanics Approach to Stress Corrosion Cracking", Stress Corrosion Research, Edited by H. Arup and R.N. Parkins, 1979.

120. British Standard 5447, "Methods of Test for Plane Strain Fracture Toughness (k_{IC}) of Metallic Materials", The British Standards Institution, 1977.

121. A.H. Priest and P. McIntyre, "Factors Influencing Stress Intensity Values and Crack Propagation Rates During Stress Corrosion Cracking Tests of High Strength Steels", Proceedings of Specialists Meeting on Stress Corrosion Testing Methods, AGARD-98, 1971.

122. J.H. Payer, W.E. Berry and W.K. Boyd, "Constant Strain Rate Technique for Assessing Stress-Corrosion Susceptibility", pp.82-93, Stress Corrosion-New Approaches, ASTM STP 610, 1976.

123. W.G. Clark, Jr., and J.D. Landes, "An Evaluation of Rising Load k_{ISCC} Testing", pp.108-127, Stress Corrosion - New Approaches, ASTM STP 610, 1976.

124. J.B. Greer, "Results of Interlaboratory Sulphide Stress Cracking Using the NACE T-IF-9 Proposed Test Method", J. Materials Performance, pp.9-15, September 1977.

125. R.D. Kane and J.B. Greer, "Sulphide Stress Cracking of High-Strength Steels in Laboratory and Oilfield Environments", J. Petrolium Technology, pp.1483-1488, November 1977.

126. British Standard 5762, "Methods for Crack Opening Displacement (COD) Testing", The British Standards Institution, 1979.

127. "What Does the Charpy Test Really Tell Us?", Proceedings of a Symposium Held at the Annual Meeting of the American Institute of Mining, Metallurgical and Petroleum Engineers, Denver, Colorado, Feb. 27-28 1978, Edited by A.R. Rosenfield, H.L. Gegel, D.F. Hasson, B.B. Rath and J.R. Stephens.

128. British Standard 131, Part 2, "Methods for Notched Bar Tests - the Charpy V-notch Impact Test on Metals", The British Standards Institution, 1972.

129. J.F. Knott, "Fundamentals of Fracture Mechanics", Pub. Butterworths, London-Boston, 1973.

130. O. Vosikowsky and R.J. Cooke, "An Analysis of Crack Extension by Corrosion Fatigue in a Crude Oil Pipeline", Int. J. Pres. Ves. Piping, Vol.6, No.2, p.113, March 1978.

131. O. Vosikowsky, "Effects of Stress Ratio on Fatigue Crack Growth Rates in X70 Pipeline Steel in Air and Salt Water", J. Testing and Evaluation, Vol.8, No.2, p.68, Feb.1980.

132. T.V. Duggan and M.W. Procter, "The Measurement of Crack Length and Shape During Fracture and Fatigue", pp.1-27, Edited by C.J. Beevers, Pub. EMAS U.K., 1980.

133. A.C.C. Tseung, N.B. Fouzder, H.C. Chan and T. Sriskandarajah, "Corrosion Protection Method", British Provisional Patent 81.16018, May, 1981.